A Case Study in Nonlinear On-line Optimal Control

by

Felipe San-Blas C.

A thesis submitted for the degree of *Doctor of Philosophy of the University of London* and for the *Diploma of Membership of the Imperial College*

February 2003

Centre for Process Systems Engineering
Department of Chemical Engineering
Imperial College of Science, Technology and Medicine
London SW7 2BY

LONDON UNIV.

Abstract

Carbon dioxide removal in ammonia or methanol plants is a suitable application for on-line optimal control, since energy efficiency is vital, and it is necessary to maintain high product purity in the face of process disturbances with minimal steam consumption.

The optimal control problem thus involves state inequality constraints, the plant behaviour is essentially nonlinear over the operating range, and many variables of importance cannot be directly measured.

A study was therefore made of the possibility of using on-line optimal control on a pilot plant removing carbon dioxide from a nitrogen stream in an absorption-desorption process, using methanolamine as the solvent.

A nonlinear mathematical model based on material and energy balances, vapour-liquid equilibrium and chemical reaction rates was developed, and implemented using gPROMS, and relevant parameters were fitted using experimental data from the plant.

Since model predictive control (MPC) is an open-loop control algorithm, the current state of the plant must be estimated from the measurements to keep track of the process, and some parameters were also up-dated on-line to improve the adaptive properties. It was found that an extended Kalman Filter (EKF) proved suitable for the purpose, and could be used without the need for refinements such as forgetting factors or variance resetting. The filter was tuned and fully tested using both simulations and actual plant data, and its performance was also compared with that of a common Luenberger observer. The results show an improvement in accuracy of almost an order of magnitude over previous observers implemented in the plant.

Lastly, nonlinear receding-horizon optimal control of the plant was tested by simulation, using a modified model for the "real" plant, and testing the effects of various kinds of mismatch in the model used for the control algorithm. Solvent recirculation rate, steam flow and solvent feed temperature to the absorber were chosen as main control variables, keeping CO_2 concentration in the nitrogen leaving the absorber below set point and respecting other operating constraints, while minimizing steam consumption. Two main scenarios were tested: instantaneous and expected perturbations in the feed conditions. The results proved that optimal model predictive control could be successfully implemented on-line on the plant, and the controller was demonstrated to be robust and adaptive enough to handle a wide range of perturbations.

"Every day you may make progress. Every step may be fruitful. Yet there will stretch out before you an ever-lengthening, ever-ascending, ever-improving path. You know you will never get to the end of the journey. But this, so far from discouraging, only adds to the joy and glory of the climb."

Sir Winston Churchill (1874 - 1965)

Dedicated to my family.

Acknowledgements

I would like to express my deepest gratitude to my supervisors, Professors Roger Sargent and Lester Kershenbaum for their guidance and advice as well as their financial support for this project.

A great thank you goes to my Uncle and Aunt for their kind hospitality and help throughout my first year in London.

All those friends whom I met in the Centre (and also outside the College), whose company and friendship made my staying quite pleasant. Gabriel, Aileen, Jens, Indi, Usman, Ati, Tomo, David, Javier, Daniel, Arinze.

To Marfree for her constant support and love. I apologise for all the extra time I had to sacrifice for this project.

Finally, there are not enough words to thank my Mum and Dad for their constant support, not only economically but also spiritually. Their love and guidance encouraged me to complete this challenging and testing period in my life.

Contents

Abstract **2**

List of Figures **10**

List of Tables **14**

List of Symbols **16**

Chapter 1. Introduction **21**

1.1. Motivations 21

1.1.1. Highly Nonlinear Behaviour 22

1.1.2. Presence of Uncertainty 23

1.1.3. Lack of Measurements of Some State Variables 23

1.1.4. Presence of Process Constraints 24

1.2. Thesis Objectives 24

1.3. Contributions of the Thesis 25

1.4. Thesis Outline 25

Chapter 2. Model Predictive Control Background **27**

2.1. Introduction 27

2.2. Model Predictive Control Strategy 27

2.3. MPC Algorithm History 29

2.3.1. Model Algorithm Control, MAC 29

2.3.2. Dynamic Matrix Control, DMC 30

2.3.3. Quadratic Dynamic Matrix Control, QDMC 31

2.4. Nonlinear Model Predictive Control (NMPC) 32
2.4.1. Nonlinear Optimal Control Formulation 33
2.5. MPC Stability 34
2.6. State Variables and Parameter Estimation 36
2.6.1. Luenberger observer 36
2.6.2. Kalman Filters 37
2.6.2.1 Linear Kalman Filter, KF 37
2.6.2.2 Extended Kalman Filter, EKF 38

Chapter 3. Pilot Plant Modelling 43
3.1. Plant Description 43
3.2. The Nonlinear Model 46
3.3. Process Model 47
3.3.1. Absorber Column Model 48
3.3.1.1 Rate of CO_2 absorption 50
3.3.2. Absorber Gas Feed Model 52
3.3.3. Desorber Column Model 53
3.3.3.1 Pressure calculation 56
3.3.4. Reboiler Model 57
3.3.4.1 Energy balance 59
3.3.4.2 Pressure calculation 59
3.3.5. Condenser Model 60
3.3.6. Mixer Below the Condenser 61
3.3.7. Delays and Controllers 62
3.3.7.1 Desorber feed 62
3.3.7.2 Level controller in the absorber 63
3.3.7.3 Absorber feed 63
3.3.7.4 Steam Valve 64
3.3.8. Model Parameters and Physical Properties 64
3.3.9. Manipulated Variable Feasible Region 66
3.4. Steady State Performance 68

3.4.1. Liquid Temperature Effect on CO_2 Gas Concentration 70
3.4.2. Effect of the Number of Stages on Product CO_2 Concentration 72
3.4.3. Steady-State Optimal Values 74
3.4.3.1 Minimum CO_2 Concentration in the N_2 product 74
3.4.3.2 Minimum Steam Flow Rate 75
3.4.3.3 Optimal Steam Flow at Different Stage Numbers 76
3.5. Dynamic Performance 77
3.5.1. Simple Dynamic Comparison 77
3.5.2. Dynamic Simulation for Optimal Steady-State Changes 81
3.6. Conclusions 83

Chapter 4. Parameter and State Variable Estimation 84
4.1. Estimation of the State Variables 84
4.1.1. Differential States from a Steady State Approximation 84
4.1.2. Extended Kalman Filter (EKF) 85
4.1.2.1 Variables Used for the Extended Kalman Filter 89
4.1.2.2 Jacobian Matrices Used for the Extended Kalman Filter 91
4.1.3. Simulation Test 95
4.1.4. Comparison Between Two Methods 98
4.2. Unknown Parameter Estimation 102
4.2.1. Unknown Parameter Sensitivity 102
4.2.2. Joint Kalman Filter 105
4.3. Simulation Test 107
4.3.1. Benchmark 108
4.3.2. Absorption Constant (κ) 110
4.3.3. Absorption Constant (κ) and MEA Concentration (C_{mea}) 113
4.3.4. Absorption Constant (κ) and Desorber Heat Loss (Q_{ld}) 115
4.4. Estimation Interval: How Often Should Be Done? 117
4.5. Conclusion 119
4.5.1. State Variables Simulation 119
4.5.2. Joint Extended Kalman Filter Simulation 120

Chapter 5. Experimental Estimation **121**

5.1. Estimation of the State Variables 121

5.2. Servo problem in the Recirculation Flow Rate (Exp1) 122

5.3. Servo Problem in the Steam Flow Rate (Exp2) 125

5.4. Servo-Problem in the Gas Feed Flow Rate (Exp3) 130

5.5. Disturbances in the CO_2 Gas Feed Composition (Exp4) 134

5.6. Conclusions 137

Chapter 6. Optimal Model Predictive Control **139**

6.1. Introduction 139

6.2. gOPT Optimisation Tool 139

6.3. Open-Loop Optimal Control Problem 140

6.4. Tests on this Problem 142

6.4.1. Fixed Control Horizon 144

6.4.1.1 Point Constraint at End-Times of Control Intervals 144

6.4.1.2 Path Constraint 146

6.4.1.3 Path Constraint Included in the Objective Function 149

6.4.2. Optimal Horizon 153

6.4.2.1 Derivative End-point Constraint 153

6.4.2.2 Optimal Horizon with Final Weighting Factor 155

6.4.3. Inlet Temperature of Solvent as Additional Control 158

6.4.4. Effect of the Number of Stages 160

6.5. Conclusions 162

Chapter 7. MPC Closed Loop **163**

7.1. Real Optimal Control Including Estimation 163

7.1.1. Simulated Plant 164

7.1.2. Control Variables 165

7.1.3. Estimator and Measurements 166

7.1.4. Simple MPC Problem 168

7.1.5. Liquid Temperature as an Extra Control Variable 171
7.1.6. Conservative Liquid Temperature as Control Variable 174
7.1.7. Expected Perturbation 176
7.1.8. Real Gas Feeding Data 179

Chapter 8. Conclusions and Recommendation for Further Work 182
8.1. Conclusions 182
8.2. Recommendations for Further Work 184

References 185

Appendix A 190

Appendix B 195

Appendix C 197

List of Figures

Figure 2.1. MPC Strategy 28

Figure 3.1. Absorption/desorption pilot plant diagram 45

Figure 3.2 Lumped representation for an absorber stage 49

Figure 3.3. Absorber gas feed model 52

Figure 3.4 Lumped representation for a desorber stage 54

Figure 3.5. Reboiler diagram 57

Figure 3.6. Condenser diagram 60

Figure 3.7. Mixer below the condenser diagram 62

Figure 3.8. Control variables operational region 67

Figure 3.9. Effect of the solvent flow and liquid feed temperature on the leaving flow CO_2 concentration 69

Figure 3.10. Effect of the steam flow and liquid feed temperature on the leaving flow CO_2 concentration. 69

Figure 3.11. Temperature liquid feed effect in the operational range (30-55ºC) 72

Figure 3.12. CO_2 concentration dynamic in each model after a perturbation in the liquid feed temperature (-5°C) 78

Figure 3.13. Step-change in steam flow –20% 78

Figure 3.14. Step-change in solvent flow –15% 79

Figure 3.15. Step-change in $y_{c,f}$ +20% 79

Figure 3.16. Step-change in the liquid feed temperature (10°C) 80

Figure 3.17 Effect in the number of desorber stages on the CO_2 final concentration 82

Figure 3.18. Effect in the number of absorber stages on the CO_2 final concentration 82

Figure 4.1 A complete sequence of the operation of the extended Kalman filter. 89

Figure 4.2 Diagram showing the tasks of both programs for the estimation. 94

Figure 4.3 Parameterised absorber bottom liquid CO_2 concentration 96
Figure 4.4 Parameterised absorber top liquid CO_2 concentration 96
Figure 4.5 Reboiler CO_2 liquid concentration 97
Figure 4.6 Absolute errors in absorber liquid concentration 97
Figure 4.7 Absolute errors in reboiler and desorber liquid concentration 98
Figure 4.8 Experimental data obtained from Rotava's research ("Nexp 5") 100
Figure 4.9 Comparison between Extended Kalman Filter and the steady state estimation. 100
Figure 4.10 Comparison between Extended Kalman Filter and the steady state absolute errors. 101
Figure 4.11 Experimental data selected (Rotava, 1997 "Lexp1") 108
Figure 4.12. Parametric liquid CO_2 concentration in the reboiler, real and estimated 109
Figure 4.13 Estimation of the final CO_2 gas concentration. 109
Figure 4.14 Estimation of the final CO_2 gas concentration with κ as unknown parameter. 111
Figure 4.15 Absorption constant. 111
Figure 4.16 Estimation of the absorption constant. 113
Figure 4.17 Estimation of the MEA concentration. 114
Figure 4.18 Estimation of the absorption constant. 115
Figure 4.19 Estimation of the desorber heat loss. 116
Figure 4.20 Lag produced by discrete sampling 117
Figure 4.21 Comparison between different sampling times. 118
Figure 5.1 Input variables in the plant (Exp1) 123
Figure 5.2 CO_2 leaving gas concentration (Exp1) 123
Figure 5.3 Unknown Parameters (Exp1) 124
Figure 5.4 Parameterised absorber temperatures (Exp1) 124
Figure 5.5 Reboiler temperatures (Exp1) 125
Figure 5.6 Input variables in the plant (Exp2) 126
Figure 5.7 CO_2 leaving gas concentration (Exp2) 127
Figure 5.8 Unknown Parameters (Exp2) 127

Figure 5.9 Parameterised absorber temperatures (Exp2) 128
Figure 5.10 Reboiler temperature (Exp2) 128
Figure 5.11 Top and Bottom desorber temperatures (Exp2) 129
Figure 5.12 Input variables in the plant (Exp3) 130
Figure 5.13 CO_2 leaving gas concentration (Exp3) 131
Figure 5.14 Unknown Parameters (Exp3) 131
Figure 5.15 Parameterised absorber temperatures (Exp3) 132
Figure 5.16 Reboiler temperature (Exp3) 132
Figure 5.17 Top and Bottom desorber temperatures (Exp3) 133
Figure 5.18 Input variables in the plant (Exp4) 134
Figure 5.19 CO_2 leaving gas concentration (Exp4) 135
Figure 5.20 Unknown Parameters (Exp4) 135
Figure 5.21 Parameterised absorber temperatures (Exp4) 136
Figure 5.22 Reboiler temperature (Exp4) 136
Figure 5.23 Top and Bottom desorber temperatures (Exp4) 137
Figure 6.1. Uncontrolled and PI controlled system. 143
Figure 6.2. CO_2 dynamic using internal point constraint. 145
Figure 6.3. Steam and solvent recirculation flow rates. 145
Figure 6.4. Controlled system with path constraints. 147
Figure 6.5. Steam consumption for each case. 147
Figure 6.6. Solvent recirculation rate for each case. 148
Figure 6.7. Effect on the integral error under unexpected perturbation. 150
Figure 6.8. Controlled system including the path constraint in the objective function. 151
Figure 6.9. Controlled system using optimal horizon. 154
Figure 6.10. Steam and solvent flow rates using optimal horizon. 154
Figure 6.11. Controlled system using optimal horizon 156
Figure 6.12. Steam consumption comparison between both methods. 156
Figure 6.13. Solvent recirculation comparison between both methods. 157
Figure 6.14. Final CO_2 gas concentration in the absorber. 158
Figure 6.15. Steam and solvent flow rates. 159

Figure 6.16. Inlet liquid temperature in the absorber. 159
Figure 6.17. Comparison between both model under the same conditions 161
Figure 7.1. MPC closed loop 163
Figure 7.2. Diagram of the plant's measurements used by the controller 167
Figure 7.3. Input variables 169
Figure 7.4. Controlled variable: Leaving CO_2 gas concentration 170
Figure 7.5. Manipulated variables 170
Figure 7.6. Input variables 172
Figure 7.7. Controlled variable: Leaving CO_2 gas concentration 172
Figure 7.8. Manipulated variables 173
Figure 7.9. Input variables 174
Figure 7.10. Controlled variable: Leaving CO_2 gas concentration 175
Figure 7.11. Manipulated variables 176
Figure 7.12. Input variables 177
Figure 7.13. Controlled variable: Leaving CO_2 gas concentration 177
Figure 7.14. Manipulated variables 178
Figure 7.15. Input variables 179
Figure 7.16. Controlled variable: Leaving CO_2 gas concentration 180
Figure 7.17. Manipulated variables 181

List of Tables

Table 3.1. Thermodynamic and physical properties data 65

Table 3.2. Level controller, valve and delay model parameters 65

Table 3.3. Units design data 66

Table 3.4. Normal operation conditions in the plant 66

Table 3.5. Range of values for the different control and manipulated variables 68

Table 3.6. CO_2 concentration at different number of desorber stages (Absorber 20 stages) 73

Table 3.7. CO_2 concentration at different number of absorber stages (desorber 20 stages) 73

Table 3.8. Feed flow rate and CO_2 mol fraction used in runs 1, 2 and 3 74

Table 3.9. Optimal results for runs 1, 2 and 3 74

Table 3.10. Feed flow rate and CO_2 mol fraction used in runs 4, 5 and 6 75

Table 3.11. Optimal results for runs 4, 5 and 6 75

Table 3.12. Optimal steam values at different desorber's stages 76

Table 3.13. Optimal steam values at different absorber's stages 76

Table 3.14. Conditions for Runs 13 to 19 81

Table 4.1. Measurements considered for the EKF test. 95

Table 4.2. Step changes made in CO_2 feed concentration. 96

Table 4.3. Unknown parameters in the model. 102

Table 4.4. Case 1. Individual effect of each unknown parameter. 103

Table 4.5. Case 2. Individual effect of each unknown parameter. 103

Table 4.6. Case 1. Effect of each unknown parameter in tandem with κ. 104

Table 4.7. Case 2. Effect of each unknown parameter in tandem with κ. 104

Table 4.8. Case 1. Effect of each unknown parameter in tandem with κ and Q_{ld}. 105

Table 4.9. Case 2. Effect of each unknown parameter in tandem with κ and Q_{ld}. 105

Table 4.10. Absolute error averages for benchmark case. 109
Table 4.11. Comparing estimation errors between simple EKF and the joint EKF. 112
Table 4.12. Comparing estimation errors between different parameter estimations. 114
Table 4.13. Comparing estimation errors between different parameter estimations. 116
Table 4.14. Absolute error average for different sampling times. 118
Table 5.1. Measurements considered for the EKF test. 122
Table 6.1. Steam consumed for each fixed control horizon case 152
Table 6.2. Steam consumed for each optimal control horizon case 157
Table 7.1. Conditions employed in the model used as “real plant” 165
Table 7.2. Measurements used for the MPC 166
Table 7.3. “real plant” measurement absolute errors 168

List of Symbols

Chapter 2

f	Vector of model equation.
g	Vector of mixed state and control inequality constraints.
$\overline{g}$	Upper bound control vector.
$\underline{g}$	Lower bound control vector.
h_i	Impulse response model's weighting factors.
J	Objective or cost function.
K	Kalman gain.
P	Covariance Matrix.
P^+	Covariance matrix. Time update
P^-	Covariance matrix. Measurement update
Q	Process variance matrix.
R	Measurement variance matrix.
t	Time.
t_0	Initial time.
t_f	Final Time.
u	Controlled inputs
w	Process noise
x	State variables
x^+	State variable estimation. Time update
x^-	State variables estimation. Measurement update
x_0	Initial conditions
X	State space
y	Process output vector.
$\hat{y}$	Estimated process output vector.
ν	Uncontrolled inputs
θ	Unknown parameters

Chapter 3

A_i	Cross sectional area of the unit i. [m^2].
a_i	Interfacial area per unit of volume. [m^2/m^3].

A_T	Vapour flow area per desorber tray [m^2].
A_w	Antoine constant for water.
B_{SP}	Recirculation flow rate set-point [kmol/s].
B_w	Antoine constant for water [°C].
$C_{i,j,k}$	Liquid molar concentration of component i in the stage j of the column k . [kmol/m^3].
C_{gi}	Gas molar specific heat in the unit i . [kJ/kmol°C].
C_{Li}	Liquid molar specific heat in the unit i . [kJ/kmol°C].
C_{Lw}	Liquid molar specific heat of water. [kJ/kmol°C].
c_{pl_i}	Liquid molar specific heat of pure component i . [kJ/kmol°C].
$c_{pl_{i,j}}$	Average liquid phase molar specific heat in the stage i of the column j . [kJ/kmol°C].
c_{pg_i}	Gas molar specific heat of pure component i . [kJ/kmol°C].
$c_{pg_{i,j}}$	Average gas phase molar specific heat in the stage i of the column j . [kJ/kmol°C].
C_w	Antoine constant for water [°C].
D_i	Diameter of column i . [m].
$D_{i,a}$	Desorption transfer rate at the stage i in the absorber. [kmol/s].
D_c	Diffusivity of CO_2. [m^2/s].
F_i	Pure component i gas flow supply. [kmol/s].
F_f	Mixed CO_2 and N_2 flow before absorber's gas feed flow. [kmol/s].
$F_{i,j}$	Gas flow at the stage i in the column j . [kmol/s].
F_w	Cooling water flow rate in the condenser [kmol/s].
g	Gravitational constant. [9.81 m/s^2].
h	Total absorber packing height [m].
h_i	Liquid enthalpy of pure component i . [kJ/kmol].
$h_{i,j}$	Liquid phase enthalpy in the stage i of the column j . [kJ/kmol].
h_{IS}	Ideal liquid enthalpy. [kJ/kmol].
h_{ow}	Liquid height over the weir in the desorber tray. [m].
h_t	Height of a packed section in the absorber. [m].
h_w	weir height in the desorber tray. [m].
H	Henry's constant. [Pa·m^3/kmol].
H_i	Gas enthalpy of pure component i . [kJ/kmol].
$H_{i,j}$	Gas phase enthalpy in the stage i of the column j . [kJ/kmol].
H_{IS}	Ideal gas enthalpy. [kJ/kmol].
I_e	Integral of absorber bottom level error [m.s].
K_c	Proportional gain of the absorber level controller [kmol/s.m].
K_{dry}	Dry hole pressure drop coefficient in the desorber. [s^2/m].

k_r	Reaction rate constant. [m^3/kmol·s].
L_a	Liquid flow rate before the mixer. [kmol/s].
$L_{i,j}$	Liquid flow rate at the stage i in the unit j. [kmol/s].
L_m	Output liquid flow rate in the mixer below the condenser. [kmol/s].
$M_{g,j}$	Average gas molecular weight in the unit i. [kg/kmol].
$M_{l,j}$	Average liquid molecular weight in the unit i. [kg/kmol].
$N_{j,d}$	Number of trays in the stage j of the desorber model.
P_f	Pressure in the separation tank [atm].
pH_i	Liquid pH in the unit i. [pH].
$P_{i,j}$	Pressure in the stage i of the column j. [atm].
P_i^*	Vapour pressure of component i. [atm].
$P_{y,i}$	Partial pressure of component i. [atm].
Q_c	Heat transferred from the condenser [kJ/s].
Q_r	Heat transferred from the steam to the reboiler [kJ/s].
R	Recirculation flow rate. [kmol/s].
$R_{i,a}$	Absorption transfer rate at the stage i in the absorber. [kmol/s].
S	Steam flow rate. [kmol/s].
S_{SP}	Steam flow rate set-point. [kmol/s].
T_g	Temperature in the separation tank. [°C].
$T_{i,j}$	Temperature in the stage i of the column j. [°C].
T_{la}	Temperature in liquid stream before the mixer. [°C].
T_{lif}	Temperature in the absorber liquid feed stream. [°C].
T^{ref}	Temperature of reference. [°C].
$T_{w,0}$	Inlet temperature of the cooling water in the condenser. [°C].
$T_{w,1}$	Outlet temperature of the cooling water in the condenser. [°C].
$U_{i,j}$	Liquid phase hold up at stage i in the column j. [kmol]
$V_{i,j}$	Gas phase hold up at stage i in the unit j. [kmol]
$W_{i,j}$	Condensation rate at the stage i in the column j. [kmol/s].
$x_{i,j,k}$	Liquid molar fraction of component i at stage j in unit k.
$y_{i,f}$	Gas molar fraction of component i in F_f flow.
$y_{i,j,k}$	Gas molar fraction of component i at stage j in unit k.
y_P	CO_2 concentration in the N_2 product [ppm].
z_r	Liquid height in the reboiler [m].
$\alpha_{i,j}$	Carbonation ratio at stage i in the column j.
ΔH_s	Molar enthalpy of condensation of the steam in the reboiler. [kJ/kmol].

ΔH_r	Heat of reaction. [kJ/kmol].
ΔH_V	Water vaporization heat. [kJ/kmol].
$\Delta P_{j,d}$	Pressure drop for a tray in the desorber. [atm].
$\eta_{i,j}$	Ratio between absorbed CO_2 and gas phase flow rate in the stage i of the column j.
$\rho_{g,i}$	Average gas phase density in the column i. [kg/m^3].
$\rho_{l,i}$	Average liquid phase density in the column i. [kg/m^3].
$\upsilon_{g\,i,d}$	Gas flow velocity through the holes in the desorber tray i. [m/s].
τ_B	Time constant of liquid to the desorber. [s].
$\tau_{c,i}$	Time constant of concentration delay model to unit i. [s].
$\tau_{l,i}$	Time constant of liquid delay model to unit i. [s].
τ_s	Time constant of steam to the reboiler. [s].

Subscripts

Component i

c	CO_2.
m	MEA.
n	N_2.
w	Water.

Process unit k

a	Absorber.
c	Condenser.
d	Desorber.
j	Generic stage number in the absorber or desorber.
r	Reboiler.

Chapter 4

B	Liquid output flow rate in the reboiler [kmol/s].
C_{mea}	MEA concentration [kmol/m^3].
$f_{i,j}$	Jacobian of variable i respect j.
fgd	Gas flow rate vector in the desorber [kmol/s].
fld	Liquid flow rate vector in the desorber [kmol/s].
flo	Liquid flow rate vector in the absorber [kmol/s].
J	Objective or cost function.
K_k	Kalman gain
P	Covariance Matrix.
P_d	Pressure vector in the desorber [kPa].

P_r	Pressure in the reboiler [kPa].
Q_{la}	Absorber lost heat [kJ/s].
Q_{ld}	Desorber lost heat [kJ/s].
Q_{lr}	Reboiler lost heat [kJ/s].
R	CO_2 absorption rate vector in the absorber [kmol/s].
t	Time
T_1	Temperature vector in the absorber. [°C]
T_2	Temperature vector in the desorber. [°C]
T_r	Temperature vector in the reboiler. [°C]
u	Controlled inputs
V_b	Gas output flow rate in the reboiler [kmol/s]
x_0	Initial conditions.
x_1	State variables.
x_2	Algebraic variables.
x	Concentration of CO_2 in the liquid phase in the absorber. [kmol/m^3]
x_d	Concentration of CO_2 in the liquid phase in the desorber. [kmol/m^3]
x_r	Concentration of CO_2 in the liquid phase in the reboiler. [kmol/m^3]
y_{co}	Concentration of CO_2 in the gas phase in the absorber. [kmol/m^3]
ε	Desorber tray efficiency.
η_k	Measurement error vector.
κ	Absorption constant. [kmol·s$^{3/2}$/kg]
ν	Uncontrolled inputs.
θ	Uncertain parameters.

Chapter 6

J	Objective or cost function.
R	Liquid recirculation flow. [mol/s].
S	Reboiler's steam flow. [mol/s].
T_{lif}	Liquid feed temperature in the absorber. [°C].
t	Time. [s]
t_f	Time horizon. [s]
u	Controlled inputs
x	State variables
x_0	Initial conditions
$y_{\max}$	Absorber leaving CO_2 gas concentration upper limit. [ppm]
y_P	Absorber leaving CO_2 gas concentration. [ppm]
ε	Path constraint error factor. [kmol]
θ	Unknown parameters
γ	Degree of steadiness at the end of the horizon. [ppm/s]

Chapter 1

Introduction

1.1. Motivations

Modern process industry is characterised by consistently tighter product quality specifications and product demands, new environmental regulations and fast changes in the economical market. Advanced process control systems are an incremental, low-cost approach that can be highly effective in fulfilling these requirements, compared to implementing new process equipments (Kane, 1989; Mix and Dweck 1982).

In the last few decades Model Predictive Control (MPC) has been shown to respond in an effective way to these demands in many practical process control applications and has been therefore widely accepted in process industry. Literature has shown that MPC has been used successfully in industry on batch or semi-batch operations in which process conditions vary significantly over the course of a batch, or in continuous processes that are expected to experience widely varying operating conditions. Model predictive control has been widely adopted in industry as an effective means to deal with large multivariable constrained control problems.

The principal reason why model predictive control has been widely use in the industry is that it is the only control technology that currently handles process objectives, constraints and operating scenarios in a systematic way, through on-line optimisation (Prett and Garcia, 1988). These advantages are very attractive compared with classic feedback-feedforward control theory, specially in highly competitive companies that require improving their process in order to maximize benefits.

After the publication of the initial MPC paper in the late 70s, MPC has progressed rapidly. Since then, a great amount of research with brilliant results has been done in different areas such as: stability, robustness, controllability, parameter estimation, among others; accomplishing a very mature stage nowadays. However most

of the research done last decade was focused in linear models. Just in the past few years some people have tried to take the next step into nonlinear systems by extrapolating the linear theory.

The need for improved process control has become more evident in recent years and there has been growing interest in nonlinear control techniques, especially due to the advances in nonlinear systems theory and improvement in the capabilities of control hardware and software.

There are four main reasons that have moved engineer's attention to advanced nonlinear theory: highly nonlinear plant behaviour, presence of uncertainties, lack of measurements and the presence of process constraints. Obviously, linear theory is the easiest option to any control problem, however it has not completely resolved these problems, even though it has reached a very mature state.

All the above issues deserve to be further analysed.

1.1.1. Highly Nonlinear Behaviour

Chemical processes are nonlinear in nature. Typical nonlinear characteristics are the presence of multiple equilibrium points, chaotic behaviour, etc. Also physical properties such as reaction rates, liquid-vapour equilibria, heat exchange and so many others are dependent on exponential, quadratic, inverse and very nonlinear functions. Nonlinearities are often associated with physical constraints such as hysteretic or saturation limits.

Attempting to linearize a chemical process can be acceptable only when the process nonlinearities are soft or the state variable space is close enough to steady state conditions. Otherwise it is almost impossible to approximate a complete model to a linear one without incurring significant errors.

1.1.2. Presence of Uncertainty

Any mathematical model created to represent any real process will exhibit a degree of mismatch between the theoretical and the real values. This divergence comes from three main reasons: model assumptions and inaccuracies, measurement errors and unmeasured perturbation.

It is vital to maintain uncertainties to the minimum if an effective controller is the final goal. For this motive several approaches have been developed to handle uncertainties and to keep the model as close as possible to the real plant values.

1.1.3. Lack of Measurements of Some State Variables

A model-based model will require a set of initial conditions for its state variables such as temperature profile, flow rates, liquid levels that are easily measurable from the process, in order to start the simulation. However, there are others such as reaction rates, internal flow rates, thermodynamic properties, etc that cannot be obtained directly and are also required to initiate the model integration. This can be done through reconciliation algorithms or estimation techniques.

An important assumption made by most of the nonlinear control techniques proposed in the literature is the complete measurement of the system states. In practice the state variables required for controller implementation are not all measurable or are not measured with sufficient accuracy. Most of the recently proposed nonlinear control techniques rely on the complete state measurement, i.e. temperature and concentrations. But, in general, online measurements of all states of a process are rarely available.

In such cases, reliable information on the unmeasurable state variables is obtained by means of a state observer. State observers are dynamic systems based on a mathematical model and capable of reconstructing the inaccessible process variables from easy available measurements.

While in the case of linear systems the observer design problem has been studied extensively, in the nonlinear case, the methodologies proposed so far are very often problem-dependent and suitable just for a restricted class of nonlinear systems.

1.1.4. Presence of Process Constraints

Safety and environmental regulations, raw materials and product flow rates, profitability, among other restrictions are common, even mandatory issues in every chemical process. Advanced control theories, especially MPC, have addressed successfully this subject by including process constraints into the control loop; it is this point that has made MPC very attractive among process engineers.

Is also well known that the optimal operative values are generally near to the plant constraints

1.2. Thesis Objectives

The work reported here was motivated by the need to study the real applicability of all the extensive theoretical work regarding nonlinear model predictive control and estimation techniques such as the extended Kalman filter in a typical nonlinear chemical process. For this purpose a CO_2 absorption/desorption process was selected.

The behaviour of a CO_2 absorption/desorption pilot plant, located in the Chemical Engineering Department, is fully analysed at different operational conditions in the feed conditions: feed gas flow and CO_2 feed concentration, as well as changes in the manipulated variables: reboiler's steam and solvent recirculation flow and its relation with the controlled variable; the absorber leaving CO_2 gas concentration.

The objective of this project is to investigate the feasibility to apply an online nonlinear model predictive control policy in the absorption/desorption pilot plant located in the Chemical Engineering department using recursive estimation techniques like Extended Kalman filter in order to reduce plant/model mismatch.

1.3. Contributions of this Thesis

Although academia stands one step forward in innovative issues and state-of-the-art ideas, the use of theoretical scenarios and the lack of extensive results generate few practical applications from industry. Therefore more conservative and well-proven approaches such as classical controllers or linear DMC are still used.

Although many studies of Model Predictive Control (MPC) in chemical processes have been conducted, none of them involves complex and realistic processes. Literature is even scarcer about nonlinear MPC implementation, where simple cases (eg. reactors, distillation columns, etc) are used.

The main contribution of this research has been to show that the extensive theory for nonlinear model predictive control (NMPC) can be applied to the control of industrial chemical processes. It has been proved that it is possible to implement nowadays advanced nonlinear control techniques in real processes without risking the robustness and controllability properties shown by the linear controllers.

1.4. Thesis Outline

This thesis is organised as follows.

Chapter 2 is an introduction to the model predictive control, principally focused on nonlinear techniques. As an important part of the algorithm, issues such as stability, robustness and constraints are addressed. Due to the open loop control principle of the MPC, current state variables require to be constantly estimated, a review regarding estimation techniques is presented, giving a more dedicated section to Kalman filters.

Chapter 3 presents a description of the CO_2 absorption/desorption pilot plant located in the Chemical Engineering Department. From a set of assumptions a mathematical model is developed using mass and thermal balances, liquid-vapour equilibrium and other chemical properties obtained from literature. The final model is fully tested using gPROMS, a dynamic process simulator suite. From the results obtained some improvements are produced in order to generate the most suitable model to be used in the following sections.

Chapter 4 tests the model generated in the previous chapter under estimation techniques. An extended Kalman filter algorithm is implemented, the Jacobian matrices used are described, firstly the Kalman filter is used to estimate only the state variables. Through simulations the covariance matrices and other fixed variables are tuned. Later, uncertain parameters are introduced in a joint Kalman filter as extra variables. From the complete set of uncertain parameters a sensitivity test is realized to select those who can better adjust the value of the controlled variable.

Chapter 5 tests the Kalman filter developed in Chapter 4. Experimental data extracted from the pilot plant is used to test the Kalman filter under different conditions.

Chapter 6 examines the optimal controller problem using the mathematical model and estimation technique obtained from previous chapters. Optimal control is only tested under simulation, firstly using the same model as for the real plant so no mismatch is considered and secondly using a model slightly different to incorporate plant uncertainties.

Testing under simulation is the first step in exploring possible difficulties and demonstrating the applicability of the theory. Actual implementation on the plant now requires a further effort in writing the appropriate software.

Chapter 7 tests the complete MPC loop under a more realistic approach. A modified version of the model is used as the real plant, a Kalman filter is used to estimate the state variables and uncertain parameters.

Chapter 8 contains a summary of the achievements and of the main contributions of this work. The most relevant issues that still remain open or require further refinements are considered and some recommendations are made for future research directions.

Finally, Appendix A contains the gPROMS's codes used in this project. Appendix B presents the data used for the sensitivity case for the uncertain parameters. Appendix C includes a sample code used in gOPT for the optimisation part.

Chapter 2

Model Predictive Control Background

2.1. Introduction

Linear controller design techniques are widely employed in the chemical/petrochemical industries. In particular, conventional model predictive control (MPC) has enjoyed widespread acceptance and success as an effective technique for dealing with difficult control problems of industrial importance. The appeal of MPC (and other linear techniques) is partly due to the simplicity arising from the linear models used to approximate process behaviour. However, this also constitutes a potential deficiency, because such simple linear models are often inadequate if a more realistic approximation of the usually complex, nonlinear processes is desired

The nonlinear control schemes which employ more realistic, and often more complex nonlinear process descriptions typically sacrifice the simplicity associated with linear techniques in order to achieve improved performance. More importantly, these nonlinear techniques require nonlinear differential equation process models. This limits industrial application since such first principles models are not readily available in industrial practice.

This chapter discusses the current practices in MPC, design, performance and stability and future research directions.

2.2. Model Predictive Control Strategy

Model Predictive Control (MPC) is an optimal-control method to select control inputs by minimising an objective function. The objective function is defined in terms of

both present and predicted system variables and is evaluated using an explicit model to predict future process output. At each time step, an open-loop optimal control problem is solved and the input profile is injected into the plant until a new measurement becomes available. The updated plant information is used to formulate and solve a new open-loop optimal control problem.

The strategy is illustrated as shown in Figure 2.1 and described as follows

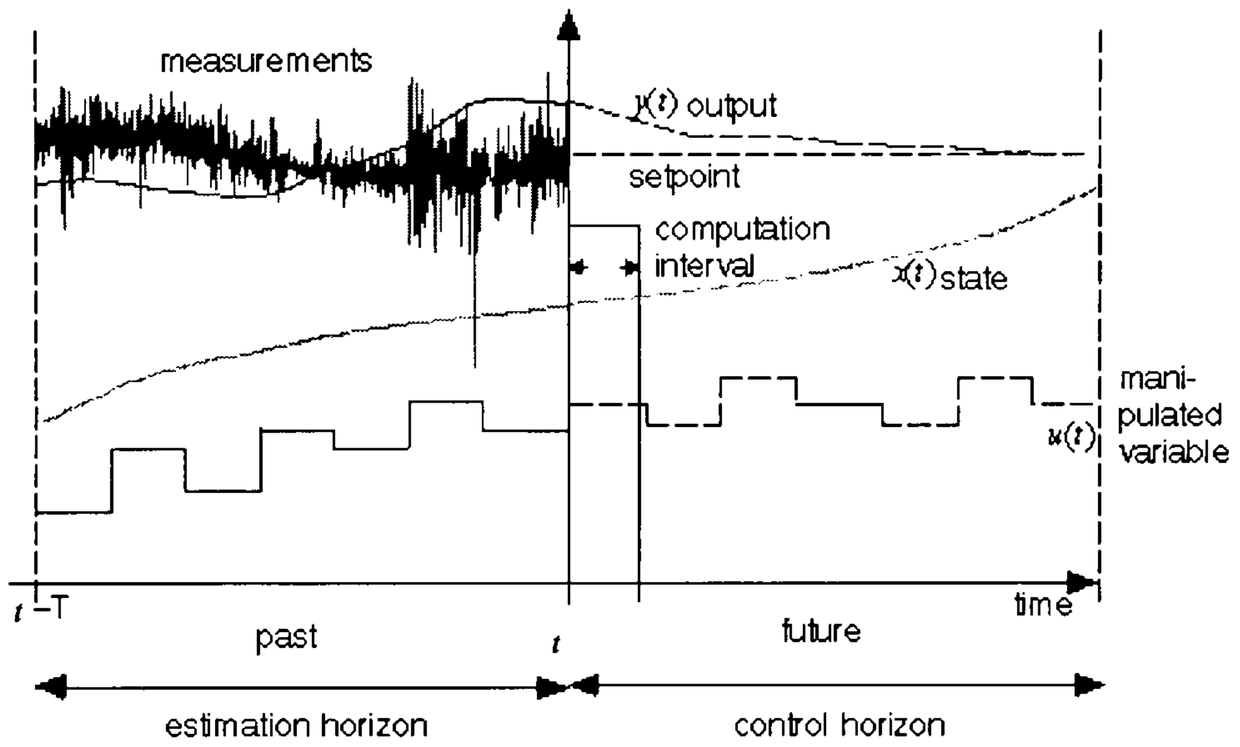


Figure 2.1. MPC Strategy

The predicted future outputs $y(t+k|t)$, $k=1,\cdots,N$ for prediction horizon N are calculated at each instant t using the process model. These depend on the known values up until time t (past inputs and outputs), including the current output (initial calculation) $y(t)$ and on the future estimates of uncontrolled inputs and control signals $u(t+k|t)$, $k=0,\cdots,N-1$ to be calculated.

A sequence of future control signals is computed to optimise a performance function, often to minimise error between a reference trajectory and predicted output. One of the main advantages of the MPC approach is its ability to take process constraints into consideration, including them in the optimisation problem (Rotava,1997).

Originally a discrete-time model was used and, only the current control signal $u(t|t)$ was transmitted to the process. At the next sampling instant $y(t+1)$ was

measured and step 1 was repeated and all sequences and data is updated. Thus $u(t+1|t+1)$ is then calculated using receding horizon techniques.

The complete MPC algorithm explained above could be compressed in three principal ideas (Camacho & Bordons, 1995):

1. The explicit use of a model to predict the process.
2. Calculation of a control sequence to optimise a performance index.
3. The implementation of a receding horizon strategy.

2.3. MPC Algorithm History

Model predictive control can be classified into two categories: Linear Model Predictive Control (LMPC) and Nonlinear model predictive control (NMPC). LMPC basically deals with a linear model of the process, has a linear or quadratic objective function, and its input and output constraints are linear functions. The response of linear dynamic systems obeys the principle of superposition, i.e. the response of the system is a linear combination of responses to each input separately. In almost any control application, linear design techniques are usually the first to be attempted, especially those involving regulation about a steady state operating point (Disli, 1996).

NMPC refers to the general case in which the process model, performance index, and constraints may be nonlinear functions of the state, inputs, and outputs (Biegler and Rawlings, 1991). Nonlinear models have no specific characteristics except that they do not include the linear case. This makes it difficult to generalise, since nonlinear models can be devised to have almost any characteristic or show any strange behaviour.

2.3.1. Model Algorithm Control, MAC

Also known as Model Predictive Heuristic Control, MHPC or IDCOM, an acronym for Identification and Command, was probably the first MPC control

application recorded. Presented by Richalet et al. at a 1976 conference and later summarized in a 1978 Automatica paper, the MAC principal features were:

- Discrete impulse response model for the plant, linear inputs or internal variables
- Quadratic performance objective function over a finite prediction horizon
- Future plant output behaviour specified by a reference trajectory
- Input and output constraints included in the formulation
- Optimal inputs computed using a heuristic iterative algorithm. Hence the "Heuristic Control" name.

The algorithm uses an impulse response model, which could be only implemented on an open-loop stable processes, and minimises the variance of the error between the output and the reference trajectory computed as a first order system. For a single input, single output (SISO) case the model looks like:

$$y_{k+j} = \sum_{i=1}^{N} h_i u_{k+j-i} \tag{2.1}$$

The model permits linear estimation, using least squares

2.3.2. Dynamic Matrix Control, DMC

Cutler and Ramaker, both engineers from Shell Oil, presented details of an unconstrained multivariable control algorithm which they named Dynamic Matrix Control (DMC), at the 1979 National AIChE meeting (C.R Cutler and B.L. Ramaker, 1979) and at the 1980 Joint Automatic Control Conference (C.R Cutler and B.L. Ramaker, 1980). The algorithm is similar to MAC but uses a step response model instead of an impulse response model. The key features of the DMC control algorithm includes:

- Linear discrete step response model for the plant
- Quadratic performance objective function over a finite prediction horizon
- Future plant output behaviour specified by trying to follow the set point as closely as possible
- Optimal input computed as the solution to a least-squares problem

The linear step response model used by the DMC algorithm relates changes in a process output to a weighted sum of past input changes, referred to as input moves. For the SISO case the step response model looks like:

$$y_{k+j} = \sum_{i=1}^{N-1} \delta_i \Delta u_{k+j-i} + \delta_N u_{k+j-N} \tag{2.2}$$

The initial MAC and DMC algorithms represent the first generation of MPC technology; they had an enormous impact on industrial process control and served to define the industrial MPC paradigm.

2.3.3. Quadratic Dynamic Matrix Control, QDMC

In order to overcome constraints and limitations, a second generation of MPC was developed in the form of quadratic dynamic matrix control (QDMC). Firstly described by Cutler et al. in a 1983 AIChE conference paper, and later described more comprehensively by Garcia and Morshedi, (QDMC; 1986). Some of the features of the QDMC indlude:

- Linear step response model for the plant
- Quadratic performance objective function over a finite prediction horizon
- Future plant output behaviour specified by trying to follow the set point as closely as possible
- Optimal input computed as the solution to a quadratic program

Extended Prediction Self Adaptive Control, EPSAC (De Keyser and Van Cauwenberghe, 1985) uses a discrete (z-transform) transfer function to model the process and a simple control law structure calculated analytically using a quadratic performance function assuming *u(t)* stays constant from instant *t*. The process model also includes measurable disturbances.

The third generation of MPC technology was presented about a decade ago, "distinguishes between several levels of constraints (hard, soft, ranked), provides some mechanism to recover from an infeasible solution, addresses the issues resulting from a control structure that changes in real time and allows for a wider range of process dynamics and controller specifications" (Qin & Badwell, 1997). Specifically, the Shell multivariable optimising control (SMOC) algorithm allows for state-space models, and state estimation via Kalman filtering (Marquis & Broustail, 1998). The subsequent evolution of commercial MPC, is well described in the last reference.

2.4. Nonlinear Model Predictive Control (NMPC)

Due to the complexity of nonlinear systems, it is not possible to develop nonlinear identification techniques by straightforward extension of the linear theory (Pearson and Ogunnaike, 1997). As an alternative, the NMPC controller may be based either on a fundamental model that is derived from either basic conservation laws or an empirical model. Hybrid nonlinear models, which are developed by a combination of the fundamental and empirical modelling approach, can also be used.

Fundamental dynamic models are derived by applying transient mass, energy and momentum balances to the process. The resulting models have the general form (Ogunnaike and Ray, 1994).

$$f\left(t, x(t), \dot{x}(t), u(t), v(t), \theta\right) = 0 \tag{2.3}$$

Subject to the following constraints

$$\underline{g} \le g\left(t, x(t), \dot{x}(t), u(t), v(t), \theta\right) \le \overline{g} \tag{2.4}$$

Where $x(t)$ is a vector of state variables, $u(t)$ are controlled inputs, $v(t)$ are the uncontrolled inputs and θ the unknown parameters.

Fundamental models have several advantages as compared to empirical models. Because fundamental models are highly constrained with respect to their structure and parameters, less process data is required for their development. Model parameters may often be estimated from laboratory experiments instead of performing time-consuming plant tests.

Another advantage is that fundamental models can be expected to extrapolate to operating regions which are not represented in the data set used for model development (Meadows and Rawlings, 1997). This property is particularly important when a process operates over a wide range of conditions. However one of the major disadvantages of the fundamental modelling approach is that the resulting dynamic model may be too complex to be useful for a NMPC design.

Once a suitable model is developed and used for NMPC design, long-term maintenance is required. Otherwise, the NMPC controller will not be used because the model will fail to provide satisfactory predictions as the plant is modified and/or operating conditions are changed.

2.4.1. Nonlinear Optimal Control Formulation

The NMPC is based on the following optimal control problem

$$\min_{u(t)} J\left(t, x(t_f), \dot{x}(t_f), u(t_f), v(t_f), \theta\right) \tag{2.5}$$

Subject to $f\left(t, x(t), \dot{x}(t), u(t), v(t), \theta(t)\right) = 0 \qquad t \in [t_0, t_f]$

$\underline{g} \le g\left(t, x(t), \dot{x}(t), u(t), v(t), \theta(t)\right) \le \overline{g} \qquad t \in [t_0, t_f]$

with initial conditions $x(t_0) = x_0$

and could include end-point constraints such as $x(t_f) = 0$ (2.6)

where

J - objective function

$x(t)$ - vector of state variables

$u(t)$ – vector of time varying control

θ – vector of parameters

f – vector of model equation

g – vector of mixed state and control inequality constraints

$\underline{g}, \overline{g}$ - vector of lower and upper bounds of control

t – time

$[t_0, t_f]$ – time interval of interest (horizon)

The solution of the optimal control problem is an admissible set of controls, given the initial state, and possibly the final time, to minimise J, subject to the conditions above. A final-time objective function covers the case of an integral of performance over the time-interval.

2.5. MPC Stability

NMPC is a nonlinear open-loop optimal control technique where feedback is incorporated via the receding horizon formulation and the disturbance estimator. It is an interesting fact that NMPC can stabilise systems, which cannot be asymptotically stabilised with continuous feedback (Meadows, Henson, Eaton and Rawlings, 1995). However, "optimality does not imply stability" (Kalman, 1960).

Until recently it was not clear under what conditions the closed loop system was stable for either the infinite or the finite horizon constraint case (Morari & Lee, 1999), thus motivating an important group of researchers to prove stability for specific cases and systems, but without obtaining a unified theory.

The primary tool for NMPC stability analysis is Lyapunov theory (Khalil, 1992). This tool was neglected for a long time until late 80's with the exception of Chen and Shaw (1982), who showed that continuous time optimal receding horizon control of unconstrained systems are stable when a terminal equality constraint is implemented, using the value function as Lyapunov function.

In recent times, after compiling results from the extensive literature, Mayne, et al., (2000) plainly presented a final set of four conditions, which ensure closed-loop asymptotic (exponential) stability on model predictive control. These conditions are stated below.

1. $X_f \subset X$, X_f closed, $0 \in X_f$ (state constraint satisfied in X_f).
2. $\kappa_f(x) \in U$, $\forall x \in X_f$ (Control constraint satisfied in X_f).
3. $f(x, \kappa_f(x)) \in X_f$, $\forall x \in X_f$ (X_f is positively invariant under $\kappa_f(\cdot)$).
4. $[F + l](x, \kappa_f(x)) \leq 0$, $\forall x \in X_f$ ($F(\cdot)$ is a local Lyapunov function)

Although the previous axioms must apply for all cases, those conditions can very rarely be verified in practice.

The terminal cost and constraint set is the version attracting most attention in current research literature. This variant of model predictive control employs both a terminal cost $F(\cdot)$ and a terminal constraint $x(N) \in X_f$ in the optimal control problem with the idea to drive the state to X_f in finite time. Several authors have studied this case (Michalska and Mayne (1993), Chisci et al. (1996) and Scokaert et al. (1999))

"In fact stability problems can usually be avoided by requiring that all controls are restricted to a closed, bounded set. Stability then becomes a controllability problem, and in the majority of cases controls can be devised so that the differential-algebraic equations generating the state variables have uniformly bounded solutions" (Disli, 1996)

2.6. State Variables and Parameter Estimation

The process of observation is the basis of any control system; therefore an important part in the complete MPC algorithm is the state variables and parameter estimation algorithm.

Normally due to the reduced number of measurable properties, many of the variables required to initialise the mathematical model must be obtained indirectly using mathematical correlations or heuristic rules employing the measurements available from the plant.

Several techniques to estimate either state variables or uncertain parameters are discussed in the next section. Basically all estimation algorithms use the same argument, the essential idea is to compare the observed system response with the output of a parameterised model over some interval of time. The parameter values are normally estimated by minimizing an error cost function or any other optimal function; typical choices might be the integral square error.

$$\theta = \min \int_0^t [y(t) - \hat{y}(t,\theta)]^2 \, dt \tag{2.7}$$

2.6.1. Luenberger observer

The Luenberger observer is a deterministic estimator that is employed when the stochastic model of the process is unknown or if the optimal filter exhibits poor performance.

This type of estimator is employed to reduce the computational requirements, making it appealing for online implementations. The estimation is carried out using the process model, given initial estimates of the state variables and input variables.

For modern chemical process control applications, computational time is generally not an issue with linear systems except in large-scale applications. However, Luenberger observers are less robust due to measurement and process noise (Ray, 1989)

Further discussion of observers for linear systems can be found in Kwakernaak and Silvan, and Kailath (Chapter 6, Model Predictive Control, "Nonlinear state estimator")

2.6.2. Kalman Filters

In 1960, R.E. Kalman published his famous paper describing a recursive solution to the discrete-data linear filtering problem. Since that time, due in large part to advances in digital computing, the Kalman filter has been the subject of extensive research and application, particularly in the area of autonomous or assisted navigation.

The Kalman filter is a set of mathematical equations that provides an efficient computational (recursive) solution of the least-squares method. The filter is very powerful in several aspects: it supports estimations of past, present, and even future states, and it can do so even when the precise nature of the modelled system is unknown.

2.6.2.1 Linear Kalman Filter, KF

The Kalman filter gives a linear, unbiased, and minimum error variance recursive algorithm to optimally estimate the unknown state of a linear dynamic system from noisy data taken at discrete real-time intervals.

The linear Kalman filter is based on a linear process model as shown below.

$$\frac{dx(t)}{dt} = F(t)x(t) + G(t)w(t)$$
$$y_k = H(t)x(t) + v(t) \tag{2.8}$$

in which F, G, H are $n\times n$, $n\times m$ and $n\times p$ respectively. The processes $w(\cdot)$ and $v(\cdot)$ define zero mean white noise.

$$E[w] = E[v] = 0 \tag{2.9}$$

$$E\left[w(t)w^T(\tau)\right] = Q(t)\delta(t-\tau) \tag{2.10}$$

$$E\left[v(t)v^T(\tau)\right] = R(t)\delta(t-\tau) \tag{2.11}$$

In the first instance, $x(t_0)$ will be assumed to be a Gaussian variable, of mean x_0 and covariance P_0. The propagation of the state variables is done by integrating the linear model (2.8) for the estimated state and an associated equation for the covariance matrix:

$$\begin{aligned} \dot{x}(t) &= F(t)x(t) \\ \dot{P}(t) &= P(t)F(t)^T + F(t)P(t) + G(t)Q(t)G(t)^T \end{aligned} \tag{2.12}$$

The measurement update is obtained using the following equations

$$K(t) = P^-(t)H(t)(H(t)P^-(t)H(t) + V(t)R(t)V(t))^{-1} \tag{2.13}$$

$$x^+(t) = x^-(t) + K(t)(y(t) - H(t)x^-(t)) \tag{2.14}$$

$$P^+(t) = (I - K(t)H(t))P^-(t) \tag{2.15}$$

where x^+ and P^+ are the corrected estimations of the state variables and the covariance matrix respectively using the current measurements while K is known as the Kalman gain. The algorithm is repeated and corrected every time a new set of measurements is received from the process.

2.6.2.2 Extended Kalman Filter, EKF

The EKF computes the optimal state estimate at each time instant using a linearized model of the nonlinear system and linear equation principles. For the case of sampled data measurements of a continuous process, a hybrid EFK is the most

appropriate. It uses the continuous-time model of the process and discrete observation for update.

Consider a nonlinear system shown below:

$$\dot{x} = f[x(t), u(t), t, \theta(t)] + w(t) \tag{2.16}$$

$$z(t) = h[x(t), u(t), t] + v(t) \tag{2.17}$$

where $u(t)$ denotes the deterministic inputs, $\theta(t)$ denotes the model parameters, and $w(t)$ represents a vector that defines how the process noise affects the state derivatives. The process noise vector, $w(t)$, is assumed to be a Gaussian random process with zero mean and covariance $Q(t)$:

$$E[w] = 0 \tag{2.18}$$

$$E[w(t)w^T(\tau)] = Q(t)\delta(t-\tau) \tag{2.19}$$

The measurement error $v(t)$, is also assumed to be a Gaussian random process, with

$$E[v] = 0 \tag{2.20}$$

$$E[v(t)v^T(\tau)] = R(t)\delta(t-\tau) \tag{2.21}$$

In the above equations, $Q(t)$ is the spectral density covariance matrix of $w(t)$, and $R(t)$ is the covariance matrix of the noise $v(t)$. Furthermore, the symmetric matrices $P(0)$ and $Q(t)$ must be positive semidefinite, while the symmetric matrix $R(t)$ must be positive definite.

The EKF formulation uses linearized models of the nonlinear system for state estimation. The nonlinear extended Kalman filter requires that the matrix F, which consists of the partial derivative of equation 2.14 with respect to each state variable, be evaluated at the current state. That is,

$$F(t,\hat{x}(t)) = \left.\frac{\partial f(x,t)}{\partial x}\right|_{x=\hat{x}(t)} \tag{2.22}$$

Then $f[x(t),t]$ can be expanded in a Taylor series about $x(t) = \hat{x}(t)$, thereby obtaining a set of linear equations in $x(t)$. Thus, for the nonlinear diferential equation

$$\dot{x} = f[x(t),t], \qquad x(t_0) = x_0 \tag{2.23}$$

we have

$$\dot{x} = f[x(t),t] = f[\hat{x}(t),t] + \left.\frac{\partial f[x(t),t]}{\partial x(t)}\right|_{x(t)=\hat{x}(t)} [x(t) - \hat{x}(t)] + \cdots \tag{2.24}$$

The same procedure applies for the observation model. The EKF recalculates the elements of the matrices F and H during each update and propagation cycle by evaluating the partial derivatives of the vector function f and h:

$$F(t,\hat{x}(t)) = \left.\frac{\partial f[x,t]}{\partial x}\right|_{x=\hat{x}(t_i^-)} = \left.\begin{bmatrix} \frac{\partial f_1(x)}{\partial x_1} & \cdots & \frac{\partial f_1(x)}{\partial x_n} \\ \vdots & & \vdots \\ \frac{\partial f_n(x)}{\partial x_1} & \cdots & \frac{\partial f_n(x)}{\partial x_n} \end{bmatrix}\right|_{x=\hat{x}(t_i^-)} \tag{2.25}$$

$$H(t,\hat{x}(t)) = \left.\frac{\partial h[x,t]}{\partial x}\right|_{x=\hat{x}(t_i^-)} = \left.\begin{bmatrix} \frac{\partial h_1(x)}{\partial x_1} & \cdots & \frac{\partial h_1(x)}{\partial x_n} \\ \vdots & & \vdots \\ \frac{\partial h_m(x)}{\partial x_1} & \cdots & \frac{\partial h_m(x)}{\partial x_n} \end{bmatrix}\right|_{x=\hat{x}(t_i^-)} \tag{2.26}$$

The propagation of the state and the state covariances is achieved by integrating the nonlinear model equation and the covariance propagation equations into the next time step. The Kalman gain is then computed. The measurement update equations are the used to estimate the state and the covariance updates. The equations that compose the different steps in the EKF are given below.

State Propagation Equation:

$$\frac{d}{dt}(x(t)) = f(x(t), u(t)) \tag{2.27}$$

Covariance Propagation Equation

$$\frac{d}{dt}(P(t)) = F(t)P(t) + P(t)F(t)^T + G(t)Q(t)G(t) \tag{2.28}$$

Kalman Gain Equation:

$$K = P^- H^T \left[H \; P^- H^T + R\right]^{-1} \tag{2.29}$$

State Update Equation

$$x^+ = x^- + K \left[z - h(x^-, t)\right] \tag{2.30}$$

Covariance Update Equation

$$P^+ = \left[I - KH\right]P^- \tag{2.31}$$

Estimation of parameters as well as states can be included by treating then as time-invariant states $\dot{\theta} = 0$

The main disadvantage of the EKF is that the covariances are determined by linearizing the dynamic equations ($x \approx Ax + Bu, y \approx Cx + Dn$), and then determining the posterior covariance matrices analytically for the linear system. As such, the EKF can be viewed as providing "first-order" approximations to the optimal terms (in the sense that expressions are approximated using a first-order Taylor series expansion of the nonlinear terms around the mean values). While "second-order" versions of the EKF exist, their increased implementation and computational complexity tend to prohibit their use.

Chapter 3

Pilot Plant Modelling

3.1. Plant Description

The process operating on the pilot plant is an important part of the conventional ammonia synthesis plant. The diagram of the pilot plant is shown in Figure 3.1. A mixed feed of carbon dioxide and nitrogen enter a packed absorption column where the CO_2 is separated from the nitrogen by contact with a solution of monoethanolamine (MEA). The absorption process occurs when carbon dioxide is absorbed chemically by the MEA solution. The column operates under pressure ($\approx$ 200 kPa). The liquid flow leaving the bottom of the absorption column is the MEA solution rich in carbon dioxide. This solution passes to the desorption column where the carbon dioxide is stripped from the solution at atmospheric pressure. Before entering the column the solution, rich in CO_2, is heated by the hot stream solution leaving the desorption column. The desorption column consists of eighteen sieve trays and a natural circulation reboiler to supply the stripping energy. Steam is the heating medium. The reboiler provides the heat needed by the desorption process. The desorption regenerates the monoethanolamine solution, which is used in a closed loop.

The lean MEA from the bottom of the stripping column, besides exchanging heat with the carbon dioxide rich MEA, is water cooled before entering the absorption column to complete the circulation loop. In an industrial plant, the carbon dioxide stripped from the MEA is normally sent to further gas processing equipment. In this pilot plant it can either be recycled and mixed with nitrogen that leaves the top of the absorption column to form the process feed or rejected.

The two main processes will be described together with condenser, reboiler, heat exchanger and cooler, delays, valves, level controller and mixers. The equations of the

model are translated into the language of the dynamic simulator (gPROMS), a software developed by the Centre for Process Systems Engineering at Imperial College, for analysis of the process and process control.

The pilot plant is linked to an on-line PC-based computing system which is used for logging and control purposes. The computer can be linked to a Unix SPARC workstation which can run programmes simultaneously, so that on-line control algorithms and strategies, simulation, estimation and optimisation can be performed.

The typical problem for this plant is to control the concentration of carbon dioxide in the gas leaving the absorption column in face of disturbances in the inlet concentration of CO_2 or inlet gas flow rate. The cost of operation of such an industrial plant is dominated by the cost of the stripping steam employed, and there is, therefore, the problem of how to control the unit to minimise energy consumption. The absorption depends upon how effectively the desorption process is carried out; the smaller the amount of CO_2 in the lean MEA, the better the absorption process will be, and the solvent circulation rate and steam flow rate must be adjusted to obtain the optimal concentration of carbon dioxide in the lean MEA solution.

The absorber, desorber and reboiler can be considered the principal components on the pilot plant. Since almost all process behaviour depends on these units, the next section will explain in more detail the criteria and assumptions made in order to obtain a mathematical representation.

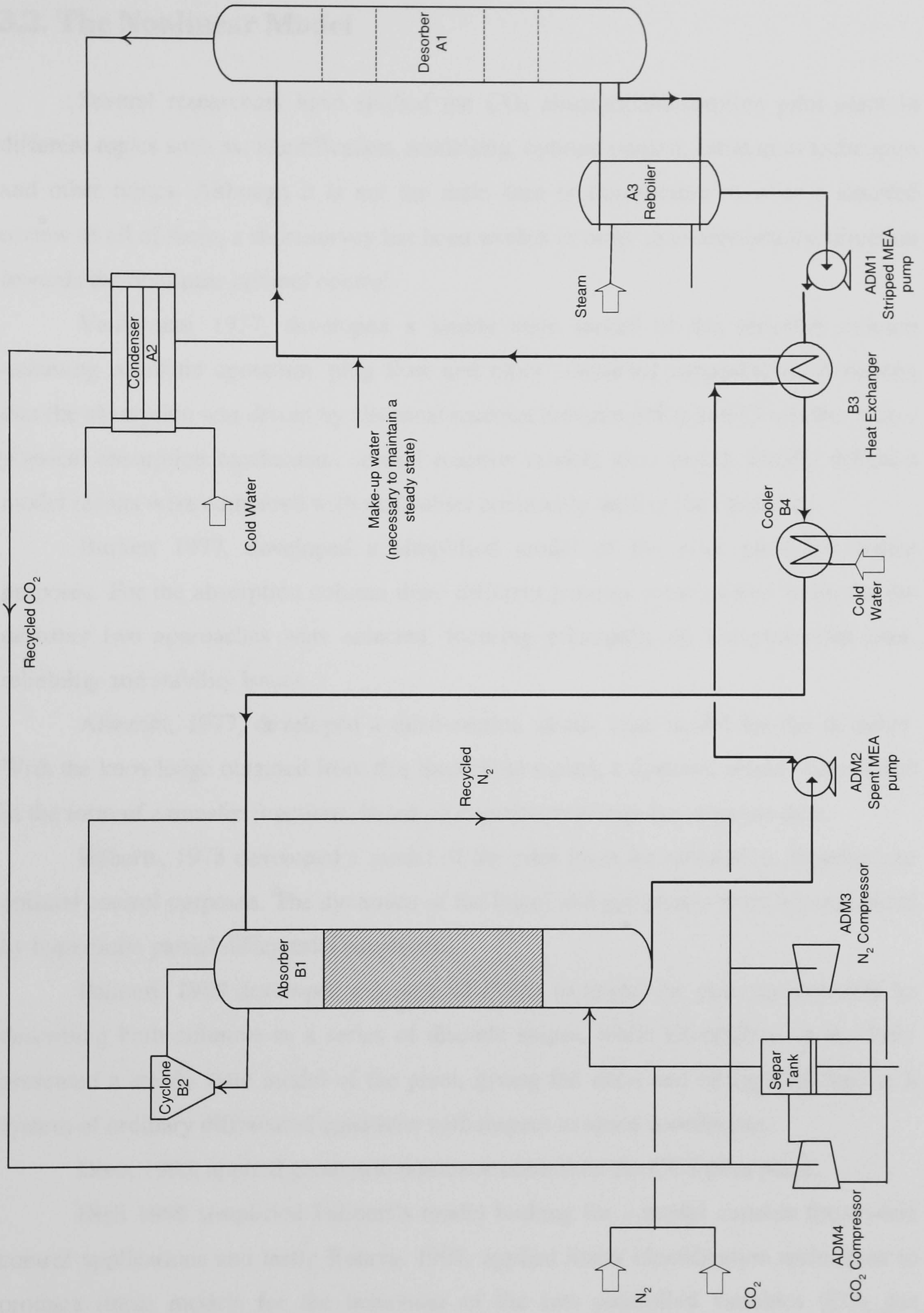


Figure 3.1. Absorption/desorption pilot plant diagram

3.2. The Nonlinear Model

Several researchers have studied the CO_2 absorption/desorption pilot plant in different topics such as: identification, modelling, optimal control, estimation techniques and other topics. Although it is not the main idea of this section to write a detailed review of all of them, a short survey has been written in order to understand the direction towards the nonlinear optimal control.

Vanichseni 1977, developed a steady state model of the absorber column assuming adiabatic operation, plug flow and other simplified suppositions. Assuming that the absorption was driven by chemical reaction between MEA and CO_2 rather than a physical absorption mechanism, several reaction models were tested. Finally different model results were compared with real values commonly used in the literature.

Burkett 1977, developed a simplified model of the pilot plant for online purposes. For the absorption column three different patterns were studied while for the desorber two approaches were selected, focusing principally on computational time, reliability and stability issues.

Albrecht, 1977, developed a three-section steady state model for the desorber. With the knowledge obtained from this theoretical model, a dynamic model was created in the form of z transfer functions, based on experimental impulse response data.

Roberts, 1978 developed a model of the pilot plant for simulation, filtering and optimal control purposes. The dynamics of the liquid and gas phases were approximated by hyperbolic partial differential equations.

Paliouri, 1989 developed a system of DAEs to model the plant dynamically by describing both columns in a series of discrete stages, while Escobillana et al., 1991 presented a steady state model of the plant, giving the mass and energy balances as a system of ordinary differential equations with respect to space coordinates.

Dore, 1993, applied geometric nonlinear control on the CO2 pilot plant.

Disli 1996 simplified Paliouri's model looking for a model suitable for on-line control applications and lastly Rotava, 1997, applied linear identification techniques to produce linear models for the behaviour of the two controlled variables (CO_2 gas concentration and reboiler liquid pH) from a set of experimental data. Once the linear model was generated, a DMC was implemented, minimizing energy costs and penalizing

controlled variables changes. Also, using Disli's approach, he developed a complete nonlinear model of the pilot plant for MPC purposes, but although the controller worked well under constrained conditions, the robustness and stability of the system was not fully proved.

3.3. Process Model

Ideal solutions are assumed (ie. no heats of mixing), so gas and liquid enthalpies can be defined as:

$$H_{IS} = \sum H_i y_i \,, \quad h_{IS} = \sum h_i x_i \tag{3.1}$$

Where H_i and h_i are the gas and liquid enthalpies of pure component i respectively. Then assuming constant component specific heats (C_{Li}, C_{gi} liquid and gas respectively) enthalpies can be approximated as:

$$h_i = C_{Li}(T - T_{ref}) \tag{3.2}$$

$$H_i = C_{Li}(T^* - T_{ref}) + \Delta H_i + C_{gi}(T - T^*) \tag{3.3}$$

Where T^* is the boiling point of the component i at the given pressure (P) and ΔH_i is the difference in enthalpy between gas and liquid at T^* (Since the liquid is mainly water, we can further take $C_{Li} \approx C_{Lw}$). If the phases are in equilibrium, we further assume ideal gases, and hence can use Raoult's law:

$$P_{y,i} = P_i^* x_i \tag{3.4}$$

where P_i^* is the vapour pressure of component i at T^* (given by the Antoine equation)

We can further simplify by assuming that MEA is non-volatile ($y_m = 0$) and nitrogen is insoluble ($x_n = 0$), so that nitrogen is present only in the absorber and its feed-tank, and MEA is not present in the condenser (in fact we can also neglect the solubility of CO_2 in the condenser without significant error)

Finally, by definition we have

$$\sum y_i = \sum x_i = 1 \tag{3.5}$$

Next we assume constant liquid hold-up in absorber and desorber stages and neglect vapour hold-up throughout.

Lastly we assume pseudo-first order reaction between CO_2 and MEA in the absorber, but reaction equilibrium in the desorber and reboiler.

3.3.1. Absorber Column Model

Modelling a CO_2 and MEA absorption system has been presented in several sources in the literature. Burkett, (1977) compared a plug flow model, a dispersion model and mixing cell model as descriptions for the absorber. Liquid phase dispersion is negligible and Burkett, (1977) concluded that plug flow representation is suitable for normal conditions. For this column, Burkett suggested 200 cells would be required in the mixing cell model to match the dispersion characteristics.

The large number of mixing cells suggested by Burkett is unsuitable for on-line control. Disli's (1996) mixing cell model of the absorption column is convenient since one of the aims of this project is to express the process (absorption-desorption pilot plant) as a system of differential algebraic equations (DAE) to be solved in a DAE solver environment (gOPT). The approach to the dynamics of the absorber proposed by Disli limits the number of cells to a few.

Each cell of the model is of fixed volume and is made up of two phases: a liquid and a gas phase. It is assumed that the two phases are at the same temperature while the pressure is constant throughout the column. None of the N_2 is absorbed into the liquid

stream and the MEA is considered non-volatile. Hold up is constant for the liquid phase. This is justified considering that the composition dynamics is much slower than liquid flow dynamics. Gas phase hold up is negligible. The following assumptions are made (Disli, 1996)

- The absorption column is adiabatic;
- There is no pressure drop along the absorption column;
- There are no radial temperature or composition gradients;
- The physical properties are constant throughout the column;

The absorption column will be represented by n_a sections or stages. Figure 3.2 shows the nomenclature used in the derivation of the equations of the model for a generic stage j. Let x be the liquid phase mole fraction (C the molar liquid phase concentration) and y the gas phase mole fraction. U is the molar liquid hold-up and V the molar gas hold-up.

The key for the nomenclature is as follows: for pure component properties, the first subscript identifies the component: n = N_2, c = CO_2, w = H_2O, m = MEA; the second subscript identifies l = liquid phase and g = gas phase. For quantities which describe properties of a process unit, a third subscript identifies the unit: a = absorber, d = desorber, c = condenser. Units not described by stages do not have the second subscript.

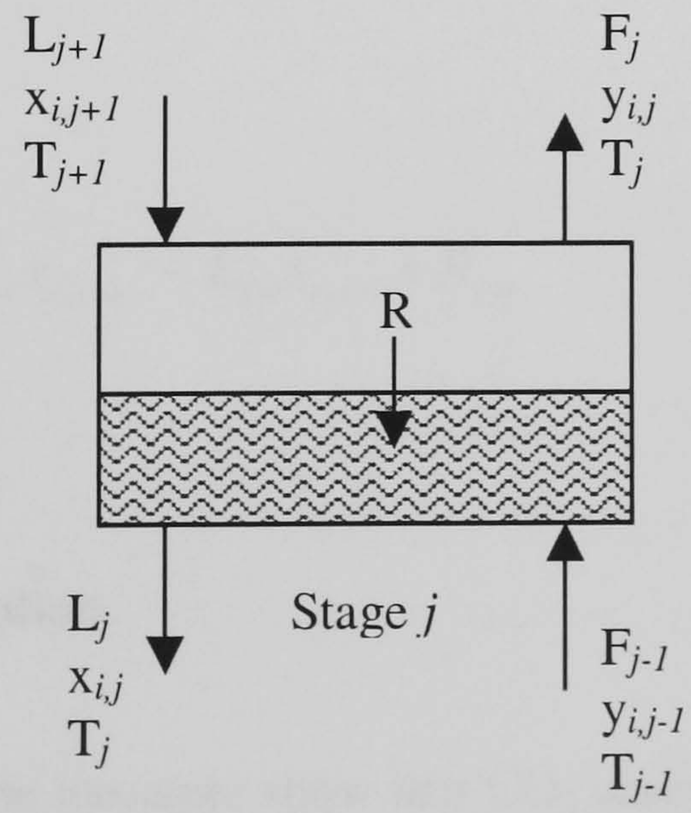


Figure 3.2 Lumped representation for an absorber stage

BIBL. LONDIN. UNIV.

The overall molar balance for stage j becomes

$$L_{j+1,a} + F_{j-1,a} - L_{j,a} - F_{j,a} = 0 \tag{3.6}$$

while the nitrogen, carbon dioxide and water gas molar balances are obtained by

$$F_{j-1,a} y_{n,j-1,a} - F_{j,a} y_{n,j,a} = 0 \tag{3.7}$$

$$F_{j-1,a} y_{c,j-1,a} - F_{j,a} y_{c,j,a} - R_{j,a} = 0 \tag{3.8}$$

$$\sum_i y_{i,j,a} = 1 \tag{3.9}$$

where $R_{j,a}$ is the rate of absorption of CO_2. If $R_{j,a}$ is positive this represents absorption, on the contrary if $R_{j,a}$ is negative it represents desorption.

Combination of Raoult's law and the Antoine equation for the saturation pressure of water produces the mol fraction of the water in the gas phase.

$$y_{w,j,a} = \frac{e^{\left(A_w - \frac{B_w}{C_w + T_{j,a}}\right)} \cdot x_w}{P_a} \tag{3.10}$$

The carbon dioxide molar balance in the liquid phase is represented by the following equation.

$$U_{j,a}\left(\frac{dx_{c,j,a}}{dt}\right) = L_{j+1,a} x_{c,j+1,a} - L_{j,a} x_{c,j,a} + R_{j,a} \tag{3.11}$$

3.3.1.1 Rate of CO_2 absorption

Several sources in the literature show that CO_2 absorption in amine solutions is a chemical reaction phenomenon rather than a physical absorption process. The

development of a local transfer flux equation was considered by Burkett (1977) and then used by Disli (1996). A complete description of the following equations can be found in Rotava (1997). The most important assumptions considered in this transfer model are.

- The chemical reaction is pseudo first order.
- Low gas resistance to diffusion of the CO_2.
- Reaction rate is smaller than diffusion rate.

The following equation results from integration of plug flow over the height of the cell.

$$R_{j,a} = F_{j-1,a}\, y_{c,j-1,a}\left(1 - e^{-\eta_{j,a}}\right) \tag{3.12}$$

where

$$\eta_{j,a} = \frac{h_t a_i A_a P_{j,a}}{F_{j,a} H} \sqrt{D_c k_r (C_{mea} - 2C_{c,j,a})} \tag{3.13}$$

The column is assumed to work under adiabatic conditions, the energy balance for stage j of the absorber becomes.

$$U_{j,a} \frac{dh_{j,a}}{dt} = L_{j+1,a} h_{j+1,a} + F_{j-1,a} H_{j-1,a} - L_{j,a} h_{j,a} + F_{j,a} H_{j,a} + R_{j,a} \Delta H_r \tag{3.14}$$

The previous formulation represents a set of 13 equations for 13 variables in each stage ($T_{j.a}$, $F_{j.a}$, $L_{j.a}$, $y_{c,j.a}$, $y_{w,j.a}$, $y_{n,j.a}$, $x_{c,j.a}$, $R_{j.a}$, $\eta_{j.a}$, $h_{j.a}$, $H_{j.a}$, $C_{p_{l,j.a}}$, $C_{p_{g,j.a}}$); therefore a complete model for the absorber is obtained. It is important to notice that 2 of the variables are differential equations; consequently two initial values are required per stage, the temperature $T_{j.a}$ and the CO_2 liquid concentration $x_{c,j.a}$.

3.3.2. Absorber Gas Feed Model

The gas feed flow injected at the bottom of the absorber is a mixture of CO_2 and N_2 that comes from either fresh sources or recycled streams from the desorber's top and absorber's top respectively.

In order to simplify the model, the feeder assumes that all gas feed comes from fresh supplies and are mixed isothermally at a given temperature and instantaneously. Hence, no dynamics are included in the model.

According to Disli (1996), the nitrogen and carbon dioxide streams are pure. However, they pass through the separation tank, which is filled with water and depending on the temperature and saturation point, the gas feeding the absorber will contain a fraction of this component.

Figure 3.3 shows the nomenclature used in the model and the equations extracted from the assumptions above.

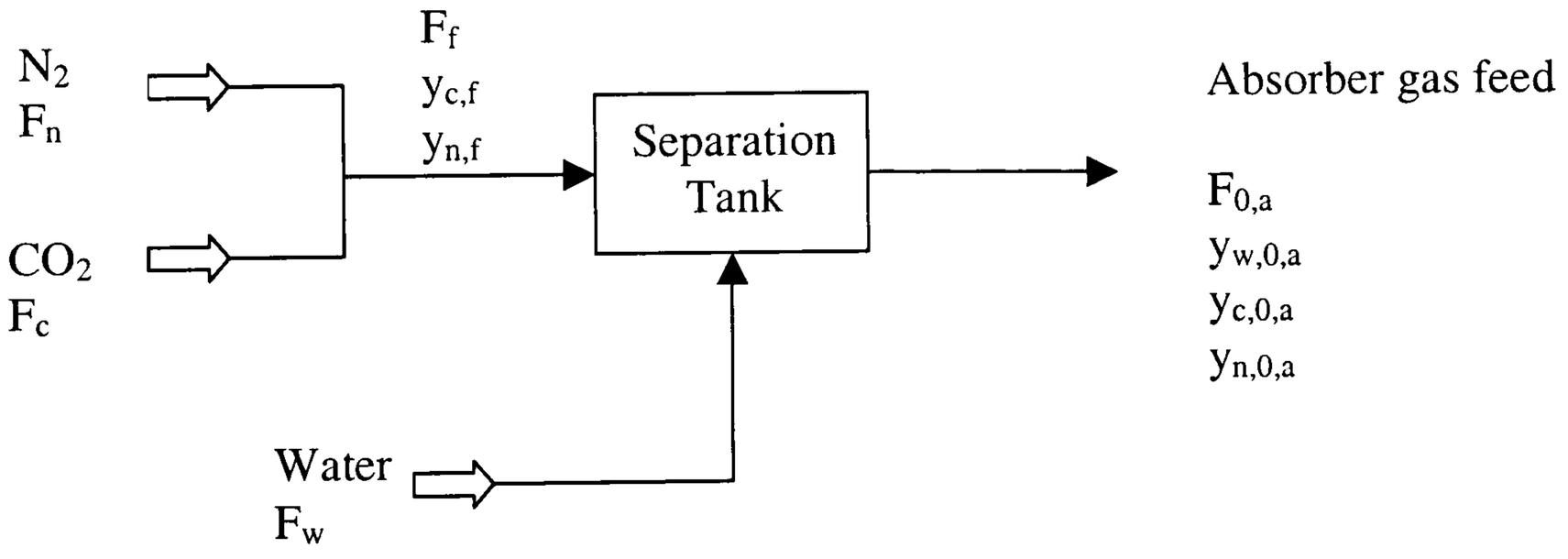


Figure 3.3. Absorber gas feed model

The overall molar balance is expressed as

$$F_n + F_c = F_f \tag{3.15}$$

$$F_f + F_w = F_{0,a} \tag{3.16}$$

Nitrogen, carbon dioxide and water molar balances

$$F_n = F_f \cdot y_{n,f} = F_{0,a} \cdot y_{n,0,a} \tag{3.17}$$

$$F_c = F_f \cdot y_{c,f} = F_{0,a} \cdot y_{c,0,a} \tag{3.18}$$

$$F_w = F_{0,a} \cdot y_{w,0,a} \tag{3.19}$$

$$y_{w,0,a} = \frac{e^{\left(A_w - \frac{B_w}{C_w + T_g}\right)} \cdot x_w}{P_f} \tag{3.20}$$

and molar fraction balances.

$$\sum_i y_{i,f} = \sum_i y_{i,0,a} = 1 \tag{3.21}$$

From this set of equations the following process inputs are known $y_{c,f}$, F_n, T_g and P_f, as well as the parameters A_w, B_w, C_w and x_w. Therefore, 8 unknown variables are accordingly expressed by 8 equations. No further specifications are required.

3.3.3. Desorber Column Model

The desorption section of the pilot plant receives aqueous MEA solution from the absorption column, which is the MEA solution rich in CO_2. The energy for the separation of the CO_2 from the liquid solution is supplied by saturated steam at approximately 140 kPa in the reboiler. The MEA rich solution in the reboiler circulates by free convection. The boiling liquid inside the reboiler forms water vapour, which passes up the unit carrying heat throughout the column.

The condenser condenses the water vapour coming from the top tray of the desorber to avoid loss water and, therefore, changes in the concentration of the MEA. Any liquid MEA carried by the vapour stream is also recovered. The condensate is returned to the desorber mixed with the feed.

The dynamic model of the plant considered here is described in works of Burkett, (1977), Disli (1996), and Dore, (1993). The modelling of the desorption column, reboiler, and condenser will be considered in the following sections and includes relevant details from these works.

According to the references above, the reversible reaction for the decomposition of carbonate to CO_2 is assumed to be instantaneous. Consequently, resistance due to the chemical kinetics is zero. The equilibrium relationship for the partial pressure of CO_2 over MEA solution as a function of the gas temperature and the liquid carbonation ratio developed by Burkett, (1977) is used in the model. The desorber is represented in terms of equivalent ideal stages.

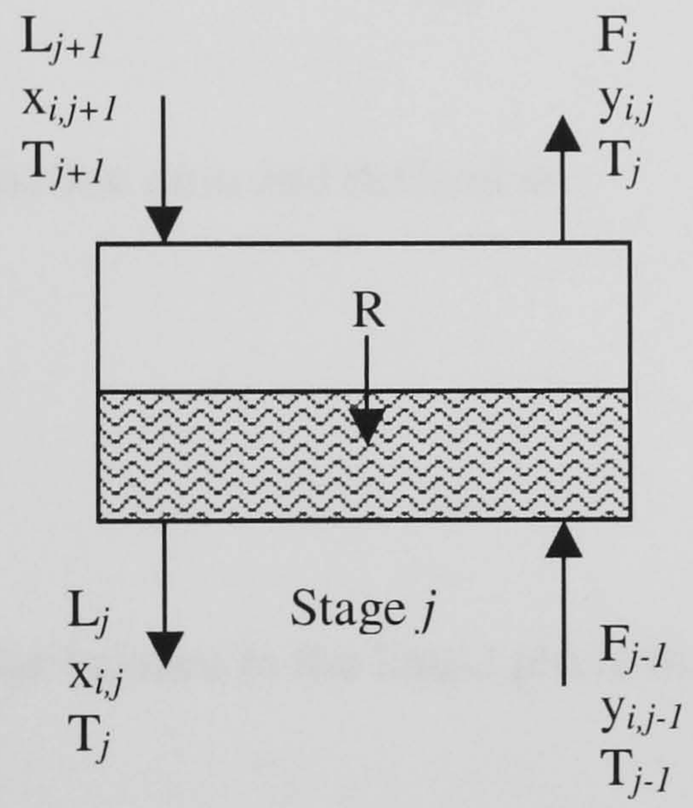


Figure 3.4 Lumped representation for a desorber stage

The whole column is represented by N_d such stages. Figure 3.2 shows the nomenclature to be used in the derivation of the equations of the model for stage j.

The overall molar balance for stage j becomes

$$L_{j+1,d} + F_{j-1,d} - L_{j,d} - F_{j,d} = 0 \tag{3.22}$$

While gas molar balance is simply expressed as

$$\sum_i y_{i,j,d} = 1 \tag{3.23}$$

while molar fractions for water and CO_2 are obtained using the following correlations

$$y_{w,j,d} = \frac{e^{\left(A_w - \frac{B_w}{C_w + T_{j,d}}\right)} \cdot x_w}{P_{j,d}} \tag{3.24}$$

$$y_{c,j,d} \cdot P_{j,d} = \frac{e^{\left((-47.91+112.8\alpha_{j,d})+(0.7615+1.668\alpha_{j,d})T_{j,d}+(-0.0029+0.007\alpha_{j,d})T_{j,d}^{\,2}\right)}}{760} \tag{3.25}$$

where $\alpha_{j,d}$ is the carbonation ratio and defined as

$$\alpha_{j,d} = \frac{x_{c,j,d}}{x_{mea}}$$

The carbon dioxide molar balance in the liquid phase in terms of concentration is

$$U_{j,d}\left(\frac{dx_{c,j,d}}{dt}\right) = L_{j+1,d}x_{c,j+1,d} - L_{j,d}x_{c,j,d} - R_{j,d} \tag{3.26}$$

Under the assumptions stated before, the energy balance for stage j of the desorber becomes

$$0 = L_{j+1,d}h_{j+1,d} + F_{j-1,d}H_{j-1,d} - L_{j,d}h_{j,d} + F_{j,d}H_{j,d} + R_{j,d}\Delta H_r \tag{3.27}$$

where $$R_{j,d} = F_{j,d}y_{c,j,d} - F_{j-1,d}y_{c,j-1,d} \tag{3.28}$$

3.3.3.1 Pressure calculation

The pressure drop in the desorber is included simply to reduce the system to index one. The index is the minimum number of times the system must be differentiated with respect to time in order to yield a pure ODE system and is needed to avoid problems with the solver. Introducing a pressure drop depending on the flow rate avoids the imposition of the constraint that the pressure is the same for all plates, which otherwise has to be differentiated.

The pressure drop in a tray of a distillation column is given by Equation 3.29 (Luyben, 1990). The coefficients shown in the Equation 3.30 were experimentally obtained by Disli (1997).

$$\Delta P_{j,d} = N_{t,j}\left(\rho_{l,d}\, g\,(h_w + h_{ow}) + K_{dry}\, g \rho_{g,d} \upsilon_{g,r}{}^2\right) \tag{3.29}$$

$$P_{j,d} - P_{j+1,d} = N_{t,j}\left(4.993 \cdot 10^{-3} + 5.481 \cdot 10^{-6} \cdot \upsilon_{g,j,d}{}^2\right) \tag{3.30}$$

$$\upsilon_{g,j,d} = \left(\frac{M_g}{A_T \cdot \rho_{g,d}}\right) F_{j,d} = 1.1515 \cdot 10^4 F_{j,d} \tag{3.31}$$

where $N_{t.d}$ is the number of trays in the stage j to compensate for the lumped approximation.The pressure is expressed in [*atm*] and the velocity is given in [*m/s*].

The complete desorber stage model is represented by a set of 11 equations with the same amount of unknown variables ($T_{j.d}$, $F_{j.d}$, $L_{j.d}$, $y_{c,j.d}$, $y_{w,j.d}$, $x_{c,j.d}$, $\alpha_{j.d}$, $h_{j.d}$, $H_{j.d}$, $P_{j.d}$, $V_{g,j.d}$);. There is one differential equation so an initial condition $x_{c,j.d}$ is necessary to complete the model.

3.3.4. Reboiler Model

The reboiler is the main heat supplier of the whole system, and is modelled as an additional desorber equilibrium stage. Unlike the other desorber stages, the reboiler has a time dependent liquid hold up. However the vapour hold up can still be ignored. The remaining assumptions for the desorber column hold. Figure 3.5 shows a diagram with the streams and variables used in the model.

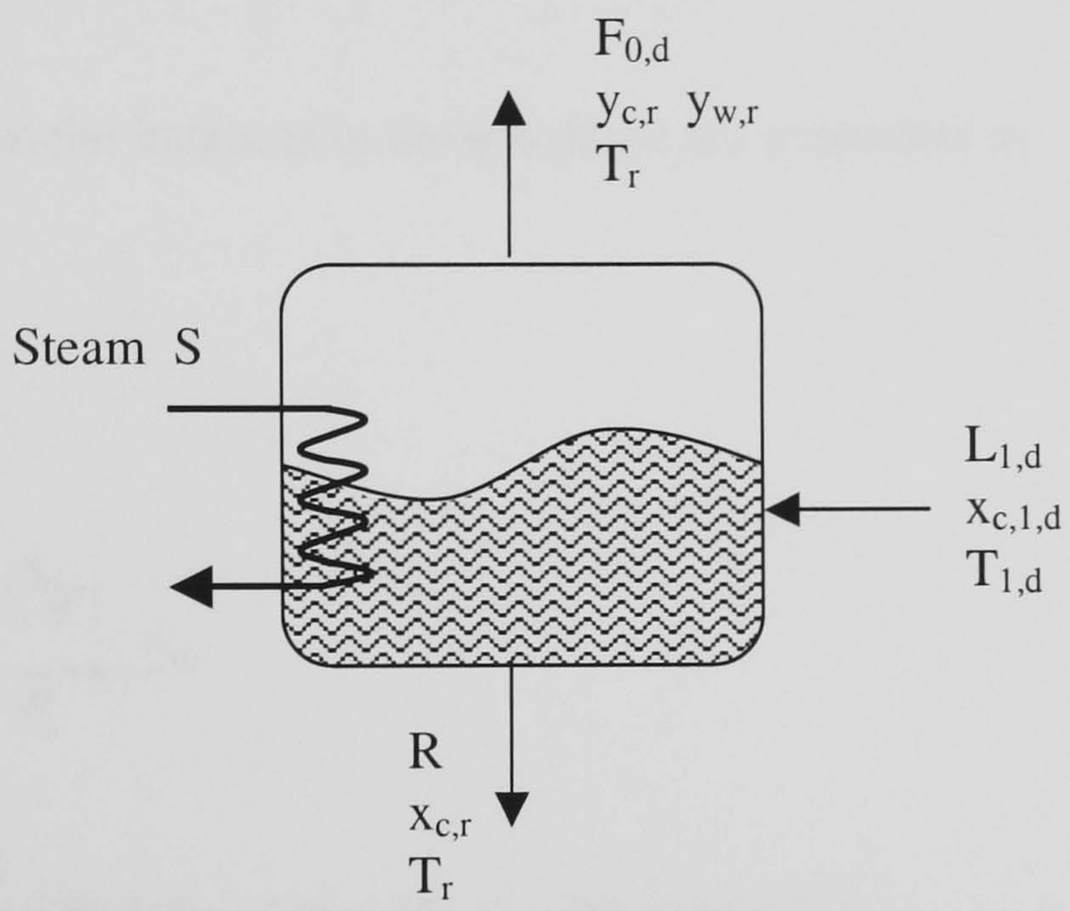


Figure 3.5. Reboiler diagram

The total balance in the reboiler becomes

$$\frac{dU_r}{dt} = L_{1,d} - R - F_{0,d} \tag{3.32}$$

which is more conveniently written in terms of the reboiler level as

$$\left(\frac{\rho_{l,r} A_r}{M_{l,r}}\right)\left(\frac{dz_r}{dt}\right) = L_{1,d} - R - F_{0,d} \tag{3.33}$$

The carbon dioxide molar balance in both phases is

$$\frac{d\left(U_r x_{c,r}\right)}{dt} = L_{1,d} x_{c,1,d} - R x_{c,r} - F_{0,d} y_{c,r} \tag{3.34}$$

By substituting equation 3.33 in the previous one the following equation is obtained

$$A_r z_r \frac{dx_{c,r}}{dt} = L_{1,d}\left(x_{c,1,d} - x_{c,r}\right) - F_{0,d}\left(y_{c,r} - x_{c,r}\right)$$

Component molar balances in the gas phase are expressed as

$$\sum_i y_{i,r} = 1 \tag{3.35}$$

$$y_{w,r} = \frac{e^{\left(A_w - \frac{B_w}{C_w + T_r}\right)} \cdot x_w}{P_r} \tag{3.36}$$

$$y_{c,r} \cdot P_r = \frac{e^{\left((-47.91+112.8\alpha_r)+(0.7615+1.668\alpha_r)T_r+(-0.0029+0.007\alpha_r)T_r^2\right)}}{760} \tag{3.37}$$

where $\alpha_{j,d}$ is the carbonation ratio and defined as

$$\alpha_r = \frac{x_{c,r}}{x_{mea}} \tag{3.38}$$

Lastly the carbonation ratio can be related to the the liquid pH using the following empirical equation (Rotava, 1997).

$$\alpha_r = -0.3024 pH_r + 3.3419 \tag{3.39}$$

3.3.4.1 Energy balance

The energy balance takes into account the energy of the entry-exit streams, the energy introduced by the steam, the desorption energy and the vaporisation/condensation of the water in the liquid solution. The gas hold up is negligible. Similar to the desorber case the energy dynamics are considered negligible.

$$h_r \frac{d(U_r)}{dt} = L_{1,d} h_{1,d} - L_r h_r - F_{0,d} H_{0,d} + R_{0,d} \Delta H_r + Q_r \tag{3.40}$$

where Q_r is the heat provided by the steam. It is assumed that all the steam is condensed; and the condensate leaves at its boiling point therefore the amount of heat transferred to the system is simply,

$$Q_r = S \cdot \Delta H_s \tag{3.41}$$

3.3.4.2 Pressure calculation

The pressure drop between the reboiler and the first tray in the desorber is obtained using the same equation used in the desorber columns.

$$P_r - P_{1,d} = N_{t,j}\left(4.993 \cdot 10^{-3} + 5.481 \cdot 10^{-6} \cdot \upsilon_{g,j,d}{}^2\right) \tag{3.42}$$

$$V_{g,r} = 1.1515 \cdot 10^4 F_{0,d} \tag{3.43}$$

The complete reboiler model is represented by a set of 10 equations with the same number of unknown variables. Two of the equations are differentiable so two initial conditions are necessary to complete the model.

3.3.5. Condenser Model

The condenser function is to condense the water from the vapour leaving the desorber and remix the water with the desorber liquid feed flow, while recycling the incondensable CO_2 to the absorber gas feed flow. The dynamic effect of the condenser in the model is found negligible. Also in order to simplify the model, the CO_2 obtained in the gas leaving flow is mixed with the fresh gas feed flow in the absorber. Figure 3.6 shows the variables and flows used in the model.

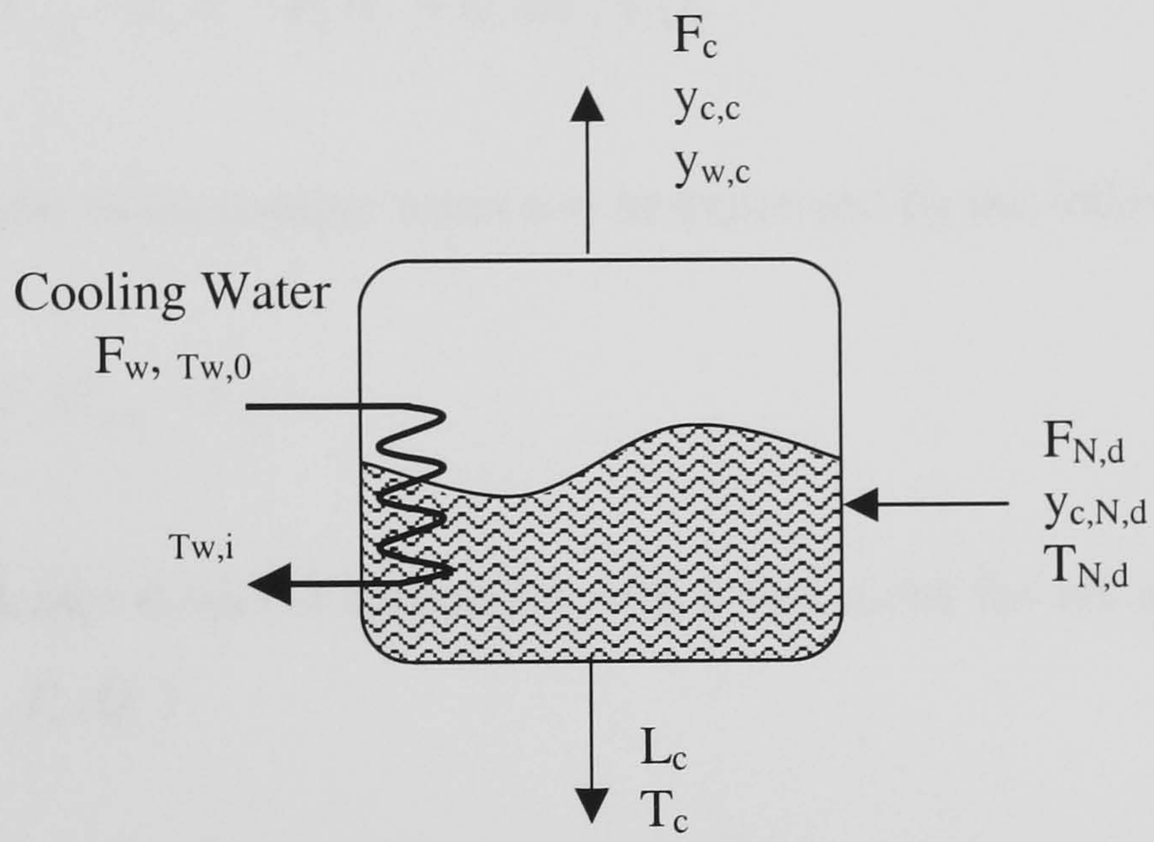


Figure 3.6. Condenser diagram

Liquid and vapour hold ups are considered negligible in the process dynamic, the overall molar balance is expressed as

$$0 = F_{N,d} - L_c - F_c \tag{3.44}$$

The carbon dioxide in the gas phase is

$$0 = F_{N,d}\, y_{c,N,d} - F_c \cdot y_{c,c} \tag{3.45}$$

The exit phase water mol fraction is given by

$$y_{w,c} = \frac{e^{\left(A_w - \frac{B_w}{C_w + T_c}\right)} \cdot x_w}{P_c} \tag{3.46}$$

$$\sum_i y_{i,c} = 1 \tag{3.47}$$

The energy balance is expressed as follows

$$0 = F_{N,d} H_{N,d} - L_c h_c - F_c H_c + L_c \Delta H_v + Q_c \tag{3.48}$$

and the heat transfer to the cooling water can be expressed by the following equation.

$$Q_c = C_{pl} F_w (T_{w,0} - T_{w,i}) \tag{3.49}$$

The condenser model is completed with 6 Equations for six unknown variables $(F_c, L_c, y_{c,c}, y_{w,c}, T_c, Q_c)$

3.3.6. Mixer Below the Condenser

The mixer below the condenser mixes the streams from the liquid condenser output and the bottom of the absorber and feed the final current in the top of the desorber column. Figure 3.7 shows a simple representation of the mixer. Dynamics are assumed negligible, therefore mass and energy balances are obtained straightforwardly.

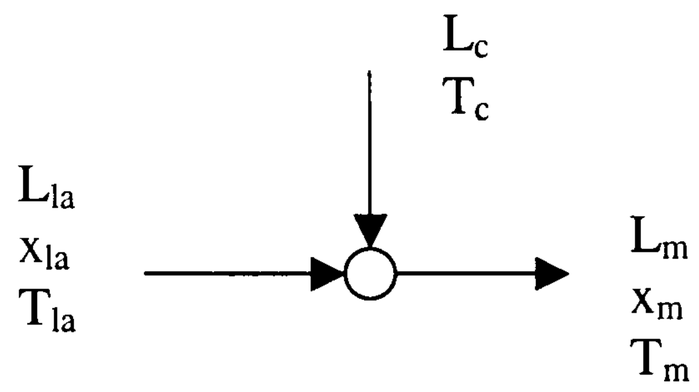


Figure 3.7. Mixer below the condenser diagram

$$0 = L_c + L_{la} - L_m \tag{3.50}$$

$$0 = L_{la} x_{la} - L_m x_m \tag{3.51}$$

$$0 = L_{la}(T_{la} - T^{ref}) + L_c(T_c - T^{ref}) - L_m(T_m - T^{ref}) \tag{3.52}$$

In order to simplify the model T_{la} is given as a constant, No further specifications are required, 3 algebraic equations for 3 unknown variables.

3.3.7. Delays and Controllers

Time delays due to mass transfer from one unit to another need to be considered in any system that involves recirculation streams. However, delays are a source of discontinuities in any mathematical model and could create infeasible solutions. A good technique to avoid this problem is by approximating delays as continuous first order differential equations.

Also the valves and safety controllers (level control) are taken into account.

3.3.7.1 Desorber feed

Equations 3.53 and 3.54 represent the transfer time delay from the bottom of the absorber to the liquid feed in the desorber

$$\tau_{l,d}\frac{dL_{la}}{dt}+L_{la}=L_{0,a} \tag{3.53}$$

$$\tau_{c,d}\frac{dx_{la}}{dt}+x_{la}=x_{1,a} \tag{3.54}$$

3.3.7.2 Level controller in the absorber

A PI controller which uses the leaving liquid flow rate as manipulated variable to control the liquid level in the absorber. The controller is expressed using the following equations.

$$\frac{\rho_{l,a}A_a}{M_{l,a}}\frac{dz_{la}}{dt}=L_{1,a}-L_{la} \tag{3.55}$$

$$e=z_{sp}-z_{la} \tag{3.56}$$

$$I_e=\int_0^t e\cdot dt \tag{3.57}$$

$$L_{0,a}=L_n+K_c(e+I_e/\tau_I) \tag{3.58}$$

3.3.7.3 Absorber feed

The liquid MEA flow and associated CO_2 composition that feed the absorber, come from the reboiler.

$$\tau_{c,a}\frac{dx_{c,n_a+1,a}}{dt}+x_{c,n_a+1,a}=x_{c,r} \tag{3.59}$$

where $\tau_{c,a}$ is the residence time of the liquid from the reboiler to the absorber. While the liquid recirculation rate is expressed using the following first order equation.

$$\tau_B \frac{dR}{dt} + R = B_{SP} \tag{3.60}$$

where τ_B is the time constant and B_{SP} is the recirculation flow rate set point.

3.3.7.4 Steam Valve

The steam valve in the reboiler is modelled using the following first order differential equation.

$$\tau_S \frac{dS}{dt} + S = S_{SP} \tag{3.61}$$

where τ_S is the time constant and S_{SP} is the steam flow rate set point.

3.3.8. Model Parameters and Physical Properties

The complete set of thermodynamics and component physical properties is obtained straightforwardly from the literature (Table 3.1). Also Table 3.2 shows the parameters used for the controllers and the time delays constant of the process, while columns design data are found from the physical dimensions of the system (Table 3.3). and table 3.4 shows the normal operation conditions of the plant.

Parameter	Value	Units	Description	Source
c_{pl_w}	79.20	kJ/kmol°C	Specific heat of liquid H_2O	Perry & Green, 1994
c_{pg_w}	33.50	kJ/kmol°C	Specific heat of vapour H_2O	Perry & Green, 1994
c_{pg_c}	41.38	kJ/kmol°C	Specific heat of CO_2	Perry & Green, 1994
c_{pg_n}	29.26	kJ/kmol°C	Specific heat of N_2	Perry & Green, 1994
ΔH_s	45400	kJ/kmol	Enthalpy of condensation	Perry & Green, 1994
ΔH_v	40000	kJ/kmol	Latent heat of vaporisation	Perry & Green, 1994
ΔH_r	102500	kJ/kmol	Heat of reaction	Disli, 1996
ρ_l	1000	kg/m^3	Density of liquid water	Perry & Green, 1994
M_l	20.13	kg/kmol	Liquid molecular weight	Periodic Table

Table 3.1. Thermodynamic and physical properties data

Considering that the liquid phase is around 95% water, the liquid density is approximated to the liquid water density. The molecular liquid weight is calculated by assuming a MEA liquid concentration of 2.5 $kmol/m^3$.

Parameter	Value	Units	Description
z_{sp}	0.45	m	Level of the absorber set point
L_n	0.012	kmol/s	Output of the absorber level controller when level error is 0
K_c	0.1	kmol/s·m	Proportional gain of the absorber level controller
τ_I	184	s	Integral time of the absorber level controller
$\tau_{l,d}$	5	s	Time constant for the desorber feed valve
$\tau_{c,d}$	1.666	s	Time constant delay for the desorber concentration feed
$\tau_{c,a}$	1.6666	s	Time constant delay for the Absorber concentration feed
τ_B	5	s	Time constant for the absorber liquid feed
τ_S	5	s	Time constant for the steam valve

Table 3.2. Level controller, valve and delay model parameters

Parameter	Value	Units	Description
D_a	0.254	m	Absorber column diameter
A_a	0.0507	m^2	Absorber cross sectional area
h	6.1	m	Total absorber packing height
D_d	0.252	m	Desorber column diameter
A_d	0.0499	m^2	Desorber cross sectional area
A_r	0.1496	m^2	Reboiler cross sectional area

Table 3.3. Units design data

Parameter	Value	Units	Description
P_a	2.03	atm	Pressure in the absorber
P_f	2.03	atm	Pressure in the absorber gas feed
P_c	1.0	atm	Pressure in the condenser
C_{mea}	2.5	$kmol/m^3$	MEA liquid concentration
x_w	1	-	Liquid molar fraction of the water
T_f	30	°C	Absorber gas feed temperature
$T_{w,0}$	24.5	°C	Cooling water to the condenser
$T_{w,1}$	36.4	°C	Cooling water from the condenser
T_{la}	90	°C	Temperature of liquid to desorber (before mixer)
F_w	0.0017	kmol/s	Cooling water to condenser

Table 3.4. Normal operation conditions in the plant

3.3.9. Manipulated Variable Feasible Region

For effective operation of the absorber, the liquid solvent flow rate must be high enough to keep the packing completely wetted and low enough to avoid flooding the column over the range of gas flow rates.

Similarly; the liquid solvent rate and steam rate must be such as to avoid excessive weeping through the desorber perforated plates and again avoid flooding the column.

These relations are of course complex, but for a given margin of gas flow rates the limits can be approximately represented by simple linear constraints in terms of steam flow rate and liquid solvent recirculation rate shown in Figure 3.8. These constraints are given by the following inequalities.

$$\begin{aligned} &(M_m R - 5.926 M_w S) - 90.74 > 0 \\ &9 < R < 17.4 \\ &0.7 < S < 1.61 \end{aligned} \tag{3.62}$$

where

M_w is the molecular weight of water [g/mol]

M_m is the molecular weight of the aqueous solvent [g/mol]

S is the steam flow rate [mol/s]

R is the liquid recirculation flow rate [mol/s]

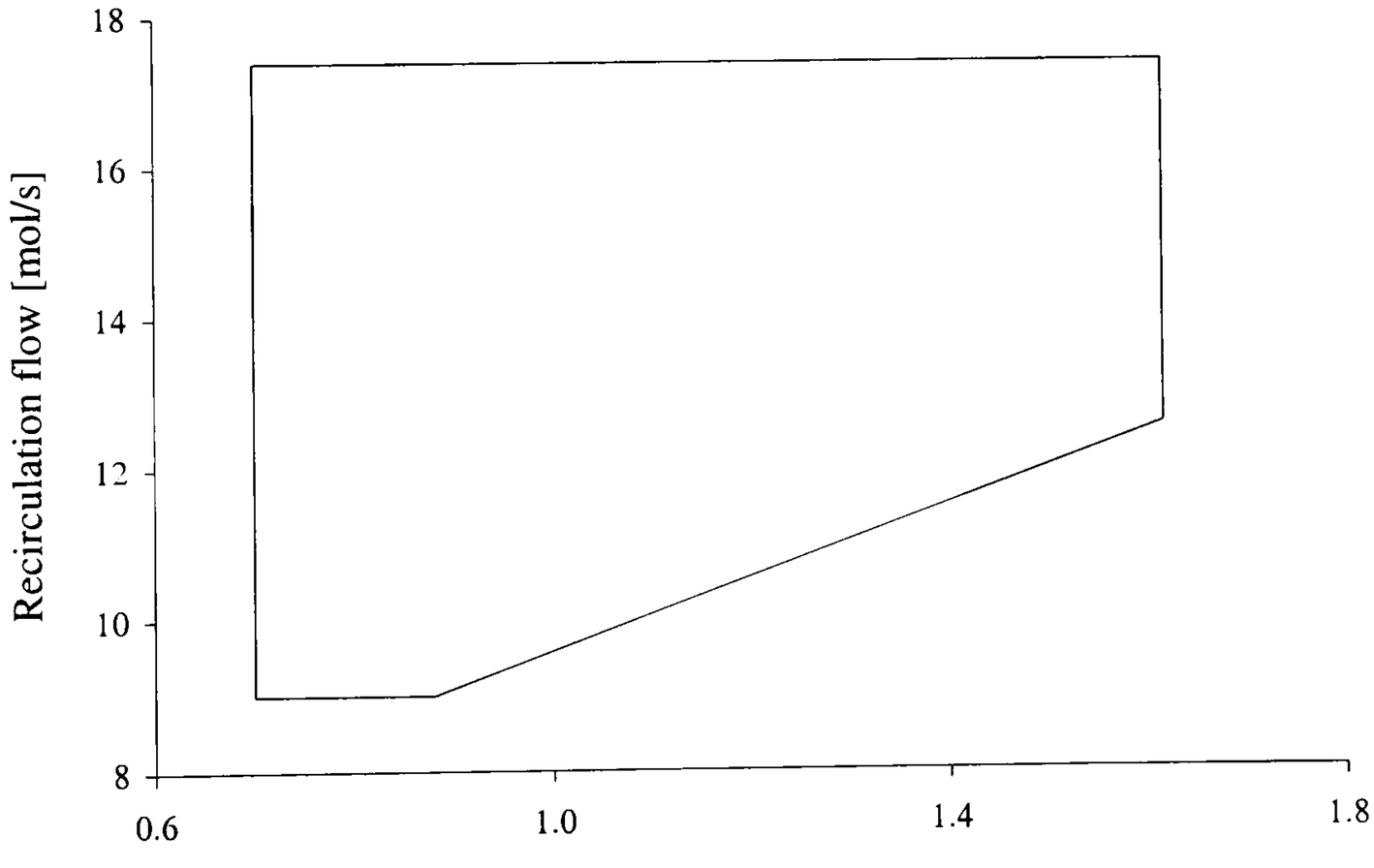


Figure 3.8. Control variables operational region

For the liquid feed temperature the limits are arbitrarily selected around the standard set point. That means between 45 and 55°C.

$$45 \leq T_{lif} \leq 55 \quad [^{o}C] \tag{3.63}$$

Where T_{lif} is the liquid feed temperature in the absorber.

Once the mathematical model was developed and written as a gPROMS file (see Appendix A), various simulations either at steady state or dynamic state were run in order to understand the process and the relationships between its multiple variables. The following sections present several studies with their respective results and analysis.

3.4. Steady State Performance

The first step is to choose the feasible region and limits for the manipulated variables. The following data (Table 3.5.) is obtained from (Rotava, 1996). Table 3.5. shows the minimum, mean and maximum values for each manipulated variable.

		Minimum	Mean	Maximum
F	Feed flow Rate [g/s]	35	40	45
y_F	Feed CO_2 mole fraction [%]	2	4	6
R	Solvent circulation [mol/s]	9	13.2	17.4
S	Steam flow rate [mol/s]	0.7	1.15	1.61

Table 3.5. Range of values for the different control and manipulated variables

Using the original model proposed by Rotava (1996) with 5 and 3 stages in the absorber and desorber respectively; the CO_2 leaving gas concentration is computed at steady state conditions, varying either the solvent recirculation or the steam flow, while keeping constant the other operational conditions at their mean values.

Figure 3.9 shows the effect of solvent recirculation flow and absorber liquid feed temperature on the CO_2 concentration in the gaseous flow leaving the absorber while Figure 3.10 plots the same relations but using steam flow as the manipulated variable instead.

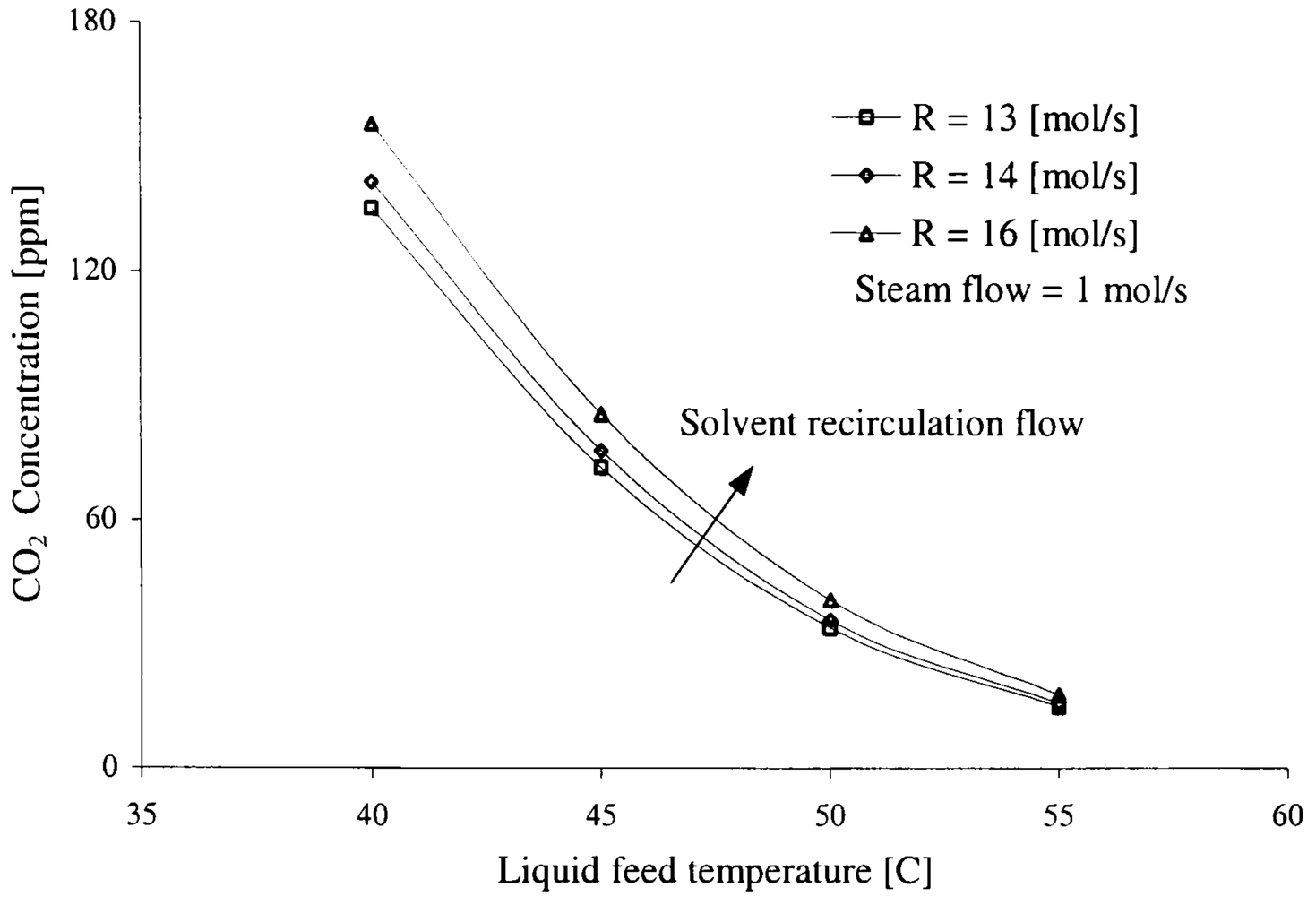


Figure 3.9. Effect of the solvent flow and liquid feed temperature on the leaving flow CO_2 concentration

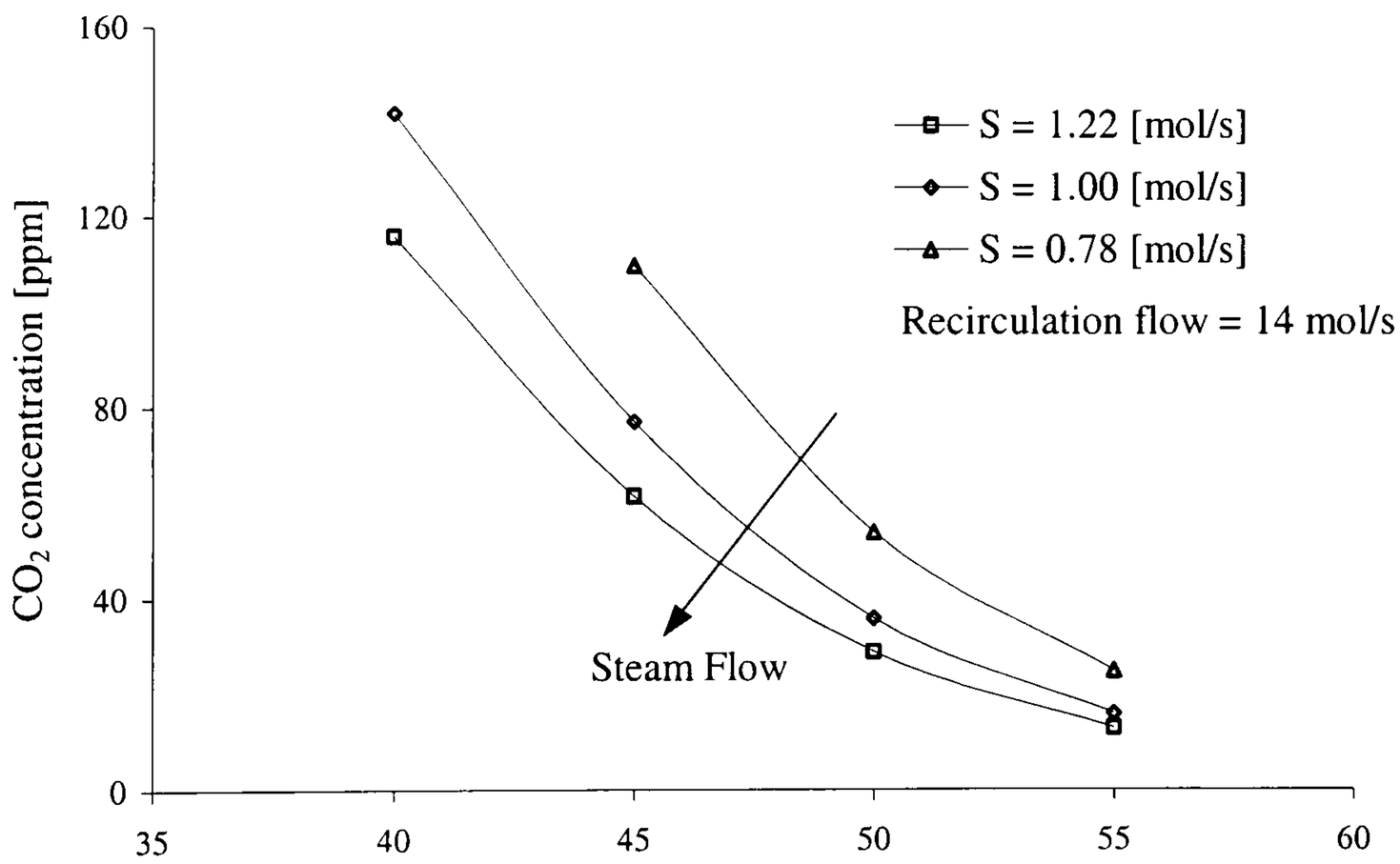


Figure 3.10. Effect of the steam flow and liquid feed temperature on the leaving flow CO_2 concentration.

From Figure 3.9 it is inferred that increasing the solvent flow rate causes an increase in the CO_2 concentration in the N_2 leaving the absorber. This is due to an effect of the reflux-ratio in the desorber where more CO_2 can be removed from the solvent.

On the other hand, Figure 3.10 shows that the higher the amount of steam employed, the lower the CO_2 final concentration leaving the absorber. With more thermal energy in the desorber, again more CO_2 can be stripped from the solvent.

However as can be seen from both figures, the liquid feed temperature has a direct relation in the absorption process, even stronger than the steam flow rate. For instance, an increase of just 5 degrees causes a reduction in the CO_2 final concentration by 50%.

The principal modifier factors in the CO_2 final composition are firstly the liquid feed temperature and the vapour steam consumption in the reboiler. The liquid recirculation flow has a more modest effect on the amount of CO_2 absorbed by the amine. These results agree with experimental results obtained by Disli, 1996 and Rotava, 1997.

3.4.1. Liquid Temperature Effect on CO_2 Gas Concentration

From the results obtained in the previous part, clearly the absorber model does not represent accurately the absorption process at temperatures above 50°C. The reaction mechanism that involves the formation of a carbamate salt (Burkett, 1977) is:

$$2HO(CH_2)_2NH_2 + CO_2 \leftrightarrow HO(CH_2)_2NHCOO^- + HO(CH_2)_2NH3^+ \qquad (3.64)$$

The equilibrium concentrations of molecular CO_2 in solution are proportional to their partial pressures in the gas phase (Henry's law applies) so absorption reactions are driven to the right by increasing acid gas partial pressure. The reaction equilibrium is also sensitive to temperature, causing the vapour pressure of absorbed acid gases to increase rapidly as the temperature is increased. As a result it is possible to strip absorbed gases from amine solutions by the application of heat (Kohl & Nielsen, 1997).

New simulations are conducted in order to check the relation between liquid feed temperature in the absorber and CO_2 gas final concentration and its possible use as a manipulated variable. Using constant mean operational conditions the liquid feed temperature was progressively changed to measure the effects on CO_2 gas concentration.

The original model neglects the desorption term in the absorption process because it is considered to have no effect at standard operational conditions; as a result the absorption reaction is assumed irreversible. However further simulations including the desorption term proves the contrary. Figure 3.11 shows the results comparing the two approaches, one with the absorption term exclusively and the proposed one that incorporates a reversible reaction in the absorber model.

$$F_{j-1,a}\,y_{c,j-1,a} - F_{j,a}\,y_{c,j,a} - R_{j,a} + D_{j,a} = 0 \tag{3.65}$$

$$U_{j,a}\left(\frac{dx_{c,j,a}}{dt}\right) = L_{j+1,a}\,x_{c,j+1,a} - L_{j,a}\,x_{c,j,a} + R_{j,a} - D_{j,a} \tag{3.66}$$

$$D_{j,a} = \frac{e^{\left((-47.91+112.8\alpha_{j,a})+(0.7615+1.668\alpha_{j,a})T_{j,a}+(-0.0029+0.007\alpha_{j,a})T_{j,a}{}^{2}\right)}}{760\cdot P_{j,a}}F_{j,a} \tag{3.67}$$

Adding the new term in the absorber CO_2 mass balance does not have any effect below 45°C. After that point the desorption term starts having a stronger weight producing a minimum value in the CO_2 gas concentration at 50°C. Above this point, the CO_2 is stripped off from the liquid phase and the gas concentration increases. Results clearly show that the desorption process has a bigger impact at higher temperatures. These results agree with the experimental data reported by Kohl and Nielsen, (1997).

In light of these results the desorption term is incorporated in the model in order to obtain a more accurate process representation.

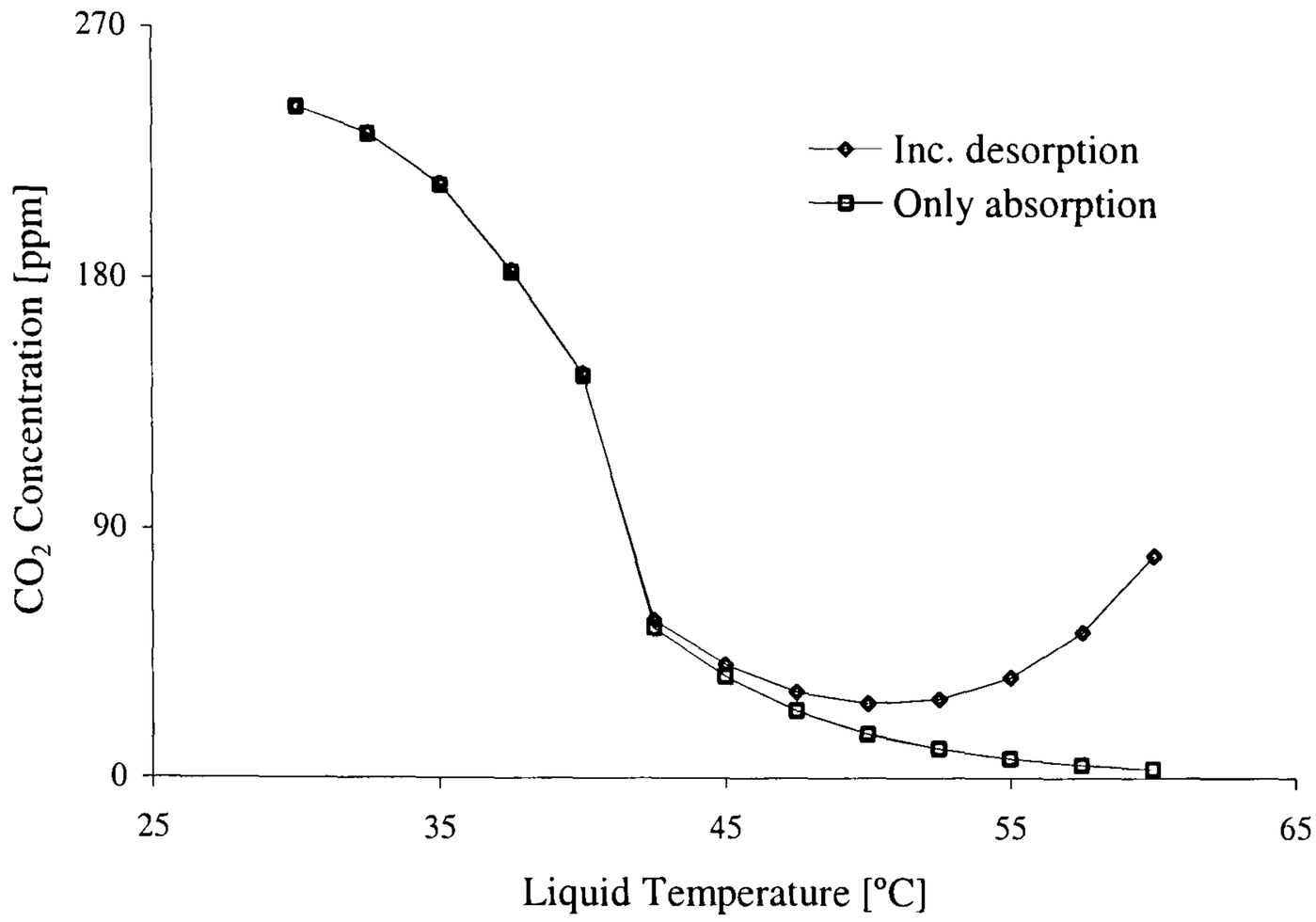


Figure 3.11. Temperature liquid feed effect in the operational range (30-55ºC)

3.4.2. Effect of the Number of Stages on Product CO_2 Concentration

Using the improved model generated from previous tests without changing the original operational condition, the effect of the number of stages either in the absorber or the desorber on the CO_2 leaving gas concentration is studied. Twenty stages were selected as the maximum number of sections to be used in each column.

In the absorber 20 lumped stages are considered large enough to closely approximate a distributed model, but keeping the simplicity and easiness to solve advantages that a distributed model does not have.

In the desorber, the column physically consists of 20 sieve trays plus a natural circulation reboiler that supplies the stripping energy.

Table 3.6 shows the CO_2 final concentration varying the number of stages in the desorber (the absorber is kept constant with 20 stages), while Table 3.7 shows the same experiment but varying the number of absorber stages and keeping constant the desorber column instead.

# of desorber stages	CO_2 ppm final concentration	Difference %
20	54.3	-
15	56.9	4.8
10	59.4	9.3
5	65.6	20.8
3	73.8	35.9

Table 3.6. CO_2 concentration at different number of desorber stages (Absorber 20 stages)

# of absorber stages	CO_2 ppm final concentration	Difference %	Difference % Disli (1996)
20	54.3	-	-
15	54.7	0.7	n/a
10	55.4	1.4	1.4
5	58.0	4.6	4.6
3	62.3	7.4	8.0

Table 3.7. CO_2 concentration at different number of absorber stages (desorber 20 stages)

In both cases (Table 3.6 and Table 3.7), a reduction in the number of stages increases the concentration of CO_2 in gas stream leaving the absorber. Due to the nature of a lumped approximation, the fewer the number of stages in each column, the more lumped the system is and consequently the larger the error.

Interestingly as Table 3.7 shows, a reduction in the number of stages in the absorber model, does not affect drastically the final CO_2 concentration at steady state conditions. The largest difference found with only 3 stages to represent the whole column has an error of 7%. Previous studies on the effect of the number of stages (Disli, 1996) arrived at the same conclusions. Table 3.7 also compares each works showing the similarities between both researches.

On the other hand Table 3.6 shows clearly that changing the number of stages in the desorber modifies considerably the final CO_2 leaving concentration. For instance a reduction from 20 to 3 stages increases more than 35% the CO_2 final concentration. Although not being directly related in the absorption process, these results show the importance of the number of stages in the desorber has in the accuracy of the model.

Previous attempts to implement an MPC in the plant failed because of poor accuracy of the match between model and the real plant. Although originally the idea

was to keep the model as simple as possible, the use of few stages in each column was reflected in bigger errors. For instance Rotava's (1996) nonlinear model generates an error of approximately 40.5% (5 stages in the absorber and 3 in the desorber).

A new model with 10 stages in the desorber and 5 in the absorber is proposed to close the mismatch between model and the process dynamics. Theoretically the new model only generates 14% of error, good enough for control purposes.

3.4.3. Steady-State Optimal Values

The objective of the next runs is to study the system behaviour at optimal steady state condition. The purpose is to try to understand the manipulated variable behaviour and limits at steady state under controlled constraints and optimal objective function.

3.4.3.1 Minimum CO_2 Concentration in the N_2 Product

The first 3 runs are conducted using 20 stages in each column while fixing the feed flow rate and feed CO_2 mole fraction for each run as shown in Table 3.8.

Run		1	2	3
F_f	[g/s]	40	45	35
$y_{c,f}$	[%]	4	6	2

Table 3.8. Feed flow rate and CO_2 mol fraction used in runs 1, 2 and 3

The minimal value of CO_2 is calculated subject to the constraints shown in Figure 3.8. The results are shown in Table 3.9.

Run		1	2	3
S	[mol/s]	1.61	1.61	1.61
R	[mol/s]	12.4	12.4	12.4
Obj Function [CO_2 concentration]		15.4	77.0	5.2

Table 3.9. Optimal results for runs 1, 2 and 3

From the results in Table 3.9 it can be concluded that the optimal values in the case when the objective is to minimise the concentration of CO_2 will be to use the maximum amount of vapour steam available, in this case 1.61 mol/s and the lowest possible solvent recirculation flow 12.4 mol/s.

3.4.3.2 Minimum Steam Flow Rate

Table 3.10 shows each run conducted using different feed conditions and 20 stages in each column. R and S are computed to minimise the consumption of steam flow rate (S), subject to previous constraints plus CO2 gas concentration limit: Results are presented in Table 3.11.

$y_P \leq 100$ ppm.

y_P represents the CO_2 concentration in the N_2 product.

Run		4	5	6
F_f	[g/s]	40	45	35
$y_{c,f}$	[%]	4	6	2

Table 3.10. Feed flow rate and CO_2 mol fraction used in runs 4, 5 and 6

Run		4	5	6
S	[mol/s]	0.720	1.19	0.7
R	[mol/s]	9	10.8	9

Table 3.11. Optimal results for runs 4, 5 and 6

Table 3.11 shows that the larger the amount of CO_2 in the feed current, the larger the steam flow rates required to achieve the CO_2 concentration end point constraint. Identically to the previous experiment, recirculation flow rate is kept as it lowest possible rate to minimise steam consumption.

3.4.3.3 Optimal Steam Flow at Different Stage Numbers

After studying the optimal steady state behaviour at different feed rates and concentration condition, the next step is to repeat the previous experiments but changing the number of stages in each column instead.

The idea is to compute the steam flow rate optimal values, varying the desorber stages while keeping fixed the number of absorber stages at 20. Values for F_f = 40 g/s and $y_{c,f}$ = 6% are used. Table 3.12 shows the results for each run and the number of stages selected for each experiment.

Run	7	8	9	10
Desorber Stages	20	10	5	2
S optimum	0.739	0.741	0.793	1.03

Table 3.12. Optimal steam values at different desorber's stages

Another set of experiments is done repeating the previous problem but changing the number of absorber stages and fixing the desorber column at 10 stages. Table 3.13 presents the results obtained in these runs.

Run	7	11	12	13
Absorber Stages	20	10	5	3
S optimum	0.739	0.752	0.778	0.778

Table 3.13. Optimal steam values at different absorber's stages

In both cases (Table 3.12. and Table 3.13.), reducing the number of stages in each column decreases the efficiency of the process, that means the amount of steam necessary to achieve the final CO_2 concentration condition is increased.

Similarly, as shown in previous sections, a reduction in the number of stages in the absorber does not affect drastically the optimal steam value, the largest difference found is only 5%. In contrast a change in the number of stages in the desorber modifies considerably the final steam quantity, with 35% being the maximum deviation.

These results confirm that increasing the number of desorber stages will be an effective way of improving the original model.

3.5. Dynamic Performance

After studying the model's steady state behaviour, focusing particularly on manipulated and control variables and their optimal values under different operational conditions and constraints, the next experiments are focused to understand the system behaviour at dynamic state.

The following sections present the results and discussion of dynamic simulation using the best model generated from previous results. Simple and optimal dynamic simulations are generated in order to obtain the best possible model to be used in a model predictive controller.

3.5.1. Simple Dynamic Comparison

A number of simulations are made using the original model proposed by Rotava, as well as with 20 stages in each column. Each run starts at steady state using the same operational conditions (see Appendix A). In order to study the dynamic behaviour of the system, a step perturbation is applied at time 0 in one of the manipulated variables, while recording the response of the controlled ones. Figures 3.12 to 3.16 show the results of some of these runs.

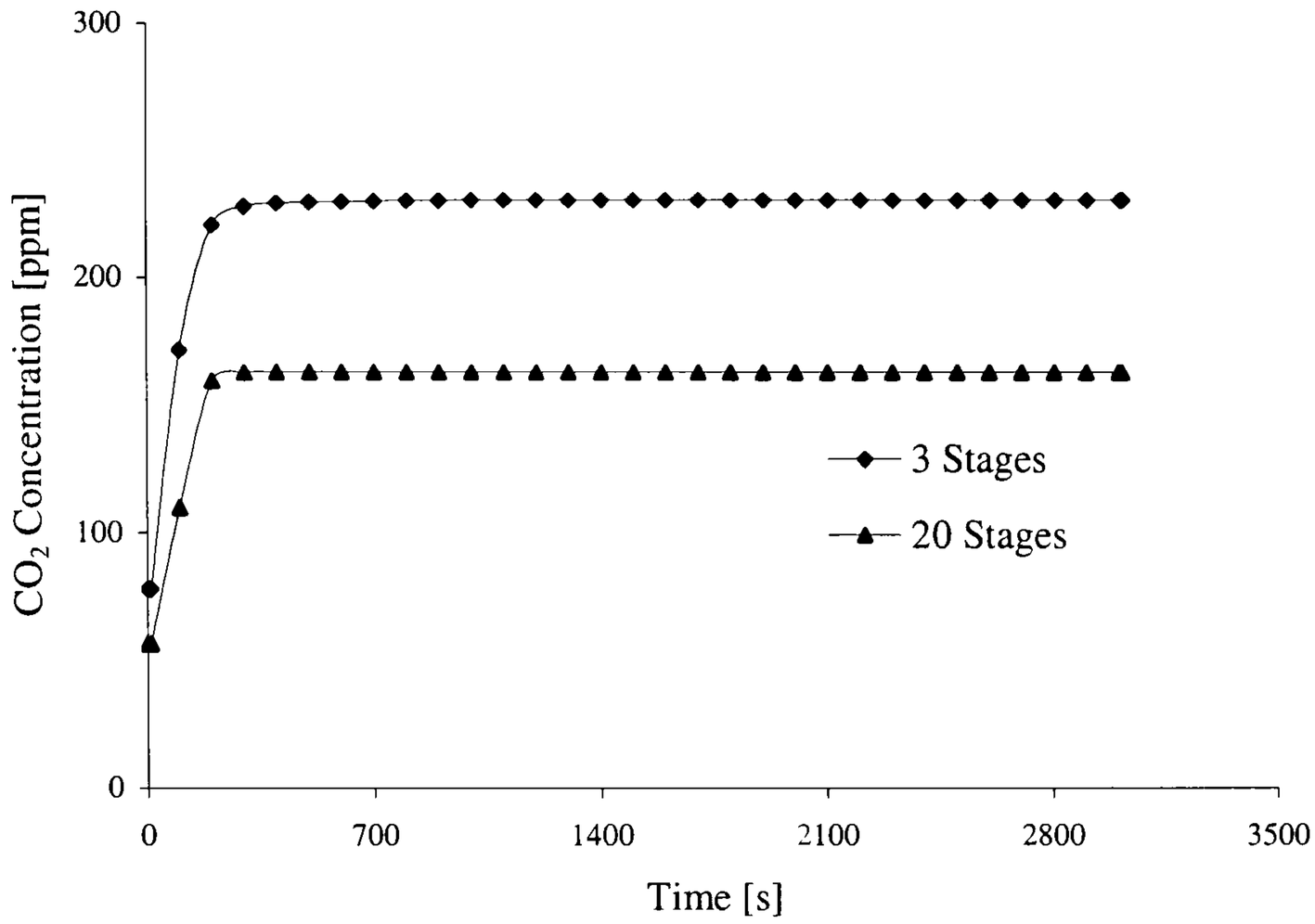


Figure 3.12. CO_2 concentration dynamic in each model after a perturbation in the liquid feed temperature (-5°C)

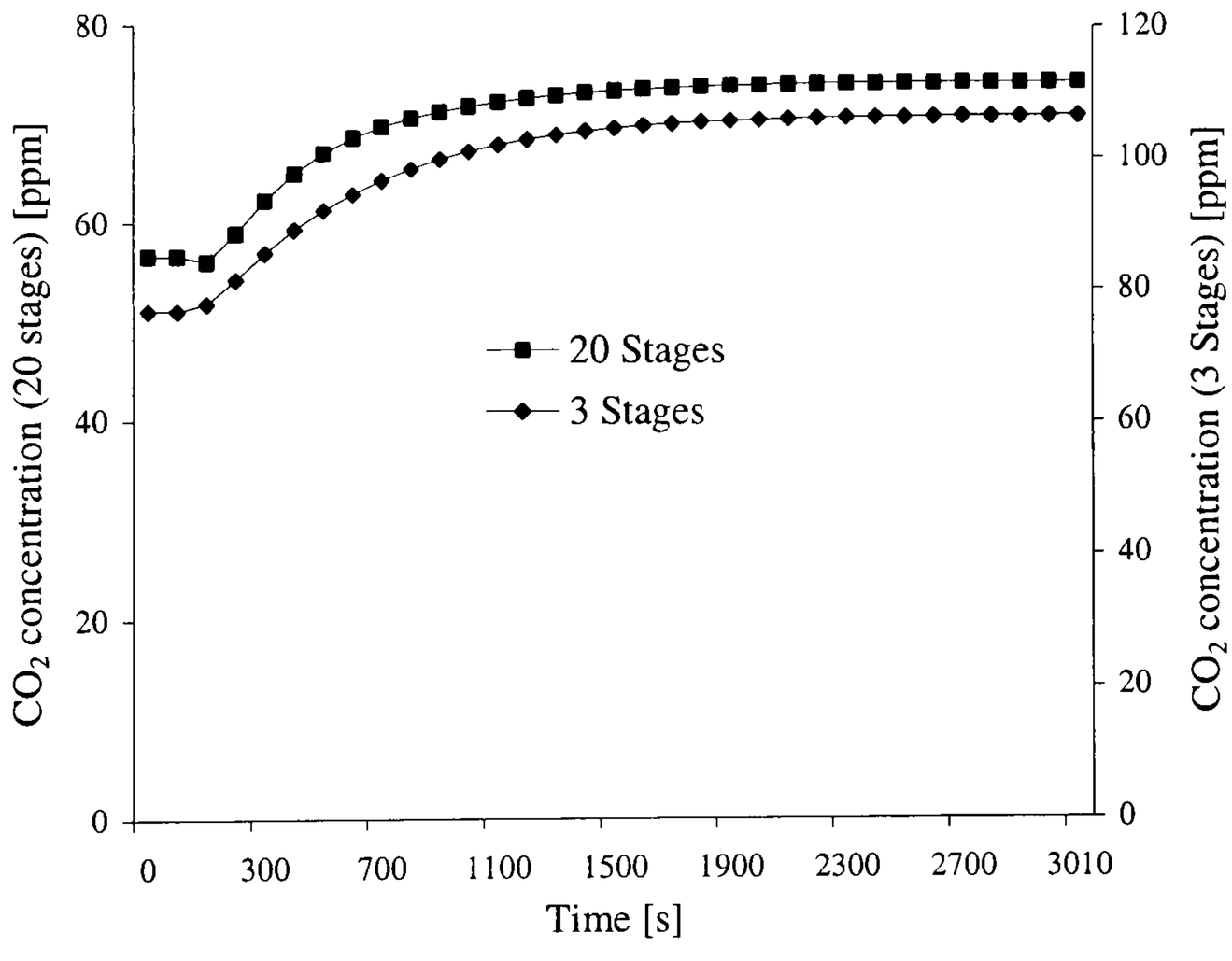


Figure 3.13. Step-change in steam flow –20%

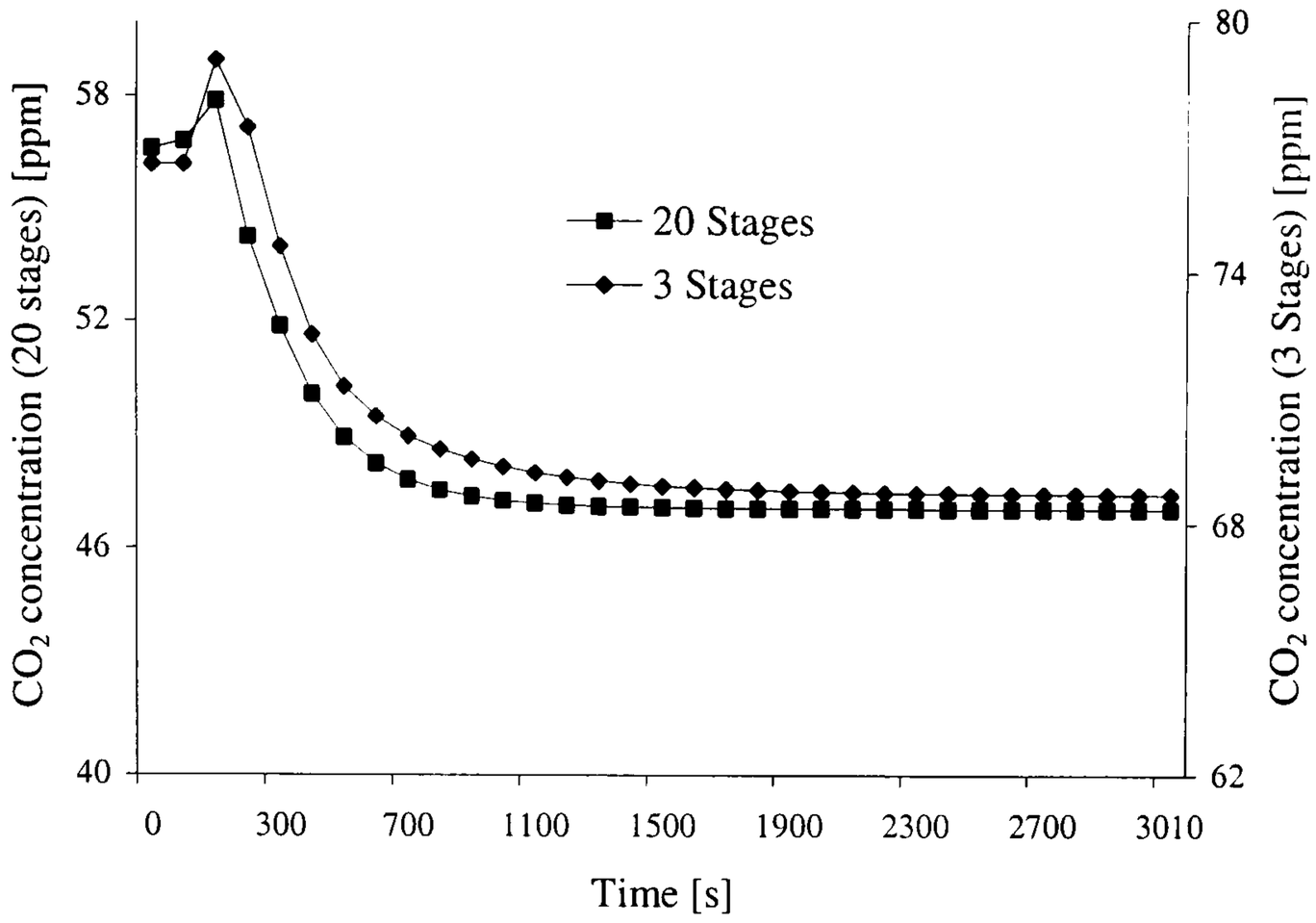


Figure 3.14. Step-change in solvent flow –15%

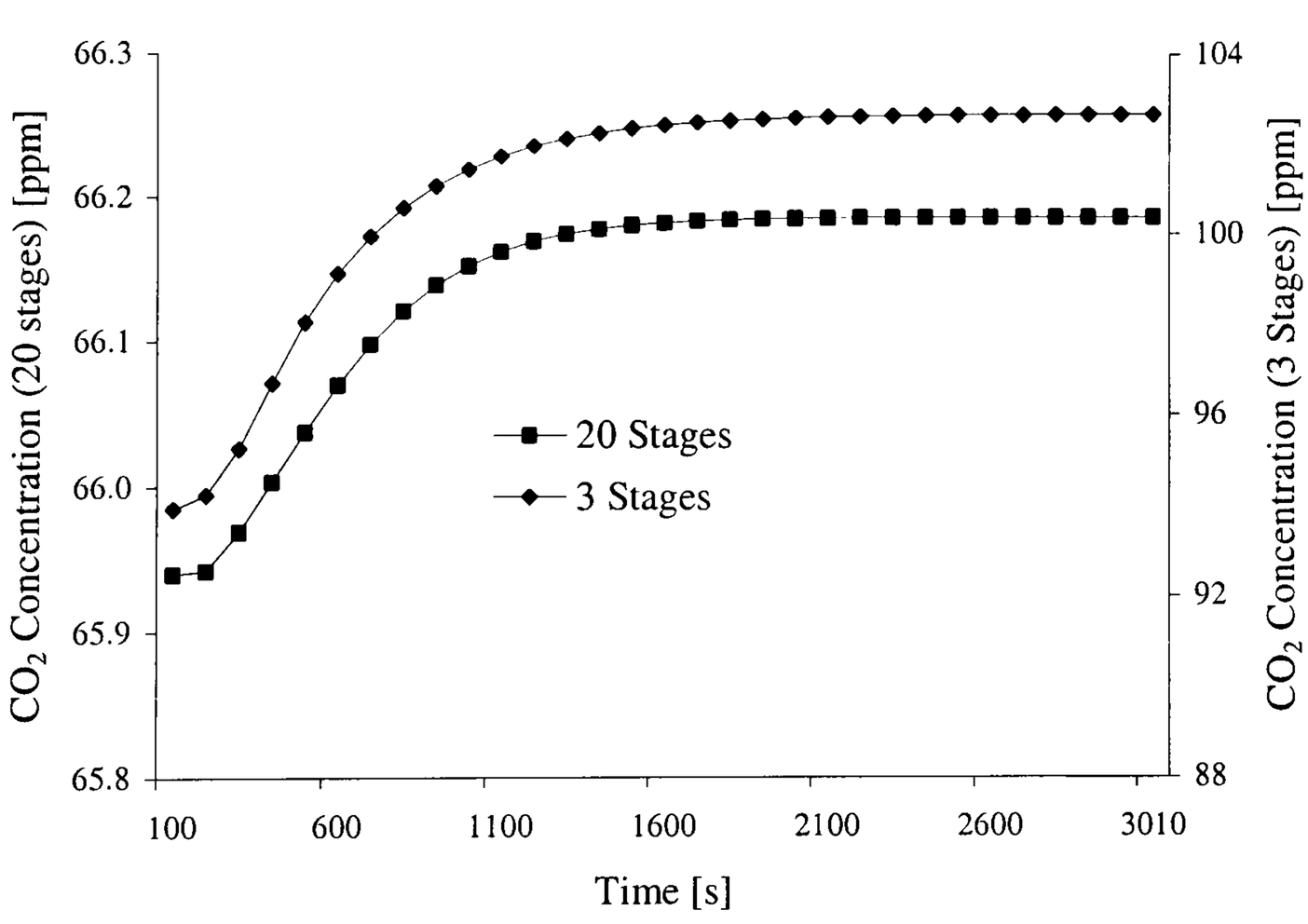


Figure 3.15. Step-change in $y_{c,f}$ +20%

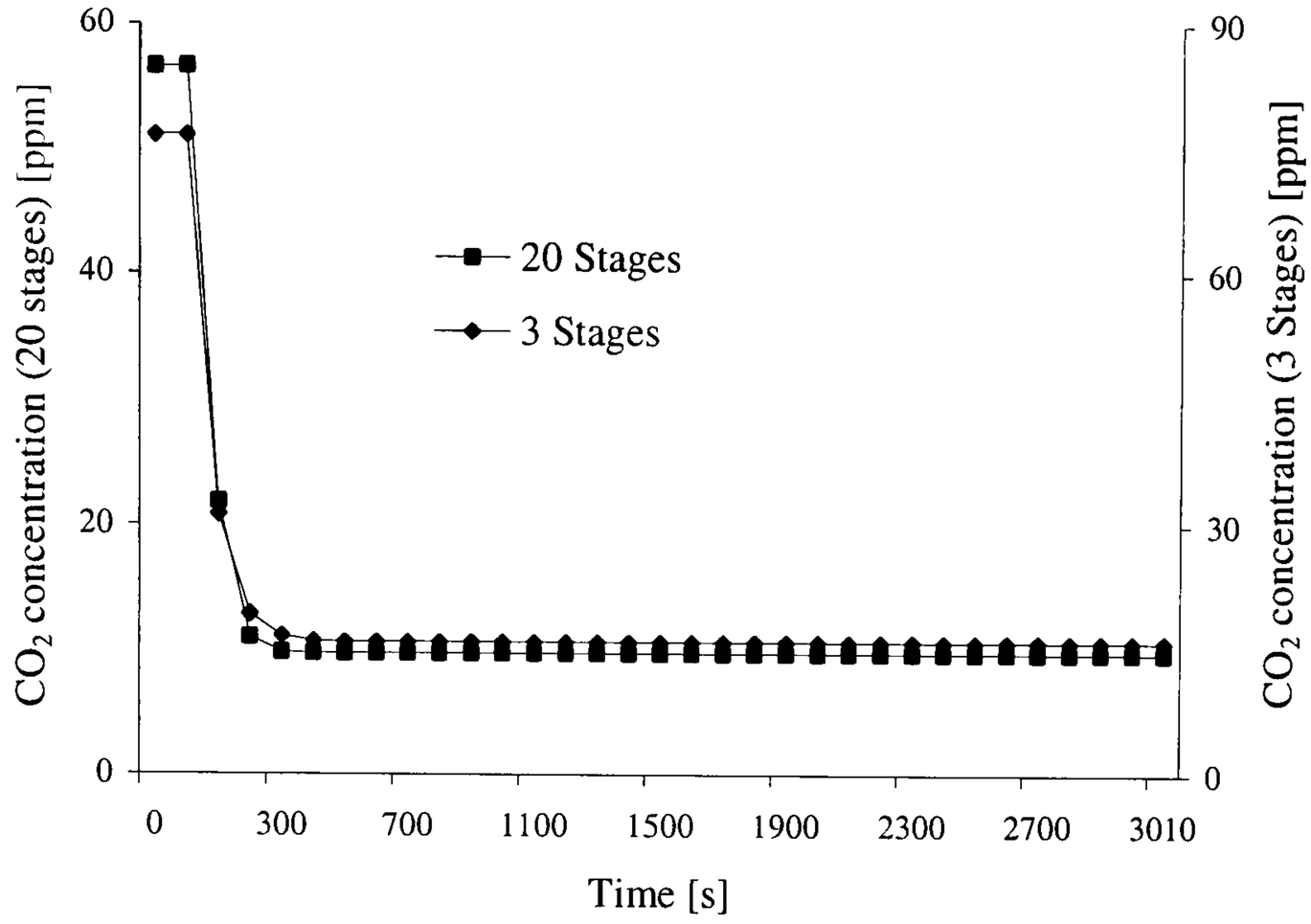


Figure 3.16. Step-change in the liquid feed temperature (10°C)

Despite the fact that each model reached distinct values at steady state, as explained in previous sections, the dynamic behaviour is identical in each case. Moreover the response time in every plot is the same, giving an indication that the new model is scaled correctly.

From these plots, it can be inferred that a model with more stages, theoretically speaking, is more accurate at steady state, however the dynamic response does not show any difference between each model. Moreover, the results for the model with 20 stages in each column can be reproduced from the simplified model by multiplying them by some factor.

Also these results show that if one wants to close the model/plant mismatch one of the better approaches will be the selection of a reliable estimation algorithm rather than using highly complex mathematical models.

As a conclusion the selection of a very complex model (20 stages in each column) may generate the most accurate results, but has the disadvantage of a very computationally demanding model. From these results, it is clear that the whole model can be simplified by reducing the number of stages in each column without deteriorating significantly the final values.

As a result a simpler model with 5 absorber stages and 10 desorber stages is chosen instead of one with 20 stages in each column. The former will give quite accurate results without making excessive computational demands. The mismatch reduction will be done using parameter estimation techniques.

3.5.2. Dynamic Simulation for Optimal Steady-State Changes

Using different numbers of stages in each column (see Table 3.14), the dynamic system behaviour at optimal steady state condition is computed. A step perturbation in the absorber gas feed flow rate is made after 500 seconds, y_F is set at its mean value throughout the whole time. At the same perturbation time the manipulated variables are set to their corresponding new optimal steady state values for the relevant periods. At these conditions, the dynamic response is computed. Figures 3.17 to 3.18 show the results obtained from these runs.

Run	13	14	15	16	17	18	19
Absorber Stages	20	20	20	20	10	5	3
Desorber stages	20	10	5	2	5	5	5

Table 3.14. Conditions for Runs 13 to 19

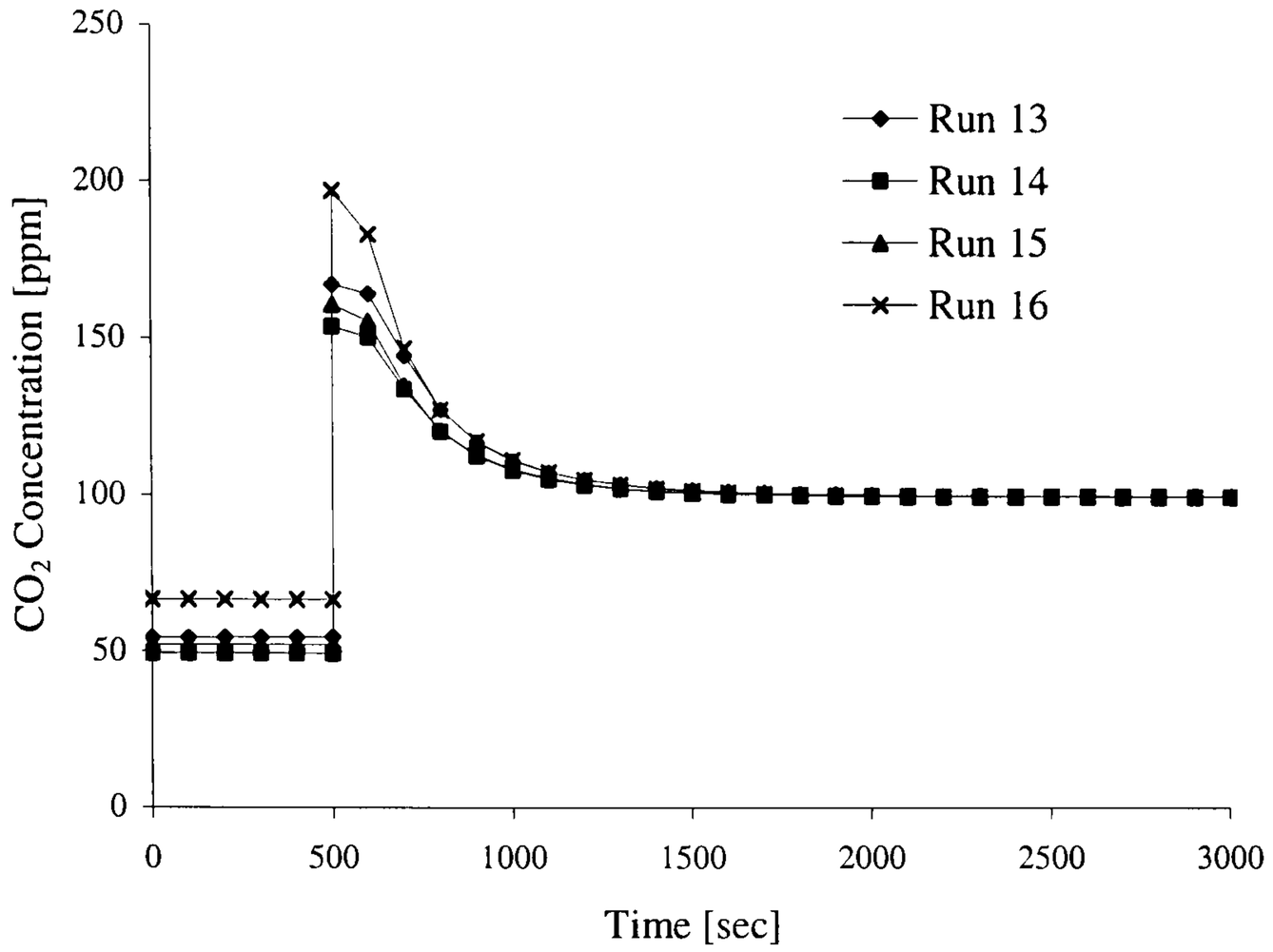


Figure 3.17 Effect in the number of desorber stages on the CO_2 final concentration

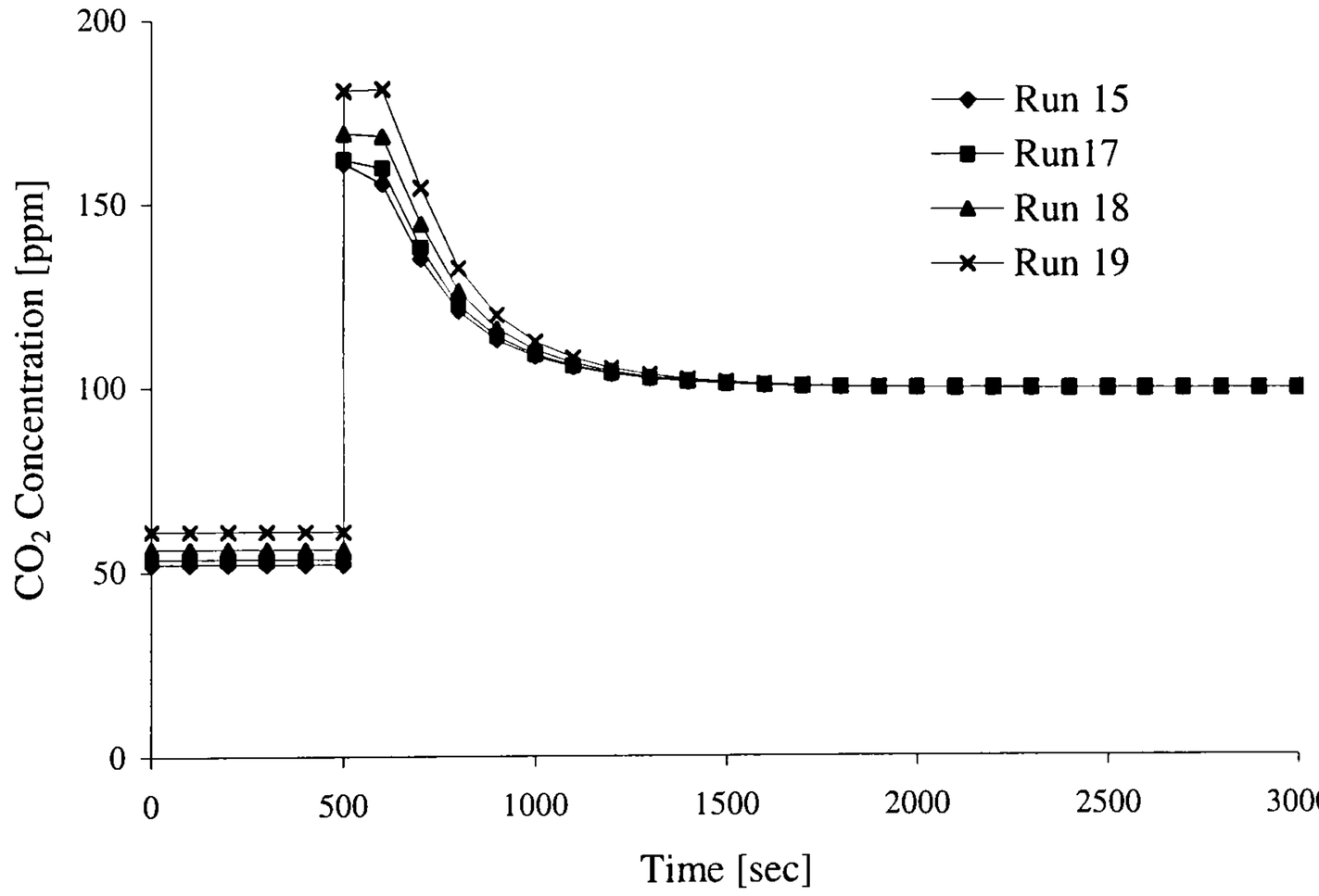


Figure 3.18. Effect in the number of absorber stages on the CO_2 final concentration

The results for runs 13 to 16 are plotted in Figure 3.17 where the number of desorber stages changes in each run. Alternatively Figure 3.18 shows the results at different absorber stages. The results show the similarity between the different models.

There is practically no difference in the dynamic behaviour, particularly in the number of absorber stages (Figure 3.18) where all the graphs are similar. It is proved again that the absorber stages are not the key factor for a better model.

In addition another interesting aspect to be considered in both figures is the similarity in the time response among all the models. It takes 1500 seconds approximately in every case to reach steady state conditions. With this time constant of approximately 25 minutes, the system is sufficiently slow to be controlled by a nonlinear optimal control scheme.

Also Figures 3.17 and 3.18 show the sensitivity of the model to the number of stages in each column. For instance the overshoots in Figure 3.18 are smaller compared with Figure 3.17 . That reflects again that the number of stages in the desorber is more sensitive to the model rather than the number of stages in the absorber. These results reconfirm the validity of the chosen model to have 5 absorber stages and 10 desorber stages.

Lastly all these runs indicate that if the poisoning of the catalyst in a downstream process needs to be avoided, the control action must be taken before the perturbation occurs. Hence the need for prediction in order to keep the final CO_2 gas concentration below the set point.

3.6. Conclusions

In this chapter a model for the absorption/desorption plant has been developed. Steady state and dynamic simulations were run in order to generate an improved model to be used for the rest of this research. Also simulations helped to define the most significant manipulated variables to control the CO_2 leaving gas concentration.

It was concluded that the best model for the controller should have 5 stages in the absorber and 10 in the desorber. Also it was proved that the model could generate the same dynamic behaviour compared with a more realistic one without generating excessive error.

Chapter 4

Parameter and State Variable Estimation

4.1. Estimation of the State Variables

Parameter and state variable estimation is a key section in the model predictive control algorithm. Due to the fact that the latter is an open loop control strategy, the former task is to keep as close as possible the plant measurements and model variables that will be used in the algorithm. Mismatch between plant and model could be the difference between a stable or unstable system, so selecting a proper estimation technique is vital for the MPC.

An extensive collection of algorithms and methods are available to choose from. Each has its advantages and disadvantages and the engineer must use his knowledge and judgment to select the most appropriate one for each case.

In order to understand the importance that the state variable estimation process has in the MPC, two estimation techniques are tested. The first one is the steady state approximation whose main virtues are its computational speed and simplicity. The second is the well-known Kalman filter which as main advantages has the stochastic and optimal properties.

4.1.1. Differential States from a Steady State Approximation

The steady state approximation is a fast way to estimate the initial conditions for the differential variables. However its lack of noise and error management tend to

produce inaccurate results. Commonly this technique is suggested when the process time is short for the system to be considered at pseudo steady state conditions for each interval.

The idea behind it is to use only the input measurements in the plant for the mathematical model and obtain straightforwardly the steady state values. Later on these values are used as initial estimates for the controller.

4.1.2. Extended Kalman Filter (EKF)

The second proposed method is the extended Kalman filter (EKF). The Kalman filter is a recursive estimation method that takes into account plant measurements, measurement errors and plant noise.

As explained in Section 2.6.2.2, the EKF consists of two stages. The first computes the evolution of the estimated state and its covariance matrix from a dynamic model of the process (also called "time update" or prediction), and the second the corrections to these as a result of the measurements made ("measurement update" or correction).

In this case we assume only measurement errors and no process "noise" so the prediction model is purely deterministic. Following there is a brief description of the Kalman filter implementation for a DAE system.

Any DAE system can be reduced to the form:

$$\begin{aligned} f^1(t,u,x_1,\dot{x}_1) &= 0 \\ f^2(t,u,x_1,x_2) &= 0 \end{aligned} \tag{4.1}$$

where x_1, x_2 and u are the state variables, algebraic variables and input variables respectively. The matrices $f^1_{\dot{x}_1}$ and $f^2_{x_2}$ are square and non-singular.

Measurements y_k are obtained at sequence of times t_k, $k = 1,2,\ldots$ which are subject to measurement noise η_k, and consist of a subset of (t,u,x_1,x_2):

$$y_k = M_k z_k + \eta_k \tag{4.2}$$

where

$$z = (z_1, z_2, z_3, z_4) \equiv (x_1, x_2, \dot{x}_1, u) \tag{4.3}$$

$$M_k = \begin{cases} 1 & if \;\; y_k^i \; measures \; z_k^i \\ 0 & otherwise \end{cases} \tag{4.4}$$

this subset need not be the same at each t_k, and measurement errors are assumed uncorrelated, with zero mean:

$$E\{\eta_k\} = 0, \qquad E\{\eta_k \eta_k{}^T\} = R_k \delta_{kk} \tag{4.5}$$

R_k is diagonal and represents the error covariance, defined by.

$$z_{t|k} = E\{z_k | y_{k'}, k' \le k\}, \qquad R_{t|k} = E\{\delta z_k \delta z_k{}^T | y_{k'}, k' \le k\} \tag{4.6}$$

For the time prediction of the algorithm $z_{t|k-1}$ is obtained over the interval (t_{k-1}, t_k) by integrating Equation 4.1, from t_{k-1} to t_k with initial values $x_{t|k-1}$.

To obtain the $P_{t|k-1}$ covariance matrix of $x_{t|k-1}$ a linearization of Equation 4.1 about $z_{t|k-1}$ is used:

$$\begin{aligned} f_{\dot{x}_1}^1 \delta\dot{x}_1 + f_{x_1}^1 \delta x_1 + f_{x_2}^1 \delta x_2 + f_u^1 \delta u = 0 \\ f_{x_2}^2 \delta x_2 + f_{x_1}^2 \delta x_1 + f_u^2 \delta u = 0 \end{aligned} \tag{4.7}$$

equivalently represented as

$$\begin{bmatrix} -f^1_{\dot{x}_1}\delta\dot{x}_1 \\ 0 \end{bmatrix} = \begin{bmatrix} f^1_{x_1} & f^1_{x_2} & f^1_u \\ f^2_{x_1} & f^2_{x_2} & f^2_u \end{bmatrix} \begin{bmatrix} \delta x_1 \\ \delta x_2 \\ \delta u \end{bmatrix} \tag{4.8}$$

$$\delta z_3 = -F_{31}\delta z_1, \qquad \delta z_2 = -F_{21}\delta z_1 \tag{4.9}$$

From (4.5) and (4.8) is then obtained:

$$\begin{aligned} P_{12}{}^T &= P_{21} = -F_{21}P_{11} \\ P_{22} &= F_{21}P_{11}F_{21}{}^T \\ P_{13}{}^T &= P_{31} = -F_{31}P_{11} \\ P_{23}{}^T &= P_{32} = F_{31}P_{11}F_{21}{}^T \\ P_{33} &= F_{31}P_{11}F_{31}{}^T \end{aligned} \tag{4.10}$$

Applying differentiation properties, the following equation is obtained.

$$\frac{d}{dt}(\delta x_1 \delta x_1{}^T) = \delta\dot{x}_1\delta x_1 + \delta x_1\delta\dot{x}_1$$

hence

$$\dot{P}_{11} = P_{31} + P_{31}{}^T \tag{4.11}$$

It is only required to integrate $f^1(\cdot) = 0$ in Equations 4.1 and 4.11 to obtain $z^1{}_{t|k-1}$ and P_{11} respectively, and then obtain algebraically $z^2{}_{t|k-1}$ from $f^2(\cdot) = 0$ and the remainder of P^- from (4.9) only at times of interest, such as t_k.

Once the estimation stage is completed, at each t_k, z^- and P^- are updated to z^+ and P^+ respectively taking account of final plant measurements (measurement update stage). Since equation 4.2 is linear, a linear minimum-variance estimate can be used.

$$z^+ = z^- + P^- M^T (MP^- M^T + Q)^{-1} (y - Mz^-) \tag{4.12}$$

$$P^+ = P^- - P^- M^T (MP^- M^T + Q)^{-1} MP^- \tag{4.13}$$

Lastly z^+ and P^+ become the initial conditions for the next iteration and the process is repeated all over. Figure 4.1 shows the complete sequence of the extended Kalman filter.

In order to avoid P^+ converging to zero and consequently no measurement update is generated, several researchers have proposed ways to tackle this effect. A forgetting factor σ can be included to put increased weight on recent measurements combined with a resetting factor for P^+ (Goodwin and Middleton, 1990). However this method has proven to be very difficult to implement in multivariable prediction cases. The most common technique is to add process noise to the covariance matrix every cycle avoiding the matrix tending to zero. Several researchers do not agree with this procedure because it artificially conditions the filter, however it has proven to be a simple and efficient solution.

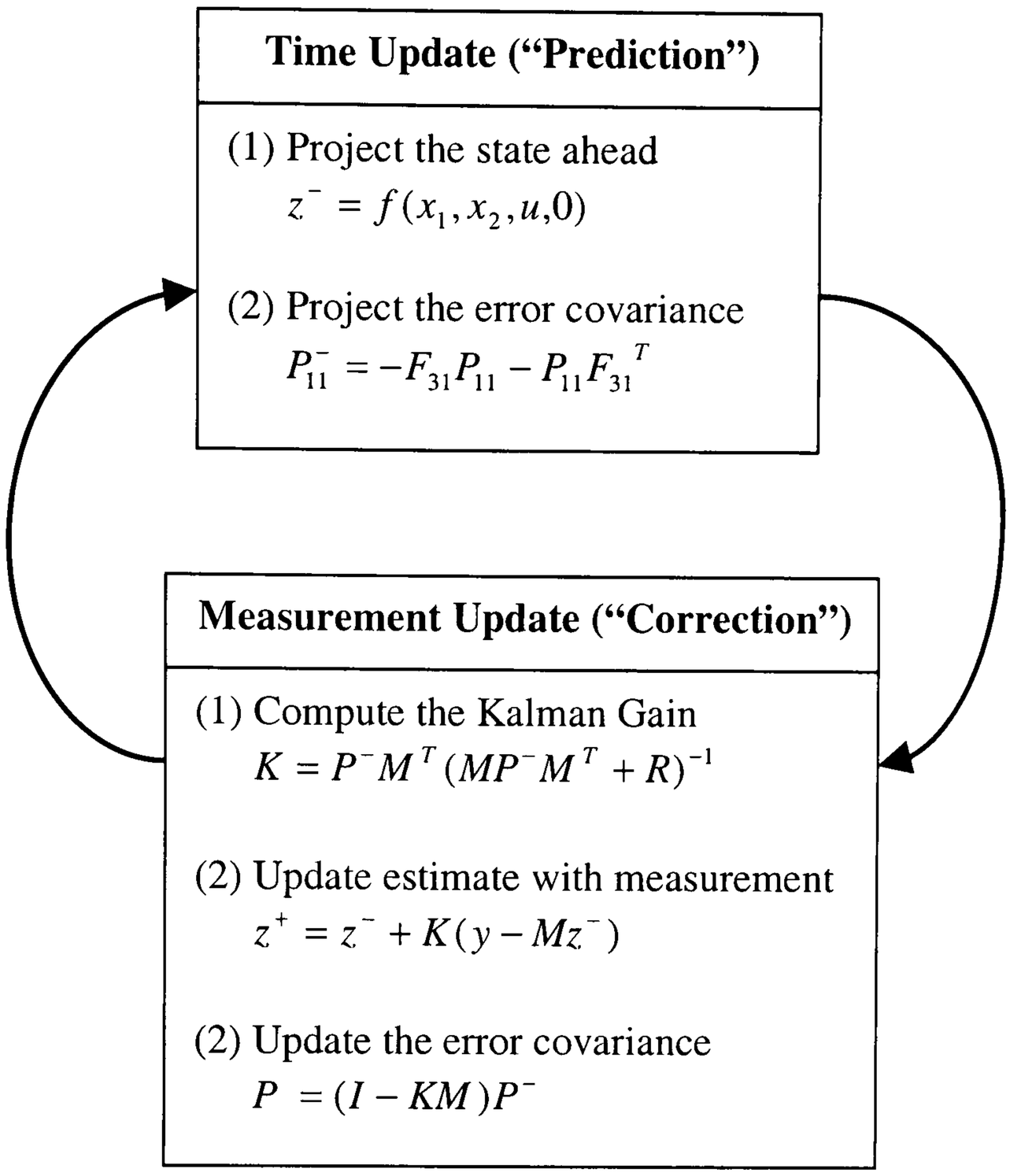


Figure 4.1 A complete sequence of the operation of the extended Kalman filter.

4.1.2.1 Variables Used for the Extended Kalman Filter

From the modelling section results, the absorber and desorber columns are modelled as lumped systems with 5 and 10 stages respectively. For the absorber each stage consists of a differential equation system in concentration and temperature. In contrast, only concentration derivatives appear in the desorber and the reboiler. In total twenty one variables are used to defined the complete state space vector which is defined as:

$$z_1 = [x^T \quad x_r \quad x_d^T \quad T_1^T]^T$$

where

x = Concentration of CO_2 in the liquid phase in the absorber (5-element vector).

x_r = Concentration of CO_2 in the liquid phase in the reboiler.

x_d = Concentration of CO_2 in the liquid phase vector in the desorber (10-element vector).

T_1 = Temperature vector in the absorber. (5-element vector).

Although some reduction of the algebraic equations is carried out, due to the nonlinearities of the model it is impossible to make a complete simplification to an ODE system. However the number of algebraic equations is condensed to 59, which is set as:

$$z_2 = [R^T \quad flo^T \quad y_{co}{}^T \quad P_r \quad T_r \quad V_b \quad B \quad P_d{}^T \quad T_2{}^T \quad fgd^T \quad fld^T]^T$$

where

R = CO_2 Absorption rate vector in the absorber. (5-element vector).

flo = Liquid flow rate vector in the absorber. (5-element vector).

y_{co} = Concentration of CO_2 in the gas phase vector in the absorber. (5-element vector).

P_r = Pressure in the reboiler.

T_r = Temperature in the reboiler.

V_b = Gas output flow rate in the reboiler.

B = Liquid output flow rate in the reboiler.

P_d = Pressure vector in the desorber. (10-element vector).

T_2 = Temperature vector in the desorber. (10-element vector).

fgd = Gas flow rate vector in the desorber. (10-element vector).

fld = Liquid flow rate vector in the desorber. (10-element vector).

4.1.2.2 Jacobian Matrices Used for the Extended Kalman Filter

This section shows the construction of the Jacobian matrices described earlier (equation 4.10). Because of its size the matrices are divided into more manageable subspaces. Each non-empty subspace is classified in one of the following four patterns.

$$Pattern1 = Diag = \begin{bmatrix} 1 & & & \\ & 1 & & \\ & & \ddots & \\ & & & 1 \end{bmatrix}, \qquad Pattern2 = \begin{bmatrix} 1 & & & \\ 1 & 1 & & \\ & \ddots & \ddots & \\ & & 1 & 1 \end{bmatrix},$$

$$Pattern3 = Pattern2^{T} = \begin{bmatrix} 1 & 1 & & \\ & \ddots & \ddots & \\ & & 1 & 1 \\ & & & 1 \end{bmatrix}, \qquad Pattern4 = \begin{bmatrix} 1 & 1 & & & \\ 1 & 1 & 1 & & \\ & \ddots & \ddots & \ddots & \\ & & 1 & 1 & 1 \\ & & & 1 & 1 \end{bmatrix}$$

where "1" in a cell means a non-null value; zero otherwise.

In order to clarify the representation used in the Jacobian matrices, three lines divide them either horizontally or vertically which represent from left to right and from top to bottom the absorber, reboiler and desorber subspaces respectively. The nomenclature used for the elements is shown below, which is simply the partial derivatives of the equations with respect to the variables.

$$f_{a,b} = \left.\frac{\partial f_a(b)}{\partial b}\right|_{a_o,b_0} \tag{4.14}$$

The $f_{x_2}^2$ Jacobian matrix is represented as follows

$$f_{x_2}^2 = \left[\begin{array}{ccc|cccc|cccc} f_{RR} & 0 & f_{R\cdot y_{CO}} & 0 & \cdots & & 0 & 0 & \cdots & & 0 \\ 0 & f_{flo\cdot flo} & f_{flo\cdot y_{CO}} & \vdots & & & f_{flo\cdot B} & \vdots & & & \vdots \\ f_{y_{CO}\cdot R} & 0 & f_{y_{CO}\cdot y_{CO}} & 0 & \cdots & & 0 & 0 & \cdots & & 0 \\ \hline 0 & \cdots & 0 & f_{\mathrm{Pr}\cdot \mathrm{Pr}} & f_{\mathrm{Pr}\cdot Tr} & 0 & 0 & 0 & 0 & 0 & 0 \\ \vdots & & \vdots & f_{Tr\cdot \mathrm{Pr}} & f_{Tr\cdot Tr} & f_{Tr\cdot Vb} & f_{Tr\cdot B} & 0 & f_{Tr\cdot T2} & 0 & f_{Tr\cdot fld} \\ & & & f_{Vb\cdot \mathrm{Pr}} & 0 & f_{Vb\cdot Vb} & 0 & f_{Vb\cdot Pd} & 0 & 0 & 0 \\ 0 & \cdots & 0 & 0 & 0 & f_{B\cdot Vb} & f_{B\cdot B} & 0 & 0 & 0 & f_{B\cdot fld} \\ \hline 0 & \cdots & 0 & 0 & 0 & 0 & 0 & f_{Pd\cdot Pd} & f_{Pd\cdot T2} & 0 & 0 \\ \vdots & & \vdots & f_{T2\cdot \mathrm{Pr}} & f_{T2\cdot Tr} & f_{T2\cdot Vb} & 0 & f_{T2\cdot Pd} & f_{T2\cdot T2} & f_{T2\cdot fgd} & f_{T2\cdot fld} \\ & & & 0 & 0 & 0 & 0 & f_{fgd\cdot Pd} & 0 & f_{fgd\cdot fgd} & 0 \\ 0 & \cdots & 0 & 0 & 0 & f_{fld\cdot Vb} & 0 & 0 & 0 & f_{fld\cdot fgd} & f_{fld\cdot fld} \end{array}\right] \tag{4.15}$$

where f_{RR}, $f_{yco,R}$, $f_{Pd,Pd}$, $f_{Pd,T2}$ and $f_{fgd,fgd}$ follow the pattern 1, $f_{R,yco}$ $f_{flo,yco}$, $f_{yco,yco}$, $f_{T2,Pd}$, $f_{T2,fgd}$ and $f_{fld,fgd}$ are pattern 2, $f_{flo,flo}$, $f_{T2,fld}$, $f_{fgd,Pd}$, $f_{fld,fld}$ are pattern 3 and $f_{T2,T2}$ is pattern 4

$f_{flo,B}$ is a column vector with the following pattern [0 0 … 1], while $f_{T2,\mathrm{Pr}}$, $f_{T2,Tr}$, $f_{T2,Vb}$, $f_{fld,Vb}$, $f_{Tr,T2}$, $f_{Tr,fld}$, $f_{Vb,Pd}$ and $f_{B,fld}$ are vectors with the pattern: [1 0 0 … 0]. $f_{\mathrm{Pr},\mathrm{Pr}}$, $f_{\mathrm{Pr},Tr}$, $f_{Tr,\mathrm{Pr}}$, $f_{Tr,Tr}$, $f_{Tr,Vb}$, $f_{Tr,B}$, $f_{Vb,\mathrm{Pr}}$, $f_{Vb,Vb}$, $f_{B,Vb}$ and $f_{B,B}$ are scalars.

The $f_{x_2}^1$ Jacobian matrix has the following shape

$$f_{x_2}^1 = \left[\begin{array}{ccc|cccc|cccc} f_{x\cdot R} & f_{x\cdot flo} & f_{x\cdot y_{CO}} & 0 & \cdots & 0 & f_{x\cdot B} & 0 & \cdots & & 0 \\ \hline 0 & 0 & 0 & f_{xr\cdot \mathrm{Pr}} & f_{xr\cdot Tr} & f_{xr\cdot Vb} & 0 & 0 & 0 & 0 & f_{xr\cdot fld} \\ \hline 0 & 0 & 0 & f_{xd\cdot \mathrm{Pr}} & f_{xd\cdot Tr} & f_{xd\cdot Vb} & 0 & f_{xd\cdot Pd} & f_{xd\cdot T2} & f_{xd\cdot fgd} & f_{xd\cdot fld} \\ \hline f_{T\cdot R} & f_{T\cdot flo} & f_{T\cdot y_{CO}} & 0 & \cdots & 0 & f_{T\cdot B} & 0 & \cdots & & 0 \end{array}\right] \tag{4.16}$$

where $f_{x,R}$, $f_{x,yco}$, and $f_{T,R}$ follow the pattern 1, $f_{T1,yco}$ $f_{xd,Pd}$, $f_{xd,T2}$ and $f_{xd,fgd}$, are pattern 2, $f_{x,flo}$, $f_{T1,flo}$, and $f_{xd,fld}$, are pattern 3, $f_{x,B}$ and $f_{T1,B}$ are column vector with the following pattern [0 … 0 1], while $f_{xr,fld}$, $f_{xd,\mathrm{Pr}}$, $f_{xd,Tr}$ and $f_{xd,Vb}$ are vectors like [1 0 … 0], and $f_{xd,\mathrm{Pr}}$, $f_{xd,Tr}$ and $f_{xd,Vb}$ are scalars

The $f_{x_1}^2$ Jacobian matrix is:

$$f_{x_1}^2 = \left[\begin{array}{c|c|c|c} f_{R\cdot X} & 0 & 0 & f_{R\cdot T1} \\ 0 & \vdots & \vdots & f_{flo\cdot T1} \\ f_{yco\cdot X} & 0 & 0 & f_{yco\cdot T1} \\ \hline 0 & f_{\Pr\cdot Xr} & 0 & 0 \\ \vdots & f_{Tr\cdot Xr} & \vdots & \vdots \\ & 0 & & \\ 0 & 0 & 0 & 0 \\ \hline 0 & 0 & f_{Pd\cdot Xd} & 0 \\ \vdots & f_{T2\cdot Xr} & f_{T2\cdot Xd} & \vdots \\ & 0 & 0 & \\ 0 & 0 & 0 & 0 \end{array}\right] \tag{4.17}$$

where $f_{R,x}$, $f_{yco,x}$ and $f_{Pd,xd}$ follow the pattern 1, $f_{R,T1}$ $f_{flo,T1}$, $f_{yco,T1}$ and $f_{T2,xd}$, are pattern 2, $f_{T2,xr}$ is a column vector with the following pattern [1 0 … 0], while $f_{\Pr,xr}$ and $f_{Tr,xr}$ are scalars

The $f_{x_1}^1$ Jacobian matrix is defined as

$$f_{x_1}^1 = \begin{bmatrix} f_{x\cdot x} & 0 & 0 & f_{x\cdot T} \\ 0 & f_{xr\cdot xr} & f_{xr\cdot xd} & 0 \\ 0 & f_{xd\cdot xr} & f_{xd\cdot xd} & 0 \\ 0 & 0 & 0 & f_{T\cdot T} \end{bmatrix} \tag{4.18}$$

where $f_{x,T1}$ follows the pattern 1, $f_{x,x}$ is pattern 3, $f_{T1,T1}$ and $f_{xd,xd}$ are pattern 4, $f_{xr,xd}$ and $f_{xd,xr}$ are vectors with the following pattern [1 0 … 0], while $f_{xr,xr}$ is a scalar.

The integration of the nonlinear model is carried out by gPROMS, while the linear integration of the covariance matrix P_{11} is done by MATLAB.

The gPROMS feature, Foreign Process Interface (FPI), is used to extract the Jacobian matrix elements from the model at the beginning of the time update interval

(simulation). Several experiments tracking those values showed no significant change rate during the sampling interval, therefore these values are assumed constant during the whole interval.

Once the Jacobian elements are exported to MATLAB, the covariance matrix is reconstructed and integrated using ODE solvers for the interval length. Later the state variables and covariance matrix are updated with the measurements from the real plant and sent back to gPROMS using again FPI commands, where they are employed as initial conditions for the next interval. Figure 4.2 shows a diagram describing the process. For more information about gPROMS's FPI commands, please refer to the "gPROMS Advanced user guide".

During the measurement update executed by Matlab, all parametric values of the state variables are bounded between lower and upper limits: 0.1 and 1.8 respectively.

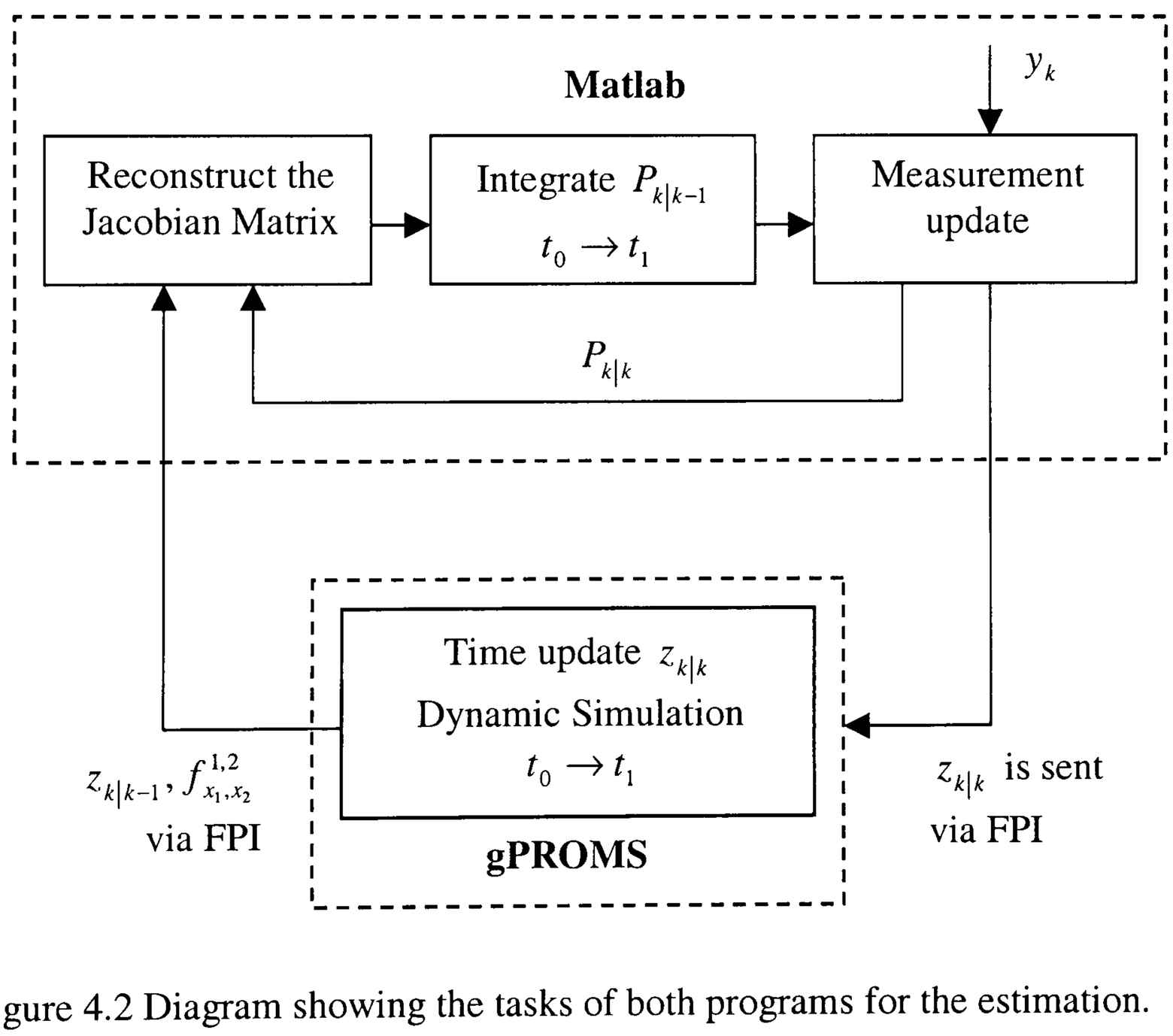


Figure 4.2 Diagram showing the tasks of both programs for the estimation.

4.1.3. Simulation Test

In order to test the Kalman filter previously developed, a simulated test is run, perturbing the feed conditions in the absorber several times.

13 measurements from the plant are used to correct the estimation in the EKF (see Table 4.1). These measurements are firstly computed offline using a perfect and undisturbed model. Later they are injected to the estimation process at their respective times with an added Gaussian noise to check the stochastic properties of the filter. The covariance values for the measurement errors are obtained from the absolute errors reported for each instrument.

To study the tracking properties of the filter, step changes in the CO_2 feed concentration are made at different intervals. Table 4.2 shows the step changes made in the CO_2 absorber feed concentration. The other input variables are fixed at their standard values. Figure 4.3 to 4.7 show the results obtained. (The results reported are the average of 20 runs).

Measurement	Element	Abs Error (±)
CO_2 final gas concentration	yco(5)	5 ppm
pH of liquid leaving the reboiler	xr	0.05 pH
pH of liquid leaving the absorber	x(1)	0.05 pH
Recirculation flow rate	B	0.01 kg/s
Temperature at top of absorber	T1(5)	0.5 °C
Temperature at half middle top of absorber	T1(4)	0.5 °C
Temperature at middle of absorber	T1(3)	0.5 °C
Temperature at half middle bottom of absorber	T1(2)	0.5 °C
Temperature at bottom of absorber	T1(1)	0.5 °C
Temperature top desorber	T2(10)	0.5 °C
Temperature middle desorber	T2(5)	0.5 °C
Temperature bottom desorber	T2(1)	0.5 °C
Temperature reboiler	Tr	0.5 °C

Table 4.1. Measurements considered for the EKF test.

Interval [s]	0 - 300	300 - 660	< 660
CO2 gas feed [%]	4	6	3

Table 4.2. Step changes made in CO_2 feed concentration.

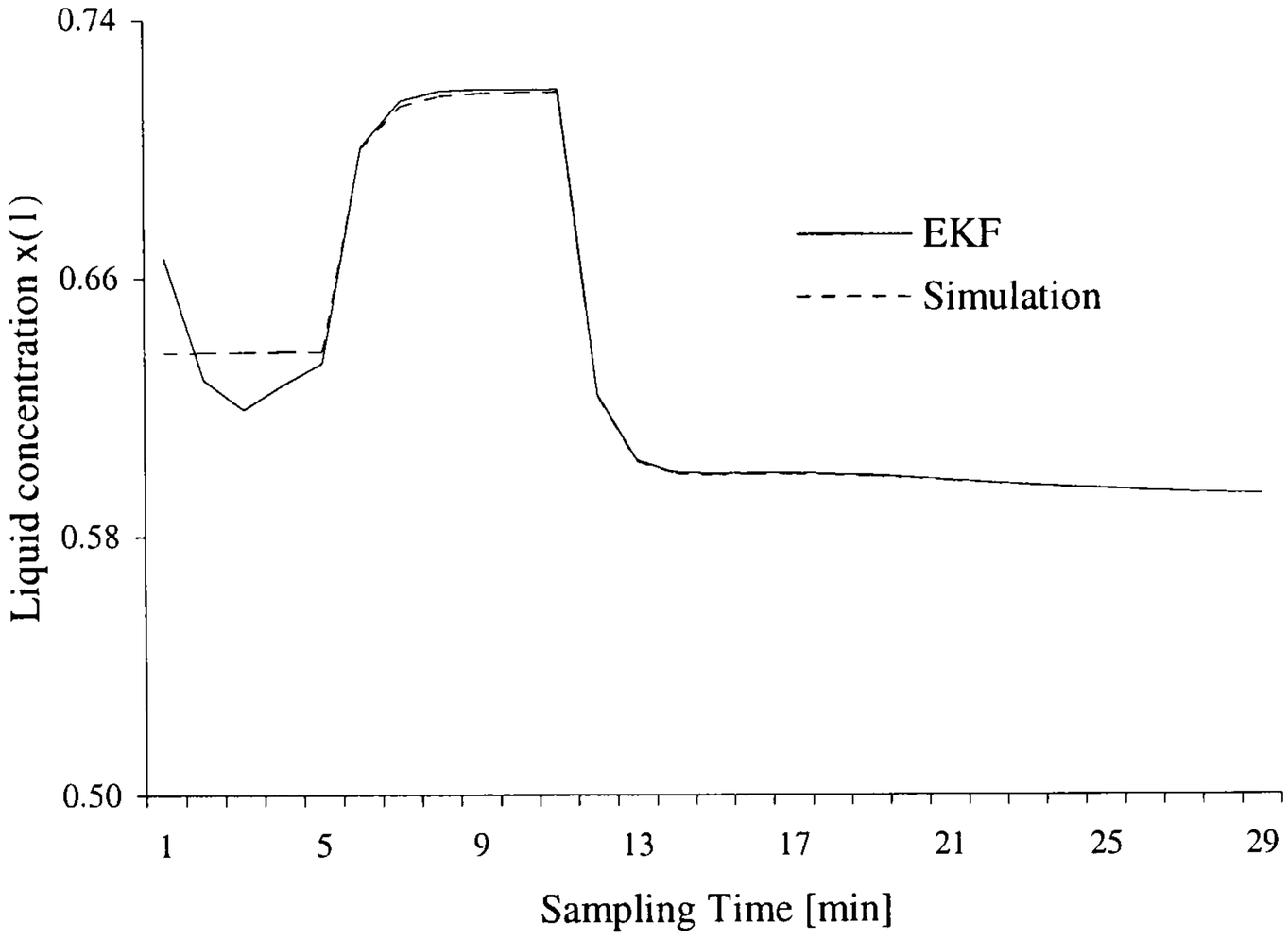


Figure 4.3 Parameterised absorber bottom liquid CO_2 concentration

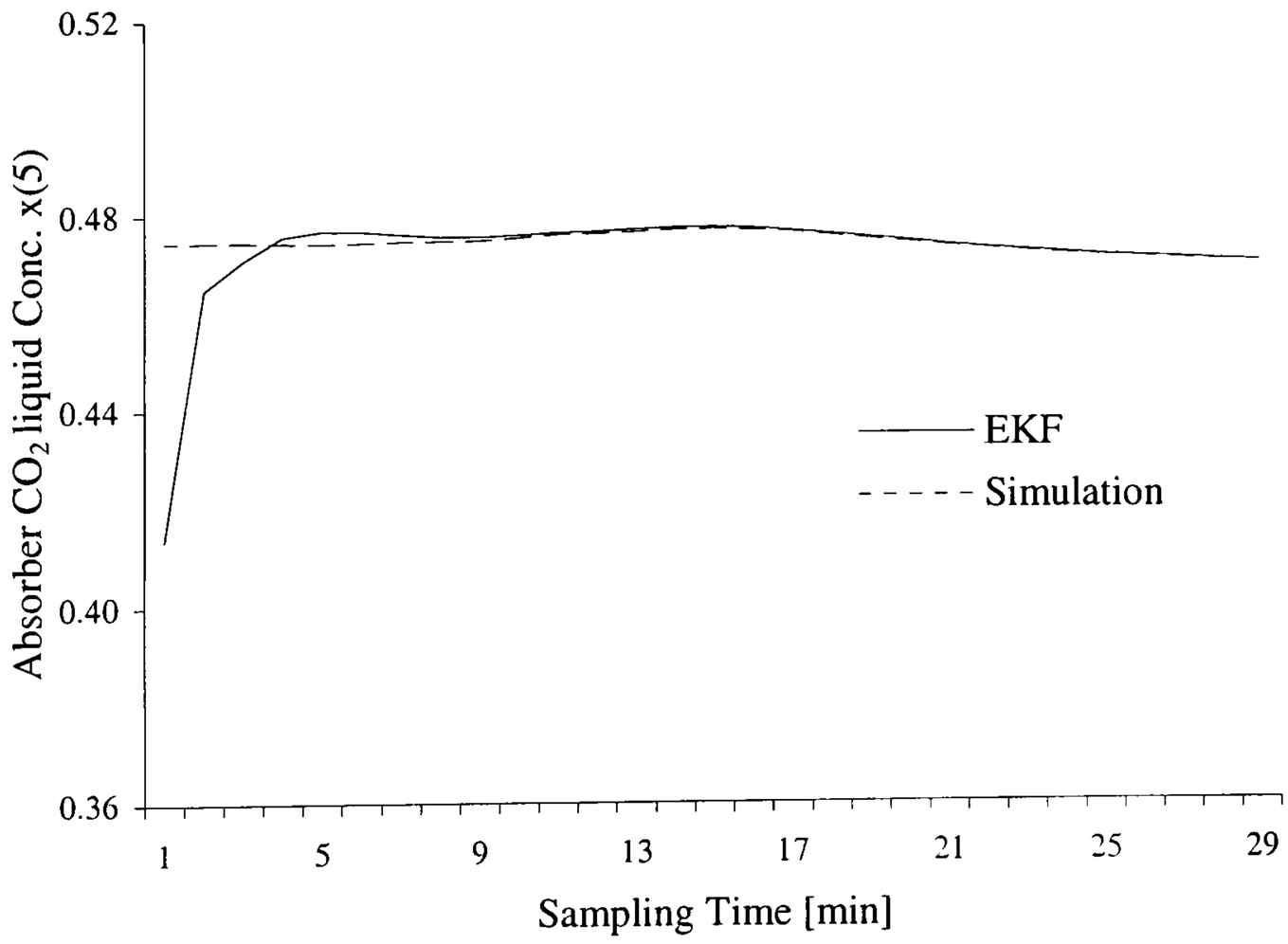


Figure 4.4 Parameterised absorber top liquid CO_2 concentration

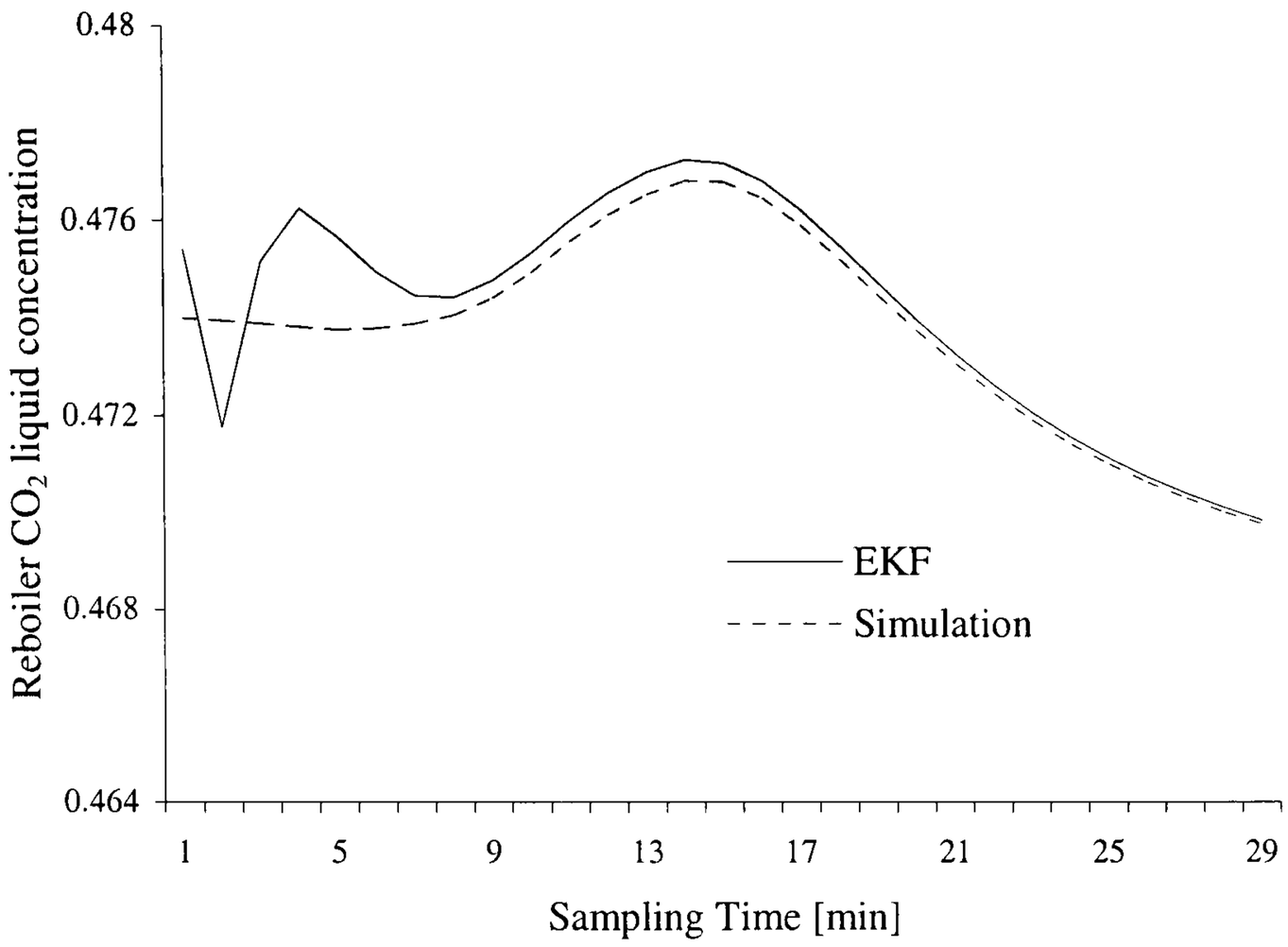


Figure 4.5 Reboiler CO_2 liquid concentration

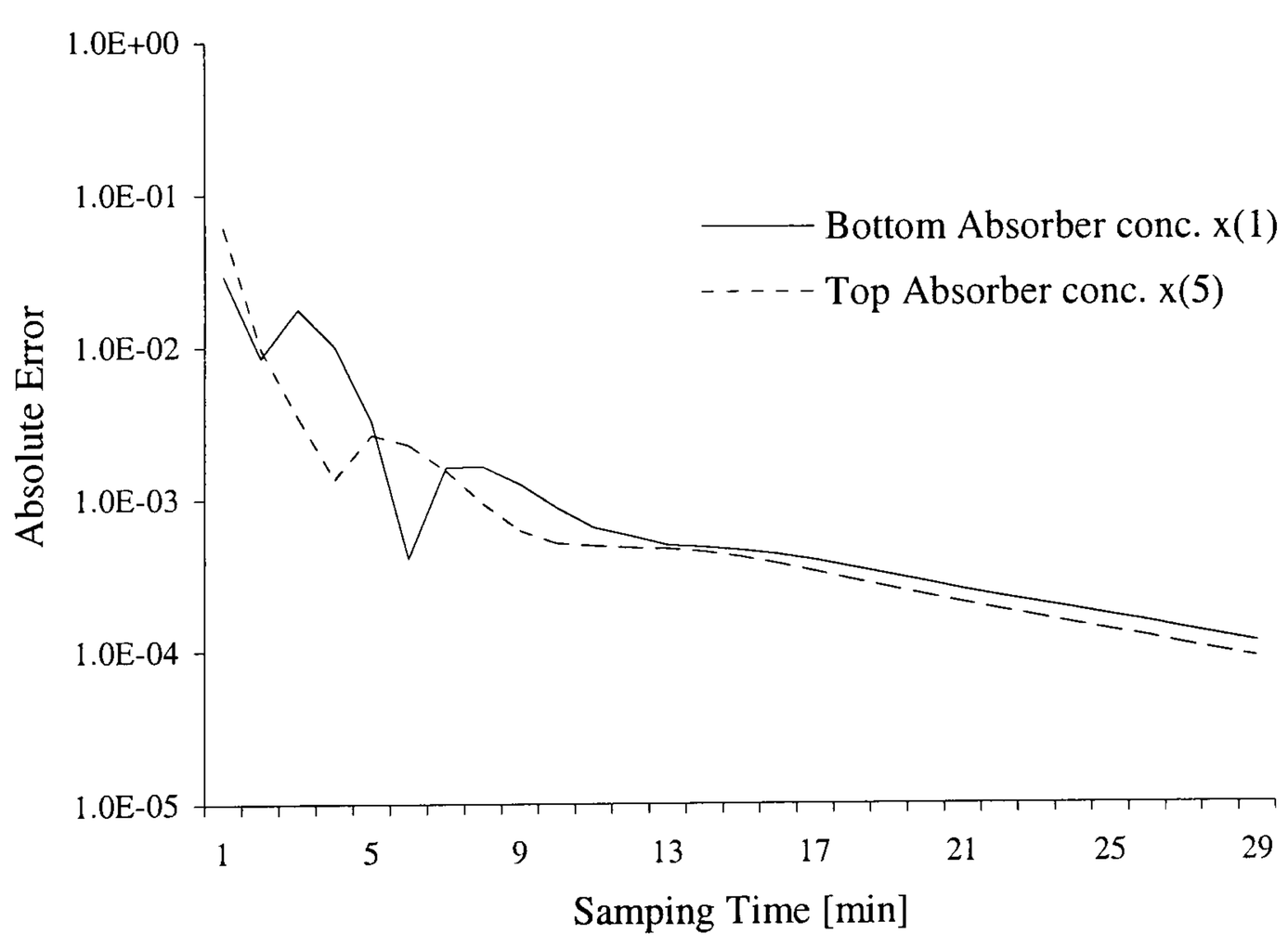


Figure 4.6 Absolute errors in absorber liquid concentration

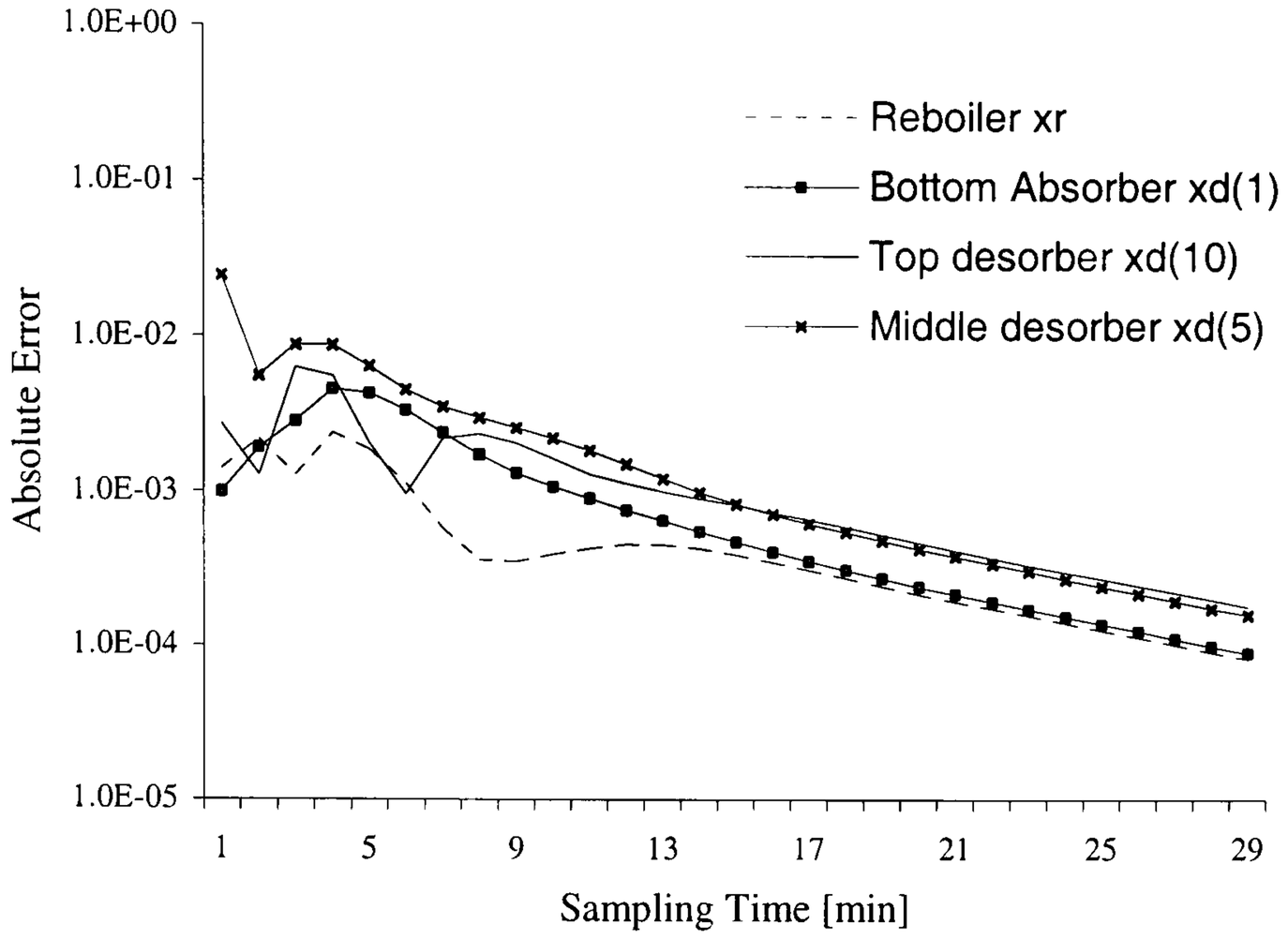


Figure 4.7 Absolute errors in reboiler and desorber liquid concentration

Under perfect conditions the Kalman filter proves outstanding at tracking all the state variables in the process. Although at the beginning the estimation has an oscillatory behaviour, mainly due to the selected initial conditions, only 4 iterations are required to converge to the real values, with an absolute error of approximately 1%, decreasing to less than 0.1% after nearly 30 intervals.

Is clear from these results that the EKF tracks exceptionally well the measured and unmeasured state variables of the simulated plant, even under noisy measurements.

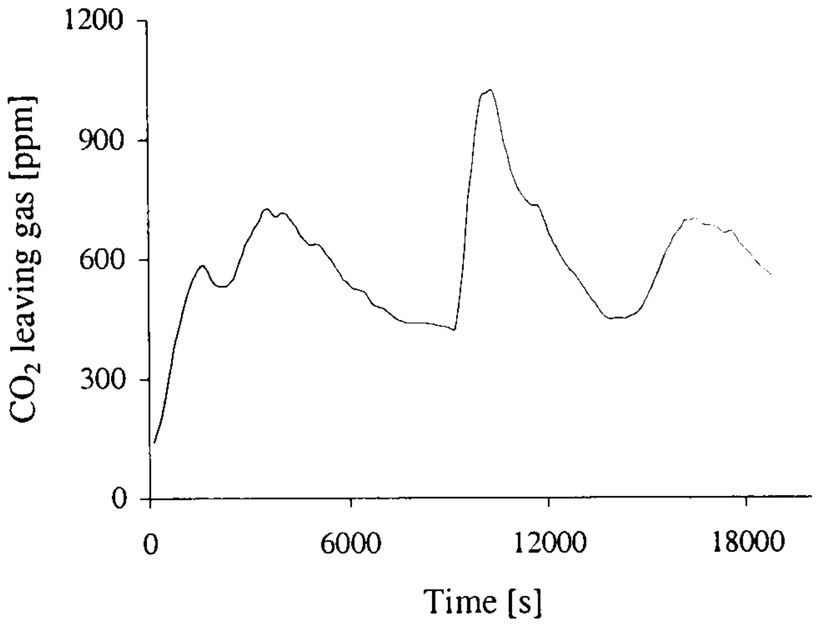
4.1.4. Comparison Between Two Methods

With the purpose of comparing the classical and well-proved steady state estimation technique (see p84) and the extended Kalman filter a set of real experimental data from the pilot plant is used to compare the estimated value of the CO_2 gas leaving concentration.

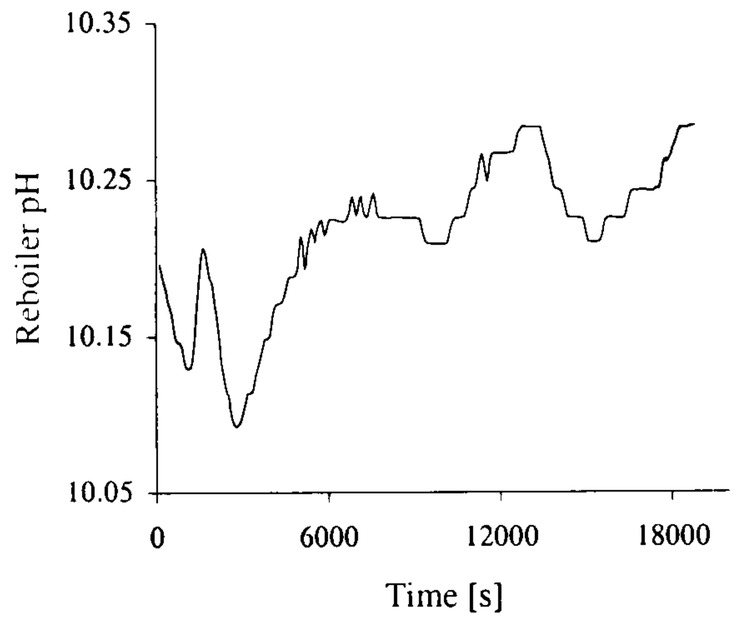
This experiment simulates a servo problem with disturbances in the gas feed CO_2 composition at t = 9300 s. The sampling interval is taken every 60 seconds.

The experiment is chosen for two reasons. The first is one of the few runs reported where the steady state approximation values are shown. In the second the plant is at dynamic conditions, so a more realistic behaviour of the estimators would be reflected as a consequence.

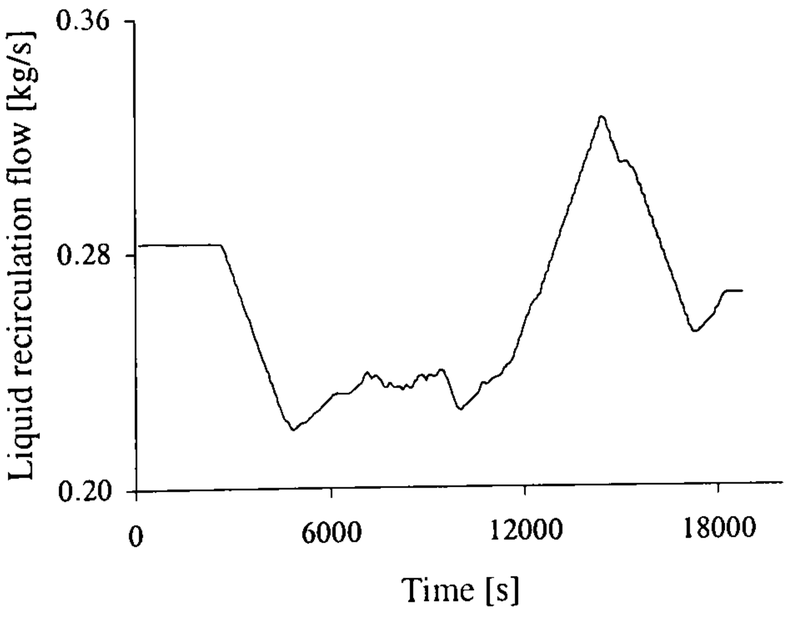
Figure 4.8 shows the real measurements from the plant



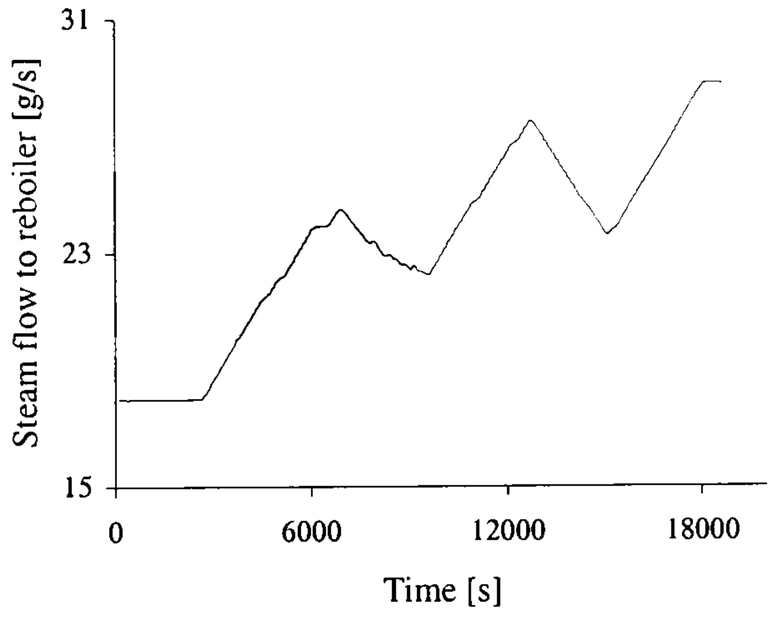
a) Gas leaving CO_2 concentratiorn



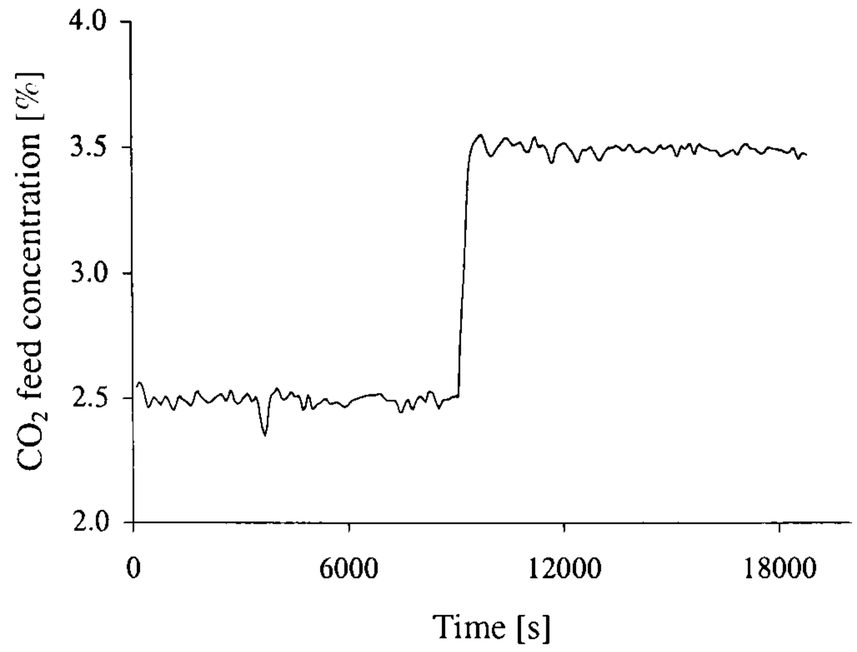
b) Liquid pH in the reboiler



c) Liquid recirculation flow



d) Steam flow



e) CO_2 gas feed composition

Figure 4.8 Experimental data obtained from Rotava's research ("Nexp 5")

The results obtained comparing both approaches are shown Figures 4.9 and Figure 4.10 .

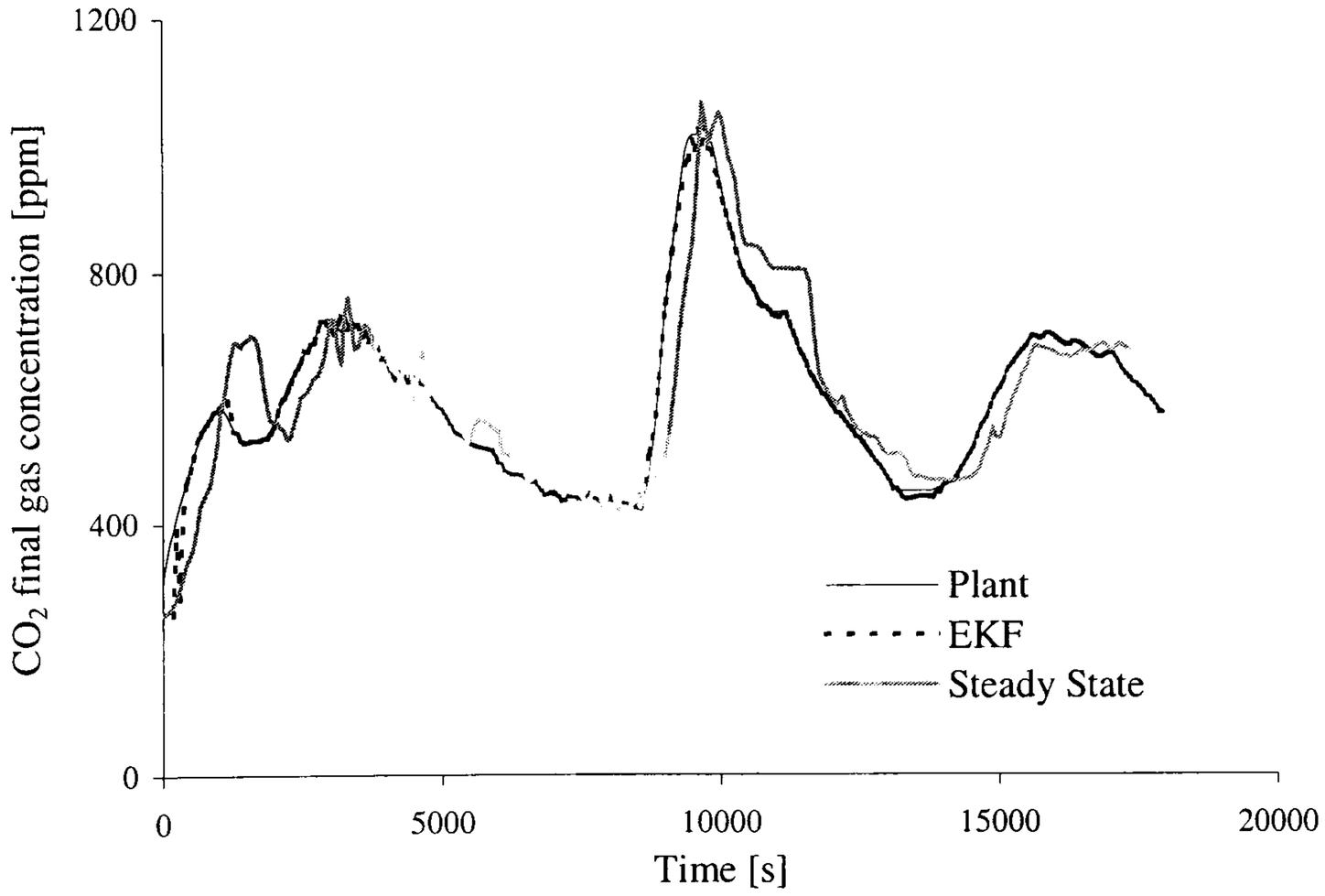


Figure 4.9 Comparison between Extended Kalman Filter and the steady state estimation.

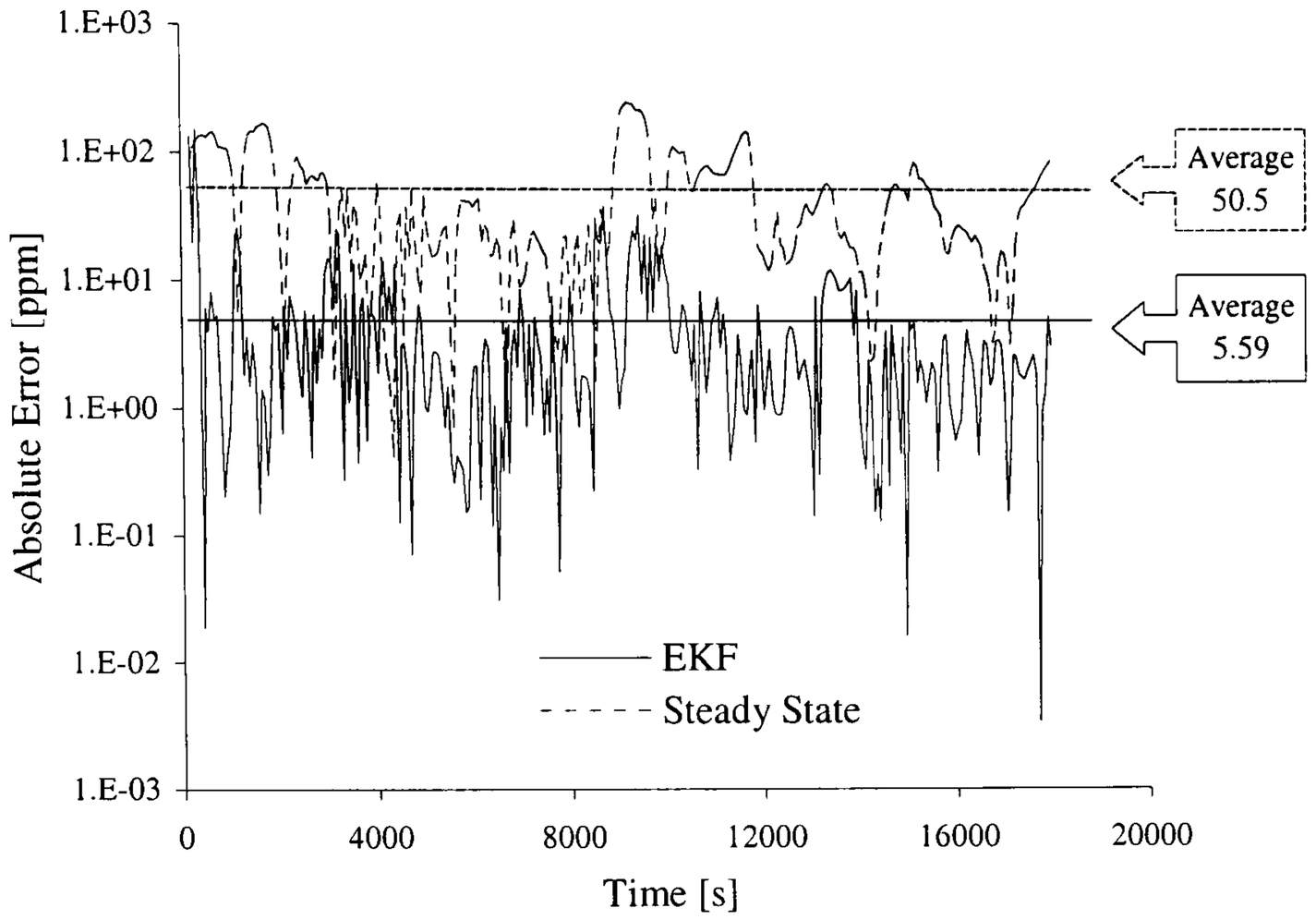


Figure 4.10 Comparison between Extended Kalman Filter and the steady state absolute errors.

It is clear that the estimation made by EKF is considerably better than that made by steady state approximation. Even the lag observed in the steady state estimation is not perceived in the EKF.

The absolute error averages reported in Figure 4.10 prove the EKF is approximately one order of magnitude more accurate than the steady state approach.

Considering that the final CO_2 gas concentration is measured in such small units, parts per million (ppm), and are quite sensitive to process noise, feed disturbances and instrument errors, the results prove the superiority of the EKF as an observer compared with a deterministic observer, with an average absolute error of nearly 5 ppm.

Due to its error management and stochastic abilities, the EKF has demonstrated being by far being the best estimation technique to be used in the MPC.

4.2. Unknown Parameter Estimation

While the state variables are computed from the present data using the previous algorithm, the estimation of unknown parameters helps to close errors between the plant and the model in the long run. The estimation techniques previously exposed could also be used to estimate unknown parameters.

Several researchers agree that although unknown parameters help to reduce the mismatch, it is not clear how many of them should be included in the formulation. Choosing too many parameters could cause stability problems and even increase the error between model and plant. For this reason it is important to carefully select the set of parameters that would be used in the estimation process.

Originally the model contains six unknown parameters: Absorption constant (κ), MEA liquid concentration (C_{mea}), desorber tray efficiency (ε) and the absorber, desorber and reboiler heat loss (Q_{la}, Q_{ld}, Q_{lr}). Table 4.3 shows the minimum and maximum values allowed for each parameter in the model.

Parameter	Units	Min value	Max value	Normal value
Absorption constant (κ)	$kmol \cdot s^{3/2}/kg$	0.0	$9.0\ 10^{-6}$	$4.5\ 10^{-6}$
MEA Concentration (C_{mea})	$kmol/m^3$	1500	5500	2500
Desorber tray efficiency (ε)	-	0.1	2	1
Absorber lost heat (Q_{la})	kJ/s	-5	5	0
Desorber lost heat (Q_{ld})	kJ/s	-50	50	0
Reboiler lost heat (Q_{lr})	kJ/s	-100	100	0

Table 4.3. Unknown parameters in the model.

4.2.1. Unknown Parameter Sensitivity

To select the best group of unknown parameters, a qualitative experiment is done. Two sets of experimental data are fitted using a minimum quadratic error (see Appendix B). The idea is to select those parameters which can significantly reduce the error in the estimation. For this process the gPROMS estimation package gEST is used.

Although this calculation is not conclusive, it gives a good indication which parameter should be used.

For the first experiment both sets of data are fitted using a single parameter. In other words, gEST must fit as well as possible a single parameter to the final value of CO_2 in the absorber and the reboiler's pH. The idea is to select those parameters that made the largest reduction in the sum of the residuals errors in the estimation. Table 4.4 and 4.5 show the results obtained.

Parameter	Value	Sum residual	Position
ε	0.232	11650	1
κ	$3.11 \cdot 10^{-6}$	60861	2
Q_{lr}	23.13	263169	3
Q_{ld}	2.44	362273	4
C_{mea}	1500.0	1220196	5
Q_{la}	3.60	1728880	6

Table 4.4. Case 1. Individual effect of each unknown parameter.

Parameter	Value	Sum residual	Position
C_{mea}	2293.5	113849	1
κ	$4.46 \cdot 10^{-6}$	120080	2
Q_{la}	0.06	142306	3
ε	2.0	498000	4
Q_{lr}	-100.0	515584	5
Q_{ld}	-31.89	688632	6

Table 4.5. Case 2. Individual effect of each unknown parameter.

From both results there is no direct indication which is the best parameter that fitted the experimental data, for instance in Case 1, the tray efficiency in the desorber ε is the best parameter, however it reaches fourth place in Case 2. On the other hand, MEA concentration C_{mea} is the best option for the Case 2 but the fifth best in the Case 1. However the only parameter that scores well in both cases is the absorption constant rate (κ) with a second place in both experiments. This first analysis shows a good correlation between this parameter and the final CO_2 gas concentration.

For the next experiments, both cases are tested again using the absorption constant κ in tandem with any other parameters. Table 4.6 and 4.7 show the results obtained.

Parameter	Value	κ value	Sum residual	Position
Q_{ld}	1.30	$3.21 \cdot 10^{-6}$	2789	1
Q_{lr}	1.35	$3.13 \cdot 10^{-6}$	2936	2
Q_{la}	0.30	$3.19 \cdot 10^{-6}$	2986	3
C_{mea}	2062.9	$3.37 \cdot 10^{-6}$	3299	4
ε	0.359	$3.77 \cdot 10^{-6}$	3836	5

Table 4.6. Case 1. Effect of each unknown parameter in tandem with κ.

Parameter	Value	κ value	Sum residual	Position
Q_{ld}	1.89	$4.70 \cdot 10^{-6}$	64146	1
C_{mea}	2017.5	$4.17 \cdot 10^{-6}$	71203	2
Q_{lr}	30.81	$4.77 \cdot 10^{-6}$	71760	3
ε	0.317	$4.76 \cdot 10^{-6}$	73142	4
Q_{la}	1.44	$4.21 \cdot 10^{-6}$	105110	5

Table 4.7. Case 2. Effect of each unknown parameter in tandem with κ.

Firstly is important to notice the reduction of the sum residual values once two parameters are implemented in tandem with the absorption constant. A reduction between 50% and 75% is obtained, making clear that dual parameter estimation is a better strategy, than using a single one. Secondly the best pair is the desorber heat loss (Q_{ld}) and the absorption constant κ. In both cases Q_{ld} scores as the best parameter, however the difference among other parameters forerunners is very close so C_{mea} and Q_{lr} are considered good options.

Continuing the procedure, the next experiment is done by estimating κ, Q_{ld} and an extra parameter. Results are shown in Tables 4.8 and 4.9.

Parameter	Value	κ value	Qld value	Sum residual	Position
Q_{la}	0.62	$3.36 \cdot 10^{-6}$	1.25	2555	1
Q_{lr}	1.74	$3.24 \cdot 10^{-6}$	1.26	2632	2
C_{mea}	1740.4	$3.65 \cdot 10^{-6}$	0.56	2781	3
ε	0.456	$3.63 \cdot 10^{-6}$	0.72	2710	4

Table 4.8. Case 1. Effect of each unknown parameter in tandem with κ and Qld.

Parameter	Value	κ value	Qld value	Sum residual	Position
C_{mea}	1756.5	$4.71 \cdot 10^{-6}$	1.16	58965	1
Q_{lr}	0.65	$4.70 \cdot 10^{-6}$	1.25	59101	2
ε	0.478	$4.69 \cdot 10^{-6}$	0.94	61143	3
Q_{la}	0.87	$4.69 \cdot 10^{-6}$	0.85	63045	4

Table 4.9. Case 2. Effect of each unknown parameter in tandem with κ and Qld.

The incorporation of a third parameter in the estimation process clearly shows that there is not real improvement in the results obtained before. Also there is not a clear parameter that leads the upgrading in both cases. It is very clear that the estimation process should be restrained to a couple of parameters to maintain the simplicity and efficiency of the estimation process.

As a conclusion, for the next step only the absorption constant κ should be used in combination with either the desorber heat loss Q_{ld} or the MEA concentration C_{mea}. The other parameters will be fixed at their optimal values throughout all the process. Further experiments are done in order to definitely select the final unknown parameters in the model.

4.2.2. Joint Kalman Filter

The previously mentioned unknown parameters can be considered extra state variables in the Kalman filter by simply extending the Jacobian matrices and assuming that their derivatives are zero. The following section shows the new Kalman formulation including the absorption constant (κ) and desorber heat loss (Q_{ld}). The matrices are divided in two zones, the greyish one is the original Kalman filter, while the white

regions represent the new additions. Note the $f_{x_2}^2$ matrix does not suffer any change because it depends exclusively on algebraic variables, so it will remain identical to the previous case (equation 4.15).

Equation 4.19 shows the new representation for the Jacobian matrix $f_{x_1}^2$.

$$f_{x_1}^2 = \left[\begin{array}{c|ccc|cc} f_{R\text{-}X} & 0 & 0 & f_{R\text{-}T1} & f_{R\text{-}\kappa} & 0 \\ 0 & \vdots & \vdots & f_{flo\text{-}T1} & 0 & \vdots \\ f_{yco\text{-}X} & 0 & 0 & f_{yco\text{-}T1} & 0 & 0 \\ \hline 0 & f_{Pr\text{-}Xr} & 0 & 0 & 0 & 0 \\ \vdots & f_{Tr\text{-}Xr} & \vdots & \vdots & \vdots & \vdots \\ & 0 & & & & \\ 0 & 0 & 0 & 0 & 0 & 0 \\ \hline 0 & 0 & f_{Td\text{-}Xd} & 0 & 0 & 0 \\ \vdots & f_{T_2\text{-}Xr} & f_{T_2\text{-}Xd} & \vdots & \vdots & f_{T_2\text{-}Q_{ld}} \\ & 0 & 0 & & & 0 \\ 0 & 0 & 0 & 0 & 0 & 0 \end{array}\right] \tag{4.19}$$

The new $f_{x_2}^1$ Jacobian matrix is represented as

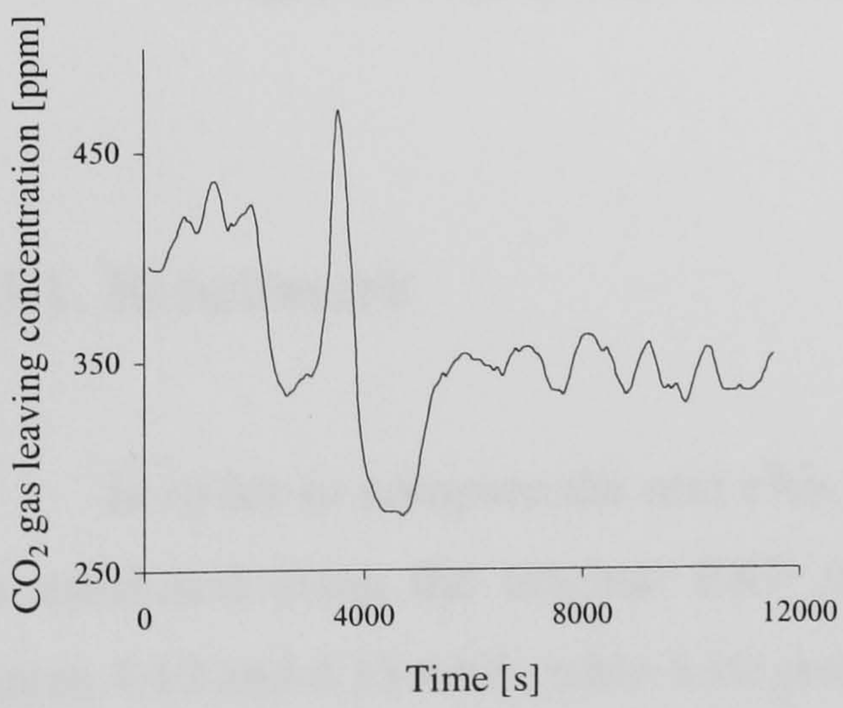
$$f_{x_2}^1 = \left[\begin{array}{ccc|ccc|c|cccc} f_{x\text{-}R} & f_{x\text{-}flo} & f_{x\text{-}y_{CO}} & 0 & \cdots & 0 & f_{x\text{-}B} & 0 & \cdots & & 0 \\ \hline 0 & 0 & 0 & f_{xr\text{-}Pr} & f_{xr\text{-}Tr} & f_{xr\text{-}Vb} & 0 & 0 & 0 & 0 & f_{xr\text{-}fld} \\ \hline 0 & 0 & 0 & f_{xd\text{-}Pr} & f_{xd\text{-}Tr} & f_{xd\text{-}Vb} & 0 & f_{xd\text{-}Pd} & f_{xd\text{-}T2} & f_{xd\text{-}fgd} & f_{xd\text{-}fld} \\ \hline f_{T\text{-}R} & f_{T\text{-}flo} & f_{T\text{-}y_{CO}} & 0 & \cdots & 0 & f_{T\text{-}B} & 0 & \cdots & & 0 \\ \hline 0 & \cdots & 0 & 0 & \cdots & & 0 & 0 & \cdots & & 0 \\ 0 & \cdots & 0 & 0 & \cdots & & 0 & 0 & \cdots & & 0 \end{array}\right] \tag{4.20}$$

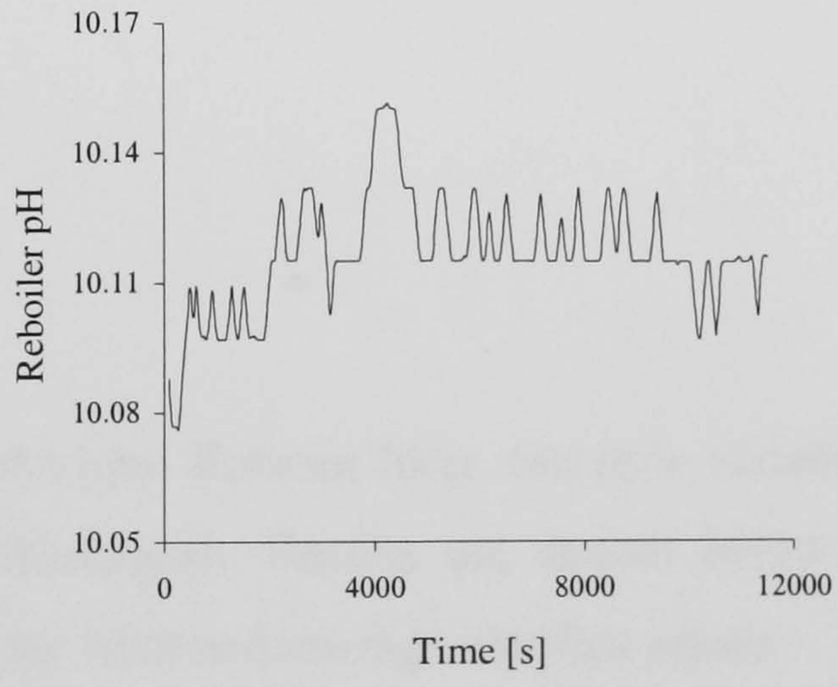
while $f_{x_1}^1$ matrix is enlarged as follows.

$$f_{x_1}^1 = \left[\begin{array}{cccc|cc} f_{x\cdot x} & 0 & 0 & f_{x\cdot T} & 0 & 0 \\ 0 & f_{xr\cdot xr} & f_{xr\cdot xd} & 0 & 0 & 0 \\ 0 & f_{xd\cdot xr} & f_{xd\cdot xd} & 0 & 0 & 0 \\ 0 & 0 & 0 & f_{T\cdot T} & 0 & 0 \\ \hline 0 & \cdots & & 0 & 0 & 0 \\ 0 & \cdots & & 0 & 0 & 0 \end{array}\right] \tag{4.21}$$

4.3. Simulation Test

In order to test the joint Kalman filter and also to finally select the best group of unknown parameters, the estimator is tested using real experimental data. Initially a simple EKF is used to estimate the state variables to have a benchmark. Later different combinations of the selected parameters are tested and compared. Figure 4.11 shows the experimental data used for these experiments.





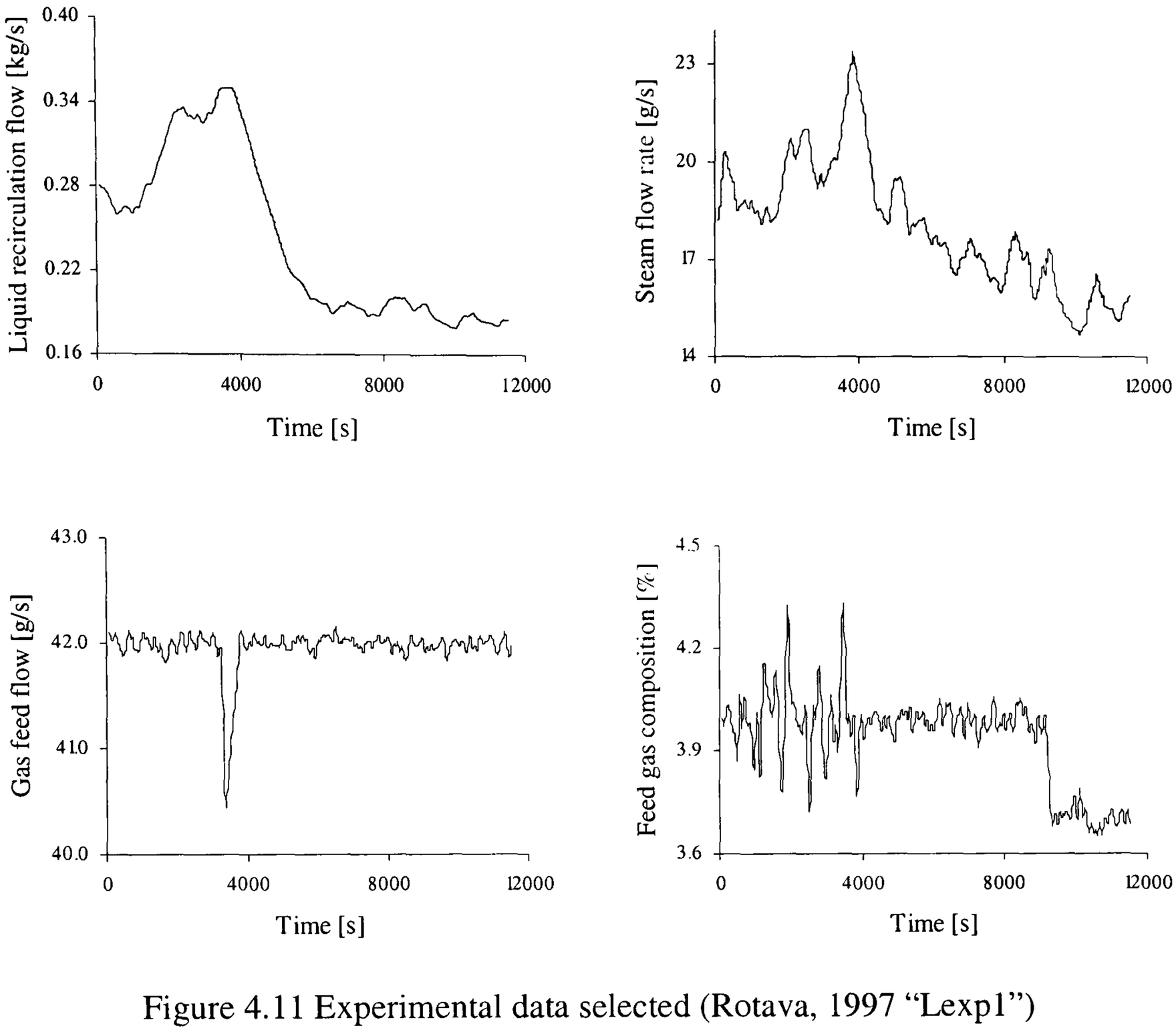


Figure 4.11 Experimental data selected (Rotava, 1997 "Lexp1")

4.3.1. Benchmark

In order to compare the real effect of the joint Kalman filter, the state variables are estimated using the original EKF as a benchmark. Results are shown below in figures 4.12 and 4.13 while table 4.10 presents the obtained average absolute errors

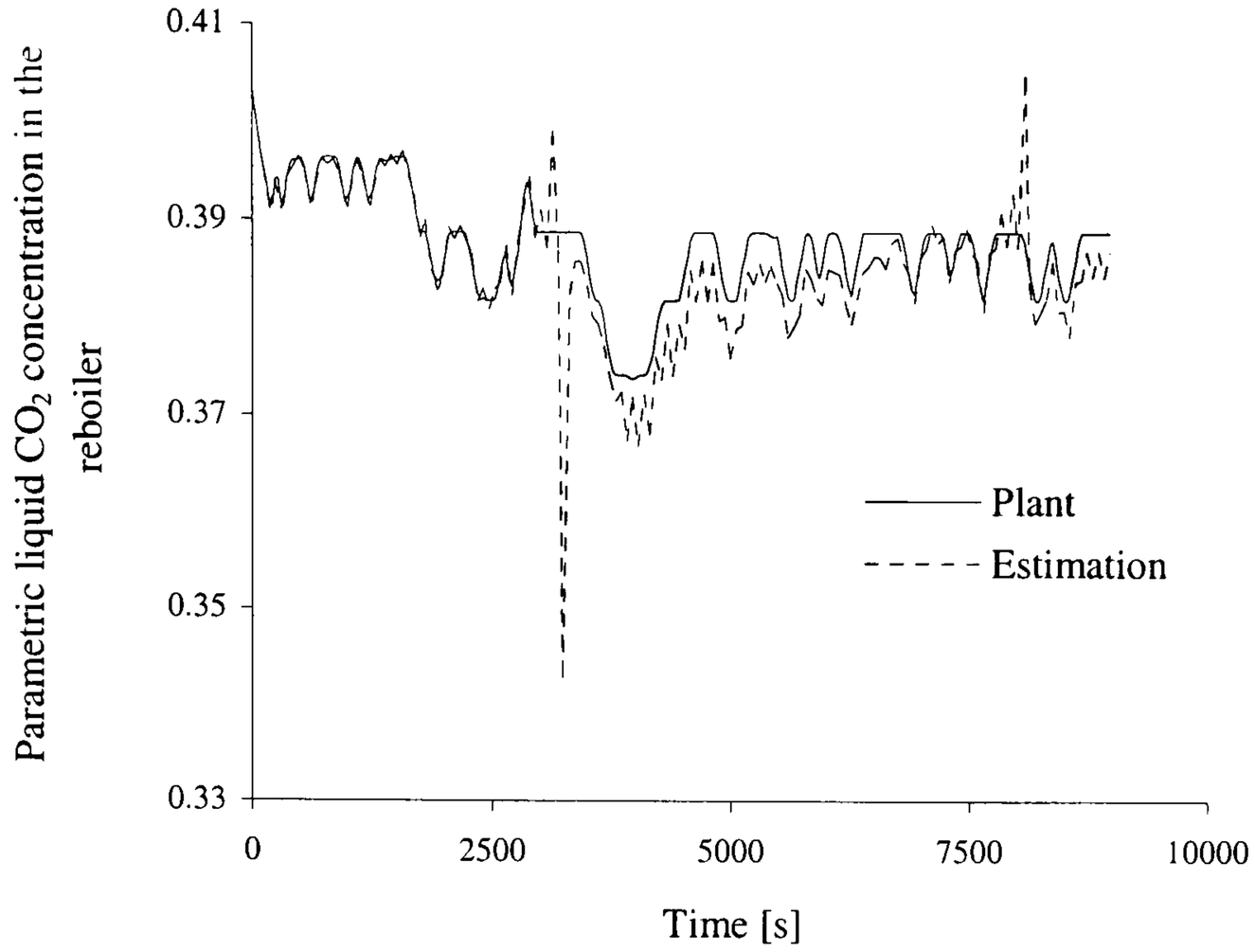


Figure 4.12. Parametric liquid CO_2 concentration in the reboiler, real and estimated

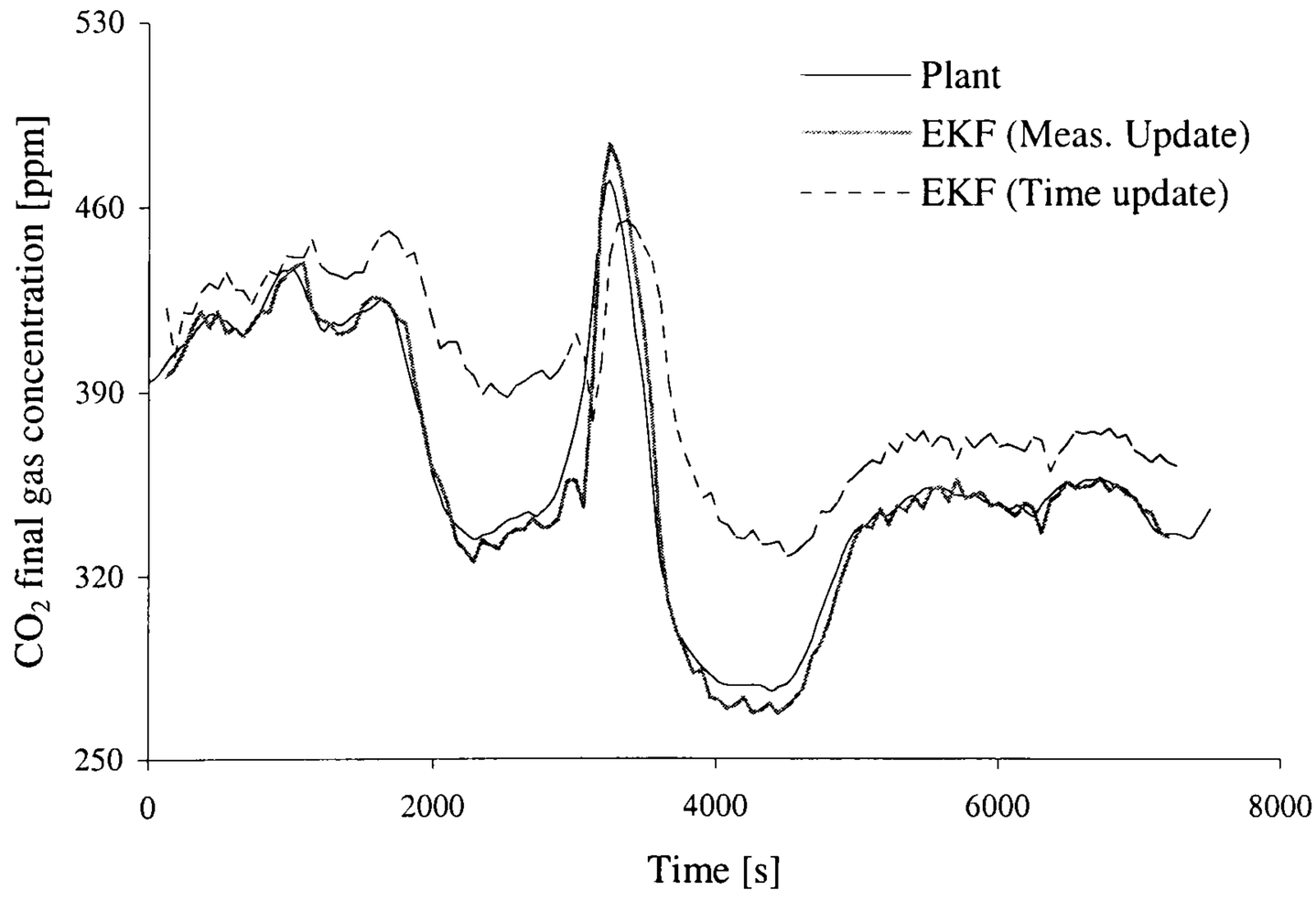


Figure 4.13 Estimation of the final CO_2 gas concentration.

	Absolute Error Average
Measurement update (x^+)	5.83
Time update (x^-)	33.20

Table 4.10. Absolute error averages for benchmark case.

As expected from the first results (Figure 4.8), the results obtained in this experiment show the same behaviour, an average absolute error of 5.85 ppm for the CO_2 final gas concentration measurement update and 33.2 ppm for the time update (see p85 and p89). The fact that the estimation process behaves similarly under different conditions and perturbations reflects the robustness of the filter.

In addition Figure 4.12 illustrates the filter's excellent tracking properties for other state variables, in this case the reboiler liquid concentration. Although some noisy pattern is obtained, the estimation kept it tight. These oscillations are presented due to the fact that the liquid concentration data comes from the acidity measurement, which is well known for having a strong nonlinear relation and oscillations sometimes are obtained.

4.3.2. Absorption Constant (κ)

The first comparison is done using exclusively the absorption constant κ as the uncertain parameter joint in the Kalman filter. Once the Kalman filter matrices are modified the estimation is redone including this parameter into the formulation.

Results of this run are presented in figures 4.14 and 4.15 .

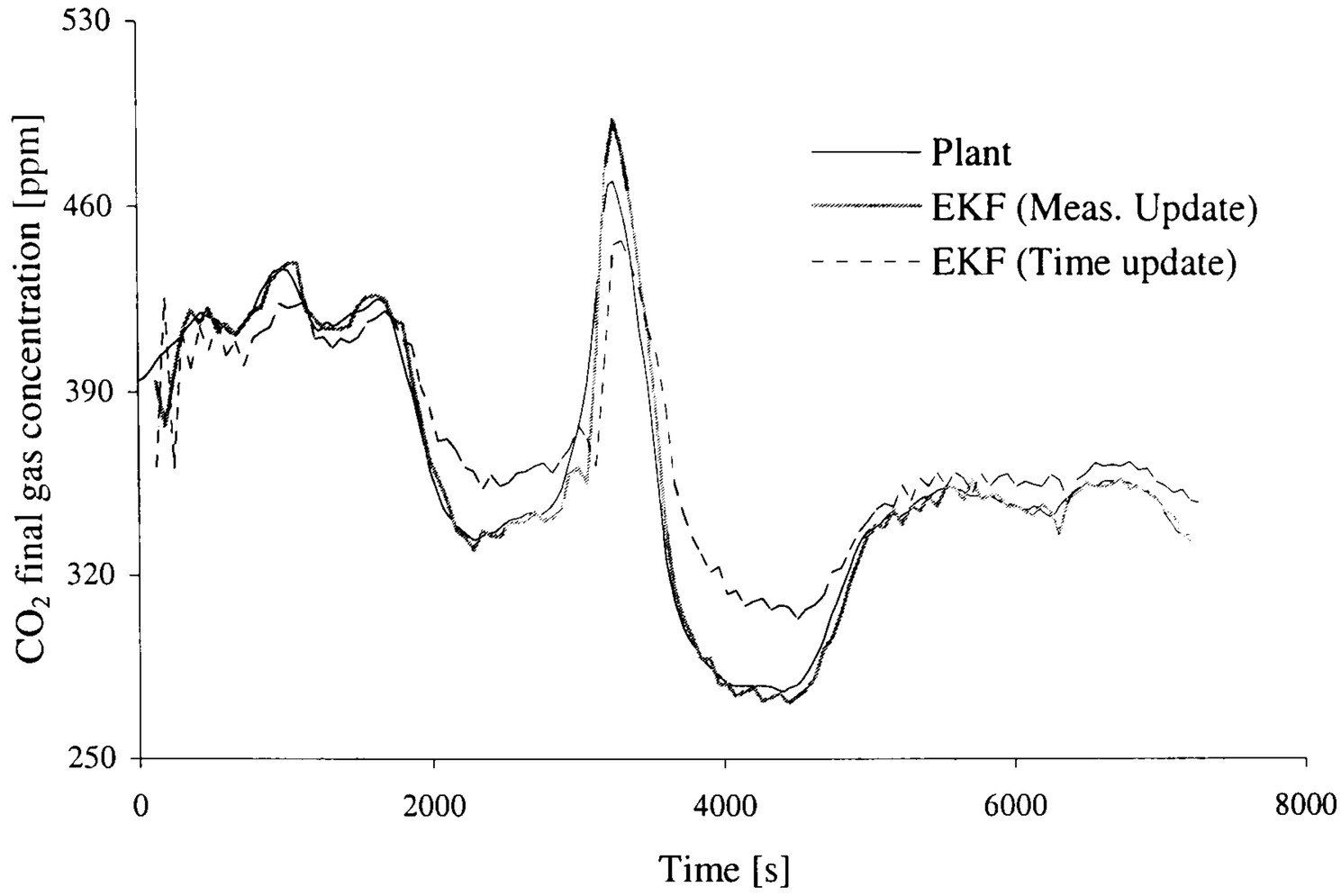


Figure 4.14 Estimation of the final CO_2 gas concentration with κ as uncertain parameter.

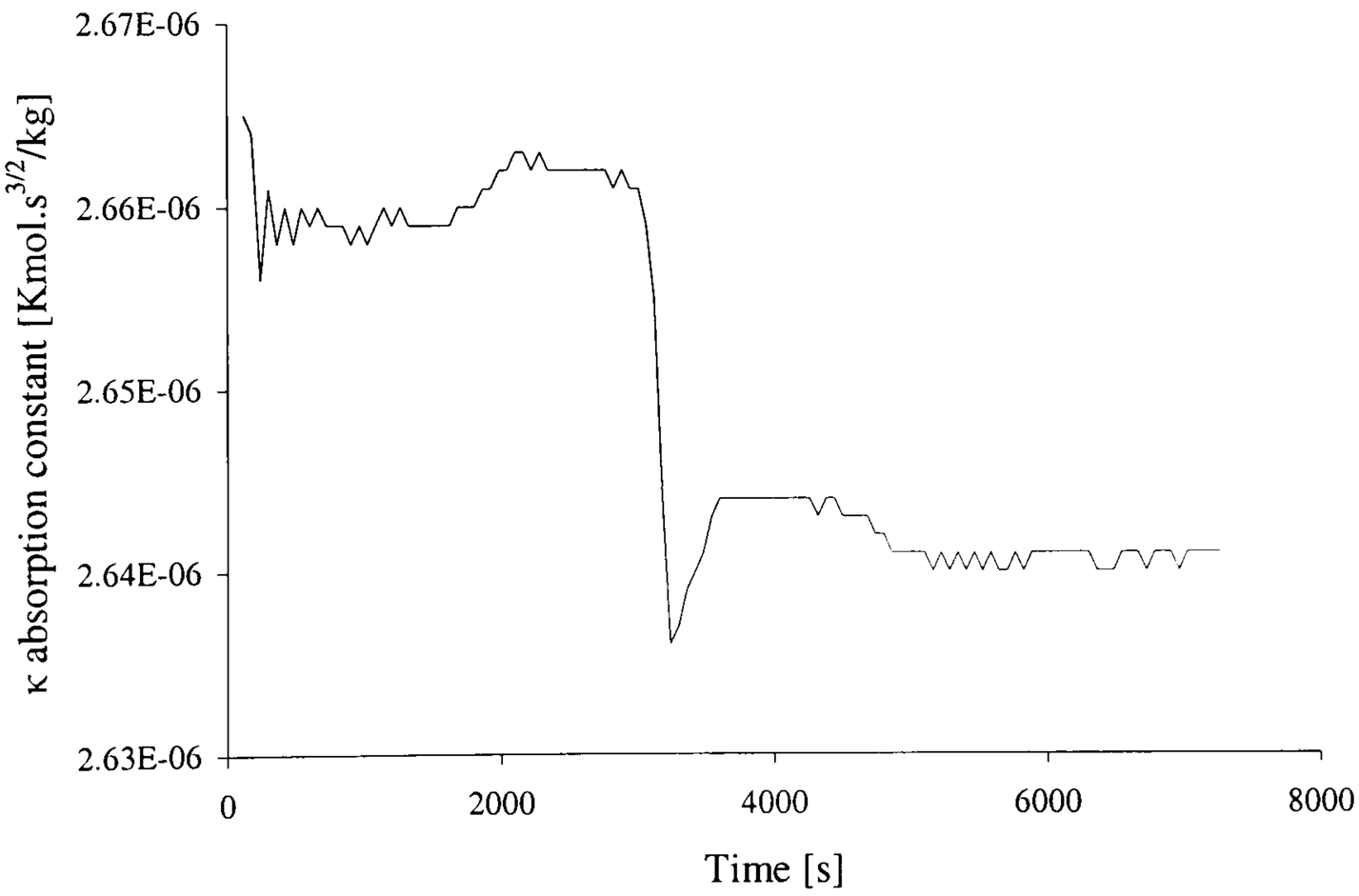


Figure 4.15 Absorption constant.

From these results, as a first impression there is a clear improvement in both the time and measurement update. Although the measurement update is not improved significantly compared with the simpler EKF, the real gain is obtained in the time update, where the average error is reduced to 16 ppm, see also table 4.11. This is very important because this is the required value in the optimisation process.

Also from graph 4.14 it can be seen that even good initial values for the parameter can lead to oscillatory behaviour for the early stages of the process, probably due to the bad values of the state variables. Nevertheless, once the values have been tuned a few intervals ahead, the model can track the plant efficiently even after strong perturbations such as the step change in the CO_2 feed flow at 3500 seconds. During this experiment some erratic behaviour was detected due to bad guesses for the unknown parameters. Estimating optimal values using gEST with the first set of measurements solves this problem.

Lastly the robustness of the absorption constant as unknown parameter is proved by the fact that it reaches almost steady state conditions for the last 2000 seconds, when the process is less oscillatory.

EKF	Absolute error average [ppm]	
	Measurement Update.	Time Update.
Simple EKF	5.83	33.2
Joint EKF	5.01	16.1

Table 4.11. Comparing estimation errors between simple EKF and the joint EKF.

4.3.3. Absorption Constant (κ) and MEA Concentration (C_{mea})

Having proved the benefits of including the absorption constant in the filter, new experiments are done to test the gain of adding further parameters. For the first case, the previous experiment is repeated but adding the MEA concentration in the liquid flow as an extra uncertain parameter.

Again in order to avoid stability problems the first measurements are used to estimate the optimal values of the parameters. Figures 4.16 and 4.17 present the values obtained for the parameters throughout the process. The CO_2 gas concentration plot is not exhibited because it is very similar to the previous results, however table 4.12 shows the average absolute errors obtained for this experiment.

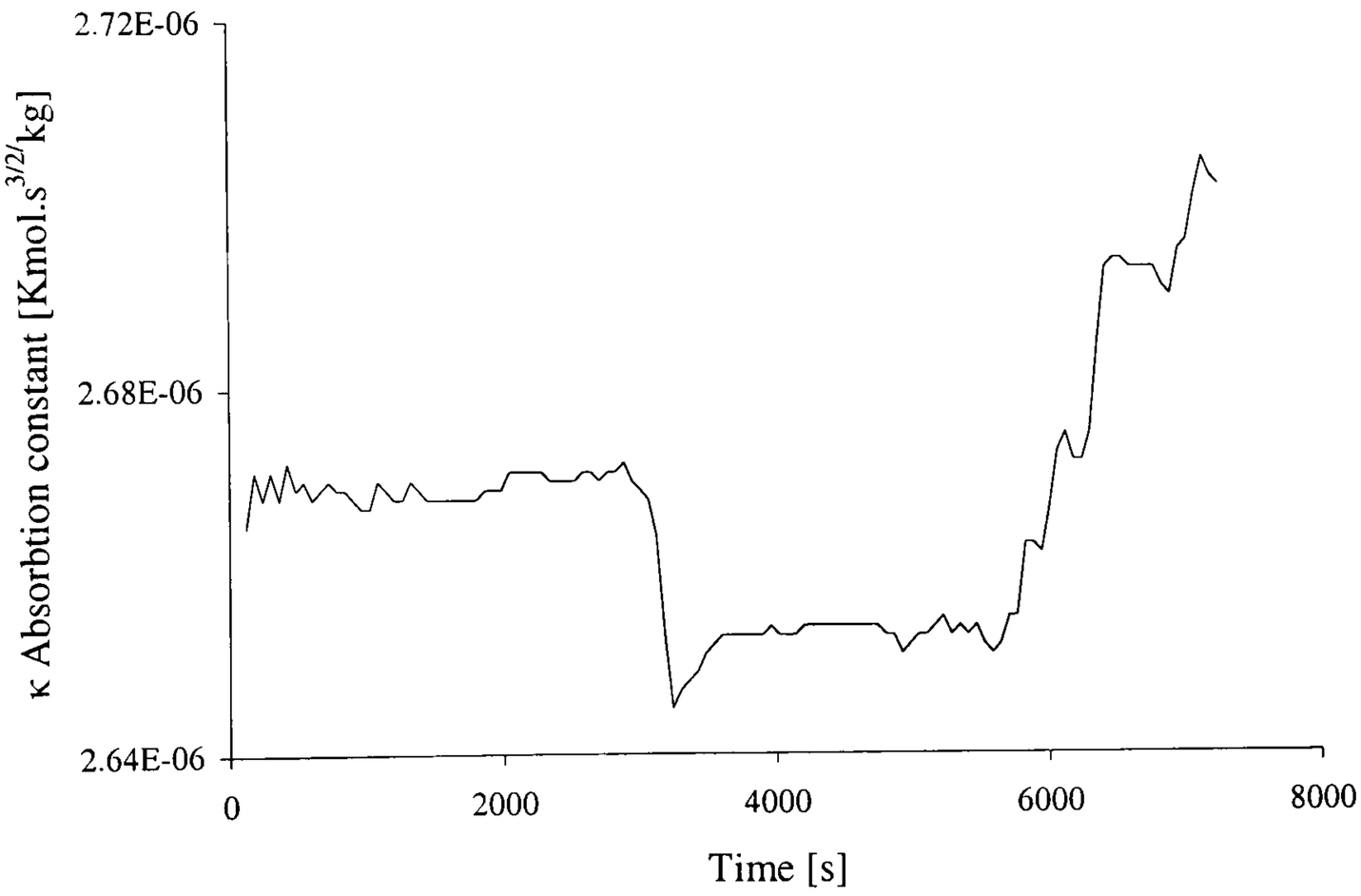


Figure 4.16 Estimation of the absorption constant.

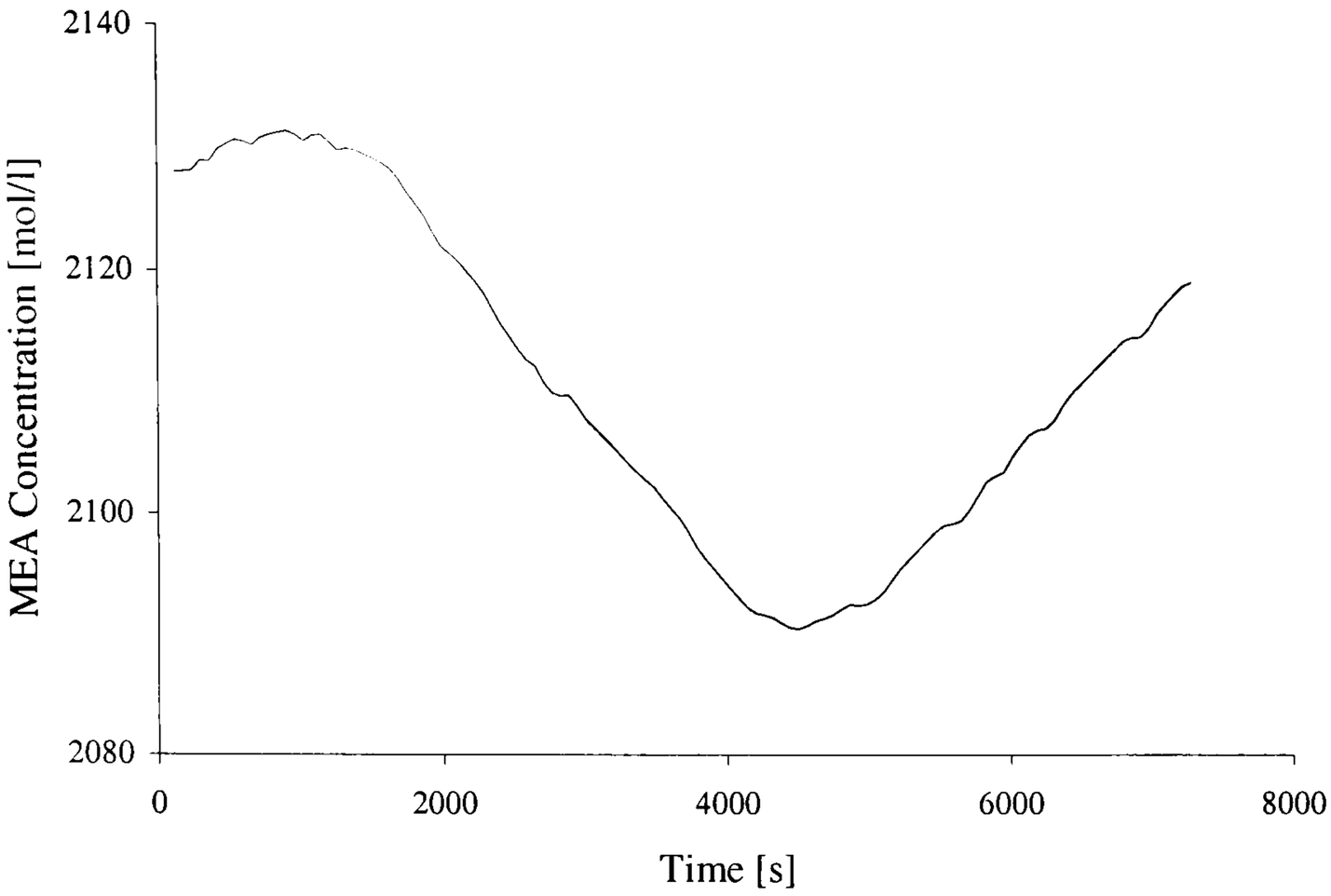


Figure 4.17 Estimation of the MEA concentration.

EKF	Absolute error average [ppm]	
	Measurement Update.	Time Update.
Only κ	5.01	16.1
κ and C_{mea}	4.85	18.2

Table 4.12. Comparing estimation errors between different parameter estimations.

From graphs 4.16 and 4.17 it is clear that the filter has problems in converging to steady state after 6000 seconds, considering that the system has in fact reached that condition. Also table 4.12 reflects this problem, although the measurement update is reduced by 3% compared with the previous case, the time update mismatch is increased, showing that in the long run the process is not as accurate as before.

This instability detected in the estimation is largely related to the fact that the MEA concentration is a variable that appears several times in different sections of the model, making it difficult for the filter to satisfy all measurements and state variables from the plant. In consequence it is harder for the EKF to converge to a single value.

These results confirm that the best approach with the MEA concentration is to find its optimal value at the beginning of the estimation process and keep it constant throughout all the process.

4.3.4. Absorption Constant (κ) and Desorber Heat Loss (Q_{ld})

The next test involved the use of the desorber heat loss (Q_{ld}) instead of the MEA concentration as the second parameter. The measurement and model conditions are identical with the previous case. Figures 4.18 and 4.19 present the final results. Again the estimated values of the CO_2 final gas concentration are omitted because its behaviour is very similar to Figure 4.14 .

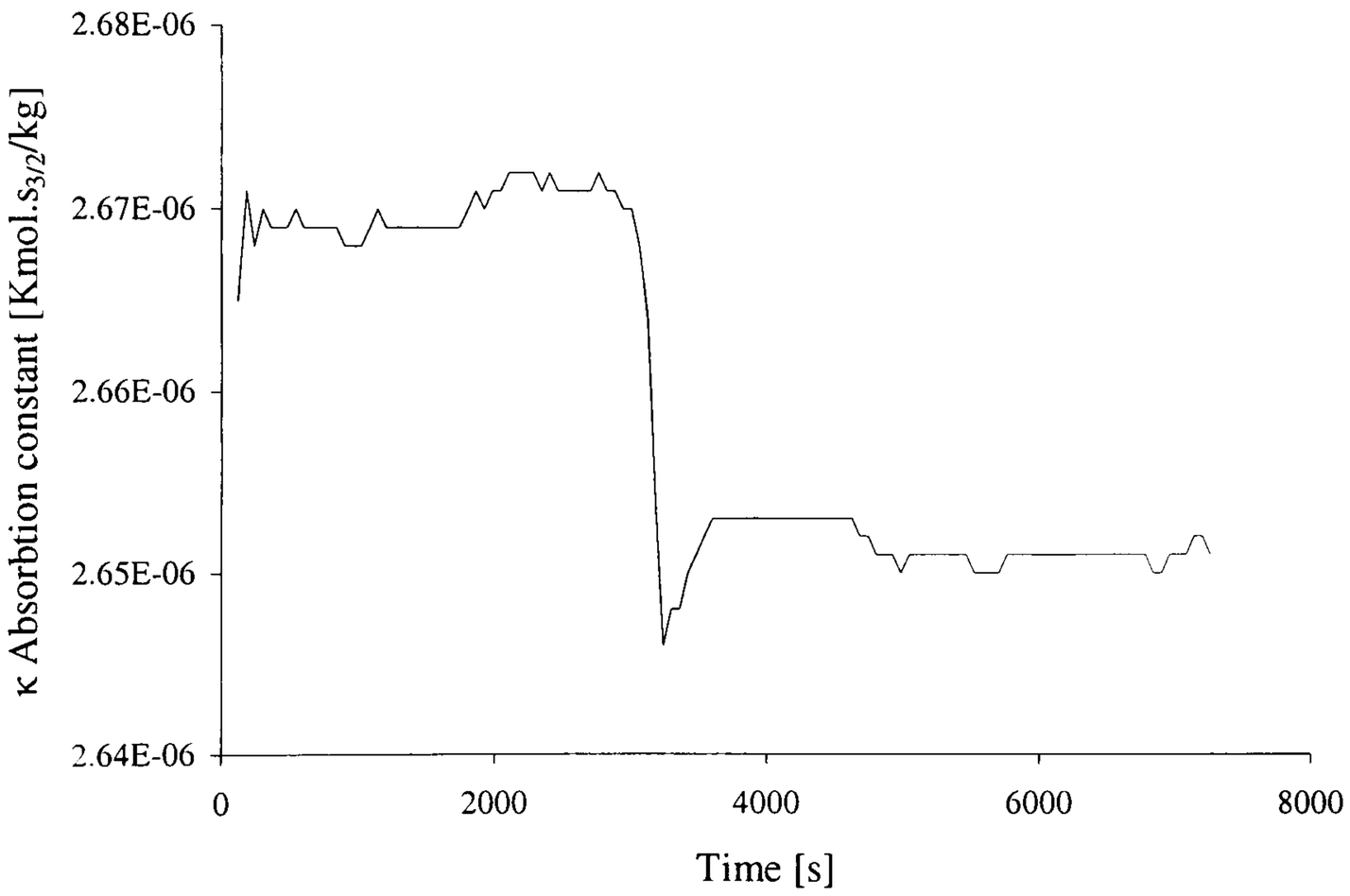


Figure 4.18 Estimation of the absorption constant.

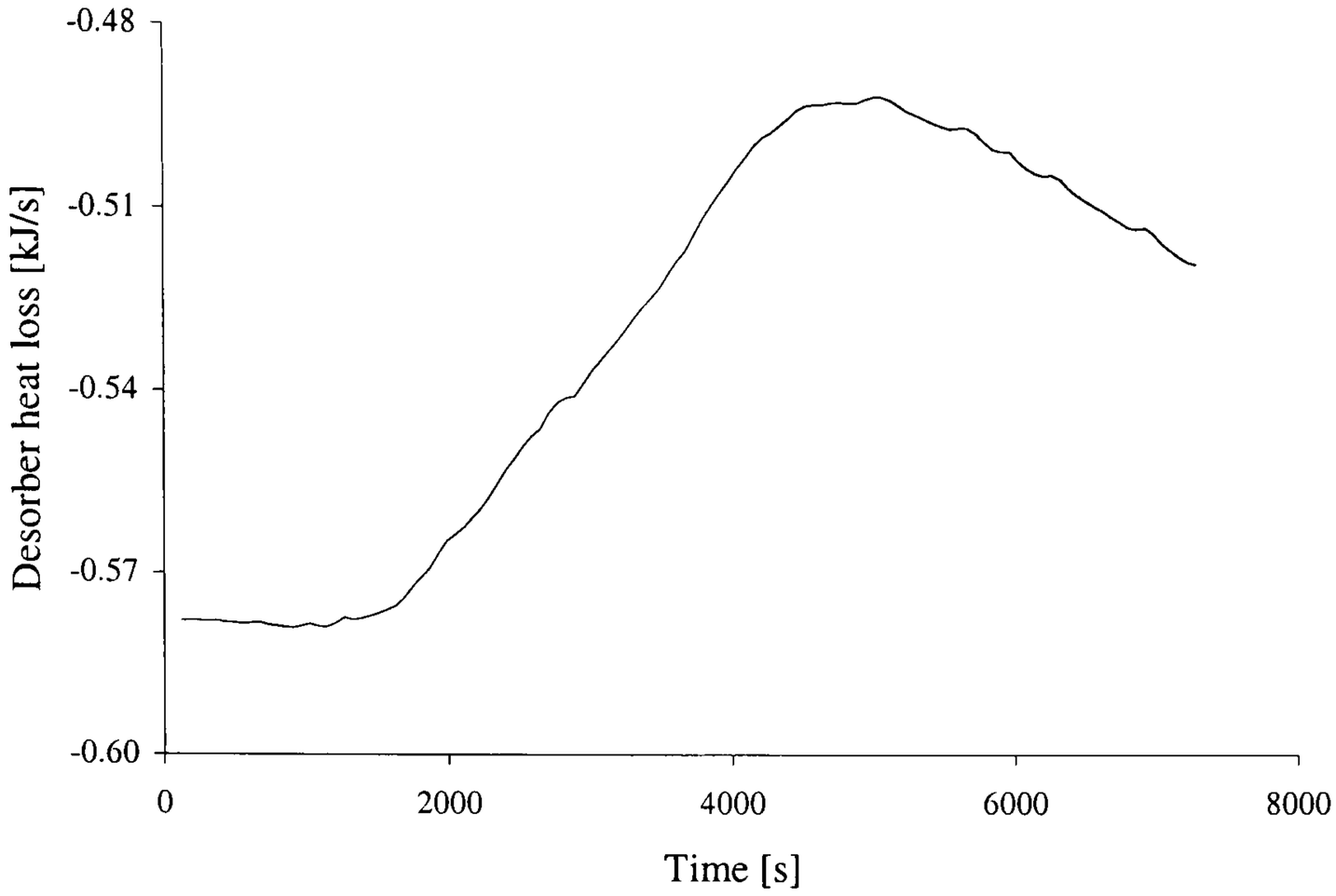


Figure 4.19 Estimation of the desorber heat loss.

EKF	Absolute error average [ppm]	
	Measurement Update.	Time Update.
Only κ	5.01	16.1
κ and Q_{ld}	4.62	16.0

Table 4.13. Comparing estimation errors between different parameter estimations.

Compared with the previous results the estimation of the desorber heat loss reduces the measurement and time update errors, although the improvement is not considerably better. However it is clear that steady state conditions are obtained once the plant reaches this condition. Even more important, these results also prove the hypothesis in the sensitivity test that more than two parameters do not bring any further benefit to the EKF.

As conclusion the unknown parameter estimation is restricted to a couple: The absorption constant (κ) and the desorber heat loss (Q_{ld}).

4.4. Estimation Interval: How Often Should be Done?

The discrete-time sampling of the controlled output is a feature that is not present in an analog control system. The value of the sampling period T affects the quality of the closed-loop response and consequently is considered as a design parameter in a digital control loop.

The intermittent sampling of the controlled output has the following two effects of the control loop:

1. During a sampling interval the digital controller controls the process using "old" and not "current" information,
2. The control loop is in effect "open" during a sampling interval and "closes" only at each sampling instant, when new information arrives.

It is clear, then, that we would like to have a sampling interval as short as possible. However as the sampling period decreases, the time and effort required by a computer increases. What, then, is an optimum sampling time rate?

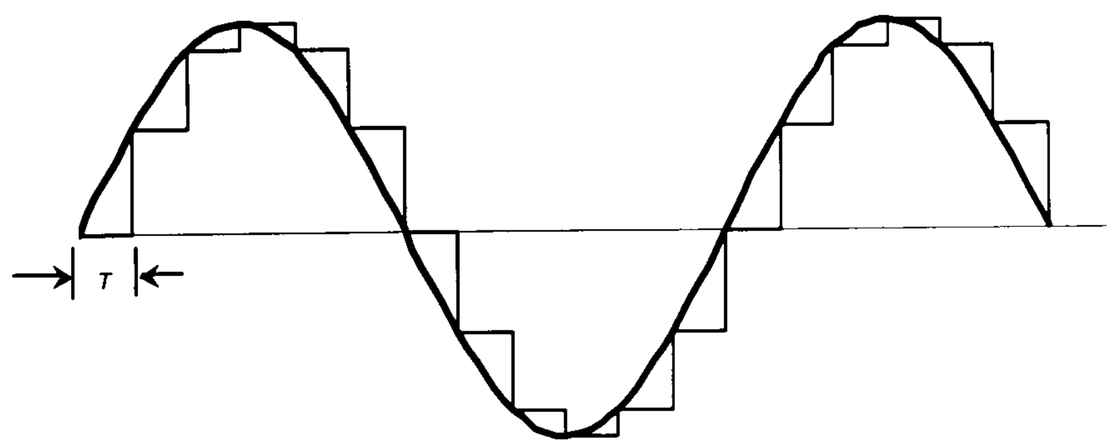


Figure 4.20 Lag produced by discrete sampling

Consider the continuous, smooth, sinusoidal wave shown in figure 4.20. Let us sample this signal every T seconds. The signal seen by the controller is a stair-step-like continuous signal. It has the same amplitude and the same frequency as the original wave, but its phase has been shifted.

There is no firm and rigorous guidelines on how to select the optimal sampling period for digital control loop. The optimal choice should always be related to the operating conditions of the controlled process. "the observer must be about ten times faster than the process" (Alvarez, 1999)

It was shown that the simulated process closed loop time was around 1000 and 1200 seconds. Hence applying the heuristic rule proposed in the literature the sampling time should be something between 50 and 60 seconds, or approximately every minute.

In order to apply a more systematic approach three different intervals are tested: 30 seconds, 60 seconds and every 120 seconds.

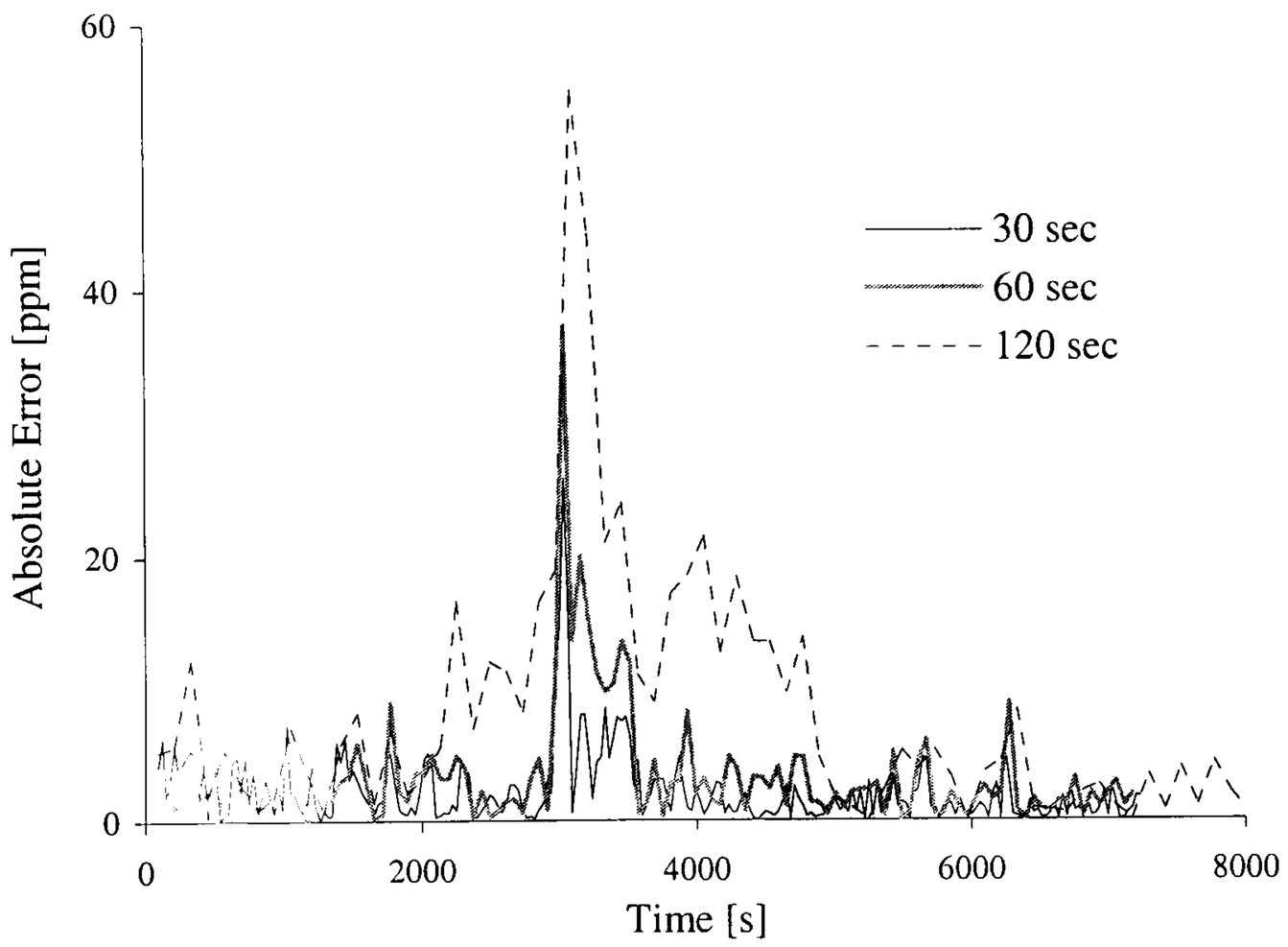


Figure 4.21 Comparison between different sampling times.

Sampling time	Absolute error average [ppm]
30 seconds	2.81
60 seconds	4.65
120 seconds	9.63

Table 4.14. Absolute error average for different sampling times.

Results obtained from different sampling times are shown in Figure 4.21 Also the absolute average error from this data is presented in Table 4.14. Using an interval of 120 seconds clearly shows that the filter sometimes finds it hard to track the plant correctly. On the other hand, selecting a small interval between 30 and 60 seconds proved to be very successful in tracking the plant, but more computationally demanding. However each iteration requires only 10 seconds to be completed, so from these results an interval of 30 seconds has enough time to estimate all variables online.

4.5. Conclusion

The results of the implementation of the EKF for either state variables alone or joint state variables and parameters reflect some concluding remarks about the reliability of the algorithm

4.5.1. State Variables Simulation

- The Kalman filter proves to be a very efficient way to track the actual process, since even under strong error measurement and process noise the estimator could converge fast. The results also show the advantage of using the Kalman filter instead of a deterministic technique as a state condition estimator. Simulations prove that EKF is approximately one order of magnitude more accurate compared with previous researches. Also the EKF showed that even at extreme initial conditions, the estimator was capable of converging to the real values in a short period of time.
- The computational time was short enough, (between 10 and 15 seconds approximately) for the estimation process to be executed online.

4.5.2. Joint Extended Kalman Filter Simulation

- It is important to keep the number of uncertain variables in the estimation as small as possible in order to assure robustness and stability. Using a simple sensitivity criterion the number of parameters manipulated by the estimator could be considerably reduced.
- Although the incorporation of uncertain parameters into the Kalman formulation does not significantly improve the final estimation, it improves the time update phase and also the process stability. However, in contrast it is important to select the initial values of the differential variables close to the real ones in order to achieve stability. Using reconciliation software such as gEST, before implementing the filter in the process, can do that.
- It is clear that not all available parameters are suitable for the estimation process. It was proved that only 2 uncertain parameters are required to reduce the plant/model mismatch. Including extra parameters only complicates the formulation and sometimes increases estimation errors and creates new sources of instability.

Chapter 5

Experimental Estimation

5.1. Estimation of the State Variables

Once the EKF previously researched was developed and tuned, several experiments were done using experimental and more complete data from the CO_2 absorption/desorption plant. In these experiments servo problems and perturbations are tested in order to study the tracking capabilities of the filter under multiple conditions.

The pilot plant located in the chemical engineering department is used to carry out all experiments. All measurements from the plant are electronically linked to a computer in the control room where the information is stored, then the data is retrieved for further manipulation and the estimation trial is executed offline. Nevertheless as shown earlier, due to the short computational time required for the estimation, the process could be easily done online providing the proper code and link between the different software is implemented.

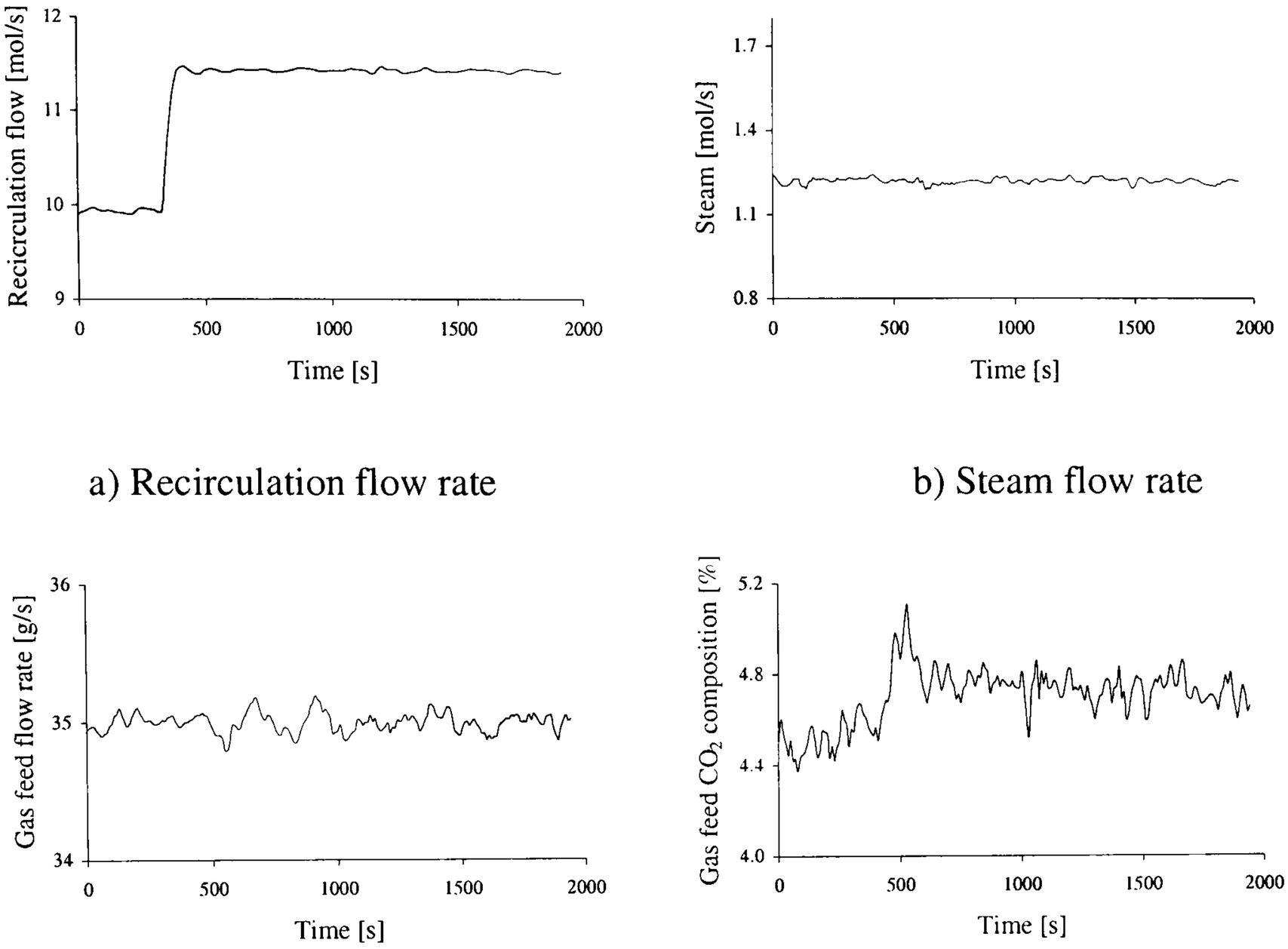
Table 5.1 shows all the measurements used for the Kalman filter with their respective absolute errors. The measurement interval is every 30 seconds.

Measurement	Abs Error (±)
CO_2 final gas concentration	5 ppm
CO_2 feed gas concentration	0.5 %
Gas feed flow rate	2 g/s
Recirculation flow rate	0.01 kg/s
Steam flow rate	1 g/s
Liquid feed temperature	0.5 °C
Temperature at top of absorber	0.5 °C
Temperature at half middle top of absorber	0.5 °C
Temperature at middle of absorber	0.5 °C
Temperature at half middle bottom of absorber	0.5 °C
Temperature at bottom of absorber	0.5 °C
Temperature top desorber	0.5 °C
Temperature middle desorber	0.5 °C

Table 5.1. Measurements considered for the EKF test.

5.2. Servo problem in the Recirculation Flow Rate (Exp1)

For the first experiment a servo problem in the recirculation flow rate is introduced, the flow rate is increased from 10 mol/s to 11.5 mol/s after 400 seconds, while the other input variables are kept constant. Figure 5.1 shows the input variables record.



a) Recirculation flow rate

b) Steam flow rate

c) Gas feed flow rate

d) CO_2 gas feed composition

Figure 5.1 Input variables in the plant (Exp1)

Some of the results obtained from the EKF are shown in figures 5.2 to 5.5 together with their measured values for comparative purposes.

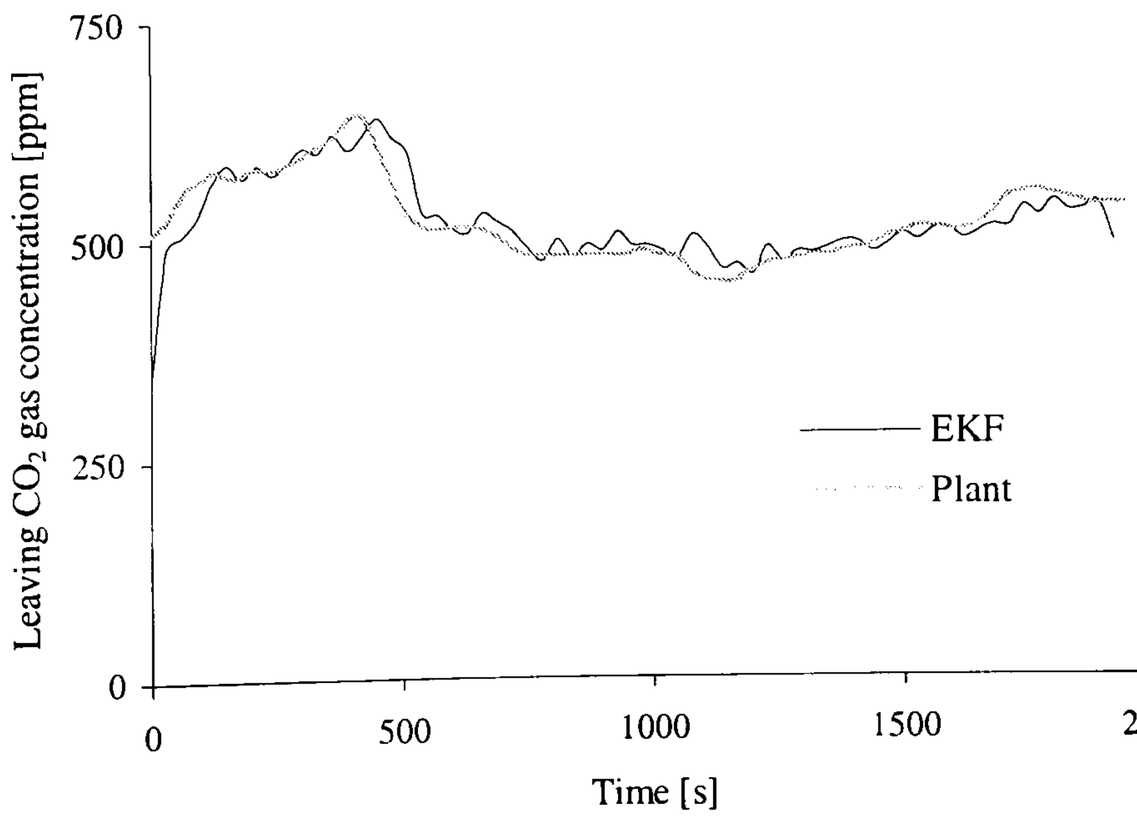


Figure 5.2 CO_2 leaving gas concentration (Exp1)

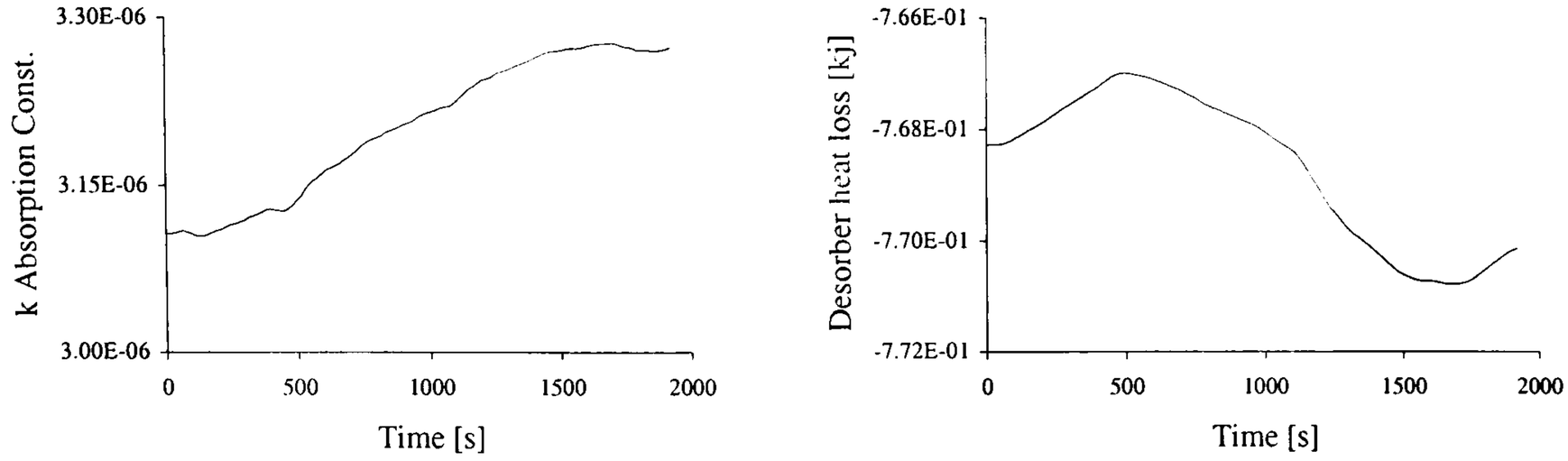


Figure 5.3 Unknown Parameters (Exp1)

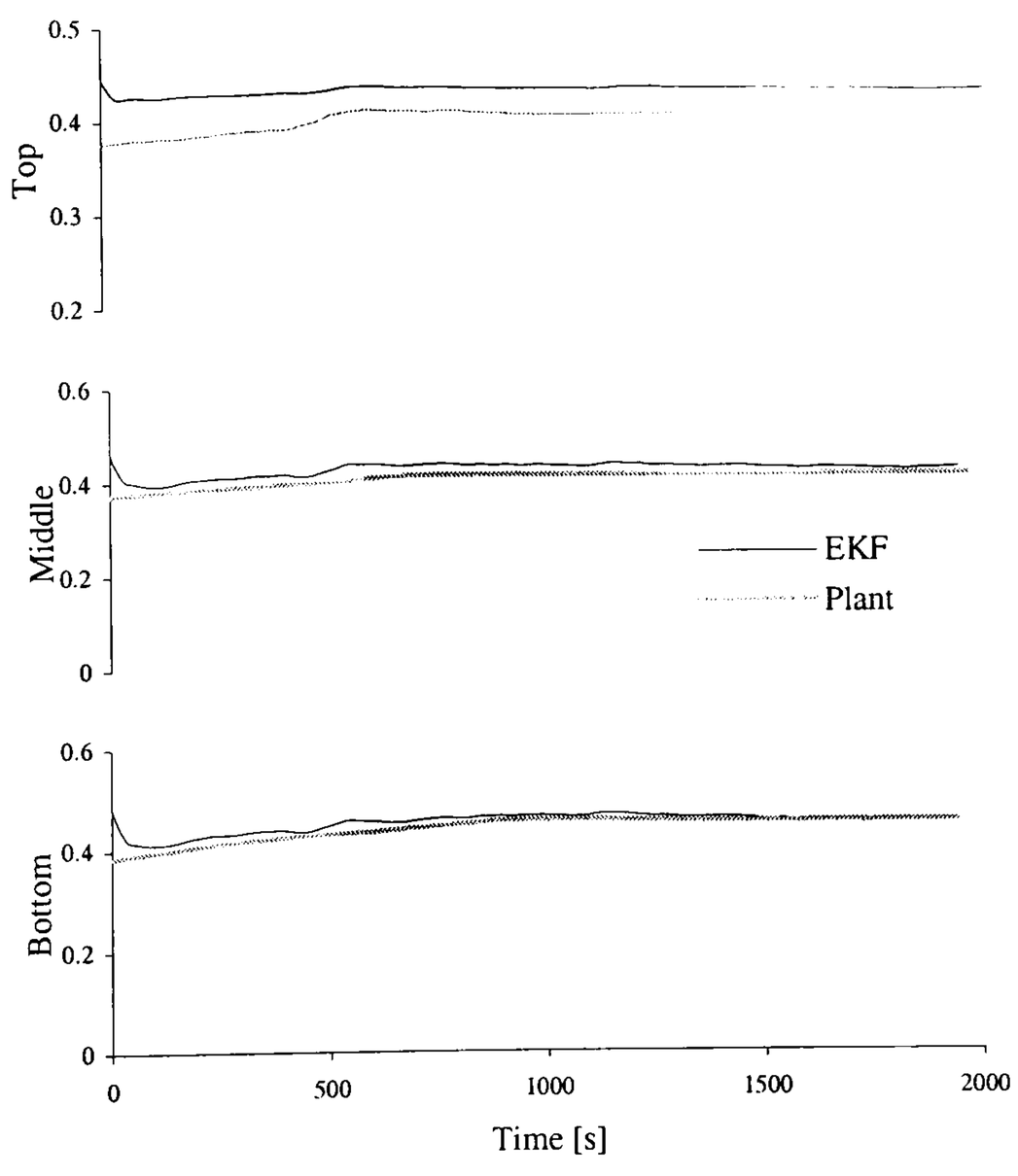


Figure 5.4 Parameterised absorber temperatures (Exp1)

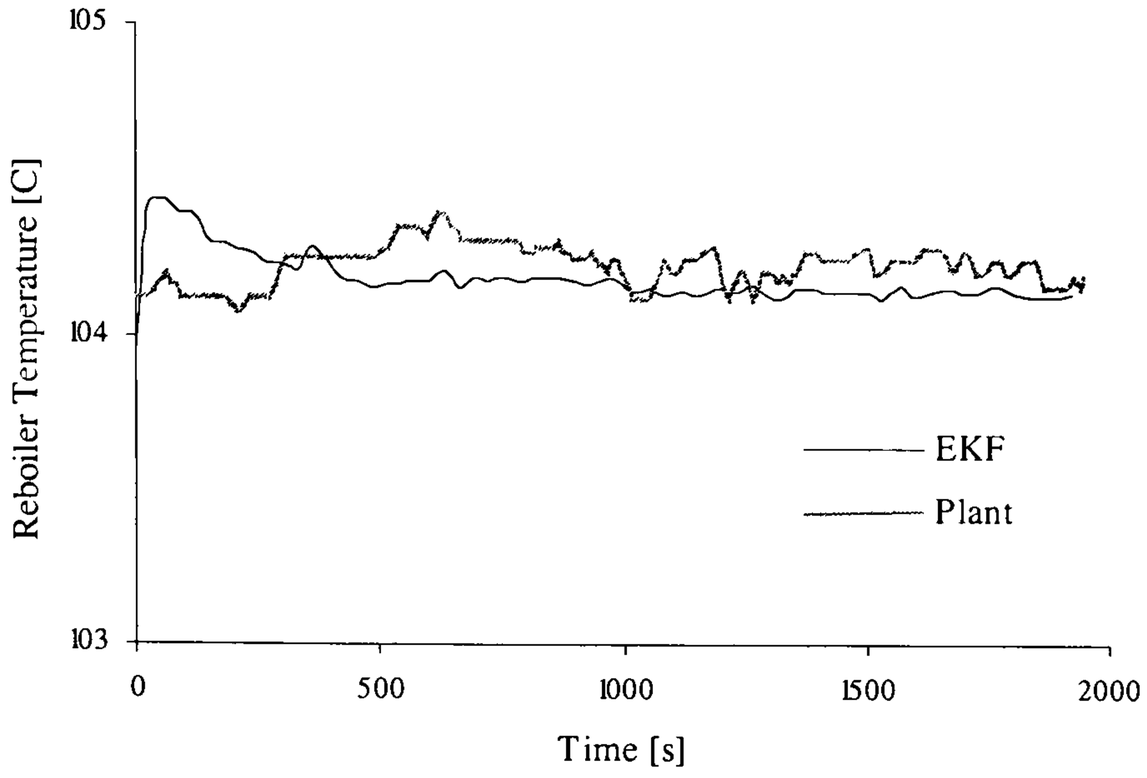


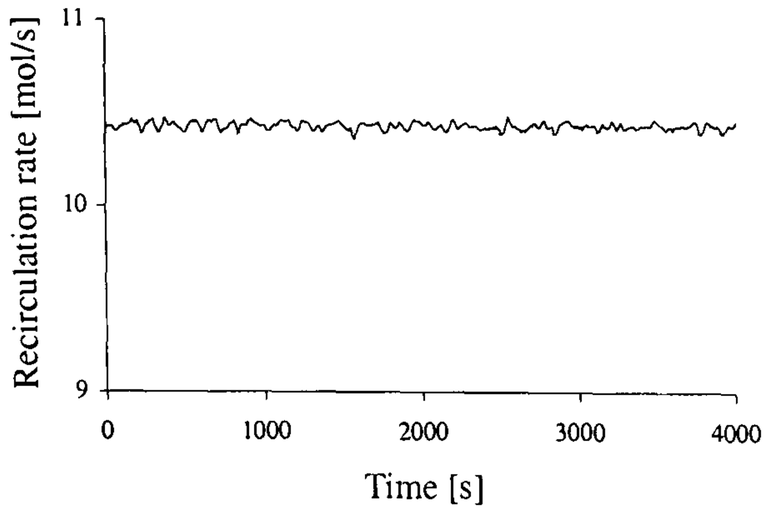
Figure 5.5 Reboiler temperatures (Exp1)

As a first impression, the results show the accuracy of the EKF to estimate the state variables in the plant. For instance the CO_2 leaving gas concentration (Figure 5.2) is kept closely estimated throughout all process time, having an average error of only 26 ppm. Also the temperature profiles in the absorber and reboiler are maintained close to their measured values with a maximum average error of only 2%.

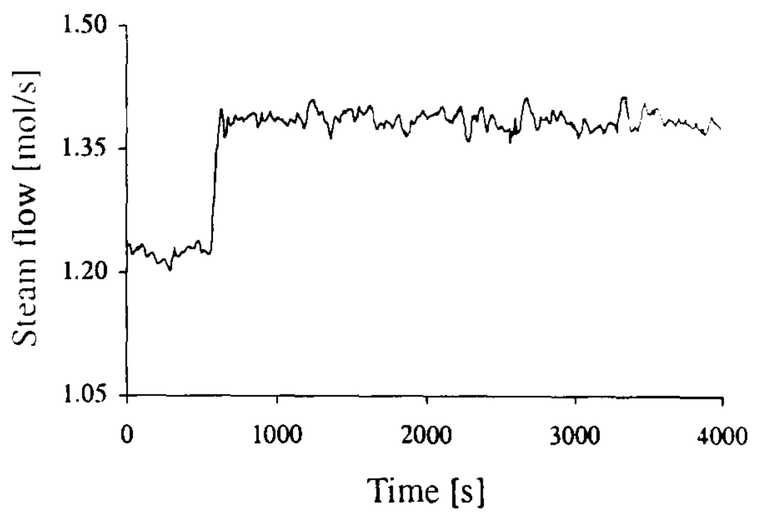
Although this experiment does not present dramatic changes or perturbations, it proves the advantages of using stochastic observers such as the extended Kalman filter, specially handling measurement errors.

5.3. Servo Problem in the Steam Flow Rate (Exp2)

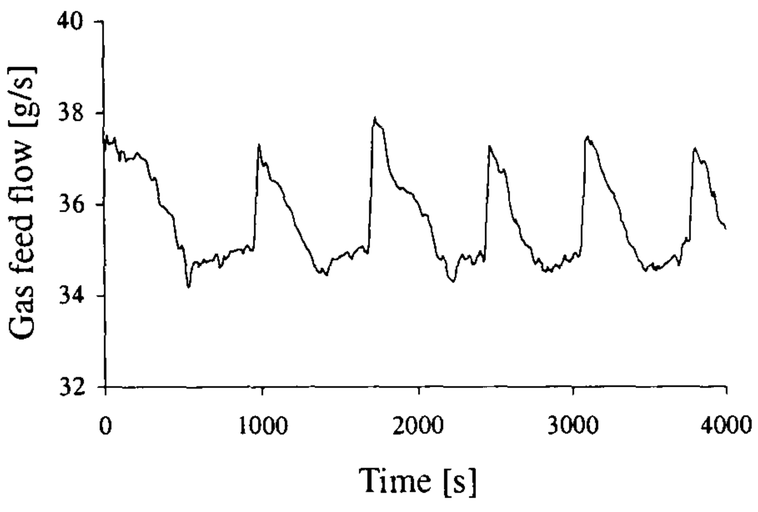
A servo problem in the steam flow rate is simulated for this experiment; where the flow rate is increased from 1.2 mol/s to 1.37 mol/s after 200 seconds. Figure 5.6 shows the input variables record.



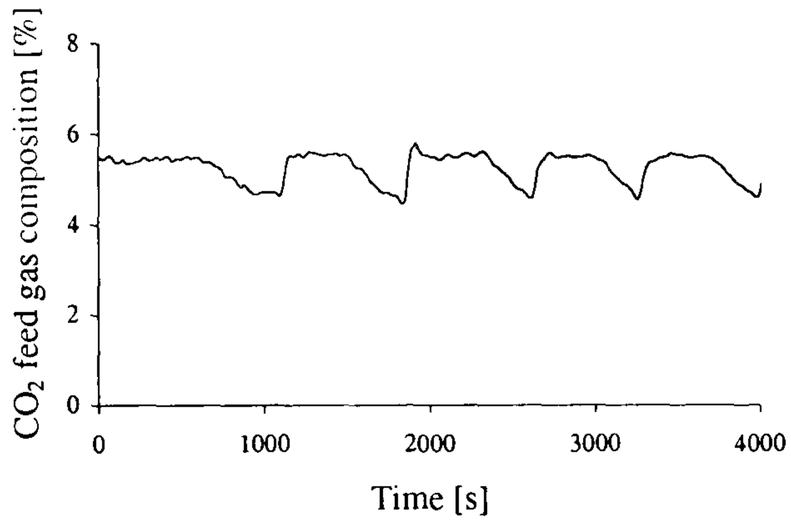
a) Recirculation flow rate



b) Steam flow rate



c) Gas feed flow rate



d) CO_2 gas feed composition

Figure 5.6 Input variables in the plant (Exp2)

The results obtained for the estimation are shown in figures 5.7 to 5.11 with their measured values for comparative purposes.

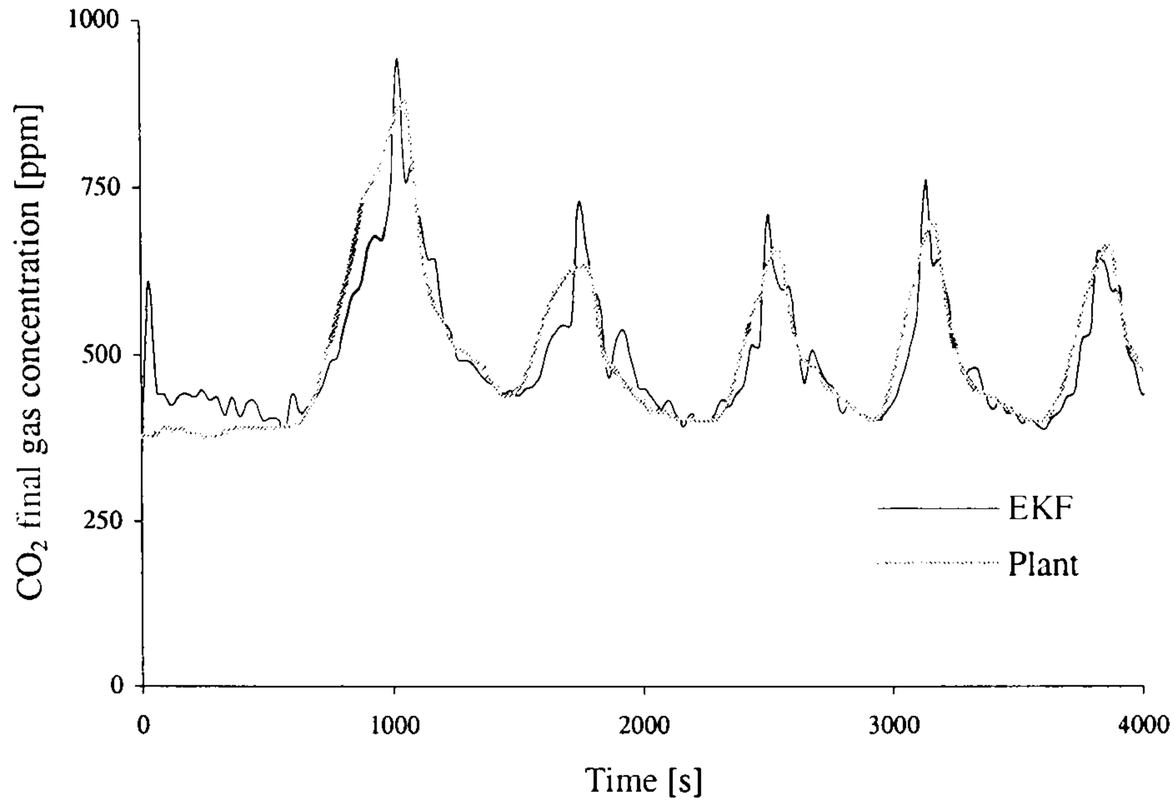


Figure 5.7 CO_2 leaving gas concentration (Exp2)

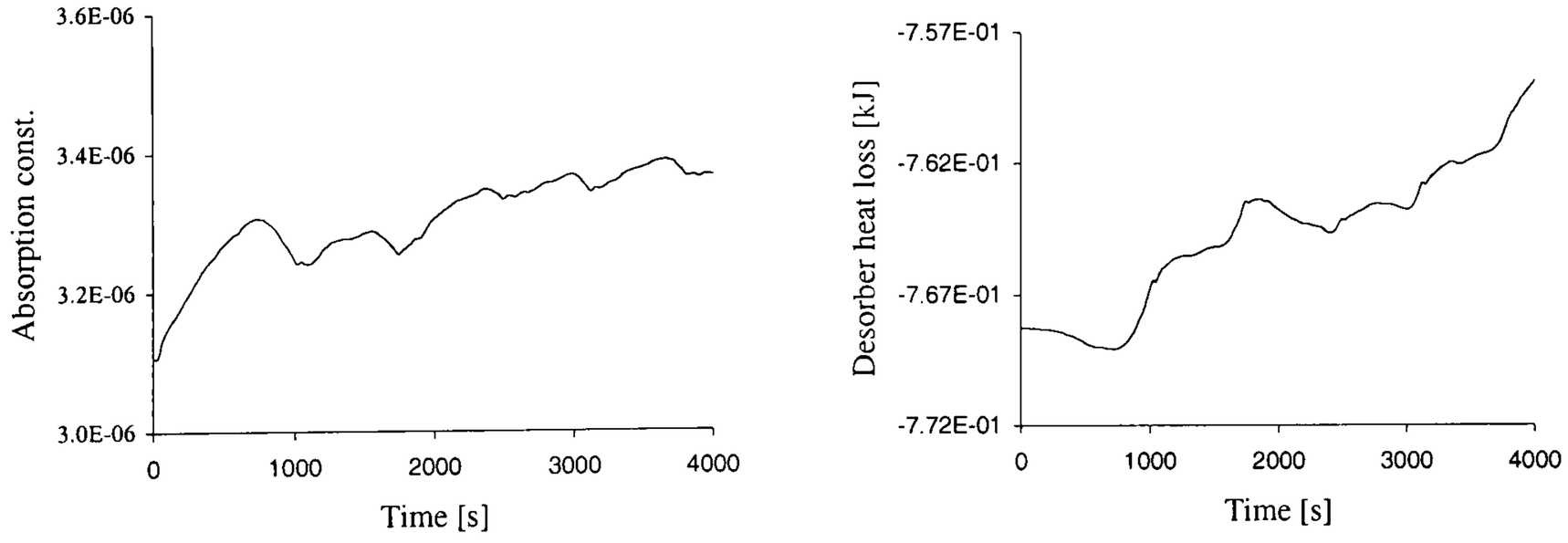


Figure 5.8 Unknown Parameters (Exp2)

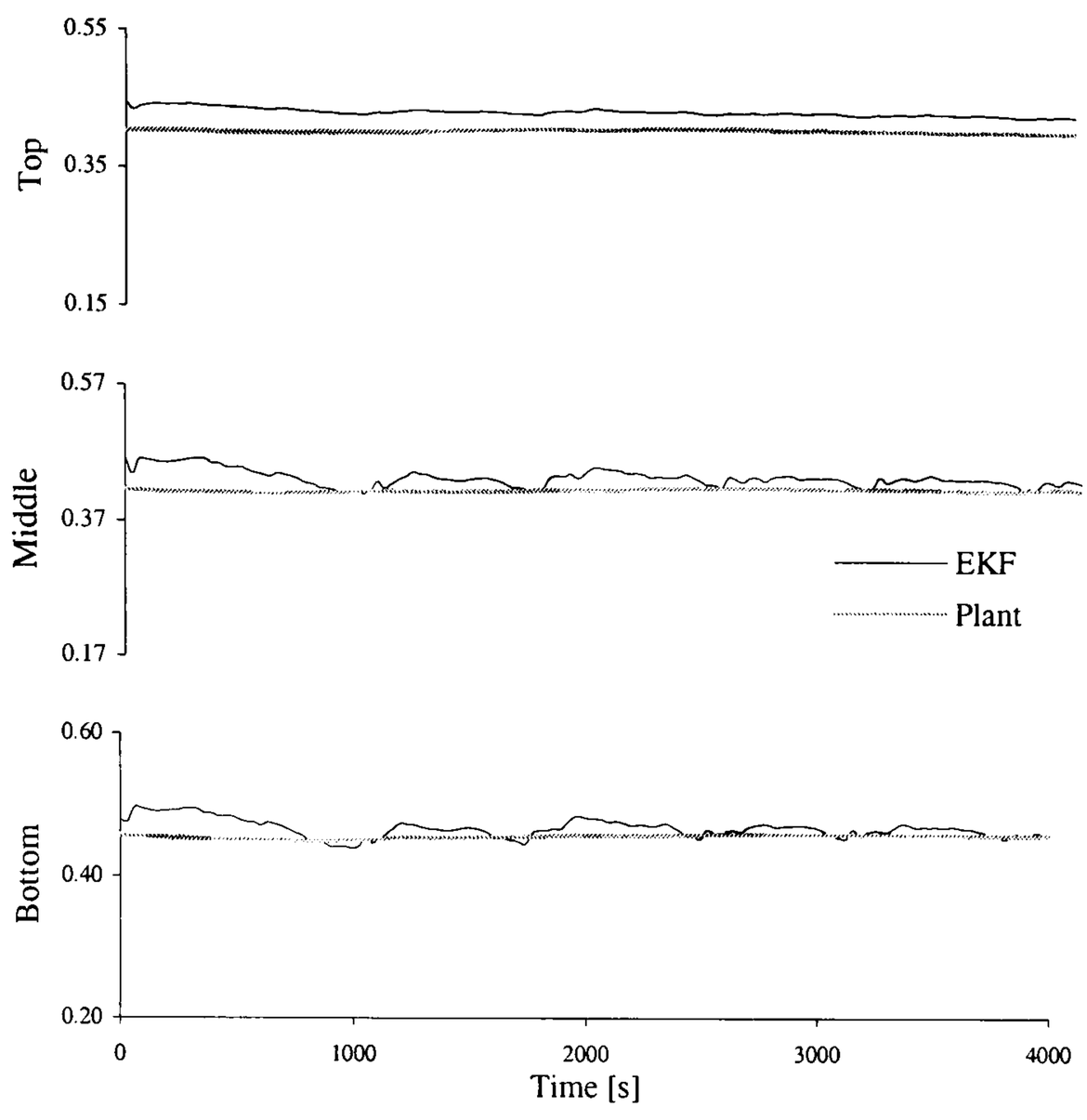


Figure 5.9 Parameterised absorber temperatures (Exp2)

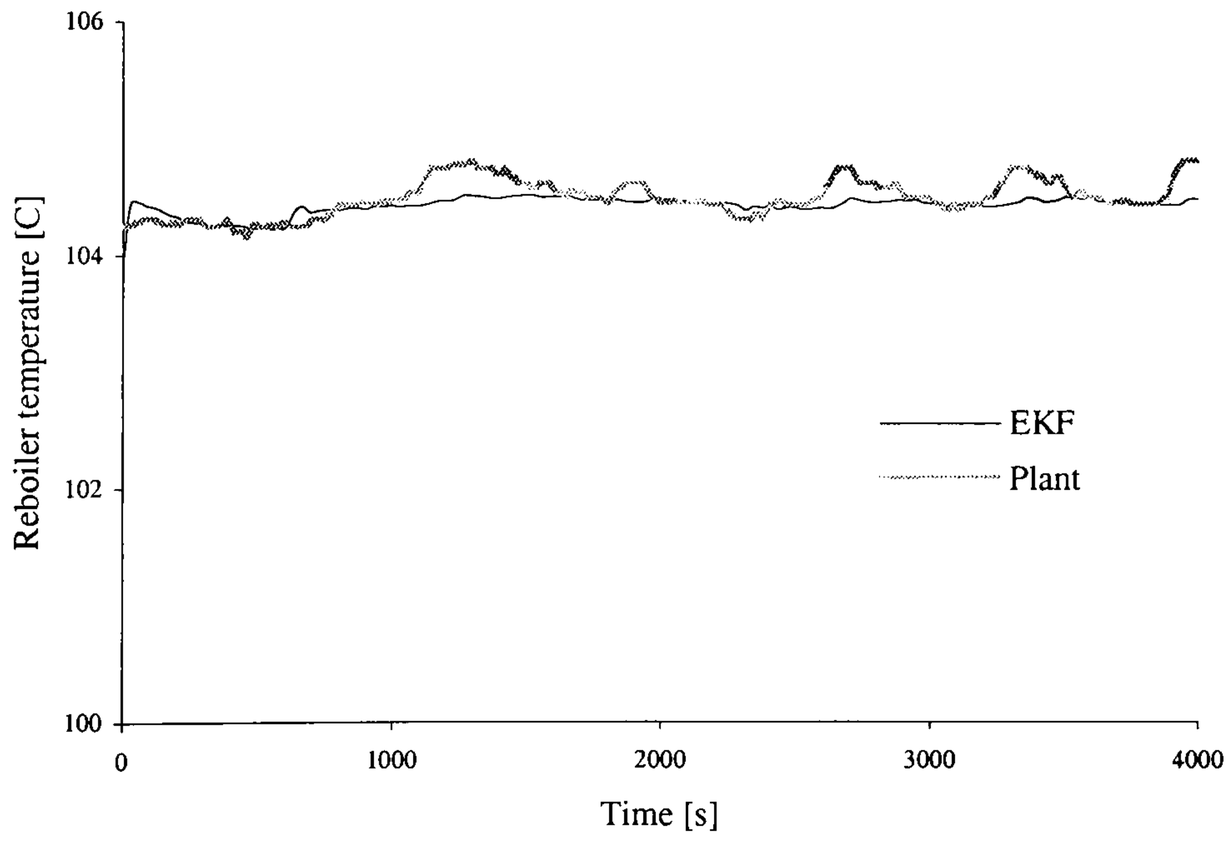


Figure 5.10 Reboiler temperature (Exp2)

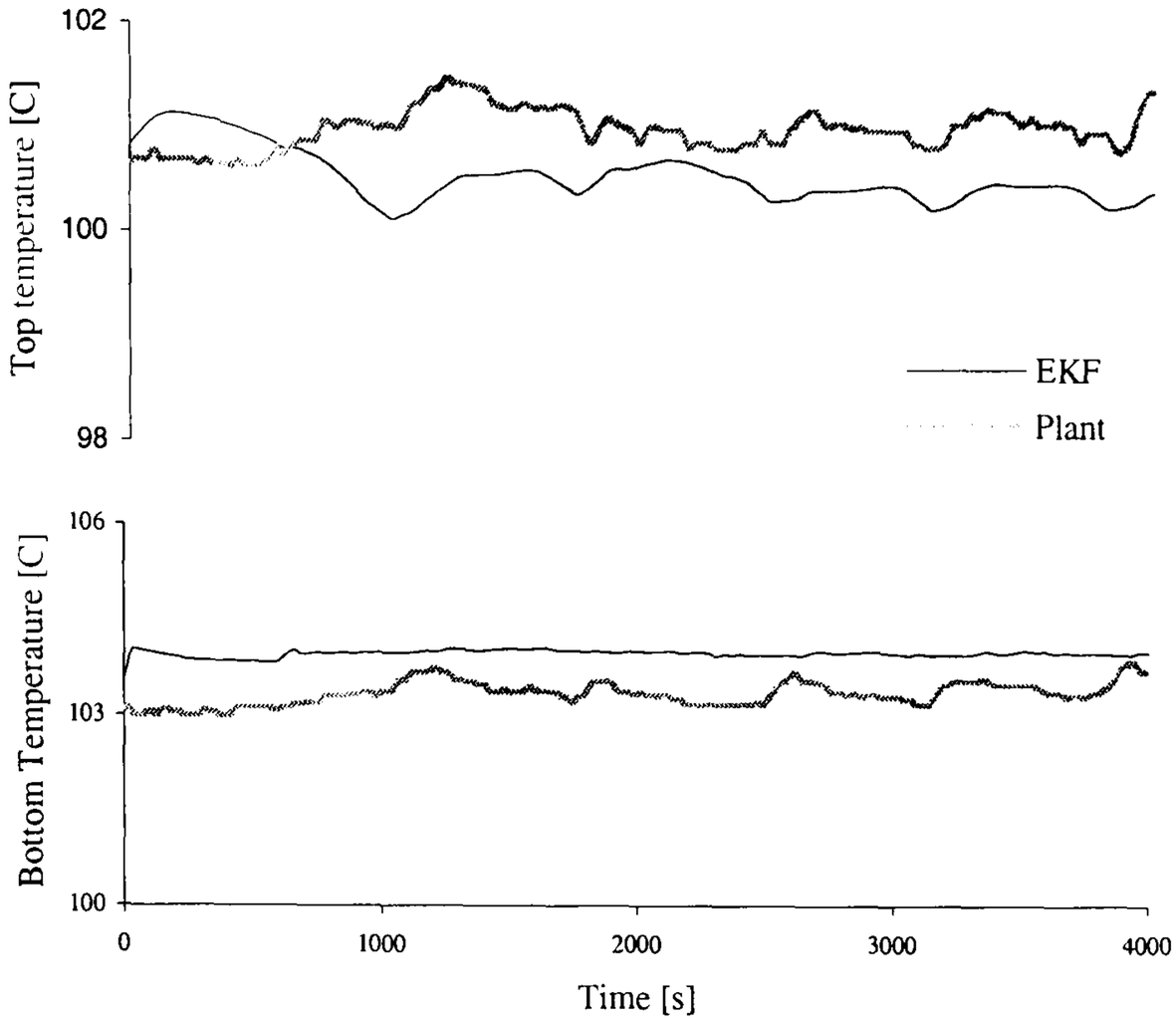


Figure 5.11 Top and Bottom desorber temperatures (Exp2)

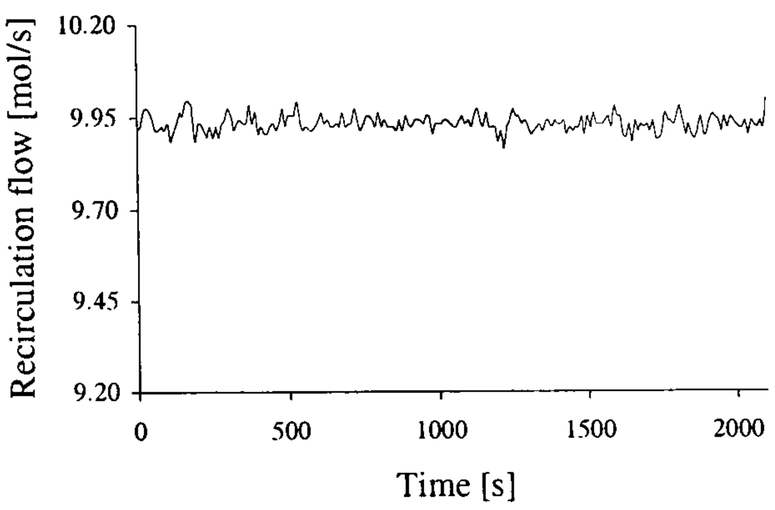
As obtained in the previous experiment, the results achieved are very good, even though the feed gas conditions in the absorber present an oscillatory pattern. This behaviour is generated from one of the closed loops in the plant, which keeps the absorber pressure constant through controlling the gas feed flow. Every time the column is depressurised the flow feed gas is incremented until the absorber reaches operational conditions.

It is important to notice how the filter is capable of achieving such accuracy in the CO_2 leaving gas concentration (Figure 5.7) considering the perturbation and changes introduced in the plant.

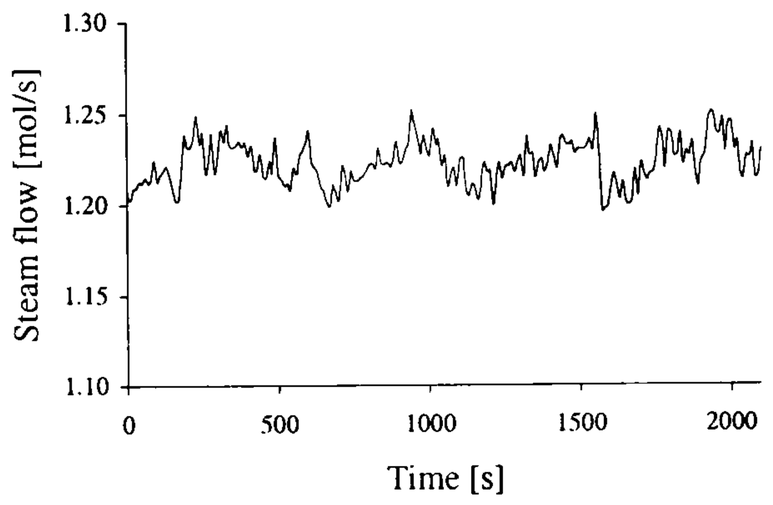
Also as seen in the previous experiment, the estimation of the temperature profiles in the absorber, desorber and reboiler are very good indeed with an average error of 1% compared with the measured values.

5.4. Servo-Problem in the Gas Feed Flow Rate (Exp3)

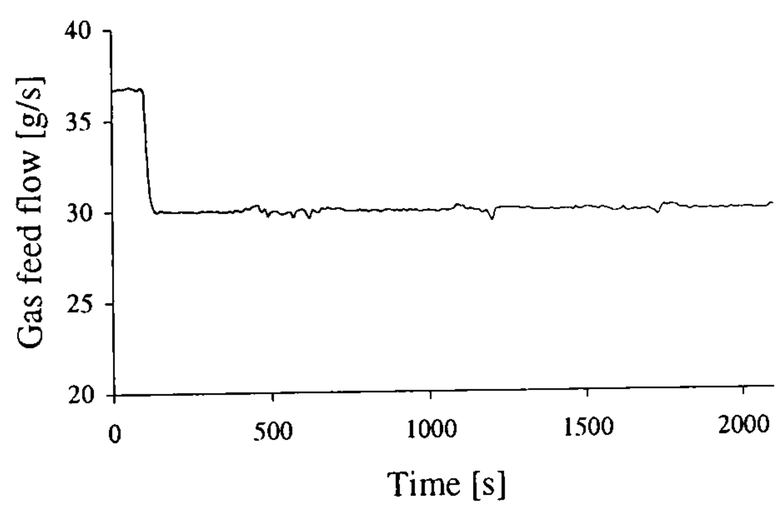
For this experiment a servo problem in the gas feed flow is simulated, the flow rate is decreased from 37 g/s to 30 g/s after 200 seconds, while the other input variables are kept constant. Figure 5.12 shows the input variables record.



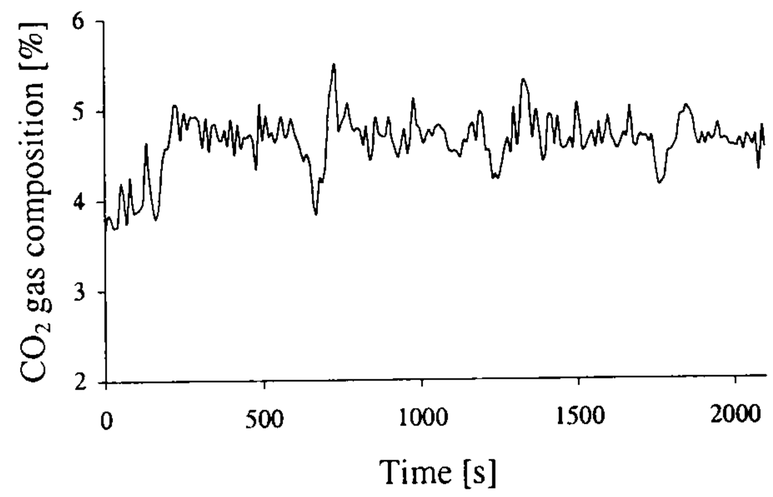
a) Recirculation flow rate



b) Steam flow rate



c) Gas feed flow rate



d) CO_2 gas feed composition

Figure 5.12 Input variables in the plant (Exp3)

The results obtained for the estimation are shown in figures 5.13 to 5.17 .

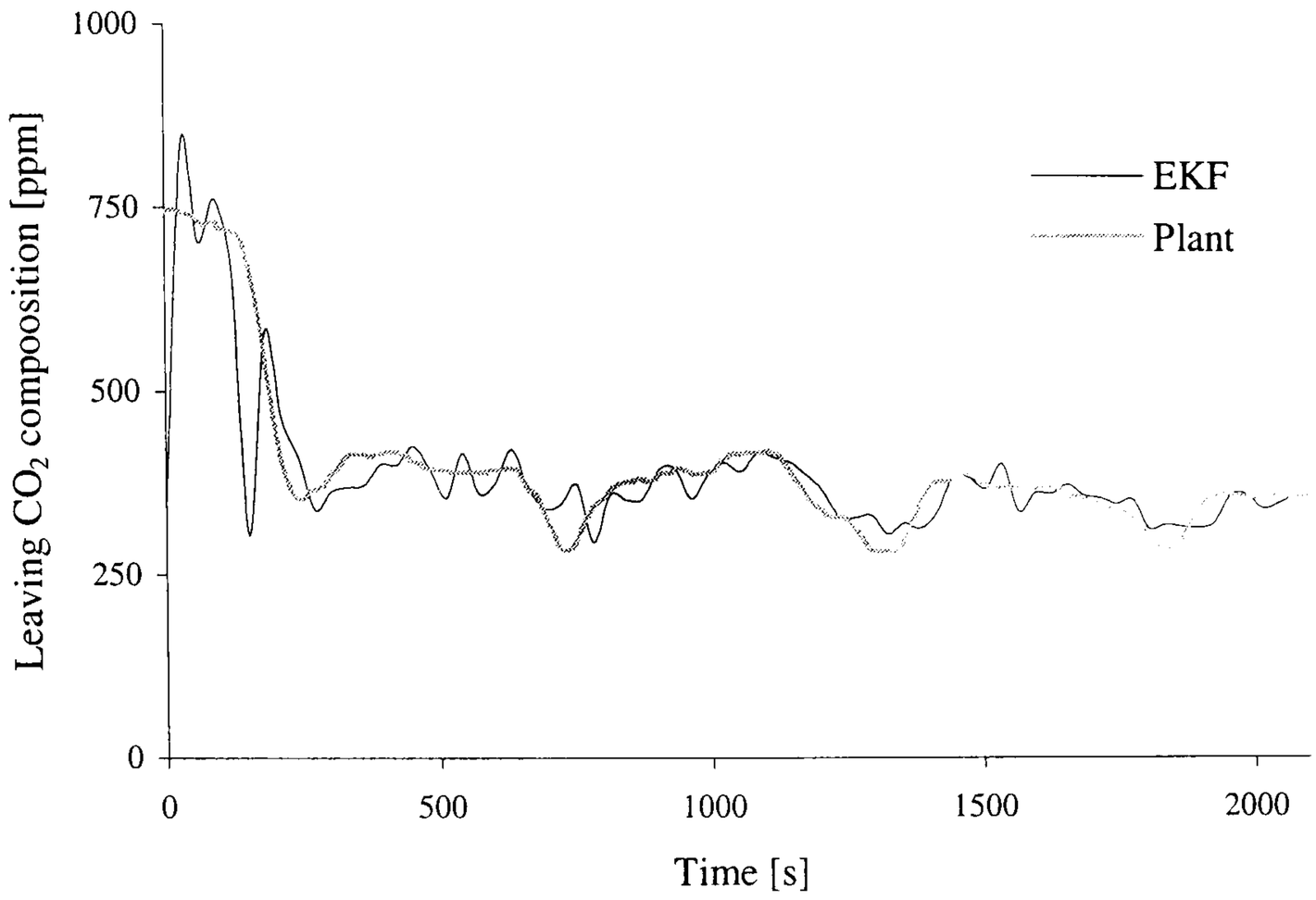


Figure 5.13 CO_2 leaving gas concentration (Exp3)

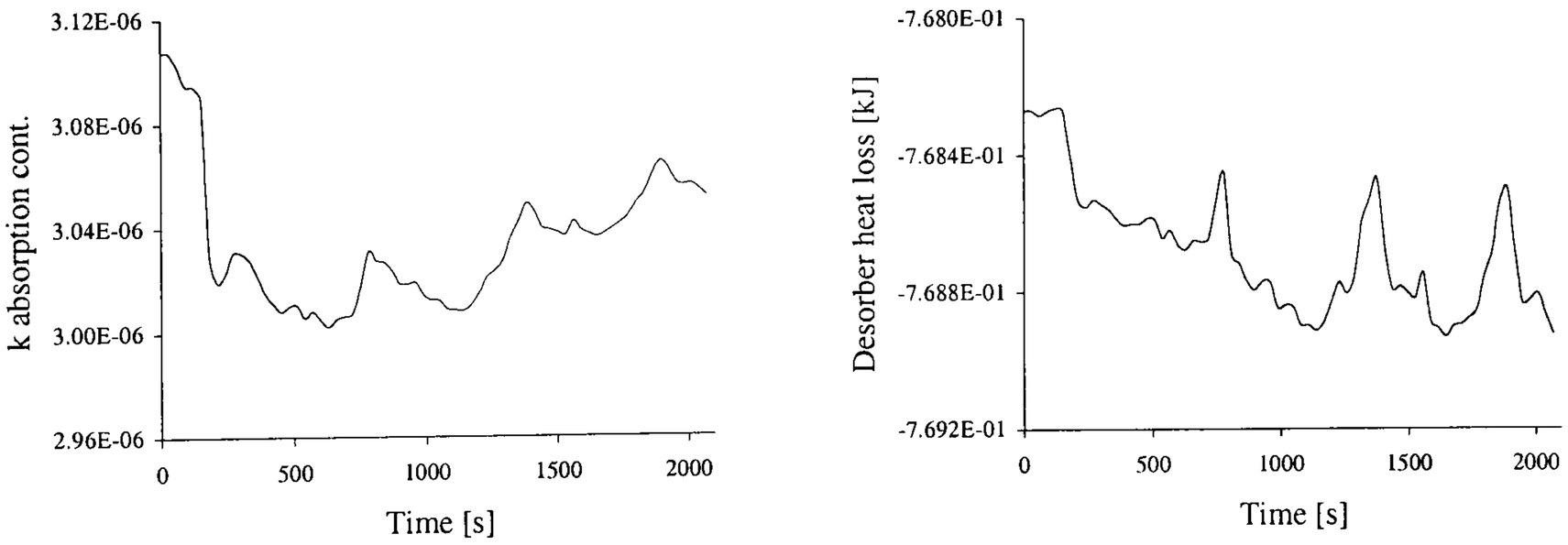


Figure 5.14 Unknown Parameters (Exp3)

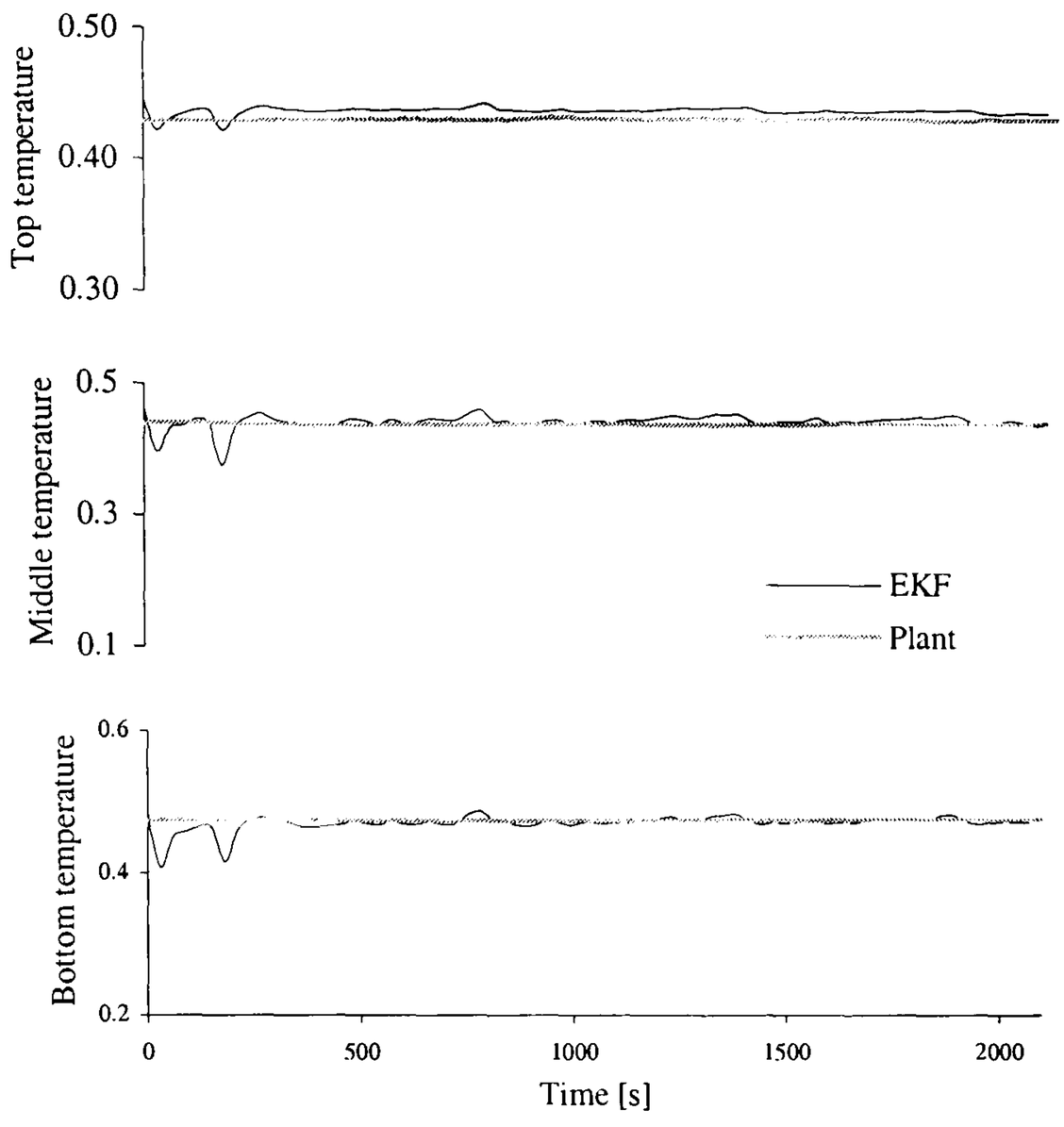


Figure 5.15 Parameterised absorber temperatures (Exp3)

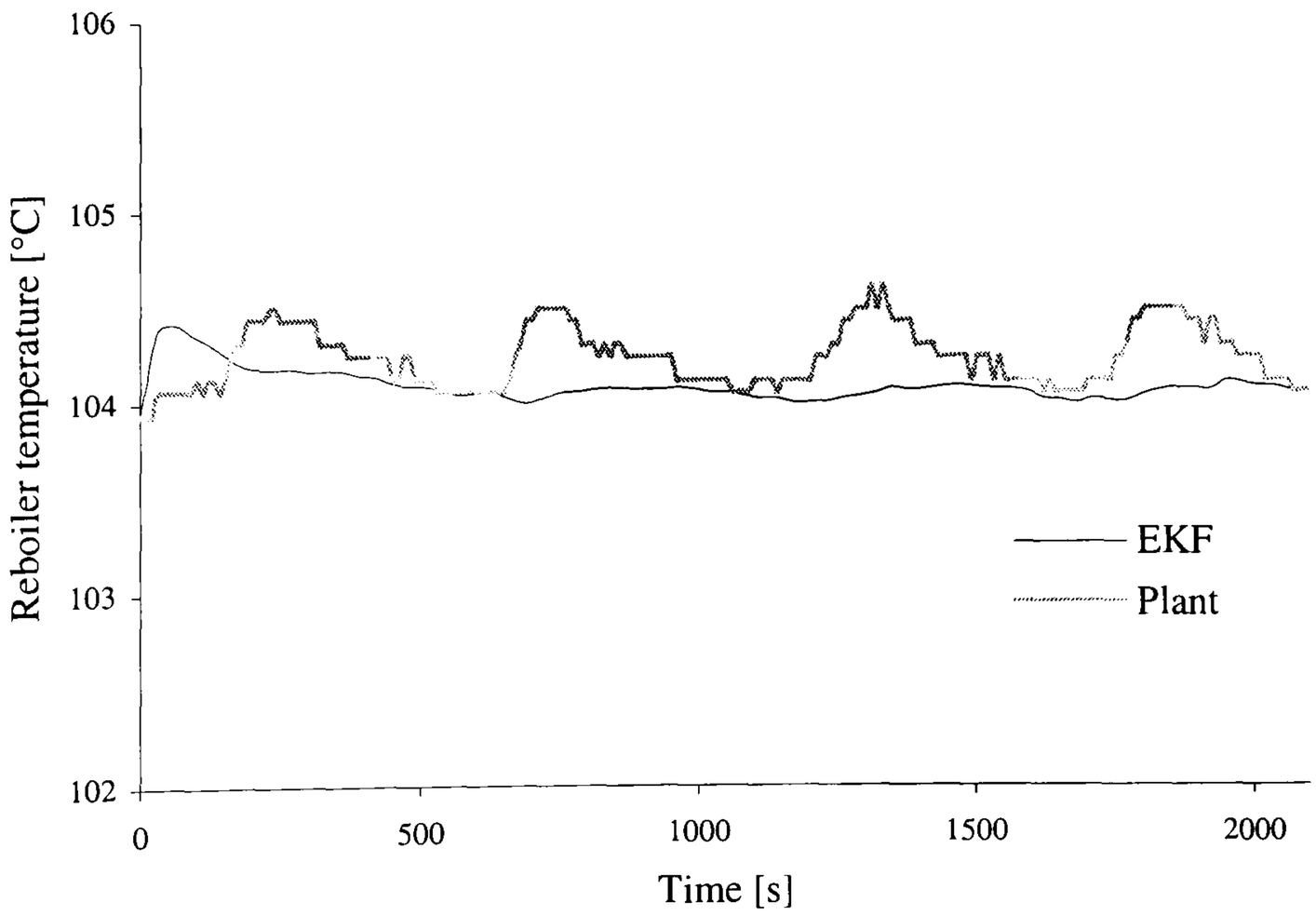


Figure 5.16 Reboiler temperature (Exp3)

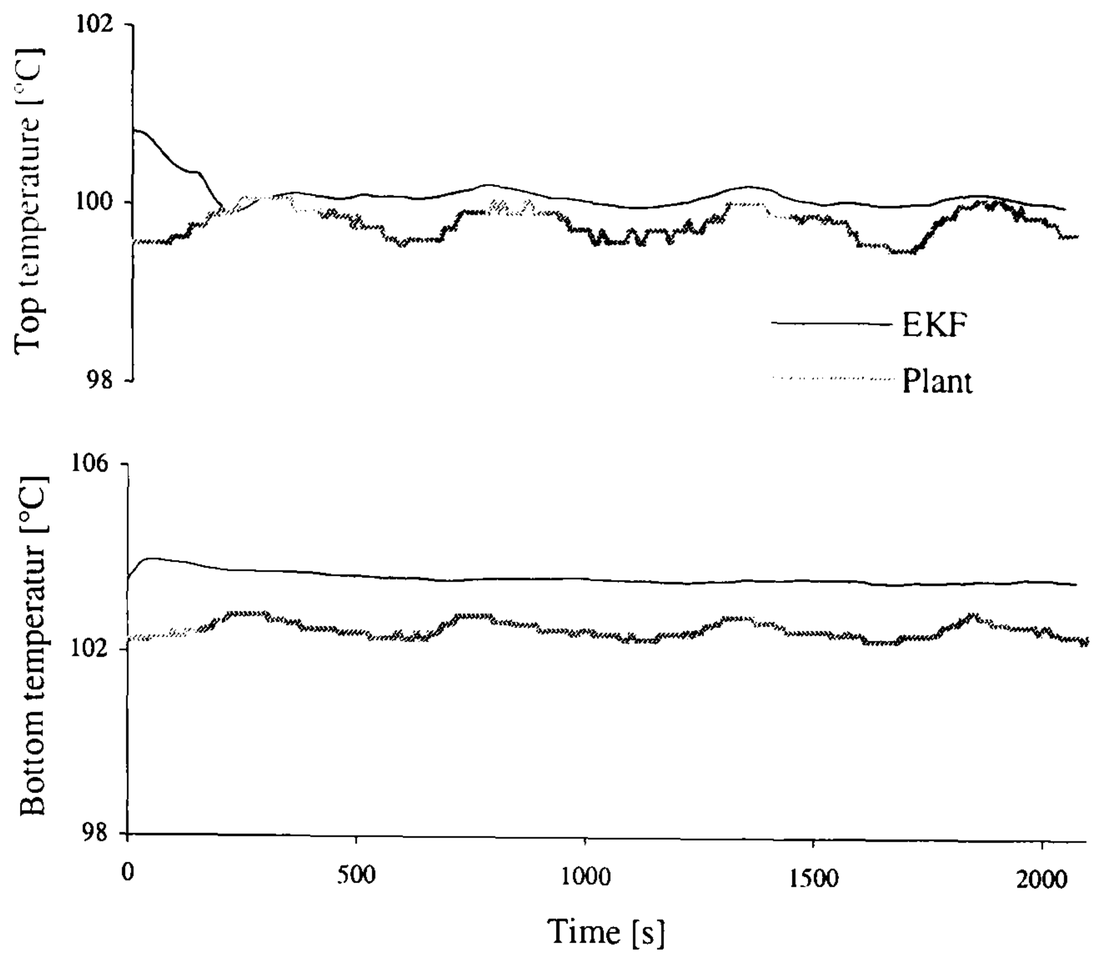


Figure 5.17 Top and Bottom desorber temperatures (Exp3)

This is a very illustrative example because the final CO_2 gas concentration in the absorber presents a deep step-change in its value; after 300 seconds the concentration drops more than 50%.

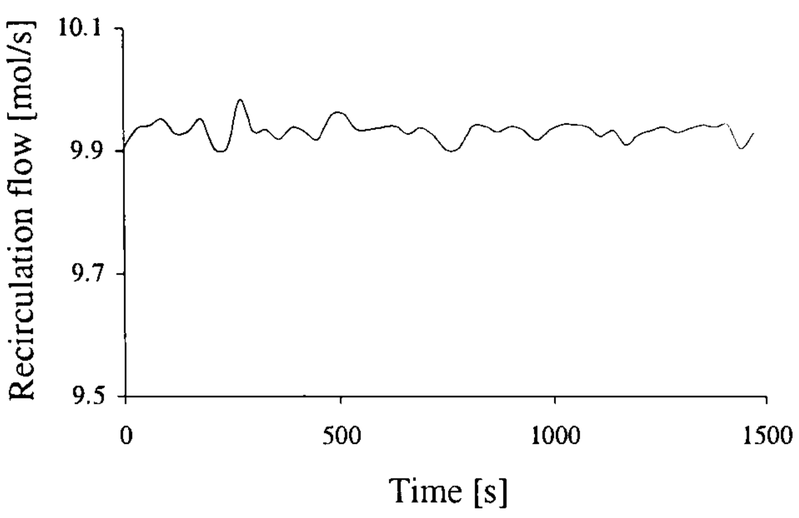
As can be seen in figure 5.13 after such a change the EKF oscillates for a couple of intervals but recovers extremely quickly without creating instabilities or unwanted behaviour. This experiment is important because it proves the robustness and stability of the EKF.

Interestingly the reboiler temperature estimation does not show the close trend exhibited by the other variables (Figure 5.16), showing an oscillatory behaviour with a span of half a degree Celsius approximately. From page 122 it can be seen that the instrument measuring the temperature has an error of that magnitude, therefore the Kalman filter hardly modified the estimated value because is still within the expected range.

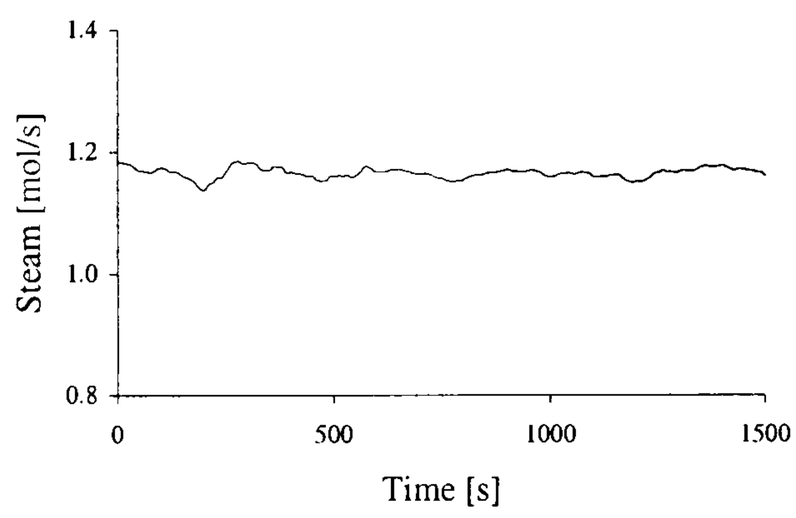
The Kalman filter integrates all measurements from the plant, therefore favouring one particular estimation could significantly degrade others and as a result degrades the overall performance of the filter.

5.5. Disturbances in the CO_2 Gas Feed Composition (Exp4)

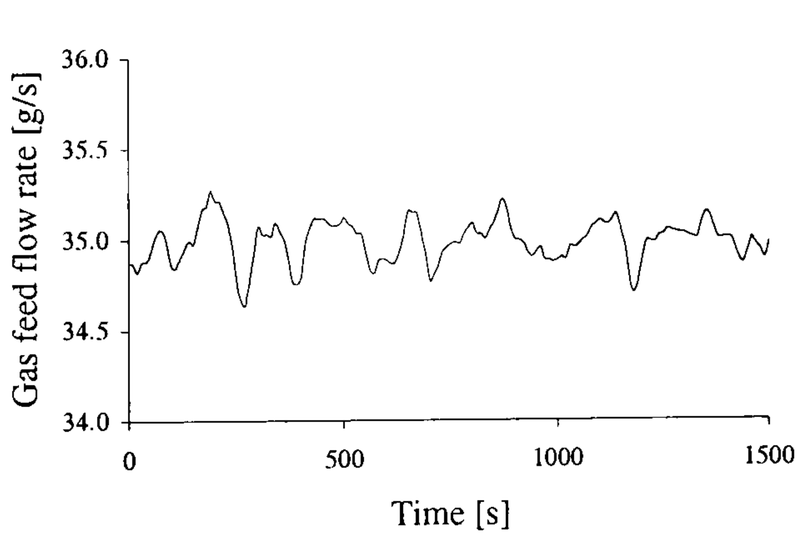
Lastly, in this experiment a disturbance in the gas feed composition is generated by introducing a pulse in the system at 300 seconds, also the composition is gradually reduced from 6% to 5%. Figure 5.18 shows the input variables record.



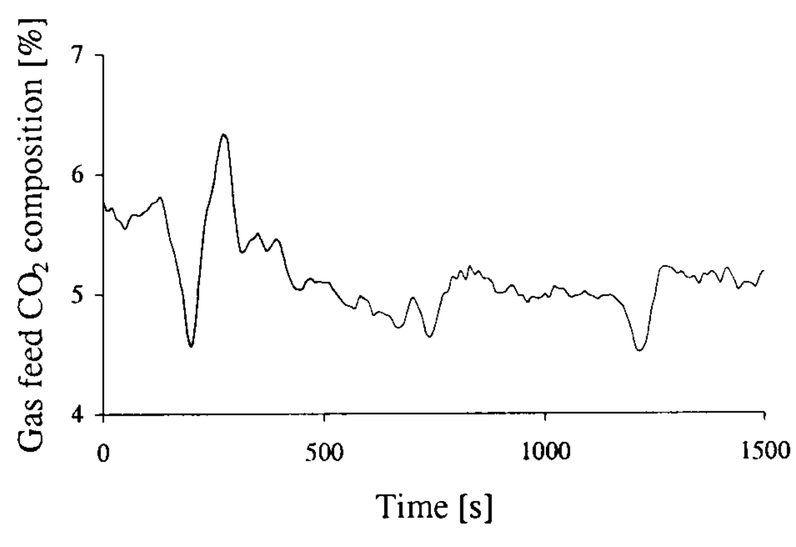
a) Recirculation flow rate



b) Steam flow rate



c) Gas feed flow rate



d) CO_2 gas feed composition

Figure 5.18 Input variables in the plant (Exp4)

The results obtained for the estimation are shown in figures 5.19 to 5.23 with their real values for comparative purposes.

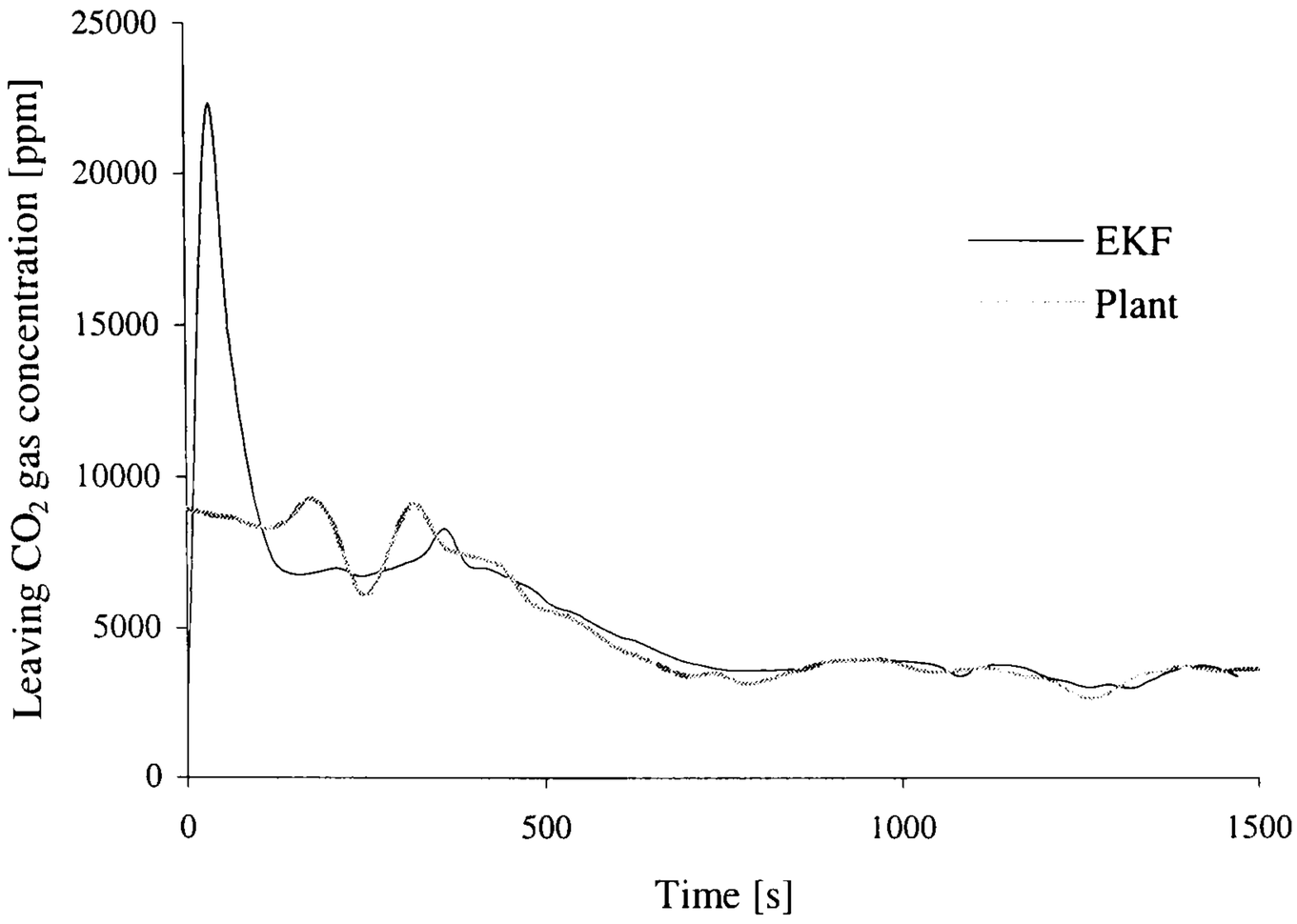


Figure 5.19 CO_2 leaving gas concentration (Exp4)

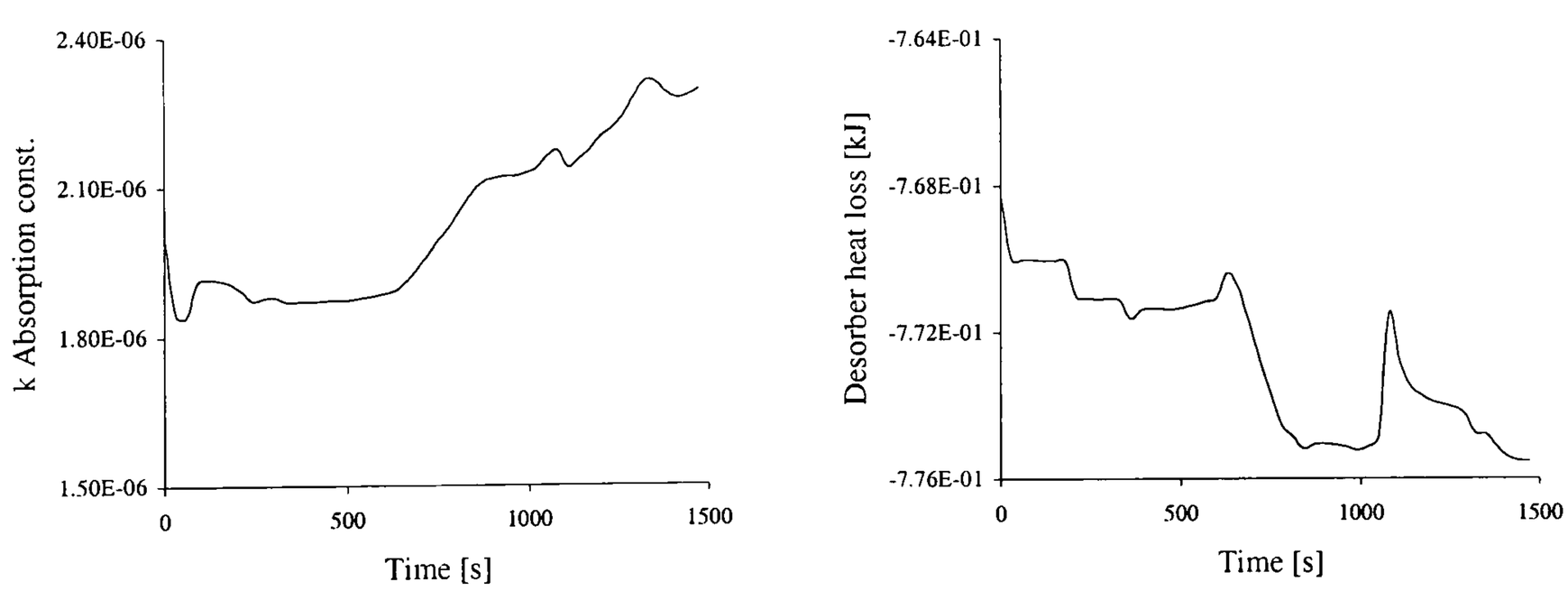


Figure 5.20 Unknown Parameters (Exp4)

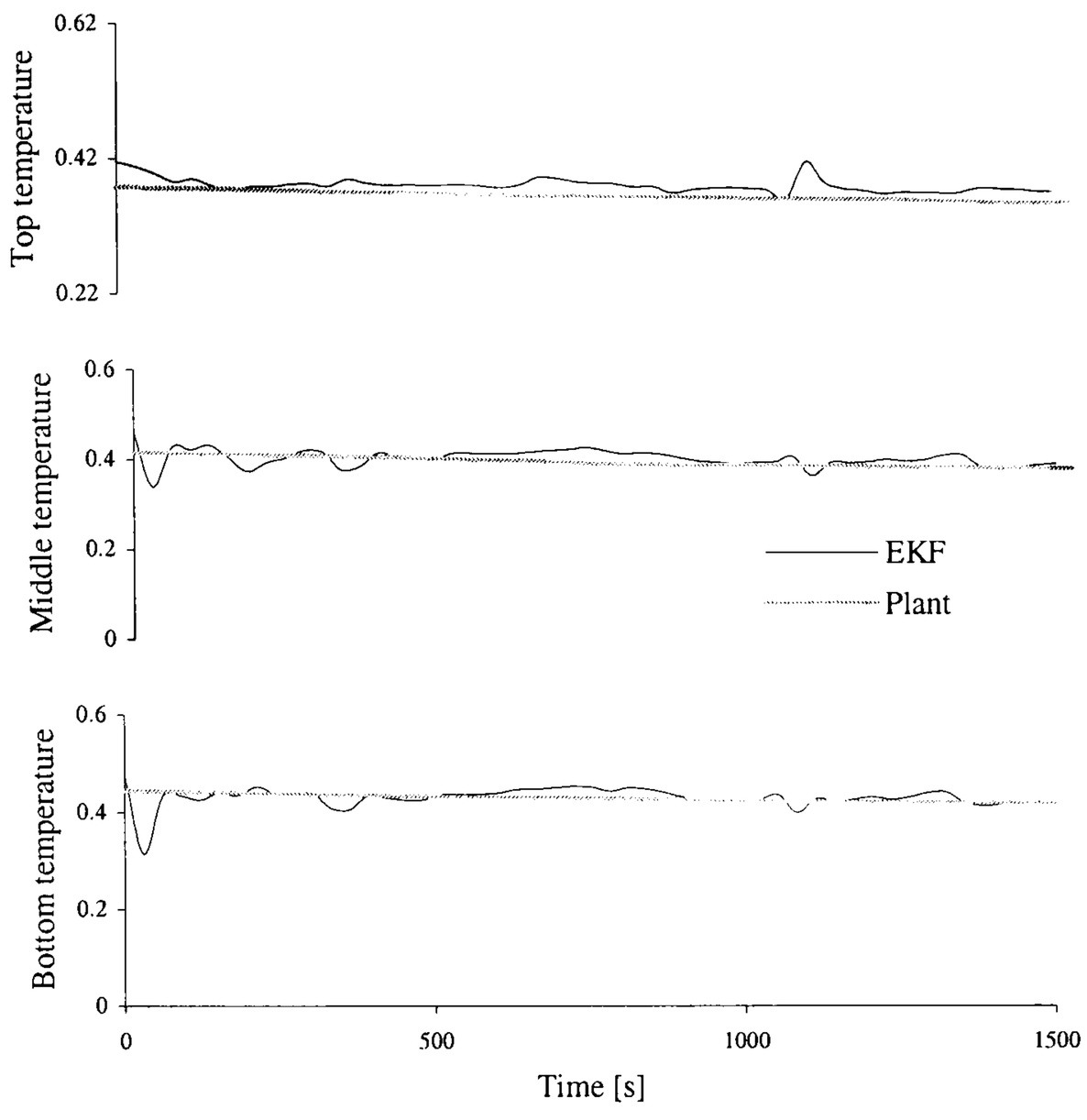


Figure 5.21 Parameterised absorber temperatures (Exp4)

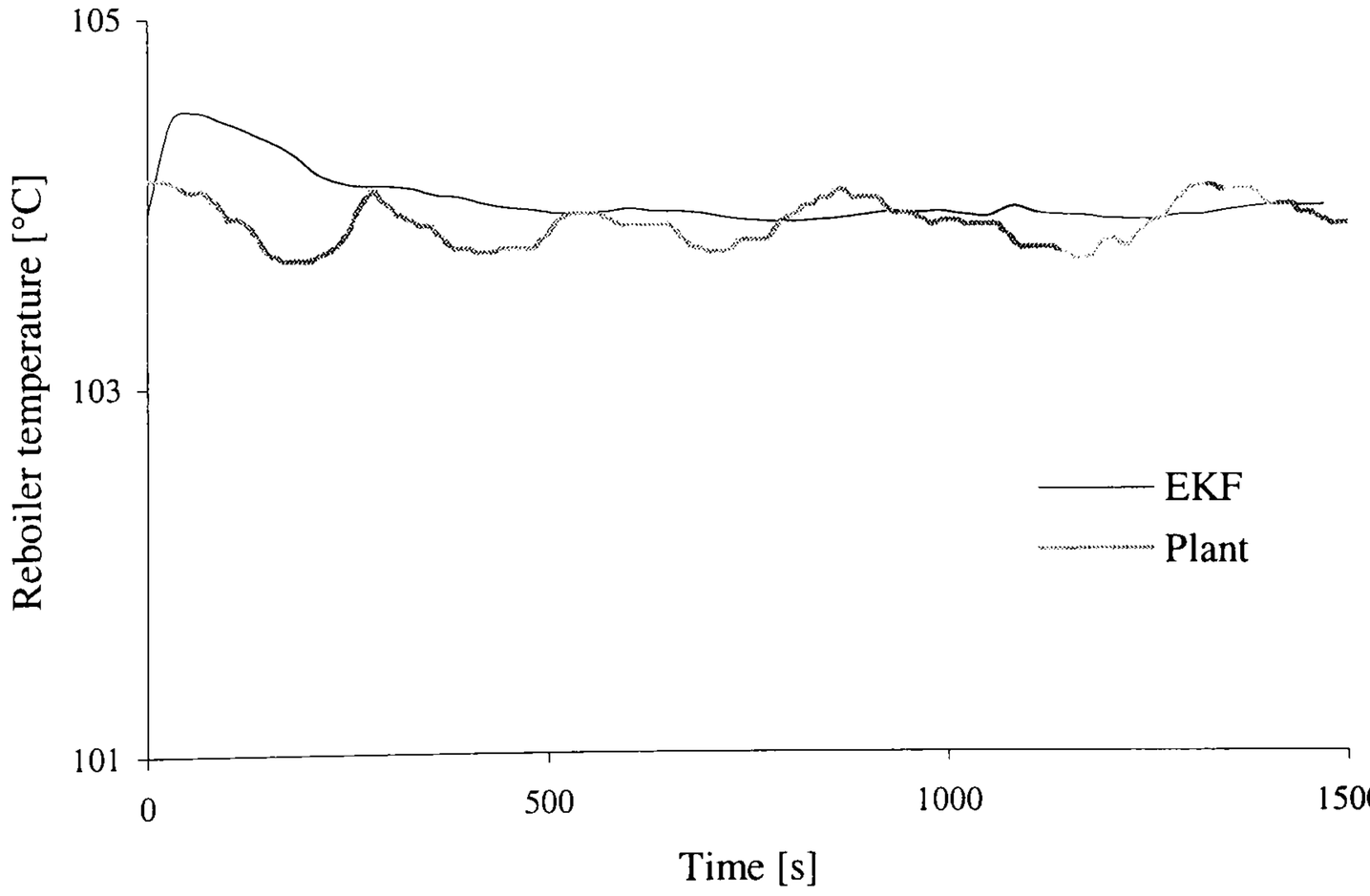


Figure 5.22 Reboiler temperature (Exp4)

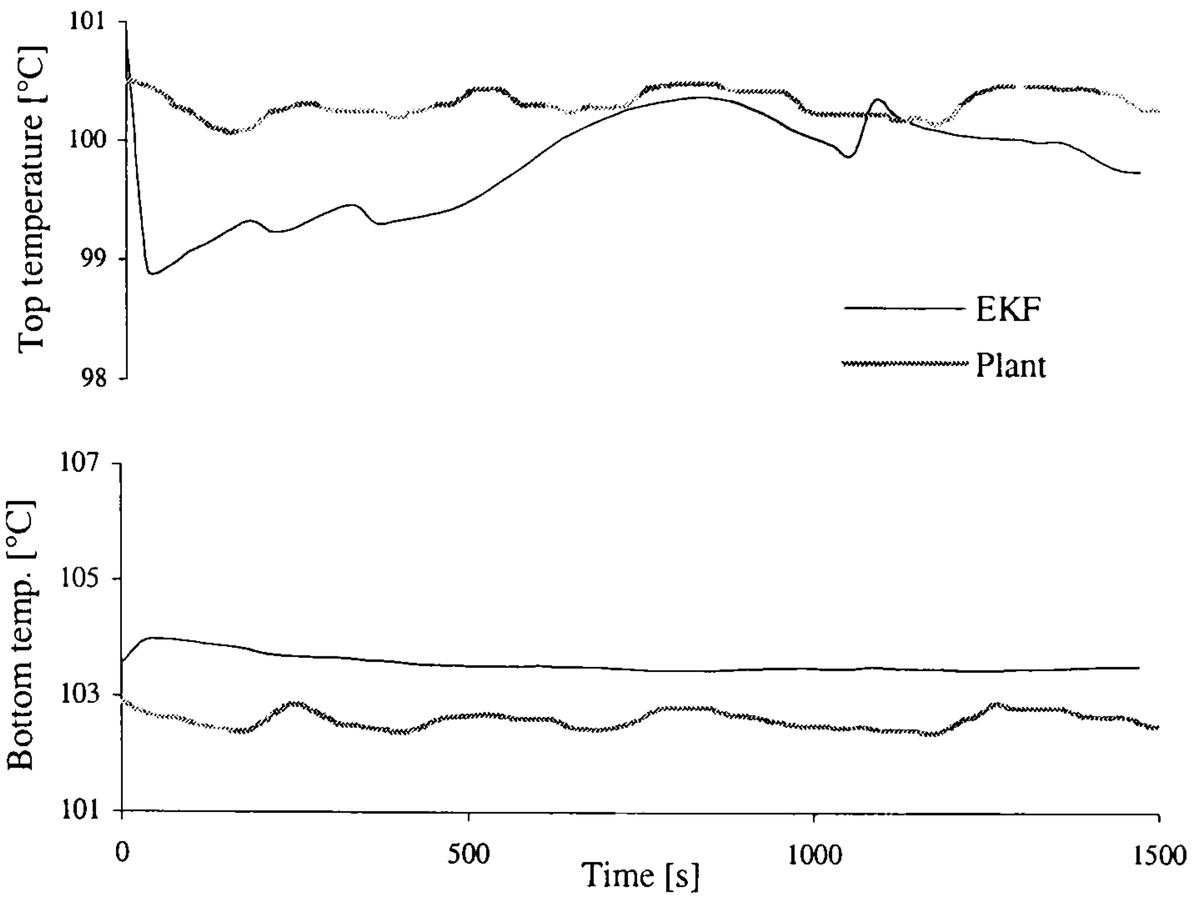


Figure 5.23 Top and Bottom desorber temperatures (Exp4)

Again this experiment shows the stability and the quick response of the estimator. Firstly due to bad guesses in the initial conditions, the Kalman filter estimate of the CO_2 gas concentration is well above its real value, however it recovers efficiently for the next interval and only needs 500 seconds to track correctly the plant. Also it is important to highlight how the EKF handles the pulse in the gas feed composition at 300 seconds, this effect is hardly noticeable in the estimation.

5.6. Conclusions

The accuracy and efficiency of the extended Kalman filter proposed in the previous section has been proved experimentally. Through different tests, including step changes and disturbances in the input variables, the filter is capable of tracking all state variables accurately with an average error of 1%. Also the Kalman filter proved to be quite stable and robust under such real conditions.

Probably more important is the fact that the CO_2 leaving gas concentration, which is the controlled variable in the MPC, is estimated extremely well. That means the controller can count on reliable data for the optimisation process.

Lastly the feasibility of implementing the estimation process online was also confirmed. The measurements are obtained at 30 seconds intervals, while the estimation process required an average of 10 seconds per cycle.

Chapter 6

Optimal Model Predictive Control

6.1. Introduction

Recall that the overall objective is to maintain the purity of the nitrogen stream in the face of variations in feed conditions, with minimum use of steam, using a receding horizon optimal predictive controller. The main control variables are the steam flow rate and the solvent recirculation rate, though the use of temperature of the solvent feed to the absorber as an additional control variable is also considered.

As explained in Chapter 2, the controller makes measurements at regular intervals, from which it estimates the current state of the plant and some parameters, then computes optimal open-loop controls over a fixed horizon for a given prediction of feed conditions over this horizon. In this chapter the use of gOPT to compute the controls is described.

6.2. gOPT Optimisation Tool

It is not intended to discuss the alternative approaches to solving optimal control problems, but give a brief description of the gOPT algorithm incorporated in the gPROMS simulation package. For more details please refer to the "gPROMS Advanced user's guide".

gOPT solves the following problem:

$$\min_{t_f,\theta,u(t),t\in[0,t_f]} z(t_f) = P(x(t),\dot{x}(t),u(t),\theta,t) \tag{6.1}$$

subject to

$$f(x(t),\dot{x}(t),y(t),u(t),\upsilon,t) = 0, \quad t\in[0,t_f] \tag{6.2}$$

$$\underline{g}^i \le g(x(t_i),\dot{x}(t_i),y(t_i),u(t_i),\upsilon(t_i),t_i) \le \overline{g}^i, \quad t_i\in[0,t_f], \quad i=1,2,\ldots \tag{6.3}$$

$$\underline{u} \le u(t) \le \overline{u}, \quad t\in[0,t_f] \tag{6.4}$$

$$\underline{\theta} \le \theta \le \overline{\theta}, \tag{6.5}$$

where t_f is the final time (horizon)

$x(t), y(t)$ are vectors describing the current state of the system, (all initial state variables $x(0)$ need to be specified).

g is a vector of constraints, $u(t)$ is a vector of controls and θ is a vector of time-invariant parameters.

Although t_f can be variable, it must be finite, and the upper and lower limits in (6.3), (6.4) and (6.5) must be given fixed values. Also at each t, equations (6.2) must be solvable for $\dot{x}(t), y(t)$ for given values of $t, u(t), \theta$.

In addition, the functions $u(t)$, are described in terms of a finite number of parameters over a sequence of time intervals; they can be piecewise constant, piecewise linear, piecewise linear continuous or piecewise polynomial (up to fourth order).

6.3. Open-Loop Optimal Control Problem

From Chapter 3 it can be seen that the model equations are already in the form of (6.2), while the general inequalities describing the operating region can be converted to equations of form (6.2) coupled with bounds in (6.4), using slack variables, which

become additional elements of $y(t)$. Some of the parameters involved can be bounded as in (6.5).

The basic objective is to minimize steam consumption over the horizon, given by:

$$J = \int_0^{t_f} S(t)dt \tag{6.6}$$

which can be converted to the form of (6.1) by defining the variable $z(t)$:

$$\dot{z}(t) = S(t), \quad z(0) = 0 \tag{6.7}$$

Finally the maintenance of the nitrogen stream purity is expressed as the "path constraint".

$$y(t) \le y_{\max}, \quad 0 \le t \le t_f \tag{6.8}$$

In fact gOPT does not provide for such constraints, though gOPT is based on the package DAEOPT developed by Vassiliadis et al 1993(a), 1993(b), who considered various ways of dealing with path constraints.

The simplest solution is to impose the path constraint at a finite number of points t_i, $i = 1,2,\ldots$ as in (6.3), which can conveniently be the end-points of the control intervals. The drawback is of course that the path constraint can be violated within the intervals, and it may be necessary to use many short intervals, resulting in a large problem.

An alternative is to convert the path constraint into an end-point constraint:

$$\int_0^{t_f} \max\left(0, \left(y_P(t) - y_{\max}\right)\right)dt \le 0 \tag{6.9}$$

and again this can be converted into a differential equation:

$$\dot{x}(t) = \max\{0, y(t) - y_{\max}\}, \quad x(0) = 0, \quad x(t_f) = 0 \tag{6.10}$$

Of course the numerical solution of the differential equations in (6.2), (6.7), (6.9) still discretize the problem, but the constraints are now imposed over a set of more closely spaced points, with the numerical integrator providing assurance of good accuracy within the interval. Nevertheless, this is a more difficult problem to solve, and this significantly increases the computational time. Vassiliadis also considered a combination of these approaches.

In later sections we compare the two approaches, explore the sensitivity of the results to model complexity, and consider how to choose an appropriate horizon.

6.4. Tests on this Problem

In order to test the previous formulation, a set of simulation experiments is planned to select the best set of constraints, objective function and time horizon. The purpose is to study multiple approaches and select the most suitable MPC algorithm for the plant.

The main cause of disturbances in the plant are the gas feed conditions, either by perturbing the feed flow rate or the feed gas concentration, or a combination of both. In order to test and compare all the experiments under the same setting the following conditions are established.

The system starts at steady state conditions. Gas feed concentration is set at 4% for all running time. Feed flow rate is set at 40 g/s for the first 500 seconds and step-changed to 45 g/s afterwards. Steam and solvent flow rates are initially set at optimal values 0.7 and 14 mol/s respectively. The inlet liquid temperature in the absorber is set constant at 45°C, however, it will be considered an extra control variable later on. The other initial conditions and parameters are fixed to their original values (see Appendix A for a complete description of the model and variables).

Under these conditions recirculation and steam flow rate values are manipulated to maintain the CO_2 leaving concentration in the absorber below 100 ppm.

For illustrative purposes, Figure 6.1 shows the system using the conditions described above in two different scenarios. The first does not involve any kind of control action, while the second uses a classical PI controller that adjusts the steam flow in the reboiler to keep the CO_2 concentration at 100 ppm.

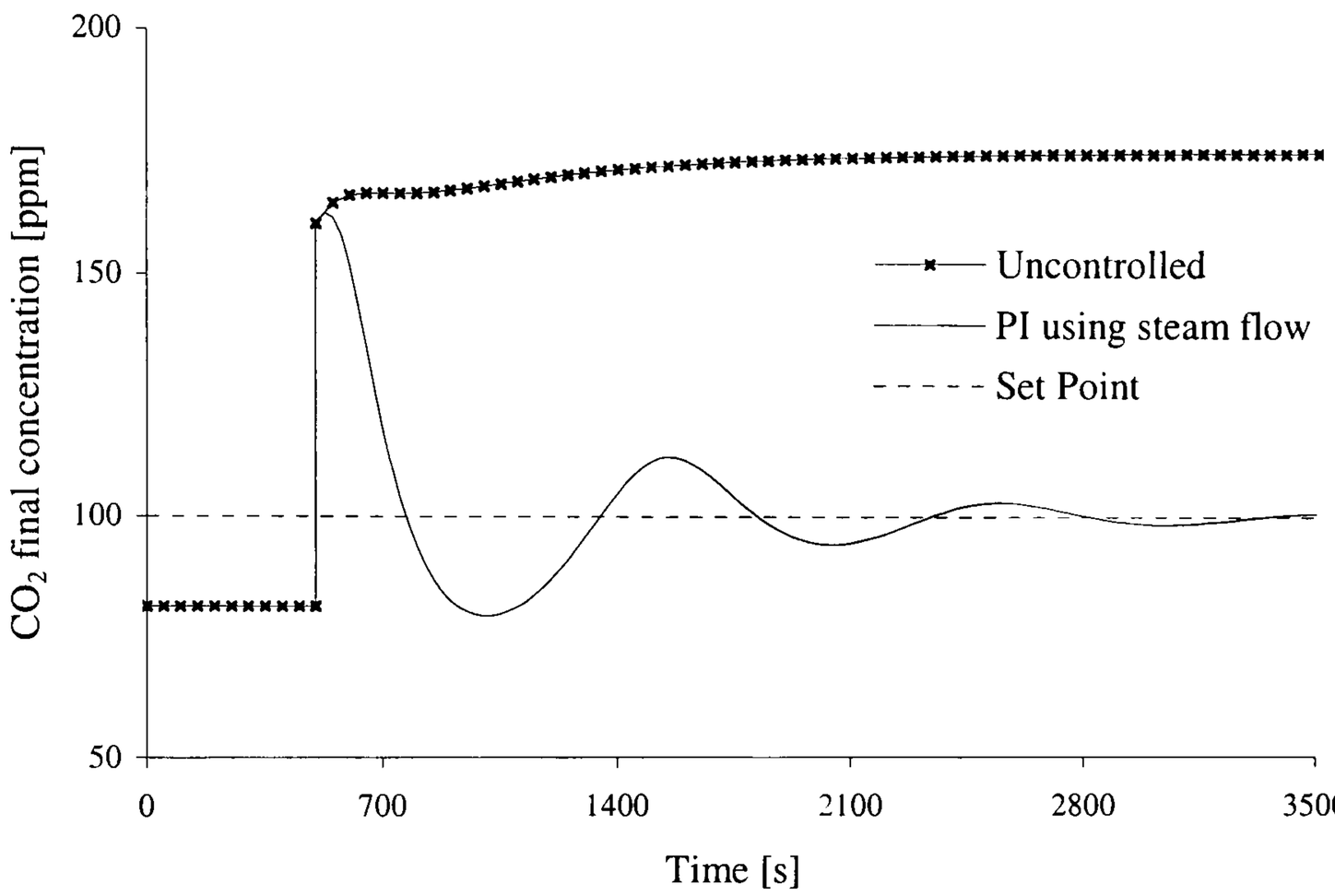


Figure 6.1. Uncontrolled and PI controlled system.

This experiment reflects that classical controllers are not capable of preventing overshoots, therefore that it is necessary to use an advanced control technique like a MPC to maintain the CO_2 concentration below the set point. When a PI controller is employed the CO_2 concentration is nearly 60% above set point at perturbation time. This value would be considered poisonous for a fictitious process downstream.

The general MPC algorithm explained in Chapter 2 is selected as the controller. The optimiser computes the best set of control changes to satisfy all the constraints while minimising the objective function (steam consumption). From the control horizon, only the first interval is implemented in the model. This procedure is repeated at fixed intervals, every 120 seconds.

Because the optimisation and simulation processes are run using the same model. no estimation step is required. State variable values at the beginning of each interval are directly copied from the simulation to the optimiser.

Lastly, it is also assumed that the feed conditions are known in advance for the next 500 seconds, therefore some control action is expected by the controller before perturbations reach the plant.

The next sections present different variations of MPC under the conditions expressed above. The idea is to compare and test diverse scenarios, selecting the best alternatives taking into account stability, robustness and controllability properties.

6.4.1. Fixed Control Horizon.

The first set of simulation experiments involves using an MPC with fixed control horizon. The whole horizon is divided into six fixed intervals, the first three have a length of 120 seconds, the fourth is 240 seconds long, the fifth 500 seconds and the last one 750 seconds, creating a control horizon of 1850 seconds, long enough to avoid stability problems (Scokaert & Rawlings, 1998). Steam and recirculation flow rates are constant during each interval.

With this setting and using the plant conditions described in the previous section, three approaches are tested: Internal point constraint, path constraint and path constraint included as a penalty term in the objective function.

6.4.1.1 Point Constraint at End-Times of Control Intervals

The first run uses exclusively internal point constraints, which means the upper limit for y_P is forced only at the end of each time interval. The clear advantage of this choice is a shorter computational time.

Figure 6.2 shows the dynamic behaviour of the CO_2 final concentration using internal point constraints, while Figure 6.3 shows the steam and solvent flow rates for each interval. The system starts at steady state using the conditions described in p142.

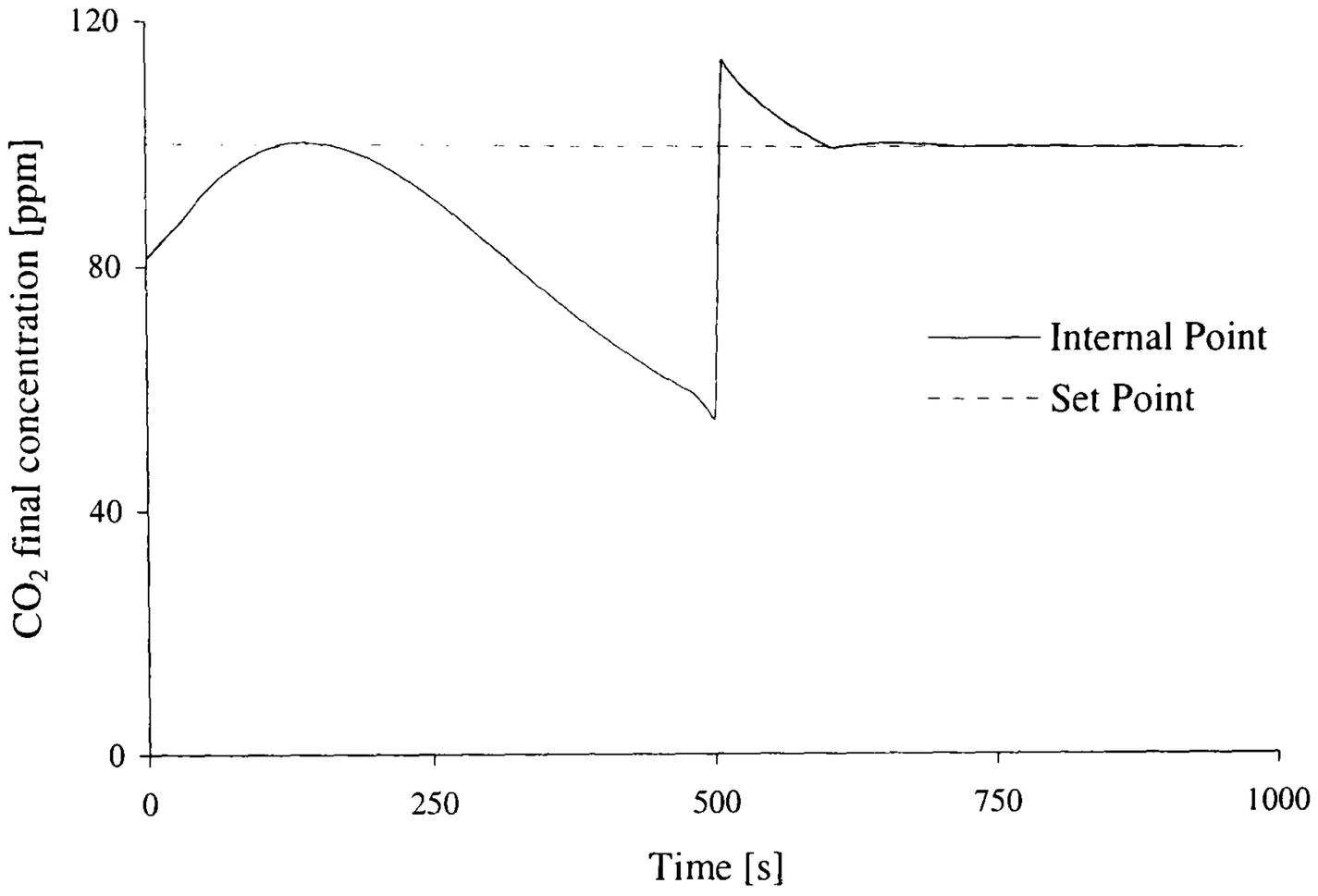


Figure 6.2. CO_2 dynamic using internal point constraint.

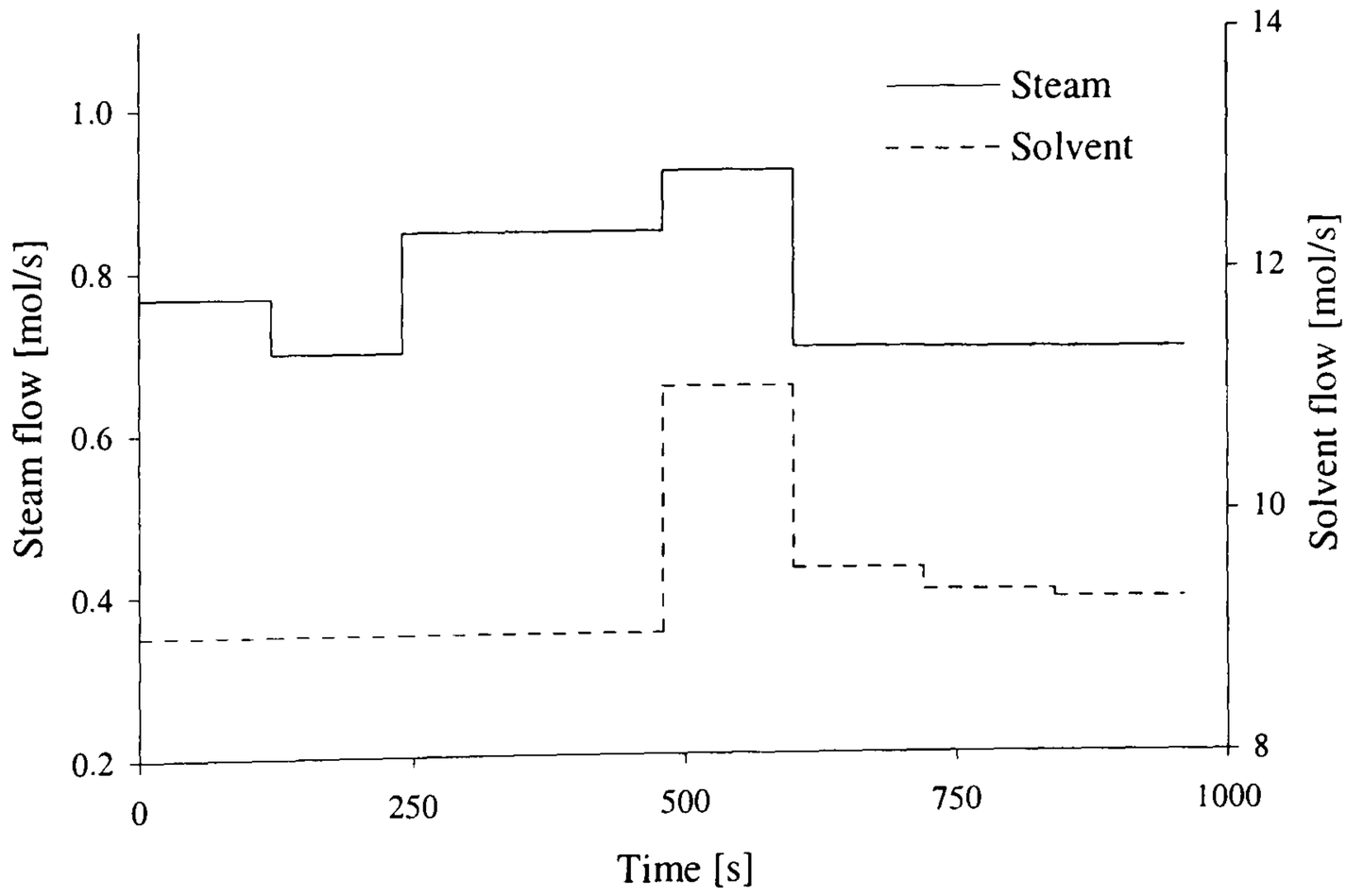


Figure 6.3. Steam and solvent recirculation flow rates.

Predictably, using point constraints at the end of each interval has the clear advantage of a shorter computational time for the optimisation process. On average, 20 iterations are required to converge to the optimal solution, which in an up to date computer can be executed in 60 seconds approximately. However as a drawback y_P crosses the upper boundary condition several times during the transient period, having a maximum value of nearly 120 ppm.

Compared with the PI controller the system reaches steady state conditions very fast (only 200 seconds after perturbation), however it will be shown later on that other approaches converge faster. Also due to the lack of tightness on the constraint, steam changes are observed only 250 seconds before perturbation.

With these results and analysis, the exclusive use of point constraints at the end of each interval for y_P does not provide a satisfactory optimal controller.

6.4.1.2 Path Constraint

For this scenario, the point constraint used earlier to control y_P is replaced by a path constraint (Equation 6.9). The difference is that the CO_2 final concentration constraint is active through the entire control horizon.

Due to the fact that gOPT does not have this option as an internal command, the following inequality is incorporated into the model. Equation (6.9) is slightly modified by substituting the right term with an error factor ε.

$$\int_0^{t_F} \max\left(0, \left(y_P(t) - y_{\max}\right)\right) dt \leq \varepsilon \tag{6.11}$$

To convert the equation into a path constraint, the new variable ε called error factor is established as an end-point constraint on gOPT. The greater the value of this factor, the softer the constraint becomes and consequently the shorter the computational time.

Using the same plant conditions as before, the effect on the ε value is tested. Figure 6.4 presents the results for three different ε values: $\varepsilon = 0.1t_f$, $\varepsilon = 0.02t_f$, $\varepsilon = 0$. Figure 6.5 and Figure 6.6 show the steam and solvent flow rates respectively.

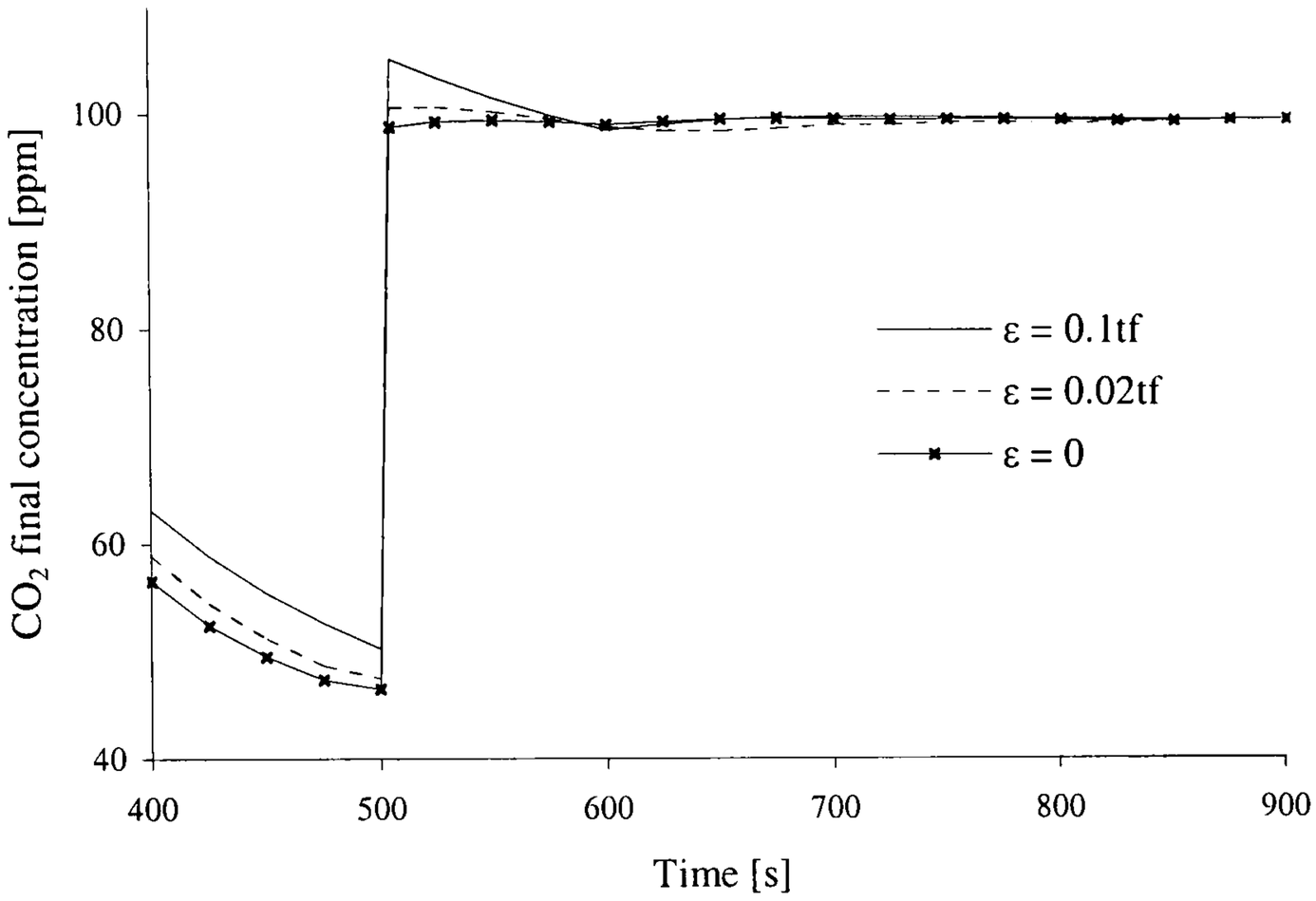


Figure 6.4. Controlled system with path constraints.

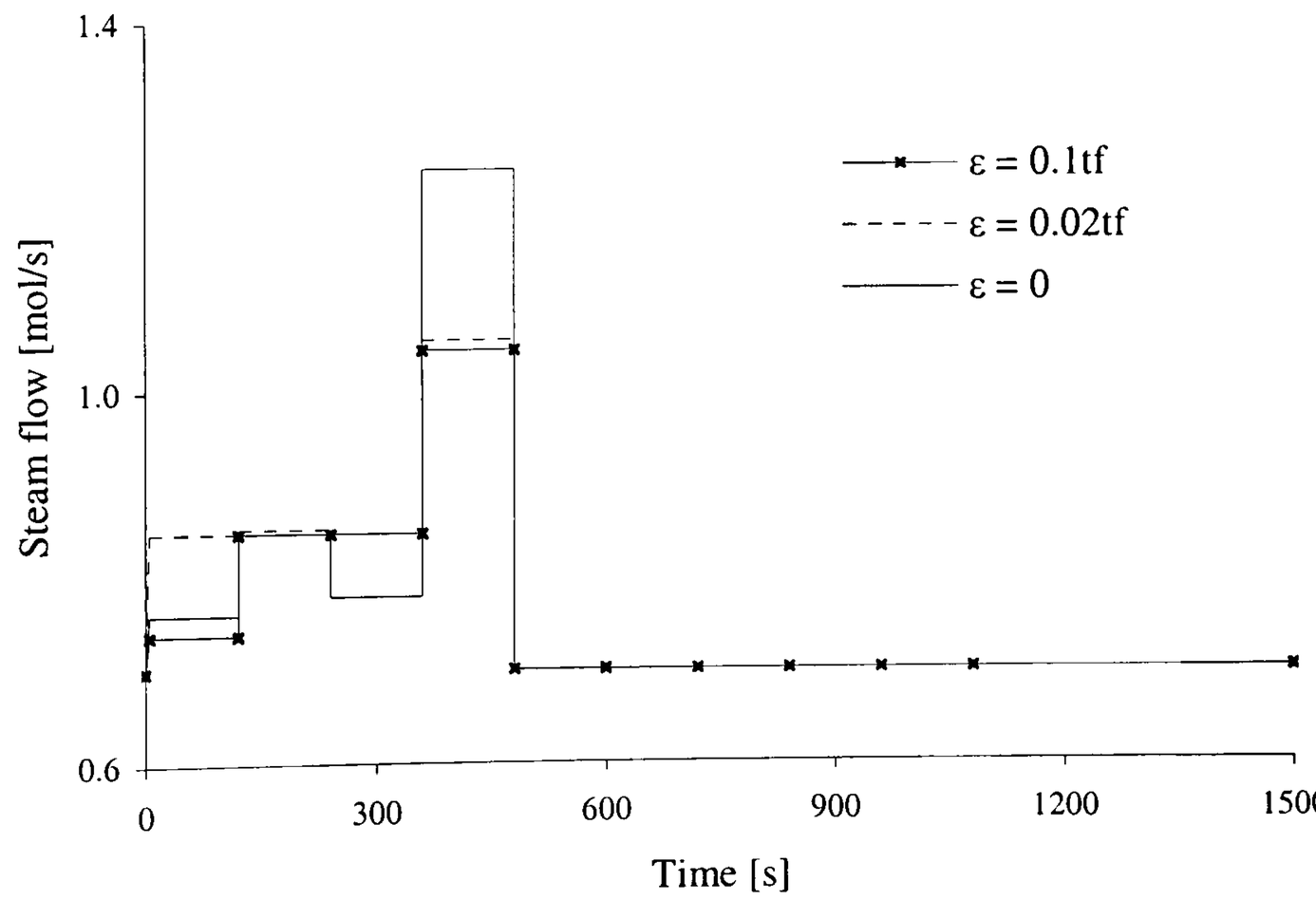


Figure 6.5. Steam consumption for each case.

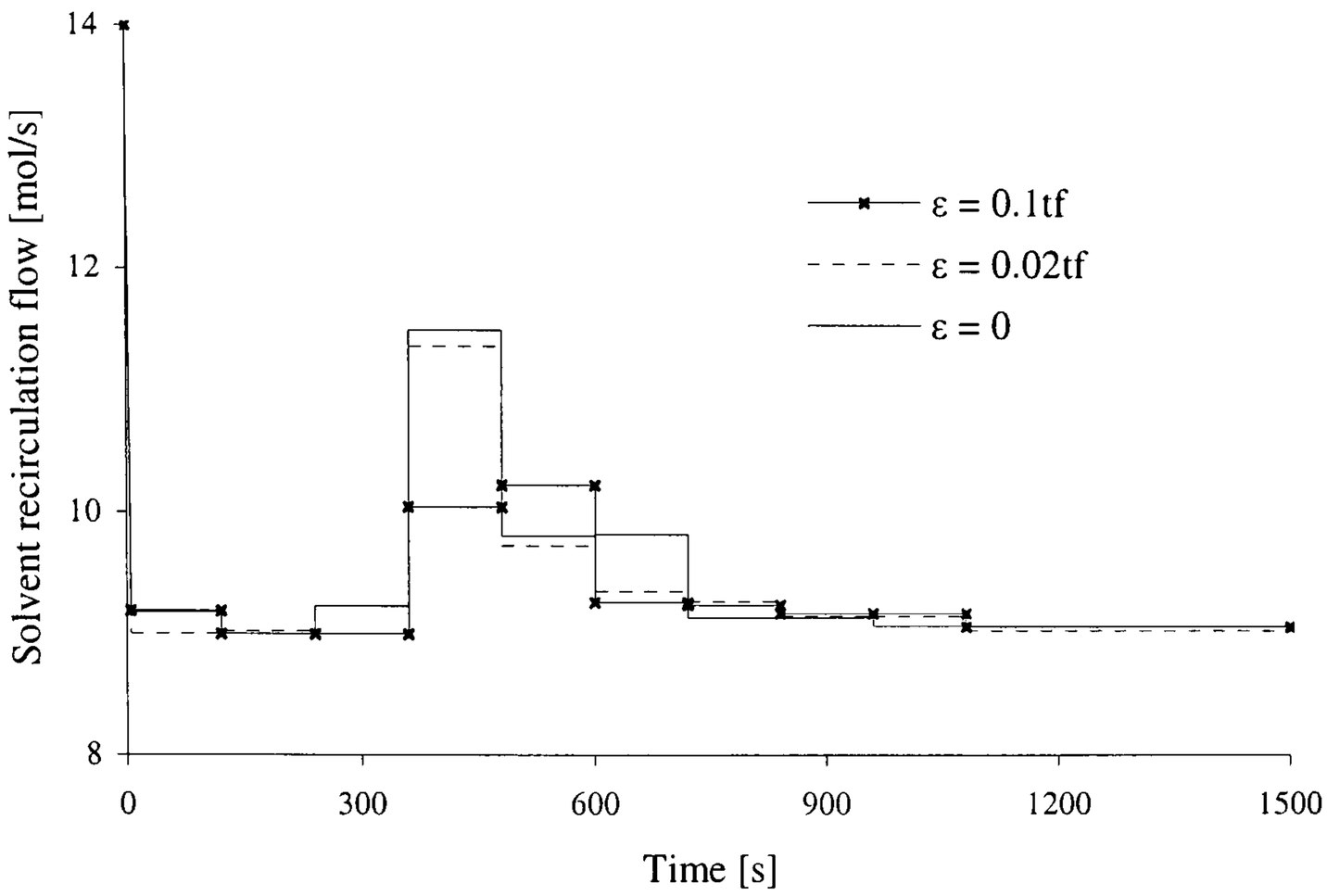


Figure 6.6. Solvent recirculation rate for each case.

Compared with the interior point constraint case, the application of a path constraint keeps the final CO_2 concentration more tightly at 100 ppm (shown in Figure 6.4) with the added benefit that the system arrives at steady state faster, only 100 seconds after the perturbation. However the computational time is increased by 7 or 8 times (600 seconds approximately) as well as the amount of steam used by the controller. Also gOPT becomes very sensitive to initial guess values, where just a small change in one of them could mean the difference between converging and not finding a feasible solution.

It is also important to highlight the effect the path constraint has in the time span required to take preventive control actions. While in the internal point constraint case only 250 seconds were necessary, the path constraint case requires 400 seconds in advance to handle effectively the perturbation. That is a good measure of the minimum time horizon needed in advance to control the CO_2 concentration level efficiently.

As explained before, lower values of ε make the constraint harder. Figure 6.4 shows that for smaller values of ε, smaller overshoots are obtained from the system, a desirable property. However the computational time required finding the optimal values increased exponentially. For this reason it is important to obtain the optimal value that is

capable of giving a shorter computational time without making the constraint too soft and as a consequence overshooting excessively the set point.

Although each case reaches similar steady state conditions and controls the plant effectively, $\varepsilon = 0.02t_f$ exhibits the best combination of controllability, steam consumption and computational time in the transient period. The overshoot is only few ppm above the set point while the computational time on average is 400 seconds.

In summary reducing the constraint ε increases the computational time requirements, however the system has a smoother behaviour with less oscillation and arrives faster to steady state condition. Both conditions are desirable for an optimal control scheme. Previously mentioned, $\varepsilon = 0.02t_f$ maintains these requirements without using too much computing effort.

6.4.1.3 Path Constraint Included in the Objective Function

So far we have assumed the optimiser knows the gas feed conditions in the plant in advance. Therefore, no unexpected perturbations are considered in the formulation, and consequently it is not clear how the previous algorithms would react under small disturbances caused by noisy measurements or unpredicted events.

In order to test this scenario an unexpected perturbation is introduced in the system. For example, the instrument that reads the feed gas CO_2 composition has an absolute error of 0.5%. Starting from optimal conditions, a disturbance of this magnitude in the gas feed stream is introduced; at the same time the steam flow rate is increased to its maximum value.

Figure 6.7 shows the value of the integral in (6.11) and the CO_2 final gas concentration.

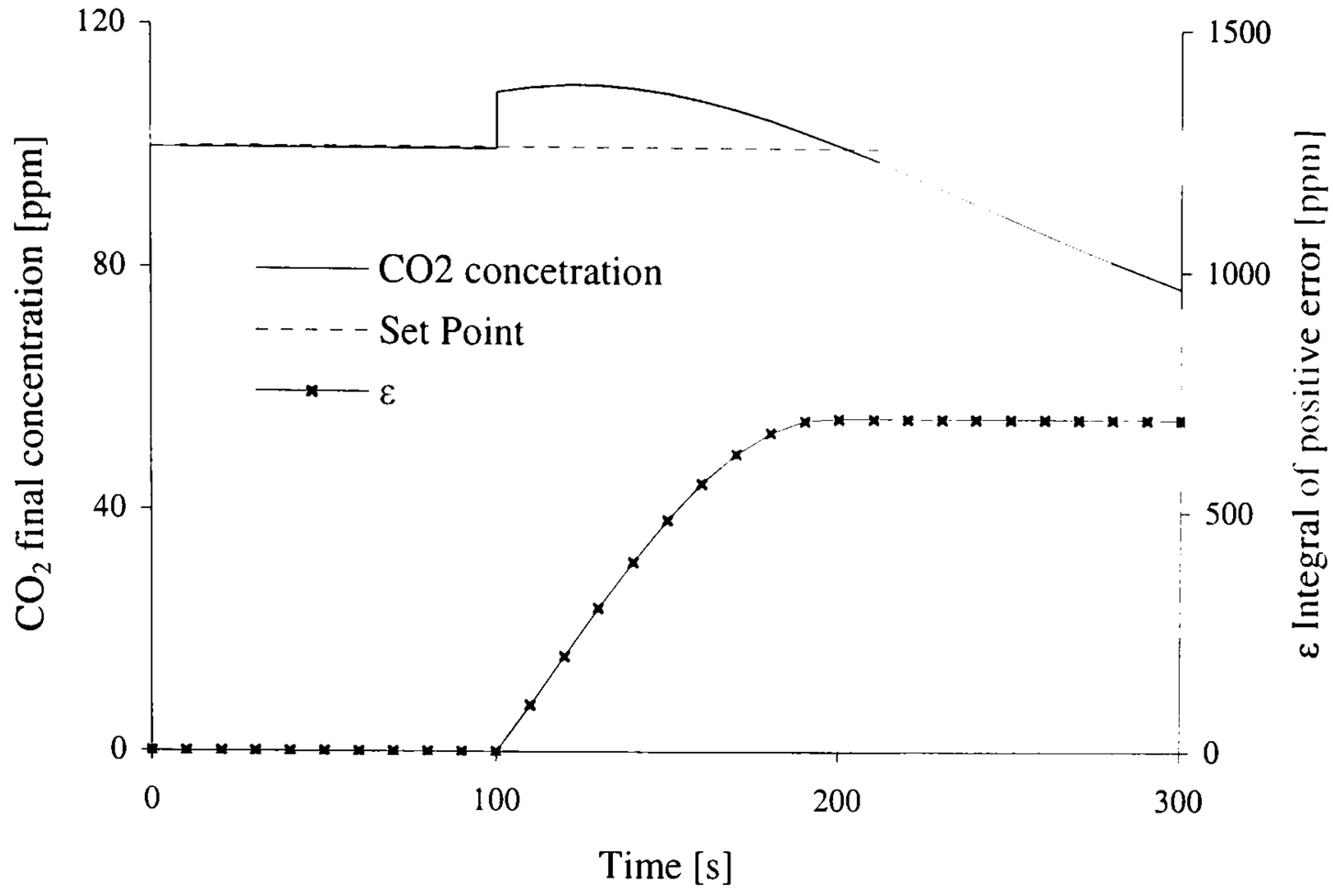


Figure 6.7. Effect on the integral error under unexpected perturbation.

With this small perturbation in the gas feed concentration and even using the maximum steam flow rate, the value of the positive error is almost 700. If any of the previous cases (internal point and path constraint) were used, it would be impossible for the solver to converge to a feasible solution due to the size of the integral.

In order to handle this situation a new scenario is tested. The idea is to include the integral of positive error ε in (6.11) into the objective function. The function is modified as:

$$J = \int_0^{t_F} \left(S(t) + \lambda \varepsilon(t) \right) dt \tag{6.12}$$

Using the new objective function (6.12) and with the process conditions and perturbations implemented before, a new simulation is run. Figure 6.8 shows dynamic behaviour obtained for the final CO_2 gas concentration.

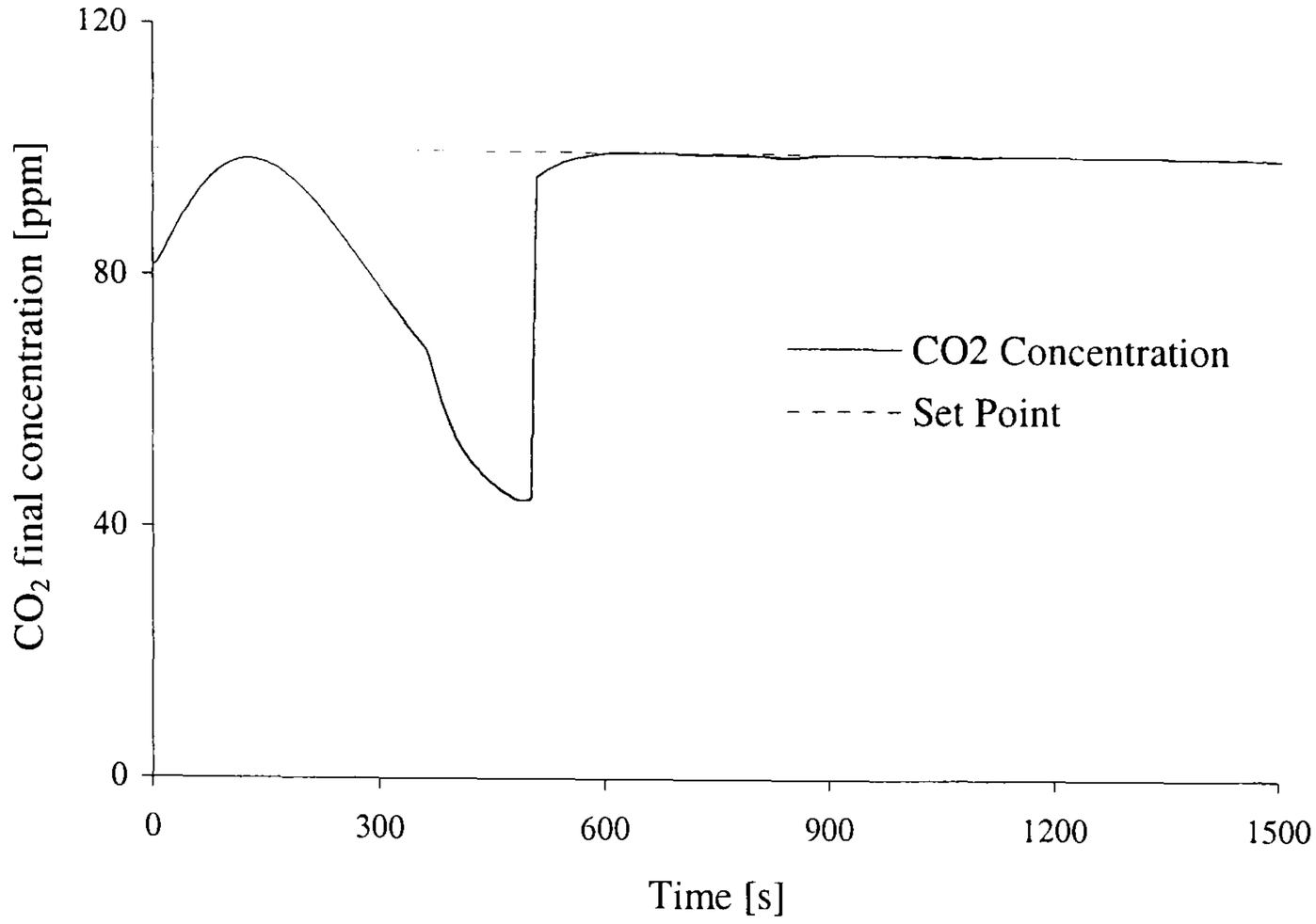


Figure 6.8. Controlled system including the path constraint in the objective function.

Although this experiment was fixed to achieve a similar response to the path constraint with $\varepsilon = 0.02t_f$, the CO_2 final gas concentration in the previous figure is more similar to the case when $\varepsilon = 0$. In fact, Table 6.1 shows that this case consumes more steam than the others, even compared with the perfect path constraint ($\varepsilon = 0$). Also the graph shows how the system gives such weight to the overshoot condition to avoid at any cost values above the set point, therefore consuming more steam.

In addition, the computational time required for this case is on average 800 seconds. This increase is probably due to the fact that the new term added in the objective function, escalates the complexity and the number of iterations required by the optimiser.

Lastly, the problem becomes more sensitive to the initial guess values selected for the first iteration in the optimiser. Sometimes is hard to find a set of values that satisfies the solver.

From this experiment it is clear that if perturbations prior their arrival (theoretical case) is not known, it is very difficult to make the solver converge in every interval unless the last scenario is used. However, including the equation 6.11 into the objective

function does not bring further benefits to the MPC; on the contrary it makes the optimisation process slower and harder to converge.

Of course the MPC algorithm would use the filter estimate of the feed CO_2 concentration rather than the instrument reading, which avoid such sudden changes, and again this experiment emphasises the need of smoothed predicted estimates of feed conditions, which is a better solution than use of 6.12.

Finally, Table 6.1 shows the total steam consumed from 0 to 1500 seconds for each of the previous cases.

Constraint	Steam consumed [mol]	Max value of CO_2 [ppm]
Interior point constraint	1122.7	112.7
Path constraint, $\varepsilon = 0.1 \cdot t_f$	1131.6	105.4
Path constraint, $\varepsilon = 0.02 \cdot t_f$	1146.6	100.9
Path constraint, $\varepsilon = 0$	1149.6	100.0
ε included in the Objective function	1159.0	99.9

Table 6.1. Steam consumed for each fixed control horizon case

The table above reaffirms previous discussions about steam consumption in each case. Due to the nature of the interior point constraint, the steam consumption is the lowest, followed by the path constraint, and the harder the constraint is, the more steam is required. Lastly the modified objective function shows the highest consumption of steam.

If it is assumed that all plant measurements are known in advance, or can be estimated; no unexpected perturbations need be considered. The path constraint with $\varepsilon = 0.02t_f$ is therefore selected as the best alternative for the following cases to keep y_P under set point.

6.4.2. Optimal Horizon

The idea of the next runs is to study the minimal control horizon time needed in an optimal control scheme without risking stability and feasibility of the process beyond the horizon.

The horizon control time t_f in (6.6) is included as an extra variable into of the optimal problem. The new optimal equation is transformed to:

$$J = \int_0^t S(t) \cdot dt \tag{6.13}$$

Again, six intervals are used but each one can vary from 120 to 500 seconds. This variability becomes part of the optimisation problem.

In order to assure stability and steady state conditions at the end of the control horizon two approaches are tested. The first one adds an end-point constraint to the rate of change in the final CO_2 gas concentration. The other, weights the final value of CO_2 in the objective function.

The following sections show the details and results of both approaches. The plant and perturbation conditions originally proposed are still used. As mentioned before a path constraint for y_P (6.11) is employed with $\varepsilon = 0.02 t_f$.

6.4.2.1 Derivative End-Point Constraint

The first run under optimal horizon constrains at time t_f the rate of change of the final CO_2 gas concentration, therefore assuring close to steady state condition at the end of the control horizon. The following equation is used:

$$\left| \dot{y}_P(t_f) \right| \leq \gamma \,, \tag{6.14}$$

where γ represents the degree of steadiness at the end of the horizon. The smaller the value is, the steadier the system is at the end of the horizon. From simple dynamic responses is found that $\gamma = 2 \cdot 10^{-3}$ is adequate to assure steady state conditions.

Figure 6.9 shows the dynamic behaviour of the final CO_2 concentration while Figure 6.10 presents the values for steam and solvent flows at each interval.

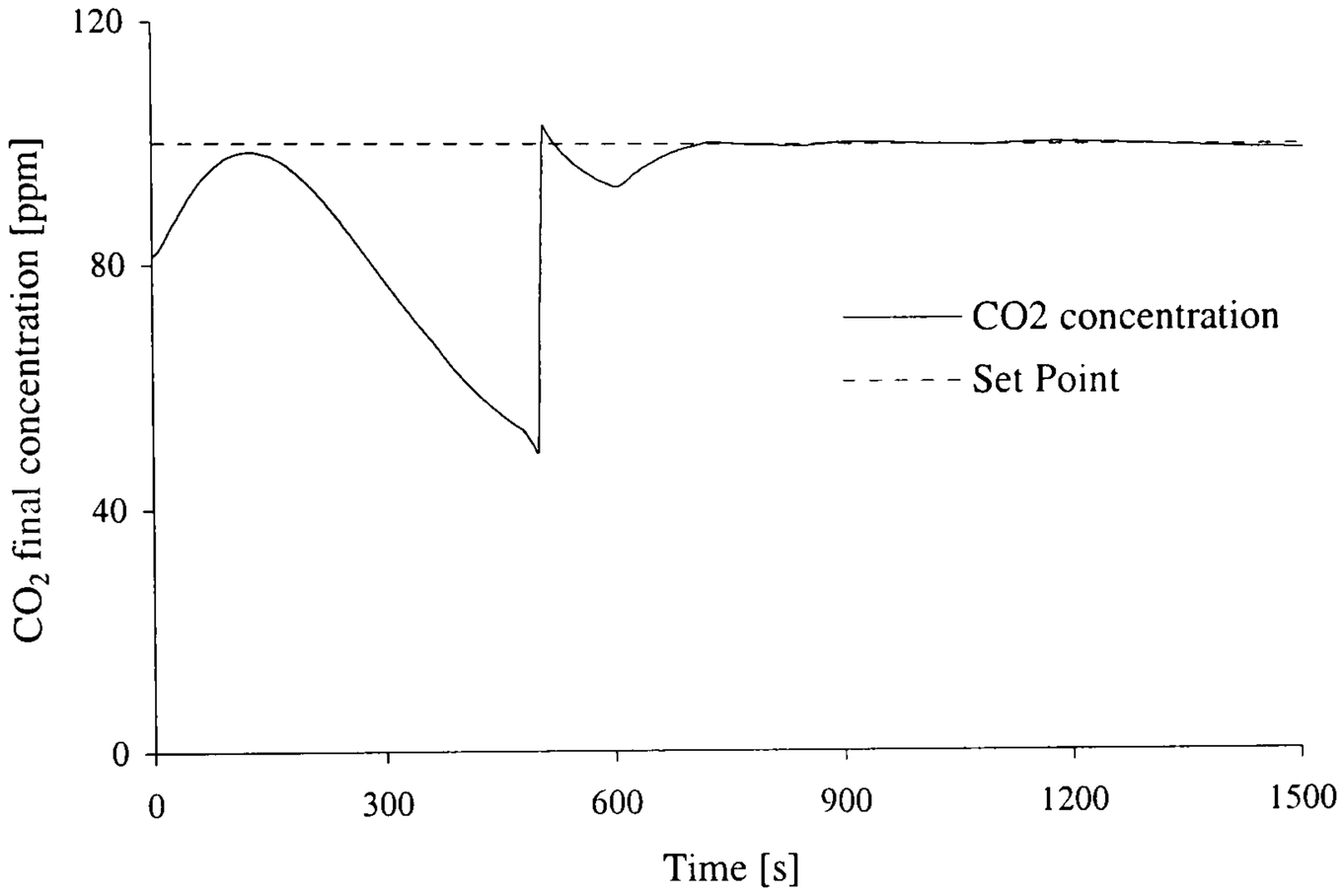


Figure 6.9. Controlled system using optimal horizon.

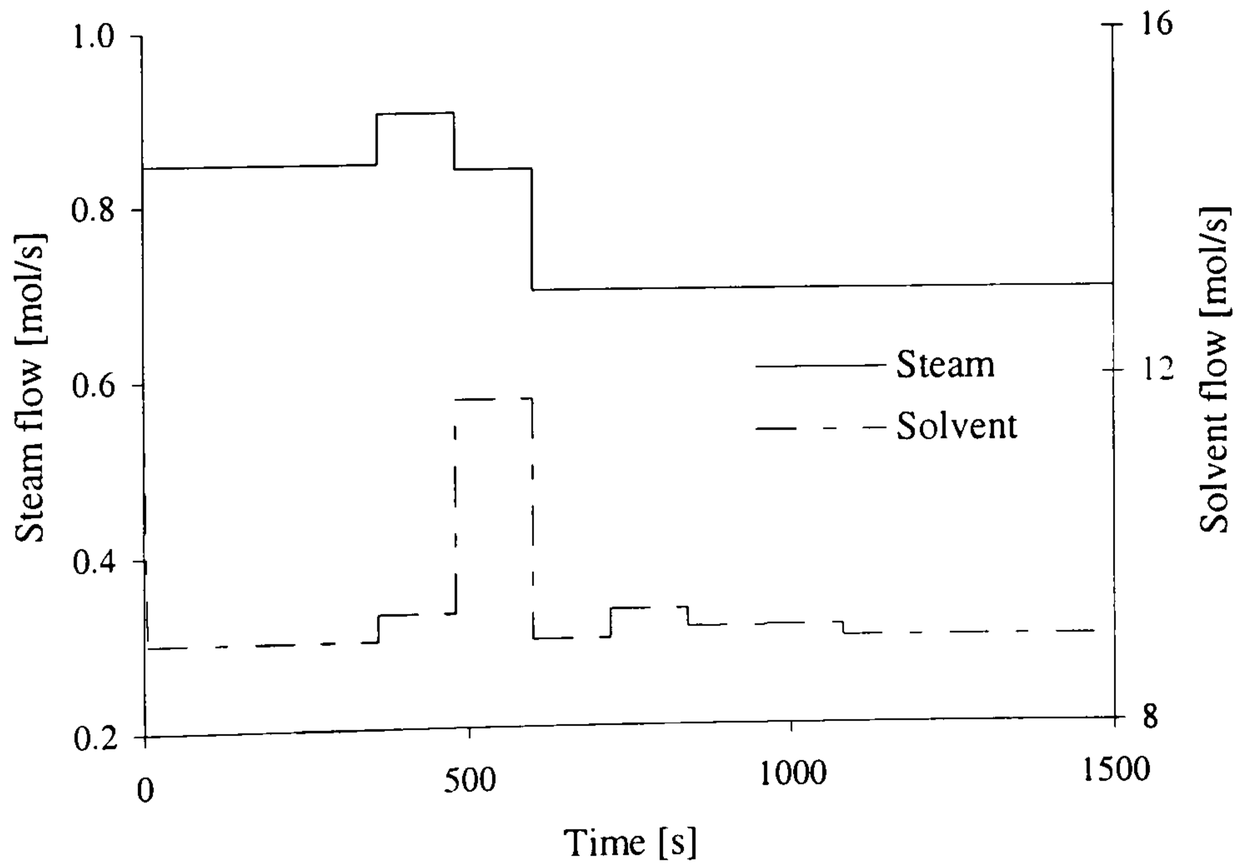


Figure 6.10. Steam and solvent flow rates using optimal horizon.

The application of an optimal control horizon in the final CO_2 concentration as shown in Figure 6.9 makes the system converge to steady state fast, the CO_2 concentration almost stays constant (100 ppm) after the perturbation takes place. Also the steam and solvent flow reach steady state condition just 200 seconds after the perturbation.

Again, even when the controller has the freedom to select the interval length, 500 seconds of control actions are required in advance to effectively avoid overshoots in the system. Also even though the control horizon is reduced to only 720 seconds, instability problems are sorted out with the inclusion of an end-point constraint to keep low the rate of change in y_P.

More important, the computational time was reduced to only 220 seconds on average. Other runs were then made using the same conditions but changing the perturbation time. The computational time required to complete the optimisation was between 180 sec and 450 sec. These results indicate the possibilities of applying an on-line MPC experimentally.

6.4.2.2 Optimal Horizon with Final Weighting Factor

The second approach involves adding a weighting factor in the objective function instead of constraining the rate of change in the CO_2 concentration. The idea is to force the optimiser to stay as close as possible to steady state conditions at the end of the control horizon.

The last experiment is repeated but adding a weighting factor in the final steam value in the objective function. The modified objective function is shown below.

$$J = \alpha \cdot S(t_f) + \int_0^{t_f} S(t) \cdot dt \tag{6.15}$$

The results of this run are shown from Figure 6.11 to Figure 6.13.

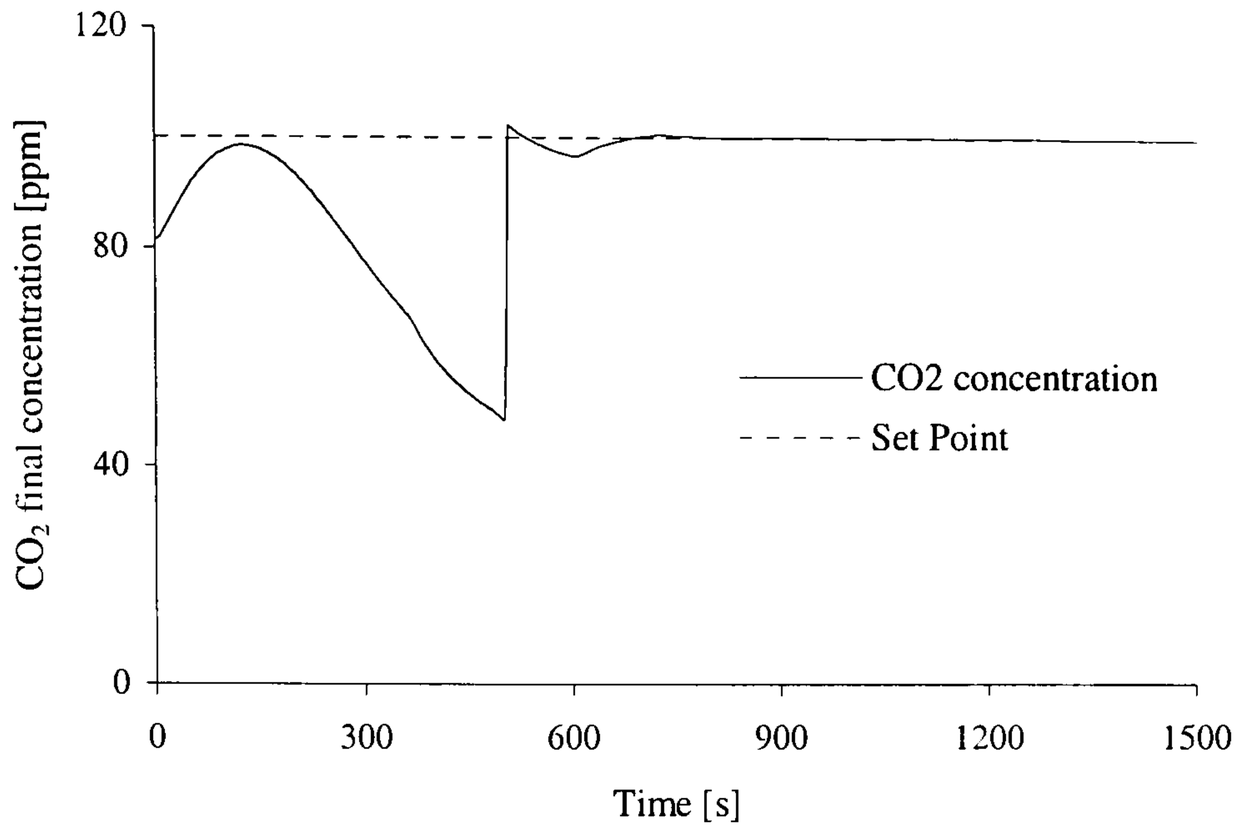


Figure 6.11. Controlled system using optimal horizon

The primary outcome is that both systems predict the vapour flow rates extremely well without overshooting the upper concentration limit during the transition period. Even more important the computational time is less than 300 seconds for a control horizon of 720 seconds. Comparing both cases, the second run has a slightly better response due to a smaller amount of oscillations. However, because gOPT requires more iterations to obtain the tightest final steam value, the introduction of the weighting factor increases the computational time by 36%.

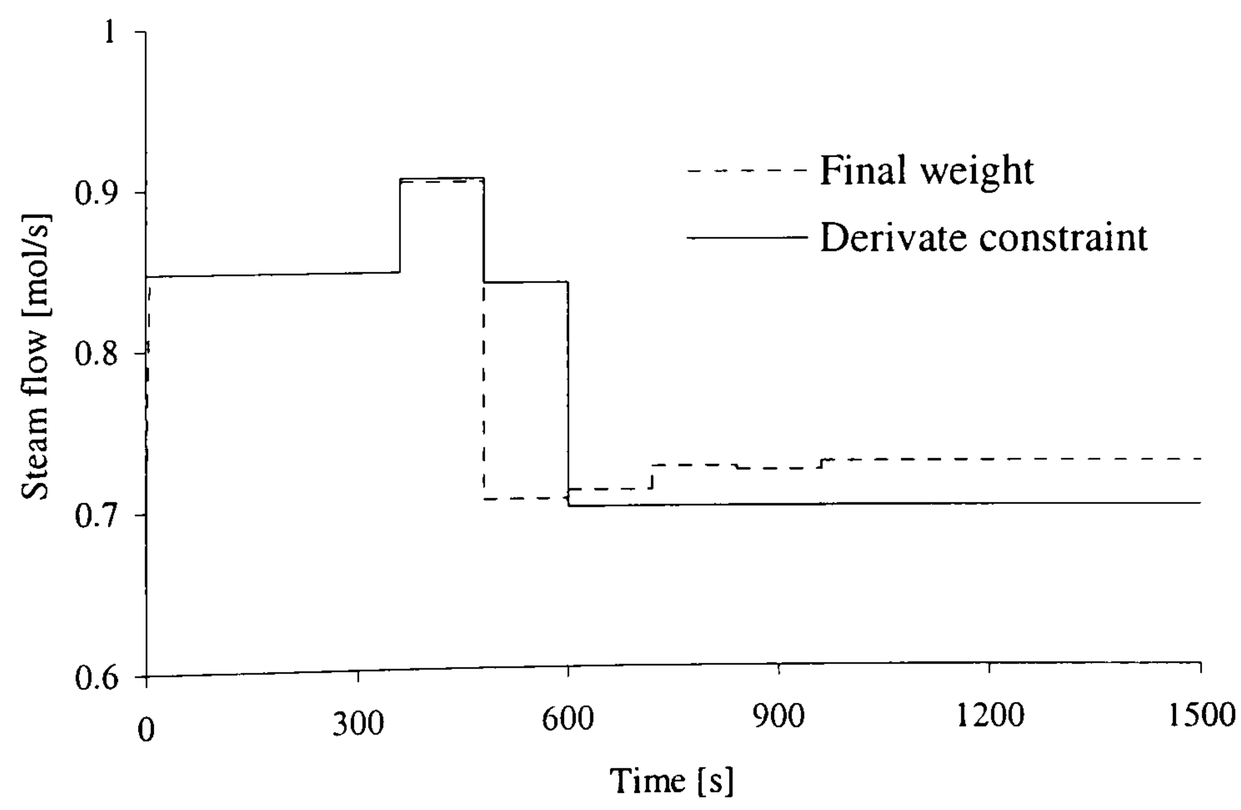


Figure 6.12. Steam consumption comparison between both methods.

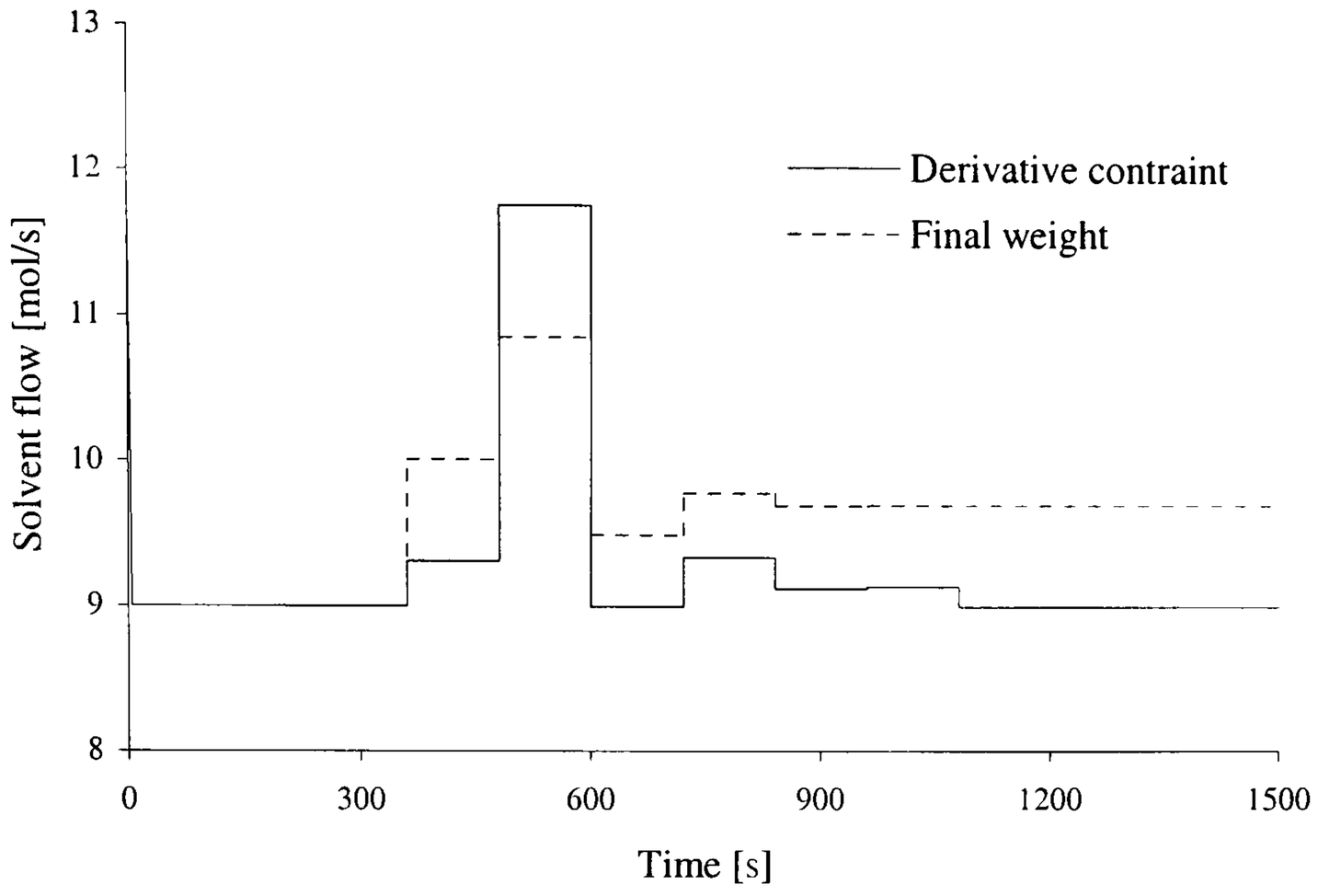


Figure 6.13. Solvent recirculation comparison between both methods.

Also a negative effect on using a final weighting factor is the difference of steam and solvent values at steady state conditions. While the other cases reach 0.7 mol/s, the latter stays at 0.73 mol/s, increasing the overall steam consumption in the long run. The reason behind the impossibility to achieve a lower level lies in the fact that the solvent flow needs to be reduced simultaneously (limits on the operational conditions), but that will create an inverse response in y_P, therefore violating the path constraint.

Nevertheless the inclusion of the final weighting factor does not make any significant contribution to the controller, on the contrary it increases considerably the computational time and consumes more steam.

Table 6.2 compares the steam consumed for each optimal time scenario with the fixed horizon case.

Path Constraint	Steam consumed [mol]
Fixed horizon	1146.6
Optimal horizon, end point constraint	1144.7
Optimal horizon, final weighting	1149.9

Table 6.2. Steam consumed for each optimal control horizon case

In summary, the significant reduction in computational time and small improvement in the steam consumption (Table 6.2) using optimal horizon with derivative end-point constraint, indicates that this option is the most appropriate. In addition a path constraint is needed to ensure the system does not overshoot the CO_2 set-point.

6.4.3. Inlet Temperature of Solvent as Additional Control

Having selected the path constraint and the derivative end-point constraint condition as the best MPC algorithm for the plant, the next step is to include the inlet liquid temperature in the absorber as an extra control variable ranging from 45 to 55°C.

The process and perturbation conditions are the same as before. The only difference is the step-change at 500 seconds in the gas feed flow rate is increased to 55 g/s instead of 45 g/s. Following previous results end-point constraint and optimal time conditions are used with $\varepsilon = 0.02t_f$ and $\gamma = 0.002$ respectively.

Figure 6.14 to Figure 6.16 show the results obtained for this experiment.

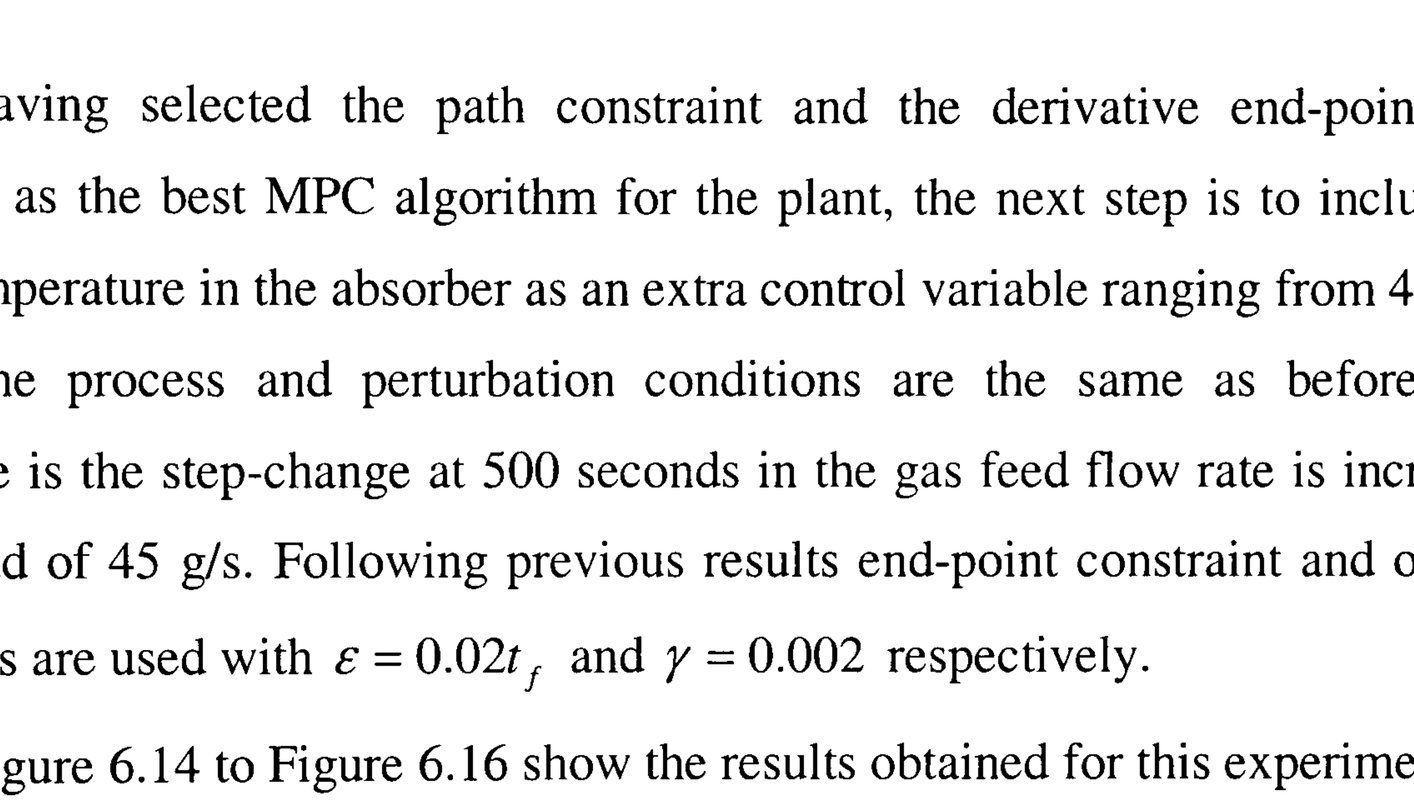


Figure 6.14. Final CO_2 gas concentration in the absorber.

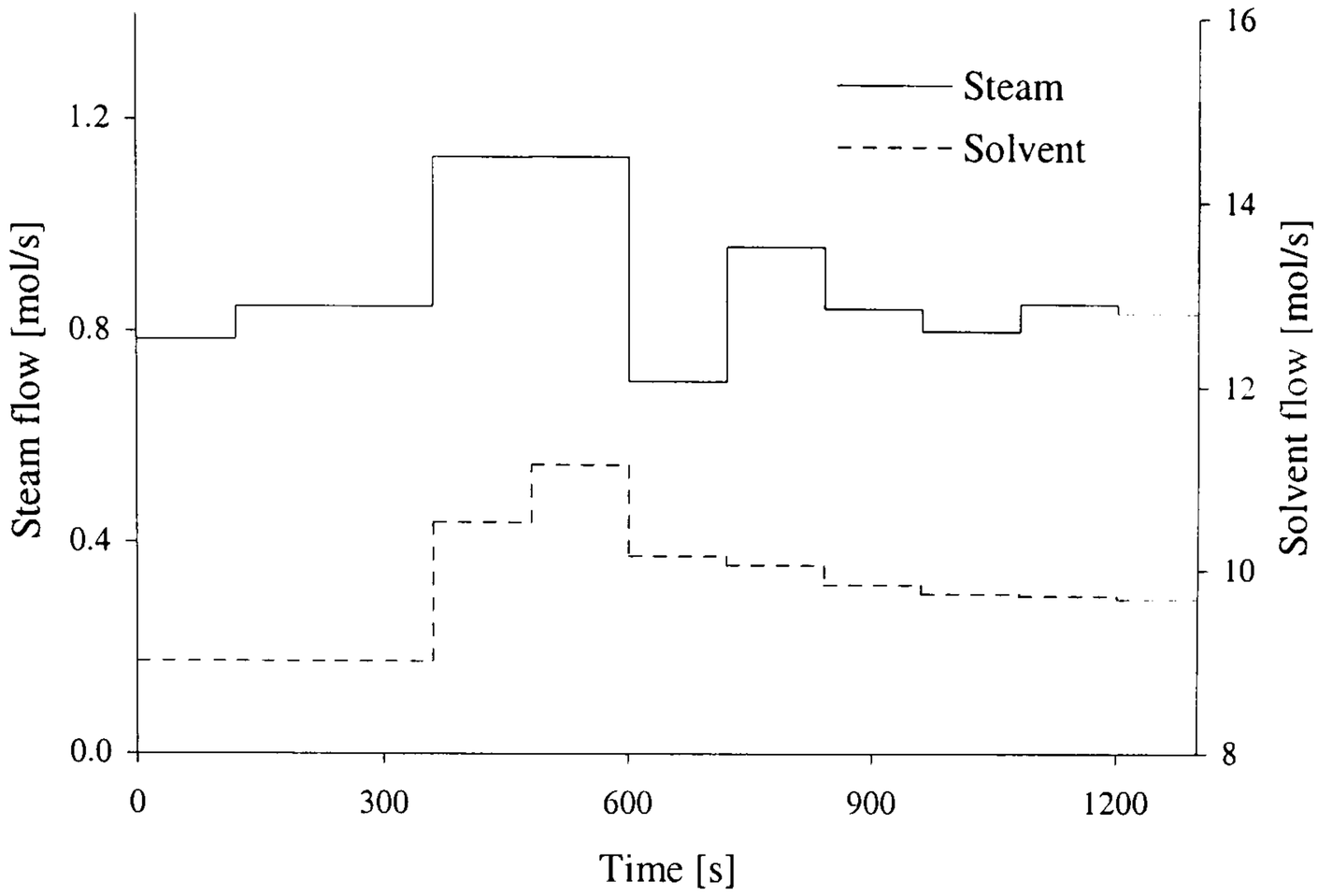


Figure 6.15. Steam and solvent flow rates.

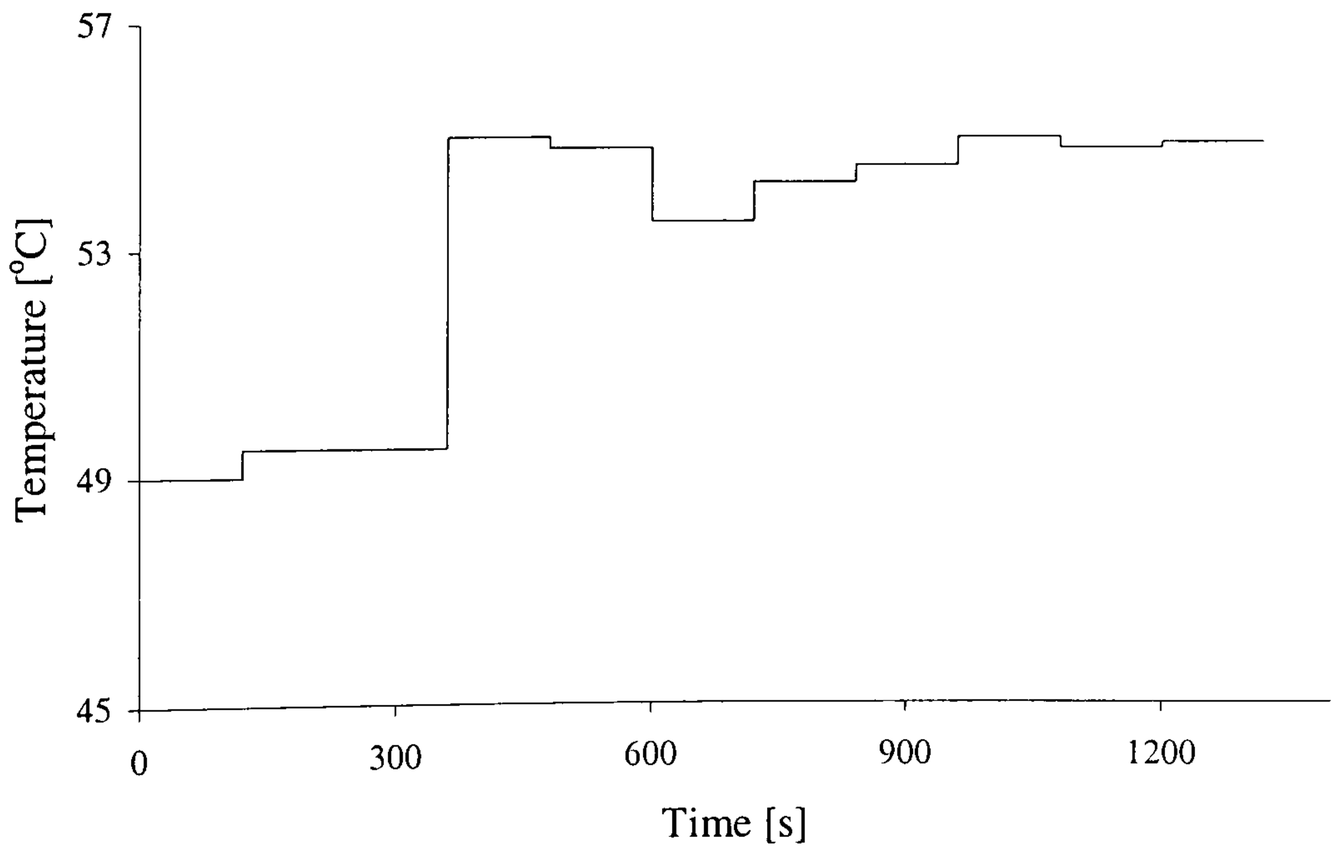


Figure 6.16. Inlet liquid temperature in the absorber.

These results show the effectiveness of using temperature as an extra control variable. Considering that the feed gas rate had an increment of 33%, the controller was capable of keeping the overshoot to just above the set point.

More important the controller makes the system reach steady state conditions only 100 seconds after the perturbation and less oscillatory compared to previous tests.

However, because of the increment of control variables in the optimiser, the computational time is somewhat increased. On average the system requires 300 seconds to find the solution.

In conclusion, including the inlet liquid temperature in the controller as an extra manipulated variable improves controllability and stability properties. Steady state conditions are reached almost immediately after perturbation. Unfortunately computational time is increased, nevertheless actual trends in computational development could solve the problem in less than 120 seconds (first control interval).

6.4.4. Effect of the Number of Stages

The last experiment handles the question how accurate is the current model (5 stages in the absorber and 10 in the desorber) compared with a more realistic one.

Figure 6.17 shows the dynamic behaviour of two different controlled systems, one proposed with 5 absorber stages and 10 desorber stages and the other with 20 stages in each column.

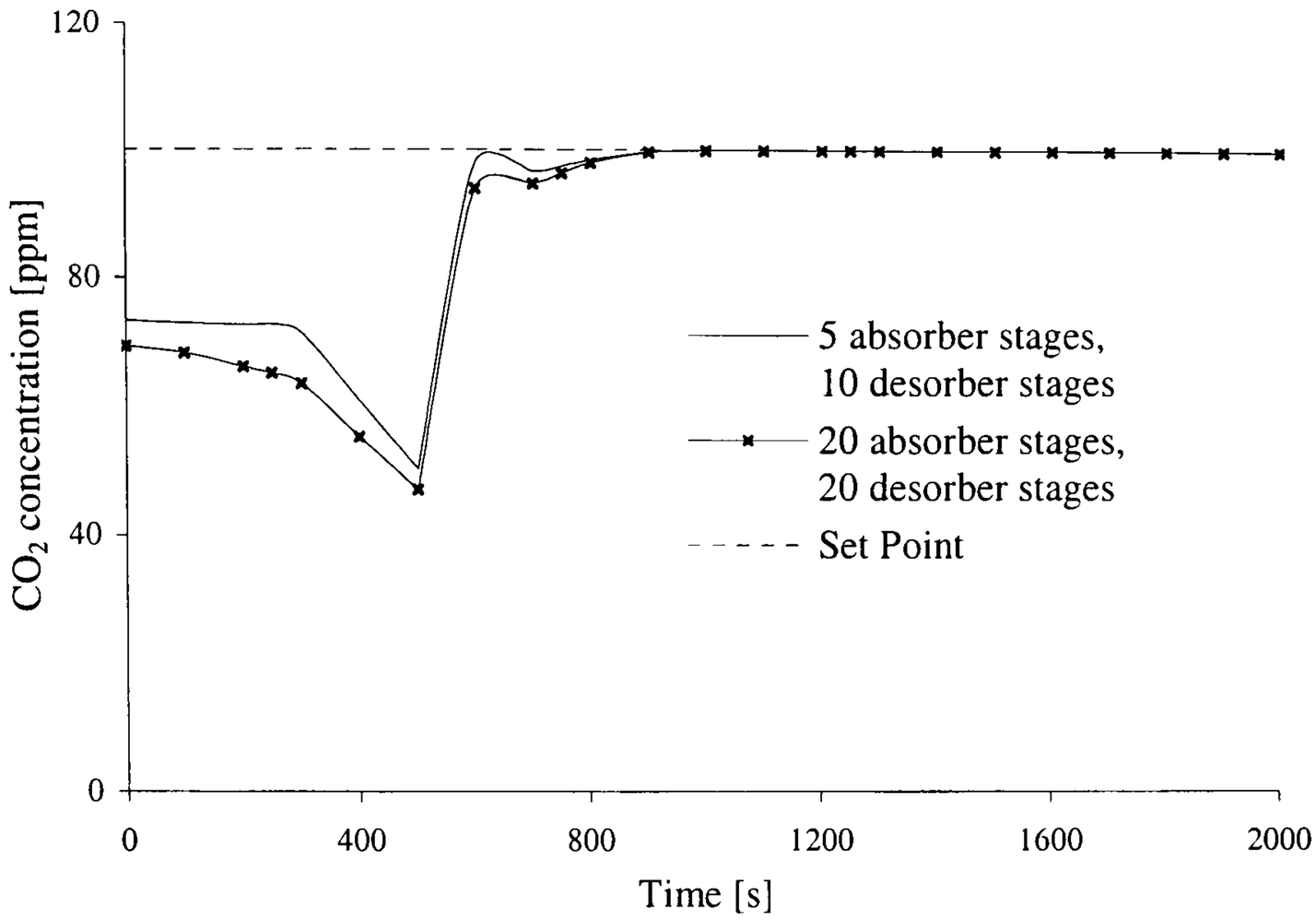


Figure 6.17. Comparison between both model under the same conditions

Figure 6.17 shows that despite the fact that a model with more stages is more accurate, the dynamic response does not show much difference between the models. As explained in the previous section, the dynamic behaviour was virtually identical in each case.

Moreover the response time in each plot is the same, giving an indication that the new model was scaled correctly. This result is very important because dynamic behaviour is normally more important than final steady state results when a controller is designed.

However, it is important to highlight the fact that the computational time using a complex model is increased by 4 times. This shows the importance of choosing the right model size in order to obtain the best balance between accuracy and computational speed.

6.5. Conclusions

In this chapter several variations of MPC's are tested and compared through simulations in order to selected the most suitable controller for the CO_2 absorption plant.

It was shown that the best option for a nonlinear MPC was to use an optimal horizon with derivative end-point constraint time in tandem with a CO_2 concentration path constraint to assure minimal use of steam without overshooting the CO_2 set-point.

It was also shown that the model could be simplified without losing the detail in the dynamic behaviour of the process systems. A less rigorous model was shown to have similar controllability and observability properties, without degrading the controller performance, all this with the benefit of faster computational time.

Chapter 7

MPC Closed Loop

7.1. Real Optimal Control Including Estimation

Once the model was successfully tested under perfect conditions, a more realistic approach was used for the next step, which includes a slightly different model as plant, with noisy measurements and different values for the unknown parameters. The optimal controller is tested under different scenarios. Figure 7.1 shows the optimal control algorithm implemented.

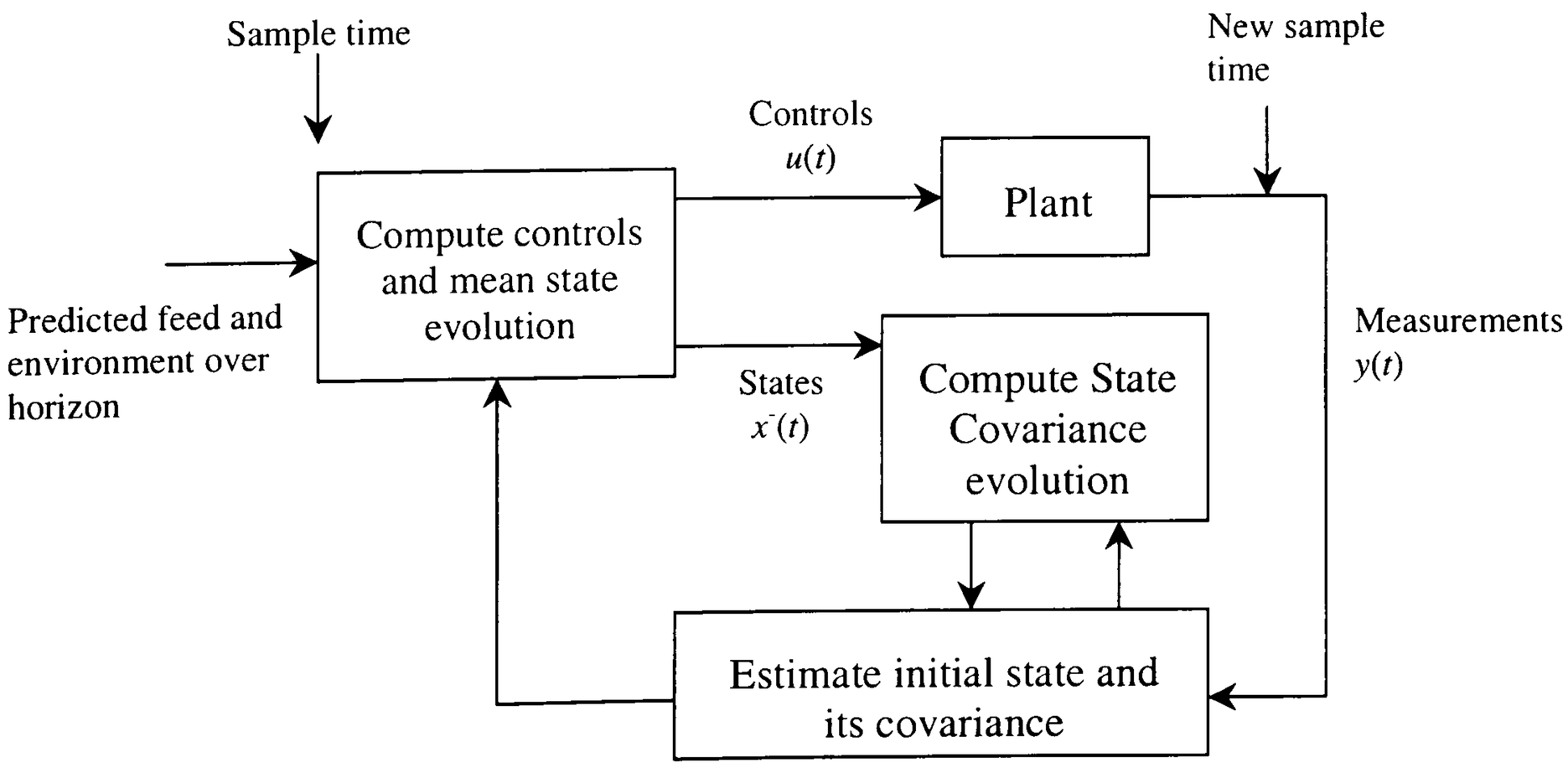


Figure 7.1. MPC closed loop

The figure above, illustrates all steps involved to control the plant using a MPC. From the plant a set of measurements is sent to the estimator; the Kalman filter, using this information plus previous estimations and known covariance errors predicts the current state variables and uncertain parameters, then using a model of the plant and predicted feed conditions, optimal controls are computed by the controller. Once a new control trajectory is computed it can be immediately implemented on the plant. The following sections will describe in more detail the model used as a plant, the measurements used by the Kalman filter, constraints and the objective function.

7.1.1. Simulated Plant

The more accurate representation of the pilot plant obtained during the modelling process was selected as the plant block in the MPC loop (see figure 7.1). The main differences between this model and the one used by the controller are the number of stages in each column, and also the numerical values of all unknown parameters. The idea is to create a constant mismatch between the plant and the model used by the controller, so the control and the estimation process are more realistic. Table 7.1 shows the conditions used in the model running as a real plant.

Please notice that the feed conditions change during the run. Also the values reported for the absorption rate and the desorber heat loss for the controller are only initial conditions, these values will change in order to close the mismatch between model and process.

The MPC was not tested in the real plant due to technical difficulties. The ageing plant requires constant and extensive maintenance making very difficult to change the current set-up. Lastly and probably the hardest part, a link between the software running the controller (gPROMS and Matlab) and the plant (Paragon) has to be written from scratch in order to implement the algorithm.

	Plant	Controller
Number of stages		
Absorber stages	20	5
Desorber stages	20	10
Uncertain Parameters		
Absorption rate constant	$3.34 \cdot 10^{-6}$	$4.50 \cdot 10^{-6}$
Desorber efficiency	1	1
MEA Concentration	2500 mol/m3	2500
Absorber heat loss	0.139	0
Desorber heat loss	-1.27	0
Reboiler heat loss	-0.84	0
Initial Conditions		
Gas feed flow	35 g/s	35 g/s
CO_2 gas feed composition	5.2 %	5.2 %
Steam flow rate	1 mol/s	1 mol/s
Recirculation flow rate	12 mol/s	12 mol/s

Table 7.1. Conditions employed in the model used as "real plant"

7.1.2. Control Variables

Physically valves open and close at a specific speed, which means control movements are also constrained. This limitation needs to be included in the optimisation problem to avoid aggressive control changes. Several researchers have incorporated those constraints into the objective function through weight factors, penalising the change rates in the control variables. However this practice brings two problems. Firstly the original model is adapted to create new variables that could be later constrained, complicating furthermore the set of equations. Secondly, the objective function is artificially modified and does not represent accurately the final objective that for this case is to minimise the energy consumption on the plant.

In order to avoid that procedure, changes in the control variables will be limited naturally through gOPT code. The gOPT file allows binding the lower and upper value of each manipulated variable for every interval.

From working experience in the pilot plant 0.2 mol/s and 2 mol/s for the steam and recirculation flow respectively are considered the maximum set point changes allowed every 2 minutes.

7.1.3. Estimator and Measurements

The set of measurements selected from the previous section used is used again to run the Kalman filter. A diagram of the plant with the selected measurements is presented in the Figure 7.2 while the measured variable and its respective process tag is shown in Table 7.2.

Variable	Instrument
CO_2 feed concentration	C1
CO_2 final gas concentration	C2
pH of concentration at reboiler	C5
Recirculation flow rate	F1
Gas feed flow rate	F2
Steam flow rate	F3
Temperature at top of absorber	T24
Temperature at half middle top of absorber	T23
Temperature at middle of absorber	T22
Temperature at half middle bottom of absorber	T21
Temperature at bottom of absorber	T20
Temperature top desorber	T8
Temperature middle desorber	T6
Temperature bottom desorber	T3
Temperature reboiler	T14

Table 7.2. Measurements used for the MPC

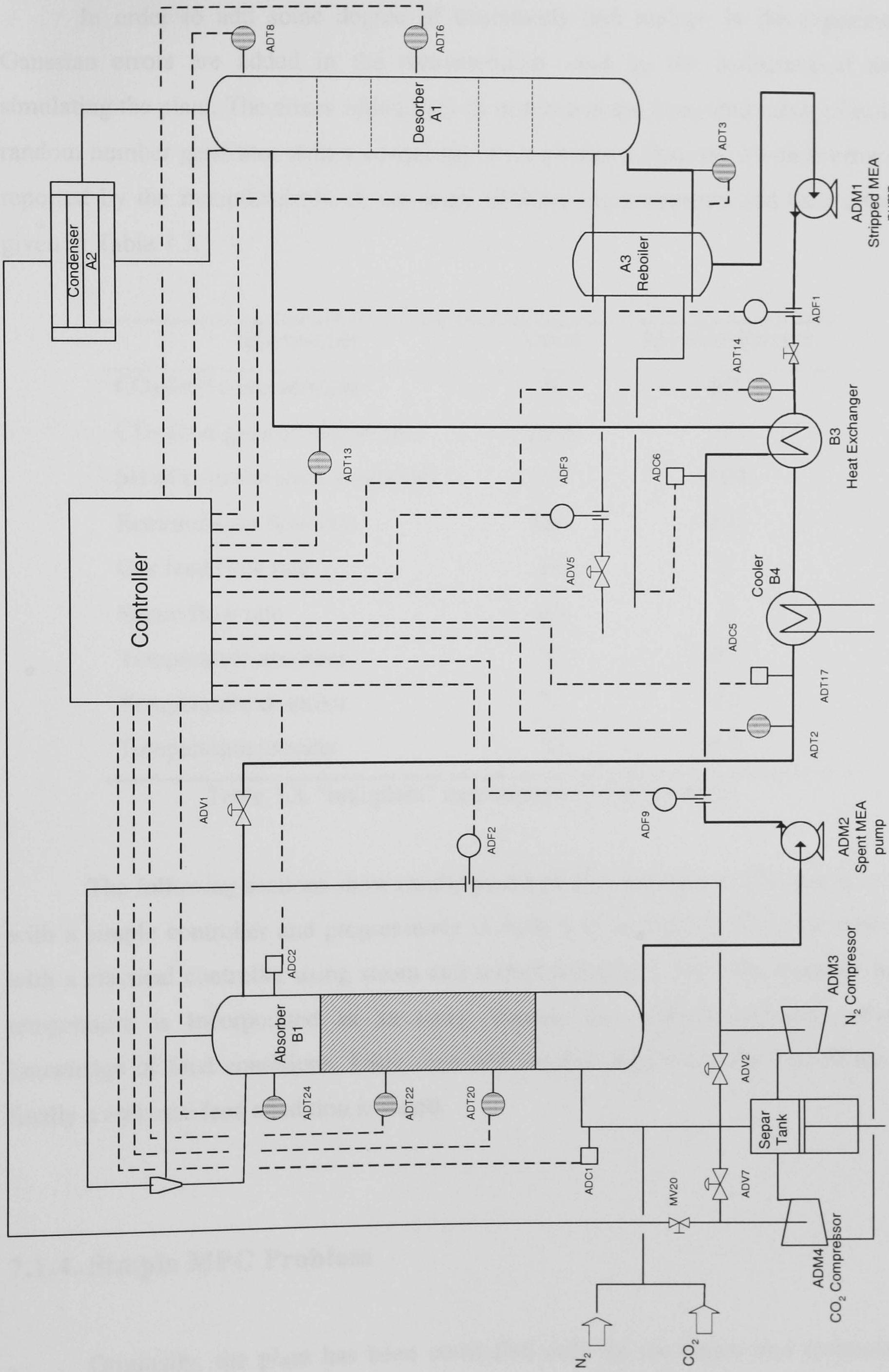


Figure 7.2. Diagram of the plant's measurements used by the controller

In order to add some degree of uncertainty and realism in the experiments, Gaussian errors are added in the measurements used by the mathematical model simulating the plant. The errors added to each instrument are generated using a Gaussian random number generator with a covariance error obtained from the absolute error data reported by the manufacturers. A summary of these measurements and their errors is given in Table 7.3.

Instruments	Units	Absolute Error ±
CO_2 feed concentration	%	0.5
CO_2 final gas concentration	ppm	5
pH of concentration at reboiler	pH	0.05
Recirculation flow rate	kg/s	0.01
Gas feed flow rate	g/s	2
Steam flow rate	g/s	1
Temperature absorber	ºC	0.5
Temperature desorber	ºC	0.5
Temperature reboiler	ºC	0.5

Table 7.3. "real plant" measurement absolute errors

The following sections show results on different experiments. The idea is to start with a simple controller and progressively include further features. The first runs deal with a classical controller using steam and recirculation flow rate. The absorber liquid temperature is incorporated as an extra variable but without including advance knowledge of feed conditions. Later runs will involve feed condition knowledge and finally a real case feed condition is tested.

7.1.4. Simple MPC Problem

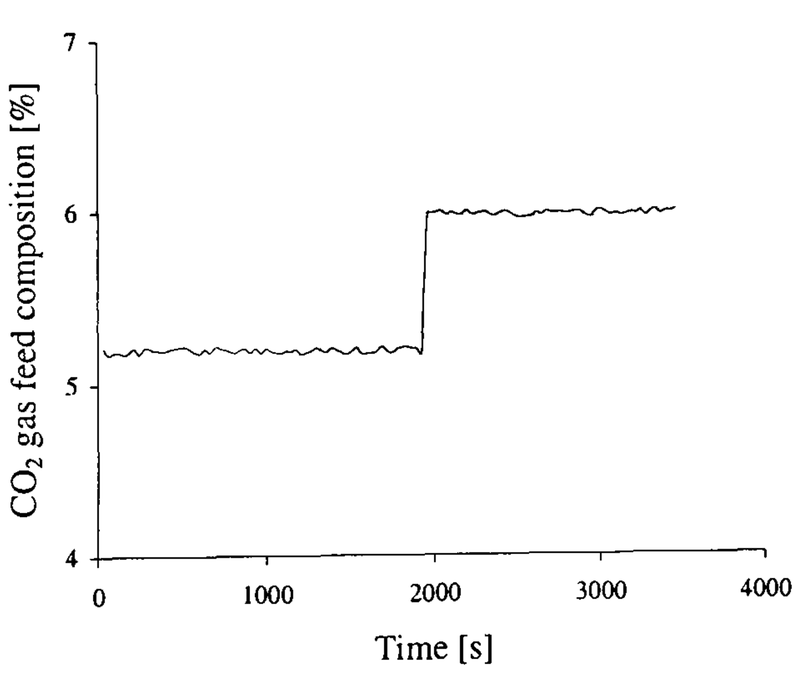
Originally, the plant has been controlled only by the steam and recirculation flow. To provide future comparisons, only the steam and the recirculation flow are used

as control variables, the liquid feed temperature is kept constant at its standard value: 45°C.

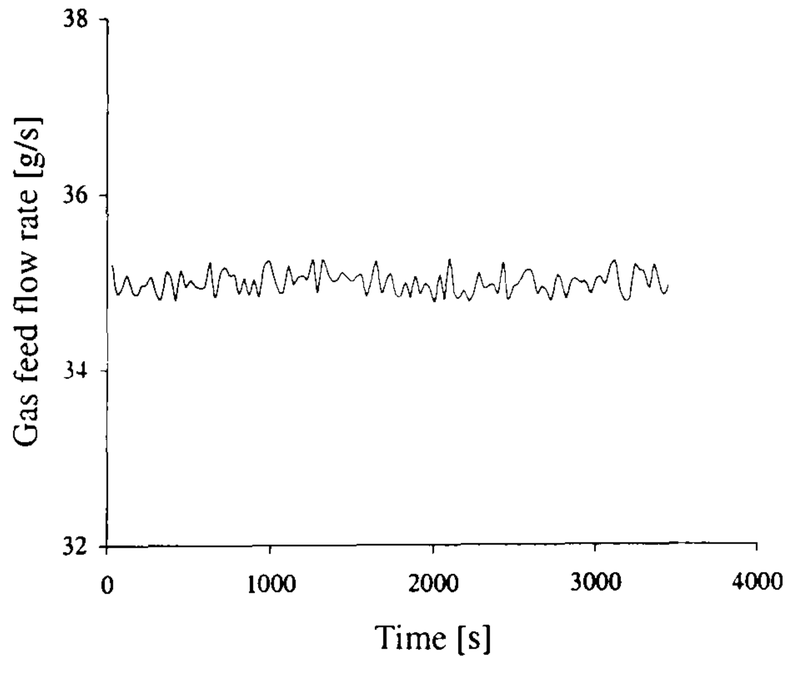
A step change in the CO_2 feed gas composition from 5.2% to 6% after 2000 seconds is introduced into the system while the feed gas rate is kept constant at 35 g/s. No information about the future feed conditions is given to the controller. The MPC only accounts present perturbations.

In order to allow the estimator to converge to stable values, the control loop is closed after 600 seconds; the reason for the time lag is to allow state variables and unknown parameters to converge before using them to compute the controls. The CO_2 leaving gas composition set point is fixed at 400 ppm.

Results of this run are shown in Figure 7.3 to Figure 7.5.



a) CO_2 feed gas composition



b) Gas feed flow

Figure 7.3. Input variables

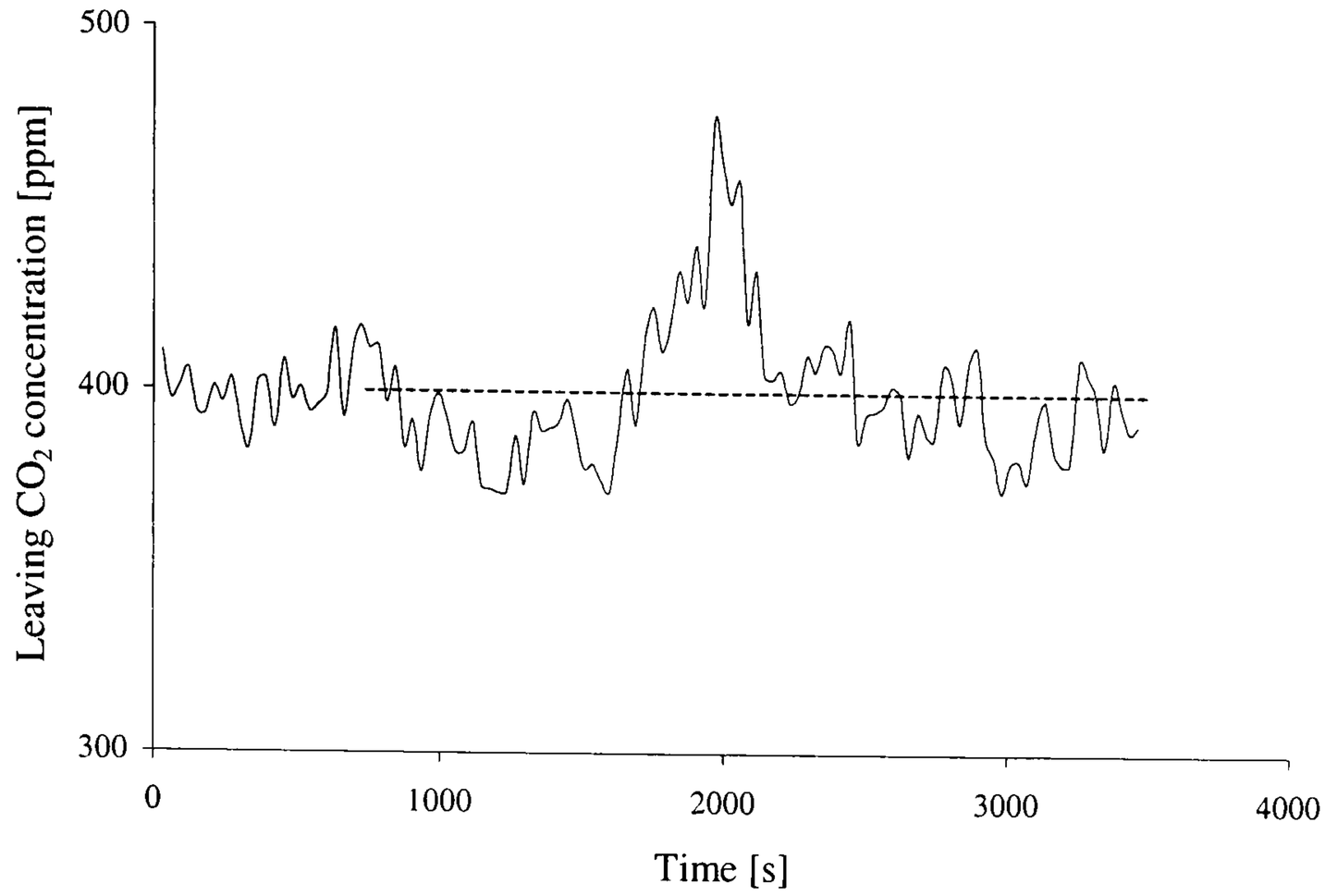
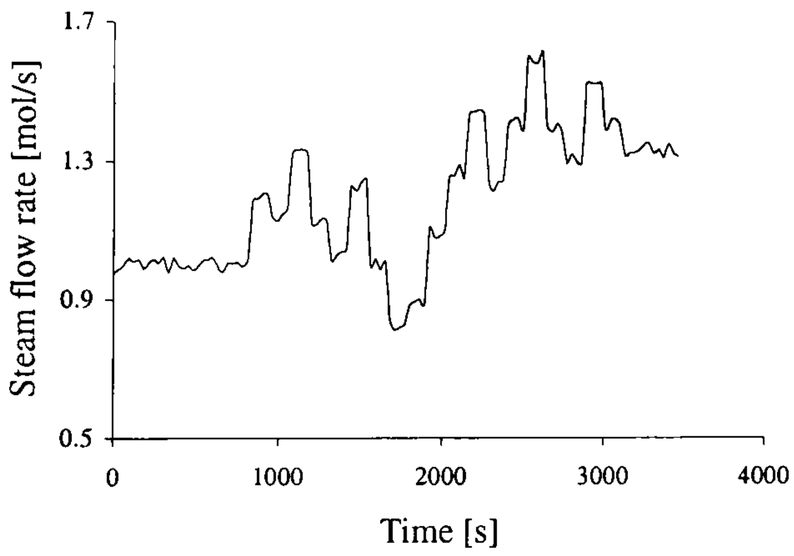
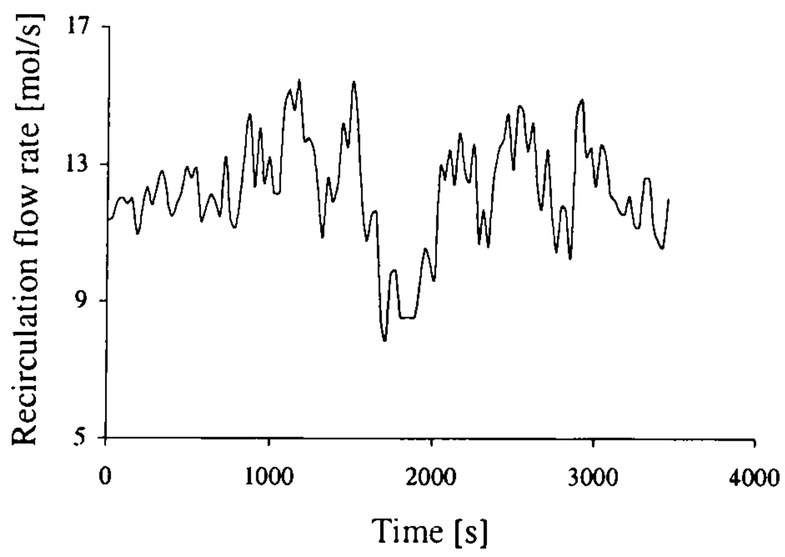


Figure 7.4. Controlled variable: Leaving CO_2 gas concentration



a) Steam flow



b) Recirculation flow

Figure 7.5. Manipulated variables

Due to the lack of information about the future feed conditions, it is impossible for the controller to take any preventive action and avoid the overshoot. Clearly this controller could not be used to avoid catalyst poisoning in a downstream process.

However, under a control and stability point of view, with the current manipulated variables the controller efficiently handles the final CO_2 concentration value. Once the controller is activated after 800 seconds the CO_2 concentration is kept

just below the set point using the minimum amount of steam and recirculation flow until the perturbation reaches the plant, as can be seen in the figure 7.4.

After the perturbation it needs 500 seconds to keep the final CO_2 concentration under set point and steady state conditions.

Although the controller is not suitable to prevent overshoots, it gives a good insight about stability and controllability issues of the controller.

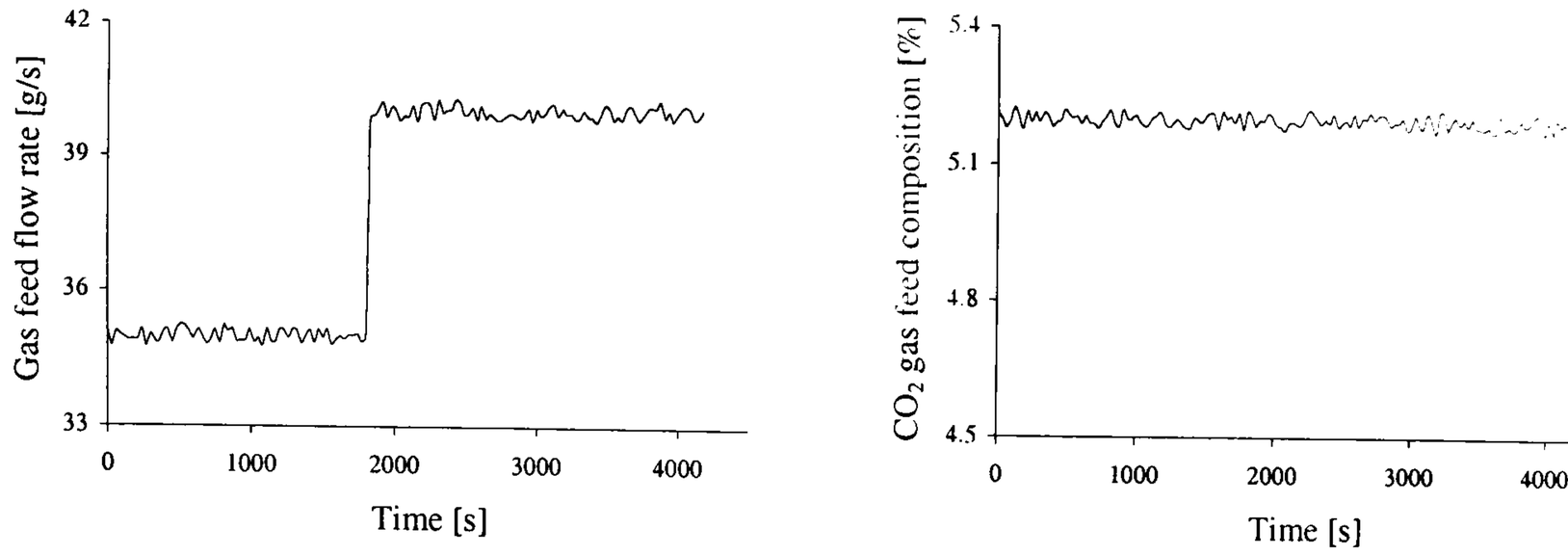
7.1.5. Liquid Temperature as an Extra Control Variable

The efficiency of the liquid feed temperature in the absorber as an additional control is tested together with the steam and recirculation flow rates. The liquid temperature was shown in previous simulations to have a very strong effect on the CO_2 gas concentration.

Originally, the idea was to use the previous conditions with this new proposed control set; however it was observed that only liquid temperature changes were required to control the system. Therefore, a bigger change in the gas feed flow rate is introduced to truly appreciate the changes and relation among the different manipulated variables.

For this case, a step change in gas feed flow from 35 g/s to 40 g/s at 1900 seconds is introduced while the CO_2 gas feed composition is kept constant at 5.2%. Also the set point is lowered to 300 ppm to make the controller task even more difficult. Again the controller does not handle any future information about perturbations or disturbances in the plant.

As a first approach, in order to avoid aggressiveness in the control dynamics a maximum change of 3°C for the absorber liquid feed temperature is allowed at every interval.



a) CO_2 feed gas composition b) Gas feed flow

Figure 7.6. Input variables

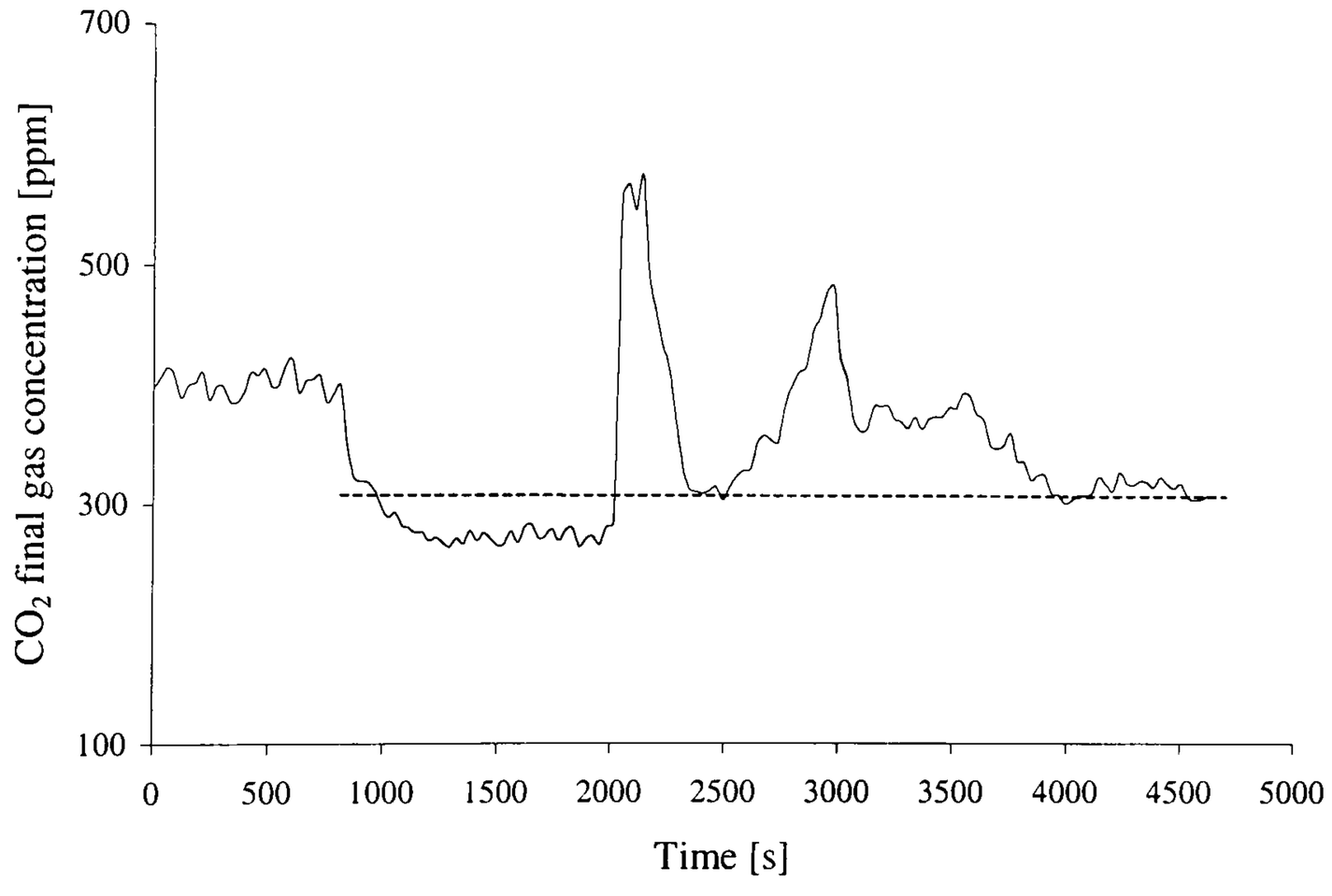
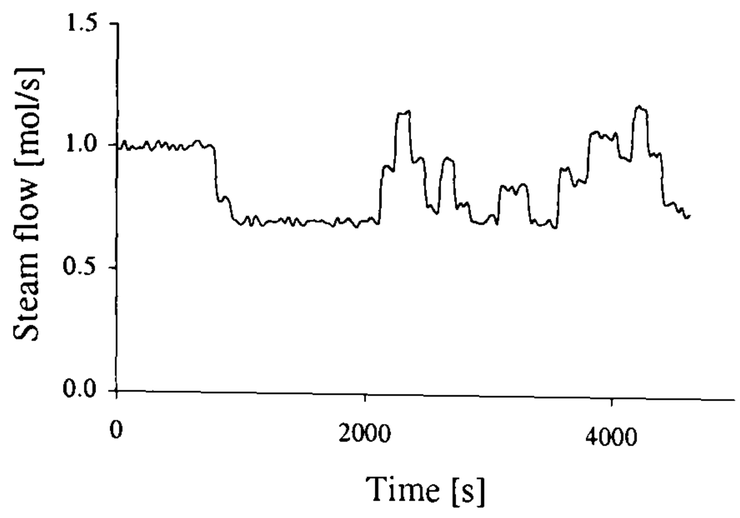
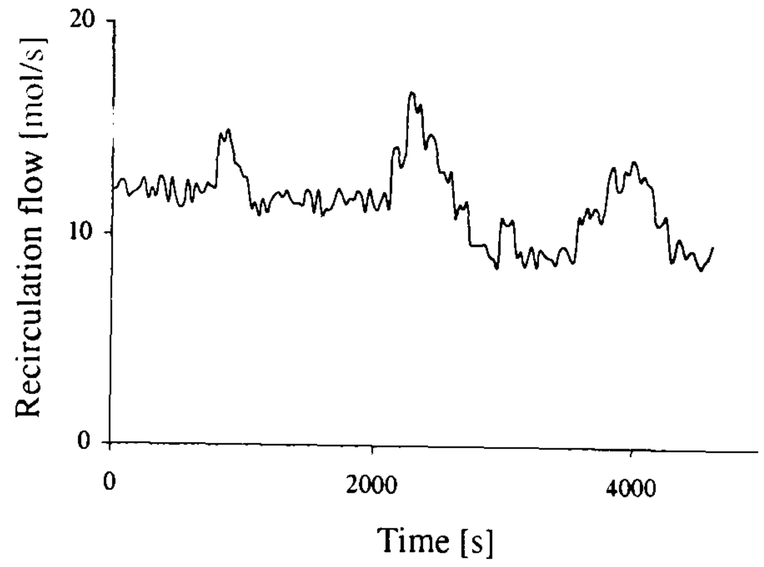


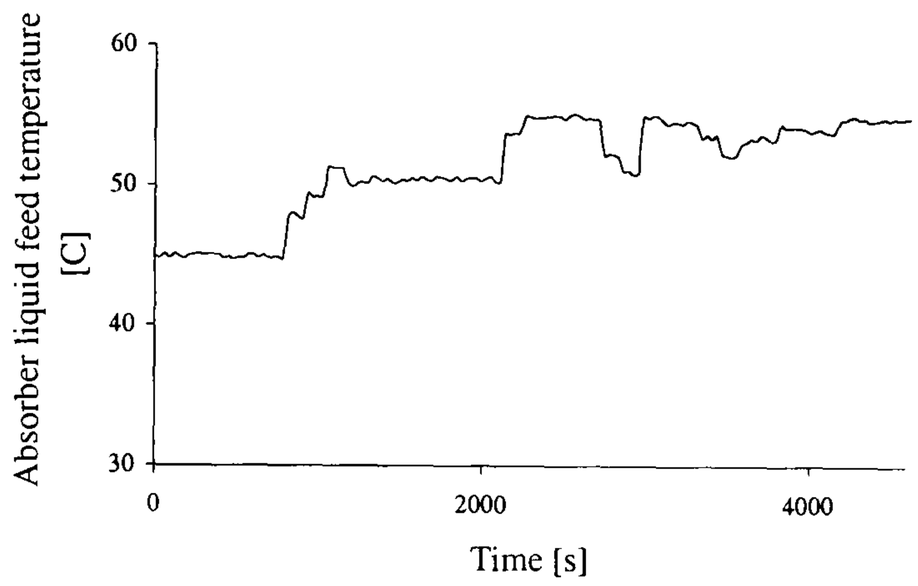
Figure 7.7. Controlled variable: Leaving CO_2 gas concentration



a) Steam flow



b) Recirculation flow



c) Liquid feed temperature

Figure 7.8. Manipulated variables

Again, as expected from the previous case, due to the lack of information about future feed conditions, it is impossible for the controller to avoid the overshoot. Also, it can be noticed that the overshoot is even bigger, nevertheless it can be explained since the step change and set point conditions are tougher for the controller.

However, it can be noticed that the controller recovers much faster from an unexpected overshoot compared with the classical case. Less than 300 seconds is needed to overcome a 300 ppm excess value (See figure 7.7). However, it can be seen that after recovering from the overshoot the controller finds some problems to keep the concentration below the set point. After struggling for 2000 seconds following the perturbation the system finally reaches steady state conditions.

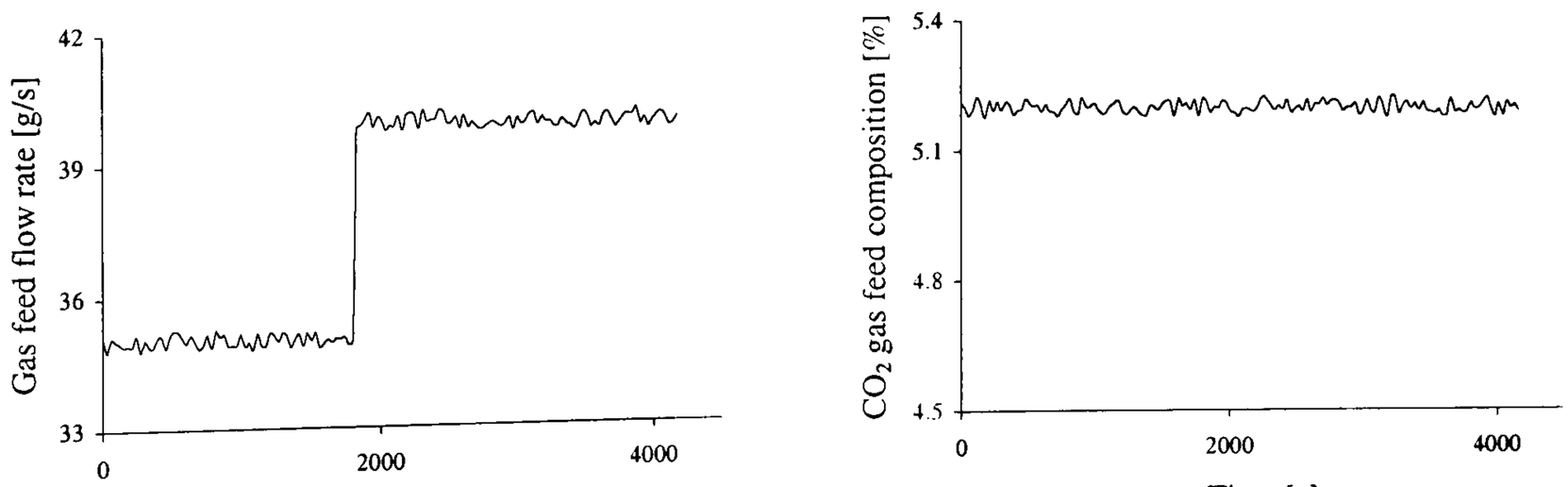
Also incorporating the liquid feed temperature in the absorber as a new control variable improves significantly the control response. For instance, once the controller is activated the CO_2 concentration is sent sharply below the set point using primarily temperature control, finding the minimum CO_2 value for those conditions (see p71). Then the controller cleverly adjusts the steam and recirculation flow rate.

Is important to notice that a conventional control scheme could never optimise like this, a good example why nonlinear MPC is more powerful than classical controllers.

Although this run was not successful, it is important because it points out the strong effect between liquid feed temperature and the CO_2 gas concentration. Due to the fact that the CO_2 gas concentration is very sensitive to the liquid temperature, the initial assumption of using the 3°C allowed change per interval is modified. This experiment is repeated but using instead 1°C change per interval.

7.1.6. Conservative Liquid Temperature as Control Variable

Because of the control aggressiveness detected previously, the last experiment is repeated but reducing the maximum temperature change allowed per interval to 1°C. Results are shown from Figure 7.9 to Figure 7.10.



a) CO_2 feed gas composition b) Gas feed flow

Figure 7.9. Input variables

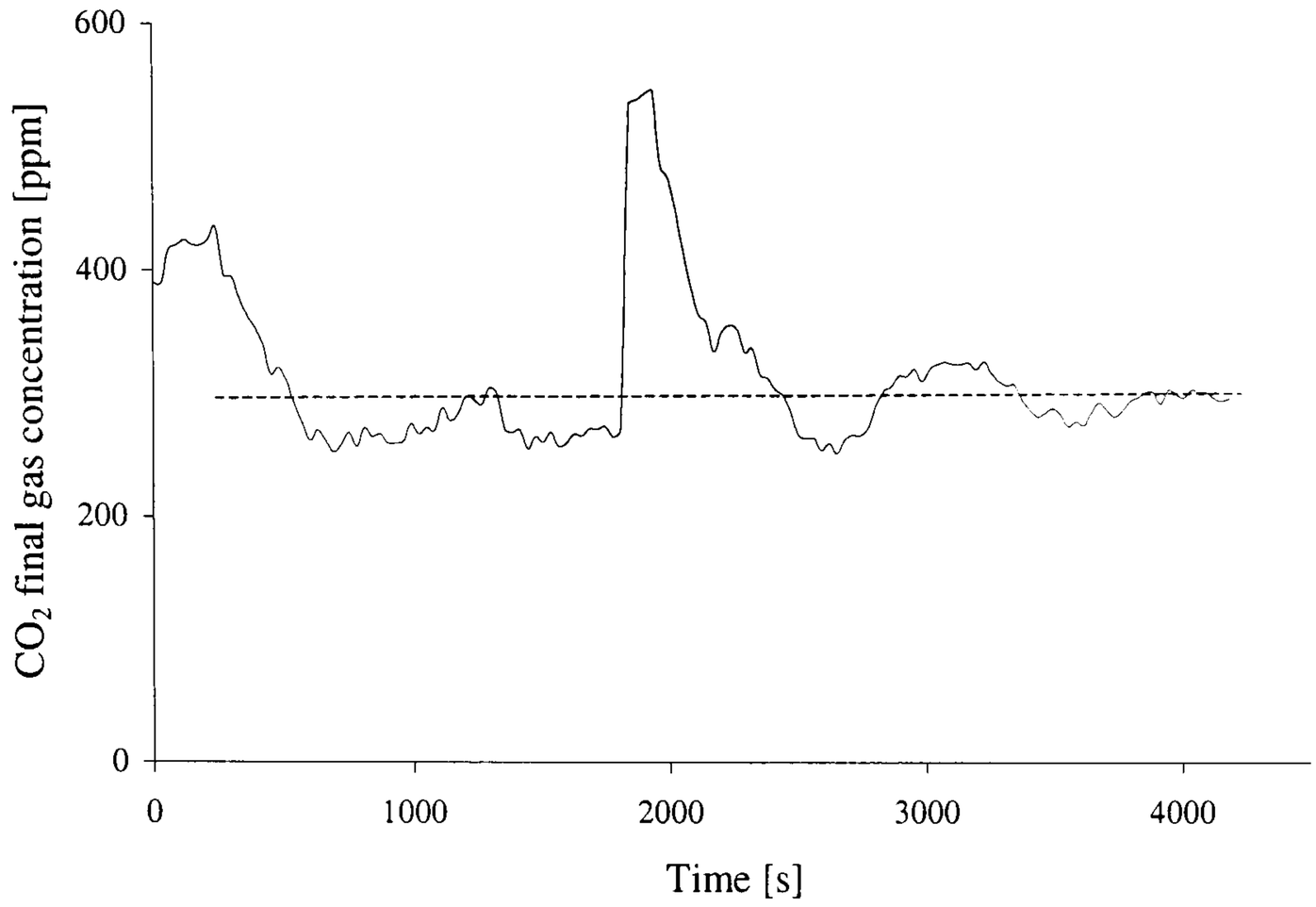
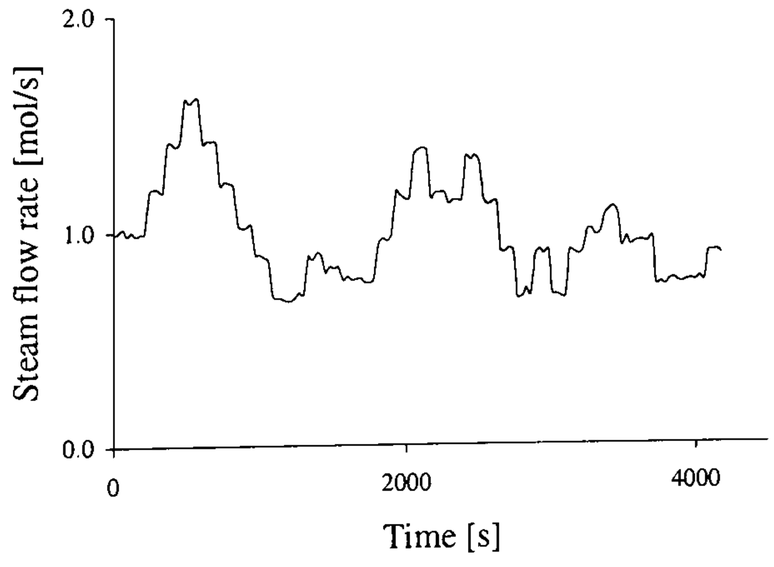
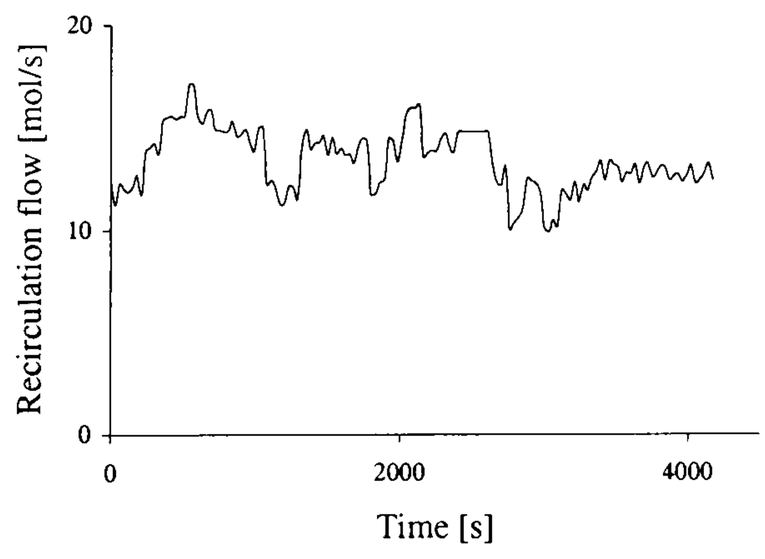


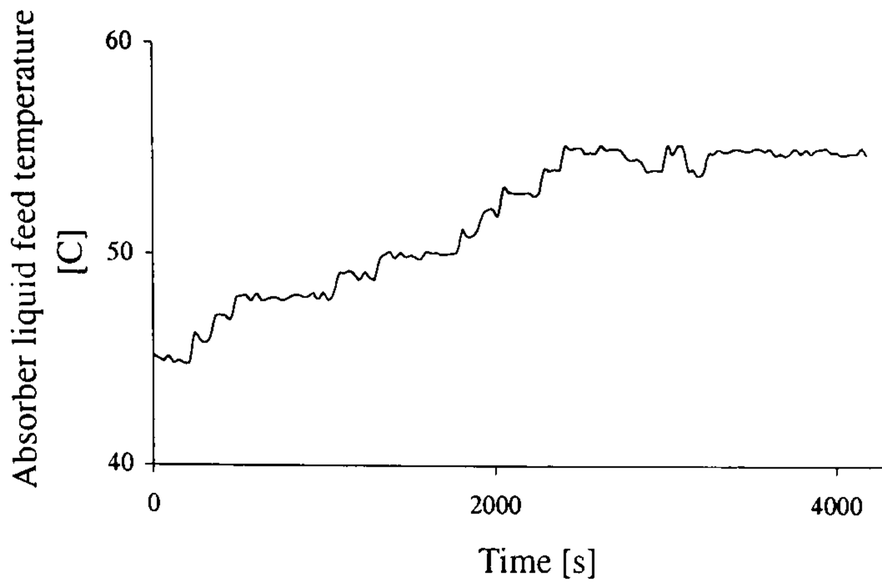
Figure 7.10. Controlled variable: Leaving CO_2 gas concentration



a) Steam flow



b) Recirculation flow



c) Absorber liquid feed temperature

Figure 7.11. Manipulated variables

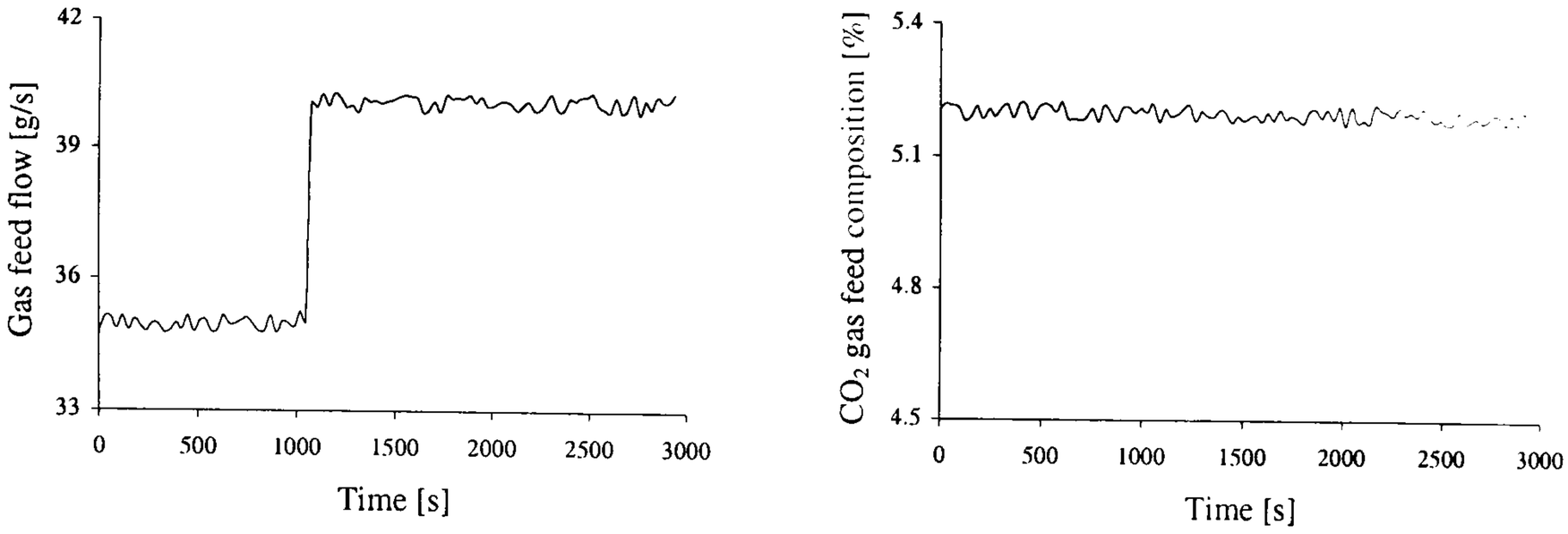
Using a less aggressive control strategy in the liquid feed temperature proved to be better for controllability purposes. Figure 7.10 exhibits the behaviour in the CO_2 gas leaving concentration in the absorber which is kept beneath the set point constantly after the perturbation. Compared with the previous case the controller requires approximately 100 extra seconds to overcome the perturbation, however it achieves steady state condition without any inconvenience. Also Figure 7.11 shows how the controller cleverly used the minimum amount of energy trying to maintain the flow close to its minimum value of 0.7 mol/s.

However, the controller cannot overcome the overshoot. The next experiment uses the same conditions but the controller has knowledge of the future feed conditions.

7.1.7. Expected Perturbation

The previous experiment is repeated again using the same conditions but with the main difference that the gas feed conditions are known by the controller five minutes in advance. Therefore some kind of control action is implemented ahead.

Results are shown from figures 7.12 to 7.14.



a) CO_2 feed gas composition b) Gas feed flow

Figure 7.12. Input variables

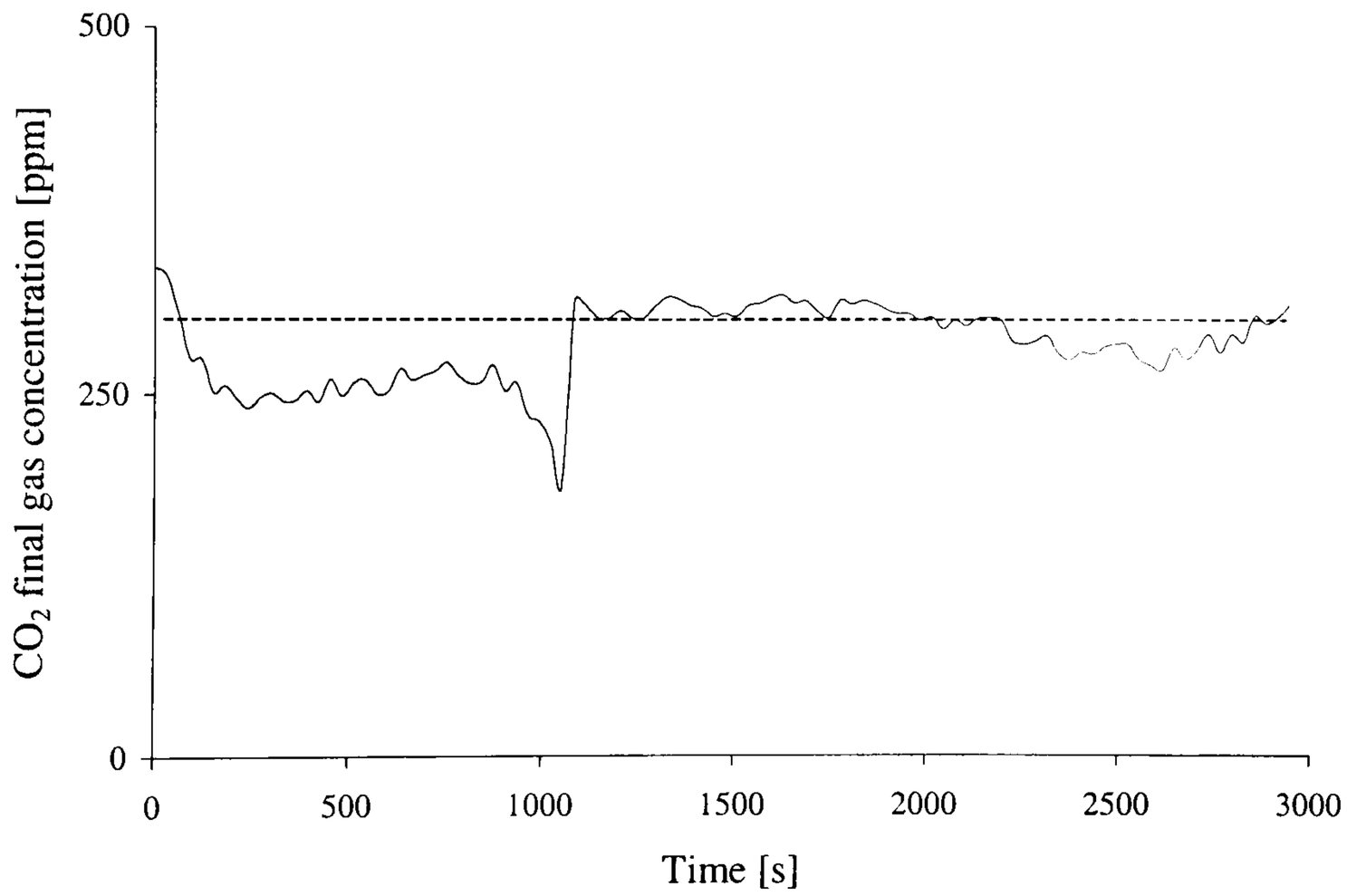
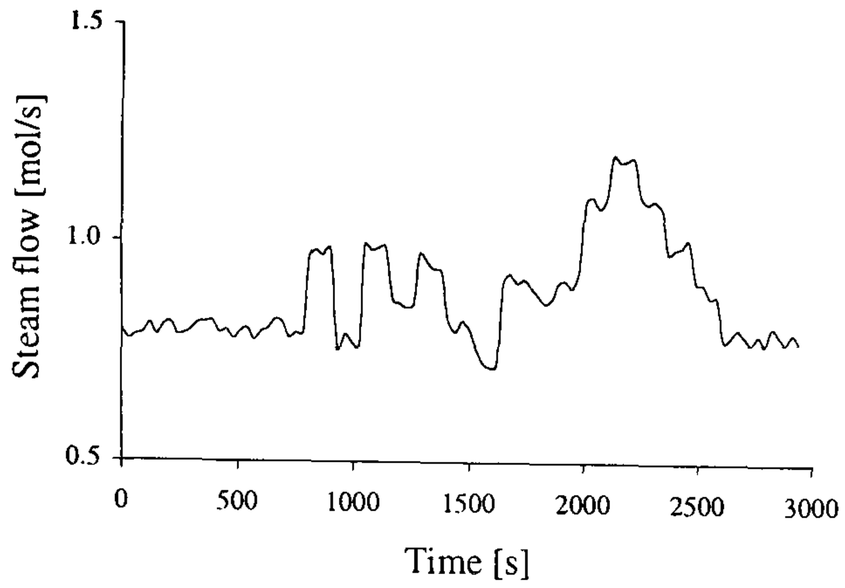
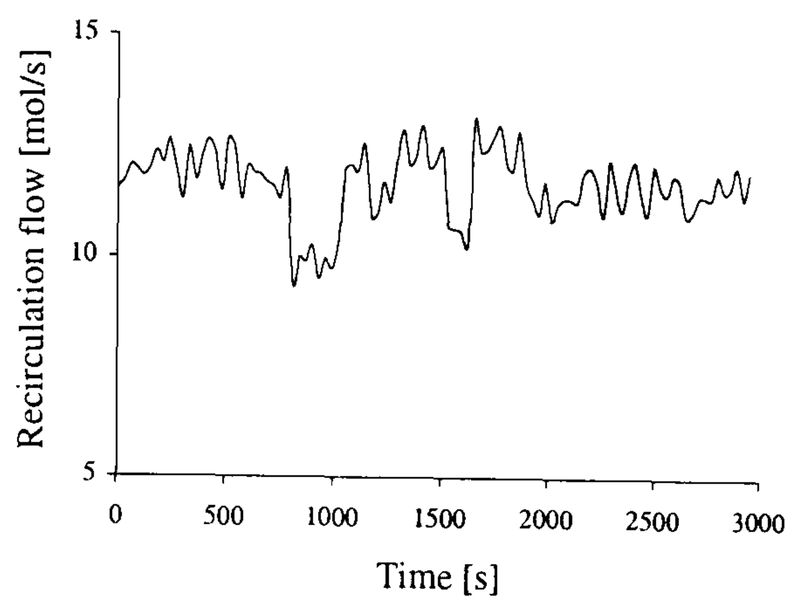


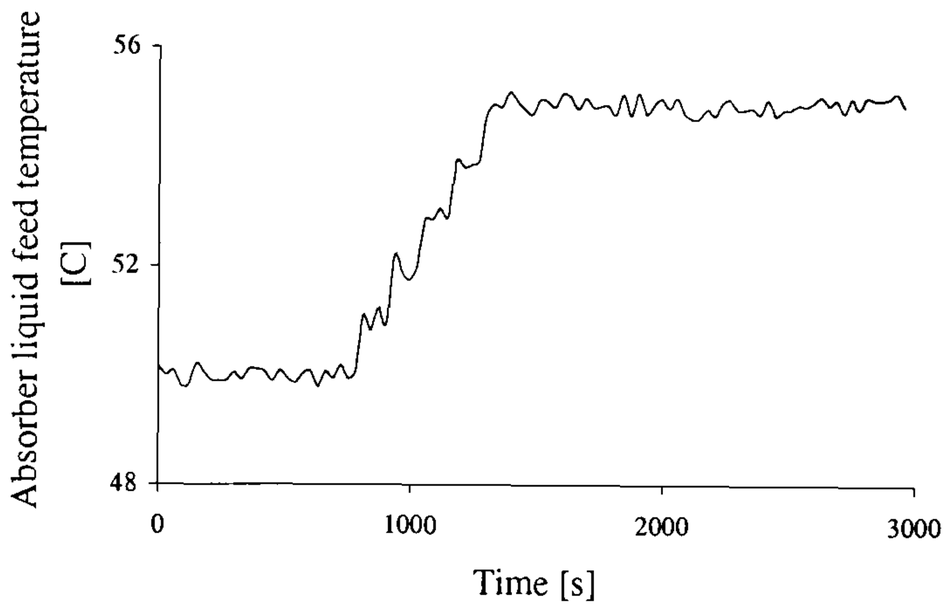
Figure 7.13. Controlled variable: Leaving CO_2 gas concentration



a) Steam flow



b) Recirculation flow



c) Absorber liquid feed temperature

Figure 7.14. Manipulated variables

As figure 7.13 proves, having advance knowledge of the future perturbation improved considerably the controller performance. It allows the controller to take some preventive action before any perturbation reaches the plant. It also improves stability and keeps the system less oscillatory compared with previous cases.

Probably more remarkable is the eradication of the overshoot seen in previous results. Although the CO_2 gas concentration is sometimes above the set point. These values are on average 10 ppm above this limit. With these results the fictitious downstream process could operate under safety conditions without risking its catalyst.

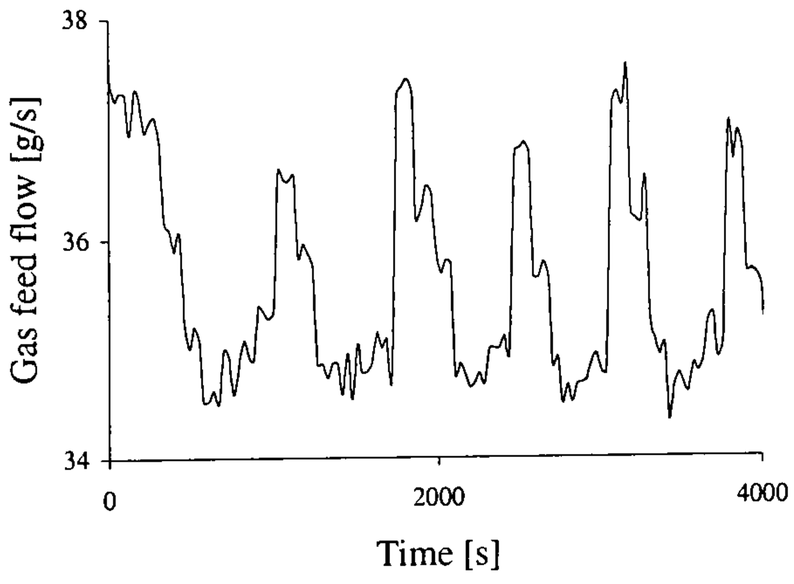
These results indicate that approximately 5 minutes advance notice is needed by the controller to effectively handle any perturbation.

Again the controller shows its preference of using liquid temperature to control the CO_2 concentration in order to save energy in the reboiler, see figures 7.14.

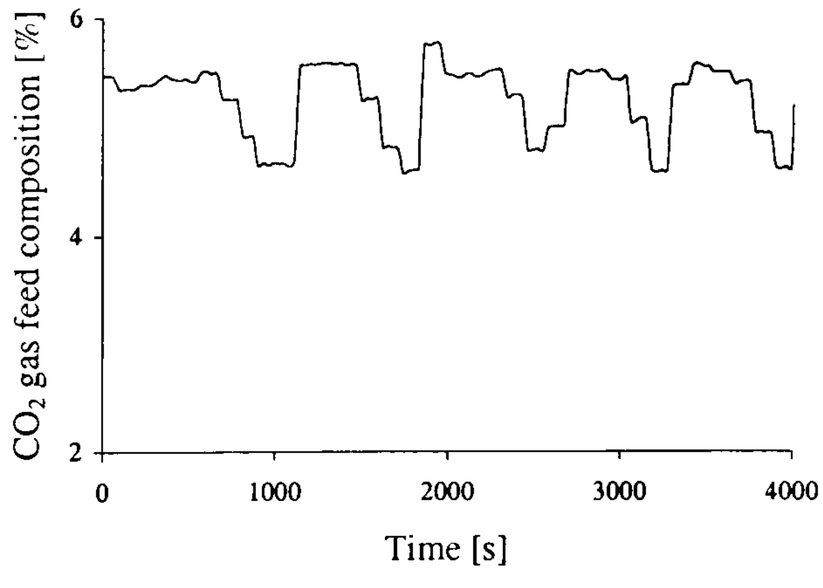
7.1.8. Real Gas Feeding Data

The last experiment tests the MPC under more realistic conditions; real feeding values obtained from one of the experiments done in the plant is used in the "simulated plant". Again the controller knows the feed conditions 5 minutes in advance.

Figure 7.15 shows the data selected for this section. It was selected among the others because its multiple oscillations in both the flow and CO_2 concentration in the gas feed present a challenging and hard task for the controller.



a) CO_2 feed gas composition



b) Gas feed flow

Figure 7.15. Input variables

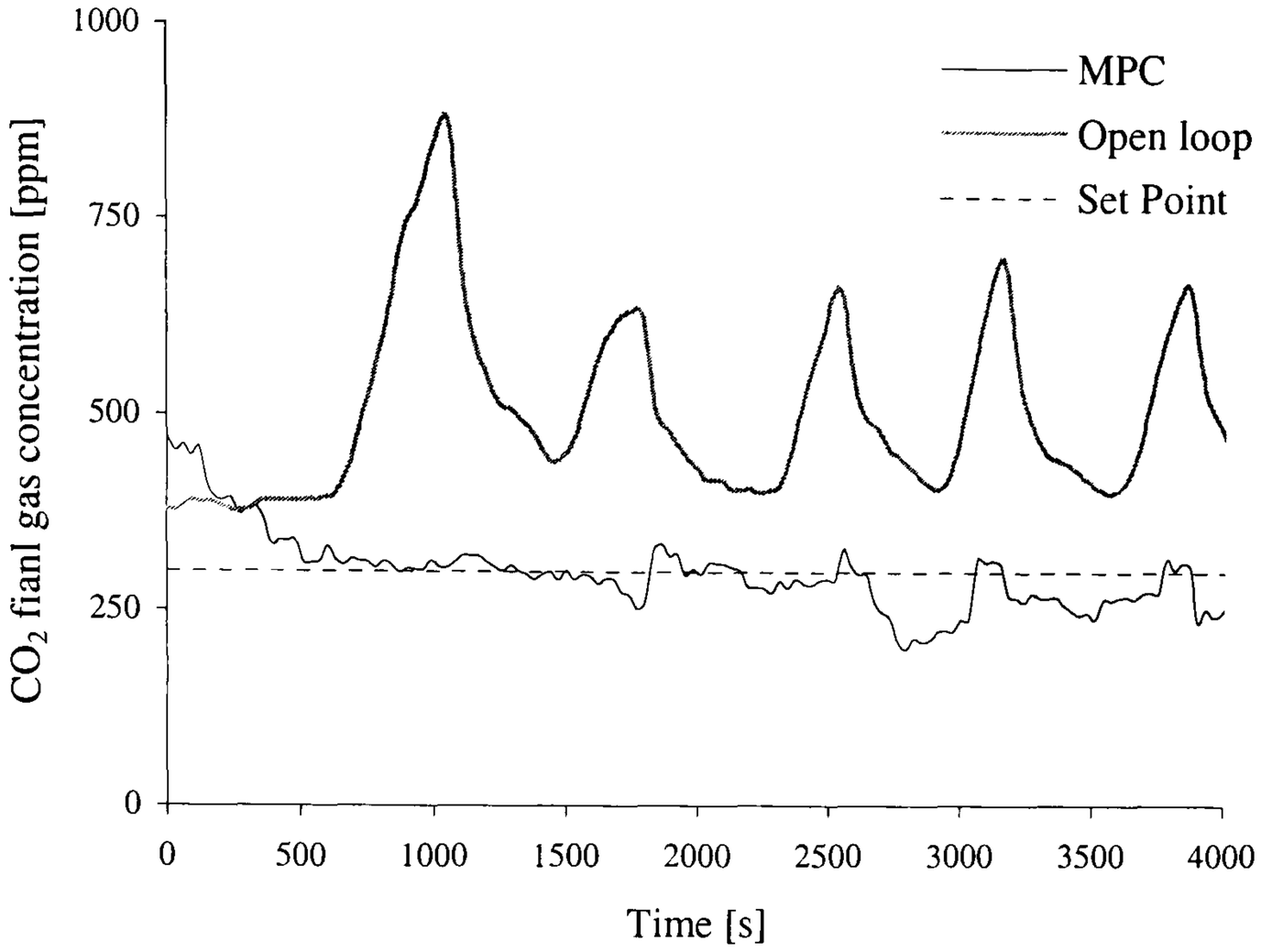
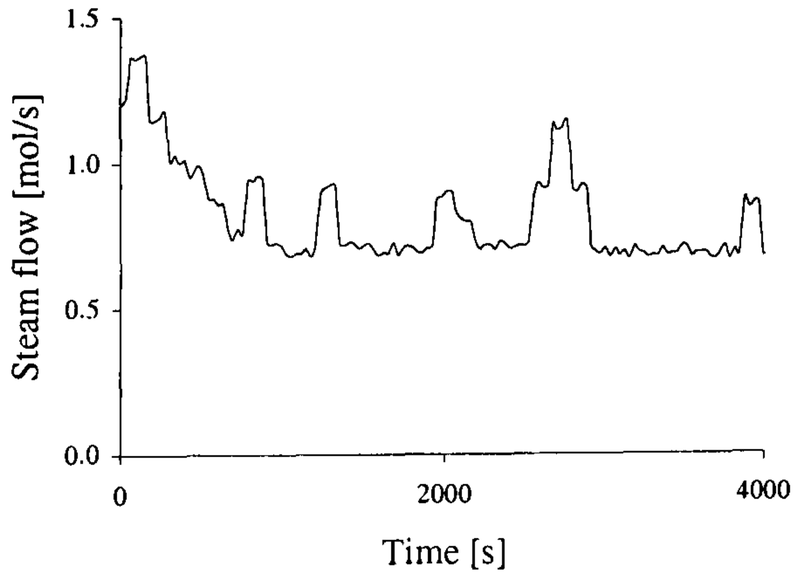
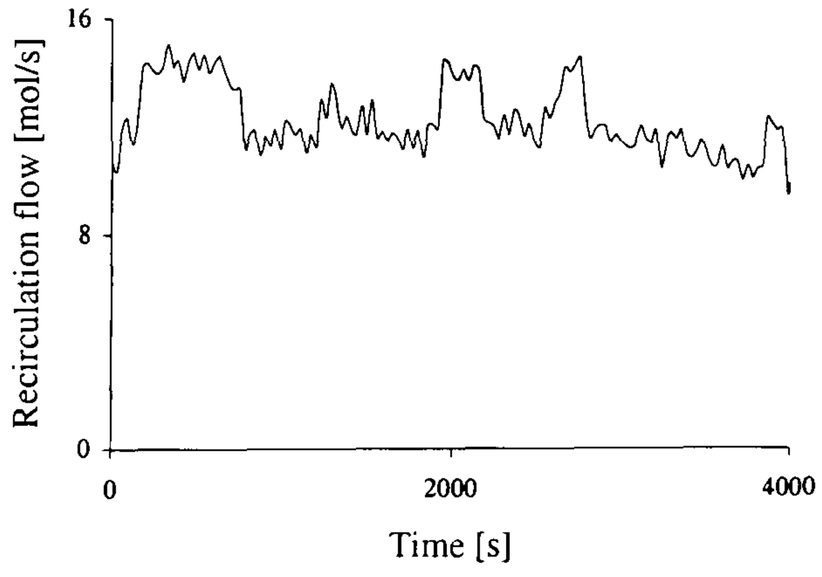


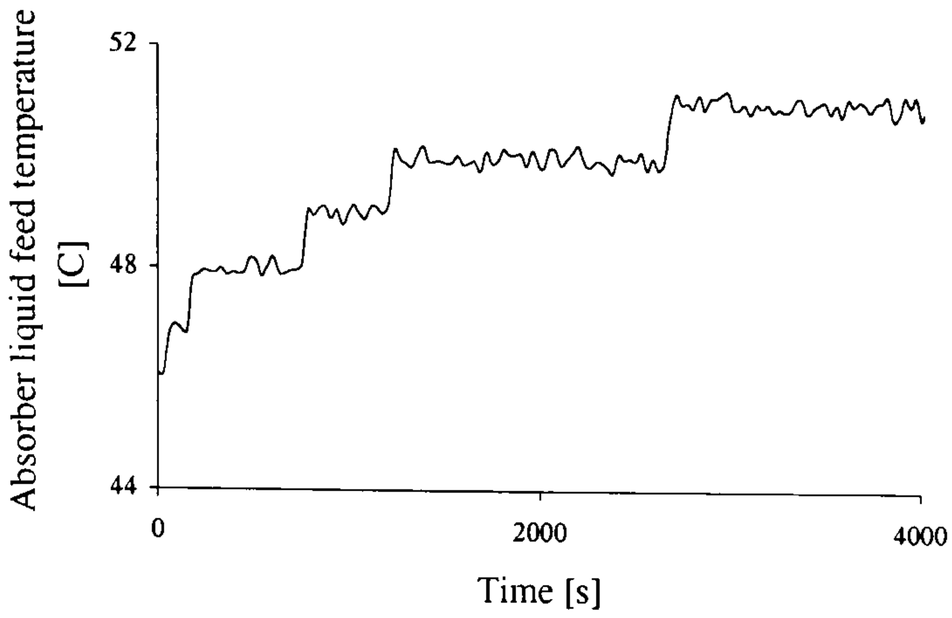
Figure 7.16. Controlled variable: Leaving CO_2 gas concentration



a) Steam flow



b) Recirculation flow



c) Absorber liquid feed temperature

Figure 7.17. Manipulated variables

This final experiment proves the feasibility to optimally control the plant under real conditions.

Although the feed conditions oscillate continuously, the controller is capable of optimally maintaining the CO_2 gas concentration below set point at all times. It can be seen from figure 7.16 that the gas concentration crosses the boundary some times, however these values are relatively small to be considered hazardous for a process downstream.

Also it is practically proved that the controller requires notice at least 5 minutes in advance to take preventive actions. This experiment shows the potential of MPC compared to other controllers.

Chapter 8

Conclusions and Recommendations for Further Work

8.1. Conclusions

Current algorithms available in the literature for nonlinear MPC, estimation and dynamic modelling have progressed remarkably in the last decade, specially issues regarding stability, controllabity, observability and robustness have been intensively studied and well documented.

This thesis has developed a new modelling and control system design for the CO_2 absorption/desorption plant. From the initial assumptions, the methodology describes the modelling process via mass and energy balances. Further improvement are developed in the model using simulation techniques, different estimation techniques are studied and lastly the feasibility to implement a nonlinear MPC is tested.

The main objective of the research was achieved; it was proved that an online nonlinear MPC could be implemented in an advanced simulation of the CO_2 pilot plant to control the leaving CO_2 gas concentration using steam flow, solvent recirculation flow and liquid feed temperature as manipulated variables while minimising energy consumption and maintaining operational constraints.

The research showed that MPC could control effectively the final CO_2 gas concentration in the absorber under noisy disturbances. The combination of terminal constraint, path constraint in the final gas concentration and optimal control horizon proved to be the best approach for an optimal solution. Also it was proved that the controller kept the plant stable under different perturbations in the feed conditions.

Previous researches have stated that steam and solvent flow were the main modifiers of the CO_2 final gas concentration in the absorber. However, this research found that the liquid feed temperature in the absorber was an excellent manipulated variable to control the leaving CO_2 gas concentration. Due to its high nonlinear effect in the controlled variable, it was recommended to change its value by a maximum of 1°C every interval.

Although the controller proved to be successful at handling unexpected perturbations, it was clear that the whole potential of the controller came when the perturbations are expected at least 5 minutes before they reach the plant. This assumption is not unrealistic considering that many chemical processes (including the CO_2 absorption/desorption) rely on products generated by an other upstream process, therefore feed conditions can be known several minutes in advance.

The extended Kalman filter proved to be an excellent estimator technique for the absorption/desorption plant. 21 state variables plus 2 uncertain parameters were optimally estimated from a set of 13 measurements in the plant. The Kalman filter was shown to be one order of magnitude more accurate compared with predecessors estimators applied in the plant such as steady state approximation or Luenberger observers.

Lastly the feasibility of implementing the estimation and control process online was also confirmed. The updated measurements are obtained at 30 seconds intervals, while the estimation process required 10 seconds per cycle on average, and the optimal control was computed within 200 seconds, well within the time required for adequate control.

The estimation of uncertain parameters reduced the mismatch between plant and model. However, overestimating the number of parameters did not bring extra benefits, specially for stability and robustness purposes. It was found that for the absorption/desorption plant, the best solution was obtained using 2 parameters (absorption rate constant and the desorber heat loss). It was also found that parameters that appear often in the model (eg. MEA concentration) should remain constant.

It is clear that MPC will become the standard in the future providing continuous improvements in computer speeds, algorithms and software.

8.2. Recommendations for Further Work

The next step would be implementing online in the real plant the complete MPC algorithm using the extended Kalman Filter as an estimator. Although the theoretical formulation has been completed and successfully tested, as difficulty would be integrating and synchronising all sections of the algorithm. Paragon Software (Plant monitor and control software) will send to Matlab at fixed intervals the updated set of measurements from the plant, and Matlab will update the estimations and send the results to gOPT. After the optimisation process is carried out, the new values for the manipulated variables are sent back to Paragon and incorporated in the real plant. All this process is executed every 2 minutes.

The simulation tests reported showed that increasing the temperature in the absorber could strip the CO_2 previously absorbed; practical experiments manipulating the liquid feed temperature in the absorber should be done and correlated with the effect on the CO_2 gas concentration in order to further improve the model. This could not be done during the experimental phase on this research due to a faulty valve controlling the cooling water.

During the practical experiments it was noticed that the liquid pH measurements in the reboiler and the absorber bottom presented numerical inconsistencies with the mathematical model. Further adjustments are required in the model in order to integrate these valuable measurements into the Kalman filter.

Lastly, gPROMS has proved to be very mature software for handling DAE systems, specially for dynamic simulations. However further improvements are required in its optimization package gOPT, in order to assure stability, robustness and convergence to feasible solutions.

References

Albrecht, J. J. *Modelling, Identification and Multivariable Control of an Absorption-Desorption System*. PhD thesis, Imperial College of Science and Technology, London, England, 1977.

Alvarez, J., and Lopez, T. Dynamic Robust State Estimator of Nonlinear Plants. *AIChE Journal*, 1999. **45**(1): 107-116

Biegler, L. T., and Rawlings J. B., Optimization Approaches to Nonlinear Model Predictive Control, CPC IV, Y. Arkun and H. Ray (eds.), *AIChE*, 543, 1991.

Bitmead, R. R., Gevers, M., and Werts, V. *Adaptive optimal control – The thinking man's GPC*. Englewood Cliffs, NJ: Prentice-Hall, 1990.

Burkett, R. J. *The Mathematical Modelling and Simulation of a Monoethanolamine-Carbon Dioxide Plant*, PhD thesis, Imperial College of Science and Technology, London, England, 1977.

Camacho, E. F., and Bordons, C. *Model Predictive Control in the Process Industry*, Springer-Verlag, London, 1995.

Chen, C. C., and Shaw, L., On receding horizon feedback control, *Automatica*, 1982, **18**: 349-352.

Chisci, L., Lombardi, A., and Mosca, E., Dual receding horizon control of constrained discrete-time systems. *European Journal of Control*, 1996, **2**: 278-285.

Cutler, C. R., Morshedi, A., and Haydel, J., An Industrial Perspective on Advanced Control, *AIChE Annual Meeting*, Washington D.C., 1983.

Cutler, C. R., and Ramaker, B. L., Dynamic Matrix Control: A Computer Control Algorithm, *AIChE National Meeting*, Houston, Texas, 1979.

Cutler, C. R., and Ramaker, B. L., Dynamic Matrix Control: A Computer Control Algorithm, *Proceedings of the Joint Automatic Conference*, 1980.

De Keyser, R. M., and Van Cauwenberghe, A. R., A self-tuning predictor as operator guide, *Proceedings of the fifth IFAC symposium on identification and system parameter estimation*, 1979, pp 1249-1256.

Disli, I. *A case Study in Optimal Process Operation: Control of a Carbon Dioxide Absorption Plant*. PhD thesis, Imperial College of Science and Technology, London, England, 1996.

Dore, S. *Application of Geometric Nonlinear Control in the Process Industries – A Case of Study*. PhD thesis, Imperial College of Science and Technology, London, England, 1993.

Escobillana, G. P., Saez, J. A., Perez-Correa, J. R., Neuburg, H. J., and Kershenbaum, L. S. Behaviour of Absorption/Stripping columns for CO_2-MEA System; Modelling and Experiments. *The Canadian Journal of Chemistry Engineering*, 1991, **69**: 969-977.

Garcia, C. E., and Morshedi, A. M., Quadratic Programming Solution of Dynamic Matrix Control (QDMC), *Chemical Engineering Communications*, 1989, **46**: 73-87.

Goodwin, G. C., and Middleton R., Digital Control and Estimation – A Unified Approach, Prentice Hall, Englewoods Clifs, New Jersey, 1990.

Kailath, T. , *Linear Systems*, Prentice-Hall, 1980.

Kalman, R. E, A new approach to Linear Filtering and Prediction Problems. *Trans. ASME. Journal of Basic Eng.*, 1960, **82**: 34-45.

Khalil, H. K, Nonlinear Systems, McMillan Pu. Co, 1992.

Kane, L., H P in perspective, *Hydrocarbon Processing*, September 1989.

Khalil H. K., *Nonlinear Systems*, Macmillan, New York, 1992.

Kohl, A., and Nielsen, R., *Gas Purification*, Gulf Publishing Company, 1997.

Kwakernaak, H., and Sivan, R.. *Linear Optimal Control Systems*. John Wiley & Sons, New York, 1972.

Marquis, P., and Broustail, J. P., SMOC, a bridge between state space model and model predictive controllers: application to the automation of a hydrotreating unit, In: T. J. McAvoy, Y. Arkun, E. Zafiriou (Eds.), *Proceedings of the IFAC workshop on model based process control*, Oxford: Pergamon Press, 1988, pp 37-43.

Mayne, D. Q., Rawlings, J. B., Rao, C. V., and Scokaert, P. O. M., Constrained Model Predictive Control: Stability and Optimality, *Automatica*, 2000, **36**: 789-814.

Meadows, E. S., Henson M. A., Eaton, J. W., and Rawlings, J. B., Receding Horizon Control and Discontinuous State Feedback Stabilization, *International Journal of Control*, 1995, **62**(5): 1217-1229.

Meadows, E. S., and Rawlings, J. B., Model Predictive Control in Nonlinear Process Control, M. A. Henson and D. E. Seborg (eds.), Prentice Hall, 1997, pp 233-310.

Michalska, H., and Mayne, D. Q., Robust receding horizon control of constrained nonlinear systems. *IEEE Transactions on Automatic Control*, 1993, **38**: 1623-1632.

Mix, T. W., and Dweck, J. S., *Conserving Energy in Distillation*, Industrial Energy Conservation Manual No. 13, MIT Press, Cambridge, Mass, 1982

Morari, M., and Lee, J. H., Model Predictive Control – Past, Present and Future, *Computers and Chemical Engineering*, 1999, **23**: 667-682.

Ogunnaike, B. A., and Ray, W. H., *Process Dynamics, Modelling and Control*, Oxford University Press, England, 1994.

Paliouri, M., A case Study in On-line Optimal Control. Technical report, process system group, Imperial College of Science, Technology and Medicine, London, England, 1989.

Pearson, R. K, and Ogunnaike, B. A., Nonlinear Process Identification in Nonlinear Process Control. M. A. Henson and D. E. Seborg (Eds.), Prentice Hall, 1997.

Prett, D. M., and Garcia, C. E., *Fundamental Process Control*, Butterworths, Stoneham, MA, 1988.

Qin, S. J., and Badgwell, T. A., An Overview of Industrial Model Predictive Control Technology. In: J. C. Kantor, C. E. Garcia, B. Carnahan (Eds), *Fifth*

International Conference on Chemical Process Control, CACHE, AIChE, 1997. pp 232-256.

Ray, W. H., *Advance Process Control*, Butterworths, Boston, USA, 1989.

Richalet, J., Rault, A., Testud, J. L., and Papon, J., Algorithmic Control of Industrial Process. *Proceedings of the 4th IFAC Symposium on Identification and System Parameter Estimation*, 1976, pp 1119-1167.

Richalet, J., Rault, A., Testud, J. L., and Papon, J., Model Predictive Heuristic Control: Application to Industrial Processes. *Automatica*, 1978, **14**: 413-428.

Roberts, M. P. *The Development and Implementation of Non-linear Optimal Control and Filtering Algorithms on an Absorption/Stripping Pilot Plant*. PhD thesis, Imperial College of Science and Technology, London, England, 1978.

Rotava, O. *Implementation of Linear and Nonlinear Techniques in a Carbon Dioxide Absorption/Desorption Plant*. PhD thesis, Imperial College of Science, Technology and Medicine, London, England, 1999.

Rotava, O., Sargent, R. W. H., and Kershenbaum, L. S. Implementation of Linear and Nonlinear Optimal Control Techniques in a CO_2 Absorption/Desorption Plant. *Computers and Chemical Engineering Supplement*, 1997, 879-882.

Scokaert, P. O. M., Mayne, D. Q., and Rawlings, J. B., Suboptimal model predictive control (feasibility implies stability). *IEEE Transactions on Automatic Control*, 1999, **44**(3): 648-654.

Scokaert, P. O. M, and Rawlings, J. B., Constrained Linear Quadratic Regulation. *IEEE Trans. Automatic Control*, 1998, **43**(8): 1163-1169,.

Vanichseni, V. *Modelling and Parameter Estimation in the Absorption of CO2 in Aqueous MEA Solution in a Pilot Plant Packed Column*. PhD thesis, Imperial College of Science and Technology, London, England, 1977.

Vassiliadis, V. S., Sargent, R. W. H., and Pantelides C. C., Solution of a Class of Multistage Dynamic Optimization Problems. 1. problems without path constraint. *Ind. Eng. Chme. Res.*, 1993, **33**(9), 2111-2122.

Vassiliadis, V. S., Sargent, R. W. H., and Pantelides C. C., Solution of a Class of Multistage Dynamic Optimization Problems. 2. problems with path constraint. *Ind. Eng. Chme. Res.*, 1993, **33**(9), 2123-2133.

Appendix A

The gPROMS Model of the CO_2 Pilot Plant

```
#
#****************************************
# CO2/N2 Pilot Plant Model
#
#  Number of stages in each column
#  5 Absorber, 10 Desorober
#****************************************
#

DECLARE

Type
  temp     = 43 : 0 : 150                UNIT = "C"
  molflow = 3.5 : -0.1 : 2.0E5           UNIT = "mol/s"
  molfrac = 0.5 : -0.0001     : 1
  kgflow   = 0.3 : 1E-5 : 3.6E5          UNIT = "kg/s"
  gflow    = 18 : 1E-5 : 3.6E5           UNIT = "g/s"
  kgliq_bound = 0.3 : .15 :.35           UNIT = "kg/s"
  molliq_bound = 14.9 : 7.4 : 17.4       UNIT = "mol/s"
  gsteam_bound = 19 : 10 : 35            UNIT = "g/s"
  molsteam_bound = 1 : 0.56 : 1.7        UNIT = "mol/s"
  molconc = 0.3 : 1E-5 : 1.5E4           UNIT = "mol/m^3"
  enthalpy = 10 : -1E3 : 1E5             UNIT = "kj/mol"
  hcapacity = 25.71 : 1E-9 : 1E8         UNIT = "kj/mol.C"
  volume   = 7E-2 : 1E-5 : 1E8           UNIT = "m^3"
  density = 1.09E-3 : 1E-9 : 1E8         UNIT = "kg/m^3"
  positive = 9 : 0   : 1E8
  absorption = -1.27E-4 : -1E4 : 20000   UNIT = "kmol/s"
  pressure = 1 : 0 : 10.5                UNIT = "atm"
  press_CO2 = 1E-3 : 1E-9 : 10           UNIT = "atm"
  notype   = 2 : -1E6 : 1E10
  level    = 0.3 : -1E6 : 1.2            UNIT = "m"
  ratio    = 0.2 : -1E8 : 1E8            UNIT = "mol/mol"
  velocity = 10 : 1E-4 : 20000           UNIT = "m/s"
  trans_unit = 3 : 1E-9 : 1000

END #Declare

MODEL CO2PLANT

  PARAMETER

  HW                              AS REAL
  dl                              AS REAL
  Cpl                             AS REAL
  A1                              AS REAL
  B1                              AS REAL
  C1                              AS REAL
  D1                              AS REAL
  A2                              AS REAL
  B2                              AS REAL
  C2                              AS REAL
  T                               AS REAL
  Cpw                             AS REAL
  Cpn                             AS REAL
  Cpc                             AS REAL
  Cplr                            AS REAL
  Hr                              AS REAL
  Hvap                            AS REAL
  Vl                              AS REAL
  Ht                              AS REAL
  A1f                             AS REAL
  B1f                             AS REAL
  C1f                             AS REAL
  Ad                              AS REAL
  NS                              AS INTEGER
  HS                              AS INTEGER
  SP                              AS REAL
  bias                            AS REAL
  gain                            AS REAL
  rset                            AS REAL
  gainvd                          AS REAL
  Tauvd                           AS REAL
  t_delayvd                       AS REAL
  gainav                          AS REAL
  tauav                           AS REAL
  t_delayav                       AS REAL
  Hst                             AS REAL
  Adr                             AS REAL
  h_dl                            AS REAL
  K_dh                            AS REAL
  pltr                            AS REAL
  gains                           AS REAL
  Taus                            AS REAL
  Q1                              AS REAL
  Q2                              AS REAL
  R2                              AS REAL
  HI                              AS INTEGER
  plt                             AS ARRAY(HS) OF REAL

  VARIABLE

  flo,fgo                         AS ARRAY(NS) OF molflow
  T1                              AS ARRAY(NS) OF temp
  x                               AS ARRAY(NS) OF molconc
  yco,ywo,yno                     AS ARRAY(NS) OF molfrac
  Cpg1,Cpgo                       AS ARRAY(NS) OF hcapacity
  K,ycoppm,xstar                  AS ARRAY(NS) OF positive
  T1star,ph,T1s,xs                AS ARRAY(NS) OF positive
  T1hat, xhat                     AS ARRAY(NS) OF notype
  R                               AS ARRAY(NS) OF absorption
  N                               AS ARRAY(NS) OF trans_unit
  Car                             AS ARRAY(NS) OF pressure
  P                               AS ARRAY(NS) OF pressure
  fgof,watern                     AS molflow
  Tg1,Tlif                        AS temp
  ycof,ywof,ynof                  AS molfrac
  Clif                            AS molconc
  realflow,waterf,fg1             AS molflow
  yc1,yn1                         AS molfrac
  ycoperc                         AS positive
  Pf                              AS pressure
  flout                           AS molflow
  z,h                             AS level
  zhat                            AS notype
  error                           AS notype
  I_error                         AS notype
  value                           AS molflow
  I_outs                          AS molflow
  I_outhat                        AS ratio
  out3                            AS molconc
  out3star, Istar                 AS positive
  out3s, Ist                      AS positive
  out3hat, Ihat                   AS notype
  flow, fl                        AS molflow
  waterc                          AS molflow
  Clow                            AS molconc
  Flom                            AS molflow
  Clom                            AS molconc
  Tlom, Tlm                       AS temp
  B                               AS molflow
  Bsp                             AS molliq_bound
  Cb                              AS molconc
  Real_Bsp                        AS kgliq_bound
  Cbstar,Bstar,Cbs,Bs             AS positive
```

```
Cbhat, Bhat                 AS notype
Sreal                       AS gflow
Breal                       AS kgflow
Vb,S                        AS molflow
Tr                          AS temp
Carr                        AS ratio
yc,yw                       AS molfrac
Q                           AS enthalpy
Cpg                         AS hcapacity
W,phr,phmul                 AS positive
xrstar,xrs, zs              AS positive
xrhat,zrhat                 AS notype
Pr                          AS pressure
zd                          AS level
Vg                          AS velocity
L,V,Fw                      AS molflow
Two,Twi,Tc                  AS temp
ycc,ywc                     AS molfrac
Qc                          AS enthalpy
Cpgi, Cpgs                  AS hcapacity
Pc                          AS pressure
Ssp                         AS molsteam_bound
Real_Ssp                    AS gsteam_bound
Sstar,Ss                    AS positive
Shat                        AS notype
CO2ppm_SP,phmul_SP          AS positive
S_ini                       AS gsteam_bound
L_ini                       AS kgliq_bound
J,Lowliq,Highliq            AS notype
fld,fgd                     AS ARRAY(HS) OF molflow
T2                          AS ARRAY(HS) OF temp
Cl                          AS ARRAY(HS) OF molconc
ycd,ywd                     AS ARRAY(HS) OF molfrac
Cpgdi,Cpgdo                 AS ARRAY(HS) OF hcapacity
Vld                         AS ARRAY(HS) OF volume
Card                        AS ARRAY(HS) OF ratio
Pd                          AS ARRAY(HS) OF pressure
Vgd                         AS ARRAY(HS) OF velocity
xdstar,xds                  AS ARRAY(HS) OF positive
xdhat                       AS ARRAY(HS) OF notype
dev_phmul,dev_CO2ppm        AS notype
K2                          AS positive
E                           AS positive
Cmea                        AS positive
xw                          AS positive
Qla                         AS enthalpy
Qld                         AS enthalpy
Qlr                         AS enthalpy
Vll                         AS notype

SET
  HI := HS;
  HW := 20.13;    #liquid average molecular weight g/mol
  dl := 1E6;      # Density g/m3
  Cpl := 75.81/1000;
  A1 := 1.68608e-3;
  B1 := -1.5319495e-1;
  C1 := 6.984763;
  D1 := -82.82877;
  A2 := 46.376592;
  B2 := -3.047119e3;
  C2 := 6.660746e4;
  T := 100;
  Cpw := 33.5/1000;    #kJ/mol*C
  Cpn := 29.26/1000;   #kJ/mol*C
  Cpc := 41.382/1000;  #kJ/mol*C
  Cplr := 79.2/1000;   #kJ/mol*C
  Hr := 1.025e2;       #kJ/mol
  Hvap := 40;          #kJ/mol
  Hst := 4.54e1;
  Vl :=0.03768/NS;       # Absorber's stage liquid Holdup
m3
  Ht := 6.1/NS;        #m Absorber stage
  A1f := 18.4;
  B1f := 3880;
  C1f := 230;
  Ad := 0.0507;
  Adr := 0.1496;
  SP := 0.55;
  bias := 12;
  gain := -100;
  rset := 184;
  gainvd := 1;
  Tauvd := 5;
  t_delayvd := 5;
  gainav := 1;
  Tauav := 5;
  t_delayav := 5;
  h_dl := 4.9289e-3;
  K_dh := 7.118e-6;
  pltr := 18/HS;
  gains := 1;
  Taus := 5;
  Q1 := 0.005*10;
  Q2 := 0.005;
  R2 := 0.026;
    FOR I := 1 TO HS -1 DO
      plt(I) := 18/HS;
    END
  plt(HS) := 3;
  NS := 5;
  HS := 10;


  EQUATION

# ABSORBER Model1

# For i := 1

# Overall Absorption Rate #
  K(1)^2 = P(1)^2*K2^2 * (A2*T1(1)^2 + B2*T1(1) +
C2)*(Cmea-2*x(1))*1000;
  N(1)*fgo(1) = K(1)*Ht;

  R(1) = fgof*ycof*(1-EXP(-N(1)));


# Overal Balance #
  fgof + flo(2) = fgo(1) + flo(1);

# Nitrogen Balance #
   fgof*ynof = fgo(1)*yno(1);

# CO2 Balance in gas
   0 = (fgof*ycof) - (fgo(1)*yco(1)) - R(1)+ (EXP((-
47.91+112.8*Car(1))+(0.7615-1.668*Car(1))*T1(1)+
    (-0.0029+0.007*Car(1))*T1(1)*T1(1))/760*fgo(1)/P(1));

# CO2 Balance in liquid #
   Vl*$xstar(1)*1250 = HW/dl*(flo(2)*x(2)-
flo(1)*x(1))+R(1)-(EXP((-47.91+112.8*Car(1))+(0.7615-
1.668*Car(1))*T1(1)+
    (-0.0029+0.007*Car(1))*T1(1)*T1(1))/760*fgo(1)/P(1));
   x(1) = 1250*xstar(1);
   xhat(1) = xstar(1) - xs(1);

# Mol balance #
   yno(1)+yco(1)+ywo(1)=1;

# Energy Balance#
   (Vl*Cpl*dl/HW)*$T1star(1)*35 = flo(2)*Cpl*(T1(2) - T)
+
       flo(1)*Cpl*(T - T1(1)) +
       fgof*Cpg1(1)*(Tg1 - T) + fgo(1)*Cpgo(1)*(T -
T1(1)) +
      (fgof*ywof - fgo(1)*ywo(1))*Hvap + R(1) * Hr -
Qla;

    T1(1)-25 = T1star(1)*35;
    T1hat(1) = T1star(1) - T1s(1);

    Cpg1(1) = Cpn*ynof + Cpc*ycof + Cpw*ywof;
    Cpgo(1) = Cpn*yno(1) + Cpc*yco(1) + Cpw*ywo(1);

    Car(1)*Cmea = x(1);
    Car(1) = -3.024e-1*ph(1) + 3.3419;

# Vapor pressure calculation #
   ywo(1)*P(1) = (A1*T1(1)^3 + B1*T1(1)^2 + C1*T1(1) +
D1)/ 760;
   ycoppm(1) = 1000000 * yco(1);


For I := 2 TO NS-1 DO

# Overall Absorption Rate #
  K(I)^2 = P(I)^2*K2^2 * (A2*T1(I)^2 + B2*T1(I) +
C2)*(Cmea-2*x(I))*1000;
  N(I)*fgo(I) = K(I)*Ht;

  R(I) = fgo(I-1)*yco(I-1)*(1-EXP(-N(I)));


# Overal Balance #
  fgo(I-1) + flo(I+1) = fgo(I) + flo(I);

# Nitrogen Balance #
   fgo(I-1)*yno(I-1) = fgo(I)*yno(I);

# CO2 Balance in gas
   0 = (fgo(I-1)*yco(I-1)) - (fgo(I)*yco(I)) - R(I) +
(EXP((-47.91+112.8*Car(I))+(0.7615-1.668*Car(I))*T1(I)+
    (-0.0029+0.007*Car(I))*T1(I)*T1(I))/760*fgo(I)/P(I));

# CO2 Balance in liquid #
   Vl*$xstar(I)*1250 = HW/dl*(flo(I+1)*x(I+1)-
flo(I)*x(I))+R(I)-(EXP((-47.91+112.8*Car(I))+(0.7615-
1.668*Car(I))*T1(I)+
    (-0.0029+0.007*Car(I))*T1(I)*T1(I))/760*fgo(I)/P(I));
   x(I) = 1250*xstar(I);
   xhat(I) = xstar(I) - xs(I);
```

```
# Mol balance #
   yno(I)+yco(I)+ywo(I)=1;

# Energy Balance#
   (Vl*Cpl*dl/HW)*$T1star(I)*35 = flo(I+1)*Cpl*(T1(I+1) -
T) +
       flo(I)*Cpl*(T - T1(I)) +
       fgo(I-1)*Cpg1(I)*(T1(I-1) - T) + fgo(I)*Cpgo(I)*(T
- T1(I)) +
       (fgo(I-1)*ywo(I-1) - fgo(I)*ywo(I))*Hvap + R(I) *
Hr - Qla;

    T1(I)-25 = T1star(I)*35;
    T1hat(I) = T1star(I) - T1s(I);

    Cpg1(I) = Cpn*yno(I-1) + Cpc*yco(I-1) + Cpw*ywo(I-1);
    Cpgo(I) = Cpn*yno(I) + Cpc*yco(I) + Cpw*ywo(I);

    Car(I)*Cmea = x(I);
    Car(I) = -3.024e-1*ph(I) + 3.3419;

# Vapor pressure calculation #
   ywo(I)*P(I) = (A1*T1(I)^3 + B1*T1(I)^2 + C1*T1(I) +
D1)/ 760;
   ycoppm(I) = 1000000 * yco(I);

   END #For

# For I := NS

# Overall Absorption Rate #
  K(NS)^2 = P(NS)^2*K2^2 * (A2*T1(NS)^2 + B2*T1(NS) +
C2)*(Cmea-2*x(NS))*1000;
  N(NS)*fgo(NS) = K(NS)*Ht;

  R(NS) = fgo(NS-1)*yco(NS-1)*(1-EXP(-N(NS)));


# Overal Balance #
  fgo(NS-1) + B = fgo(NS) + flo(NS);

# Nitrogen Balance #
   fgo(NS-1)*yno(NS-1) = fgo(NS)*yno(NS);

# CO2 Balance in gas
   0 = (fgo(NS-1)*yco(NS-1)) - (fgo(NS)*yco(NS)) -
R(NS)+(EXP((-47.91+112.8*Car(NS))+(0.7615-
1.668*Car(NS))*T1(NS)+
    (-
0.0029+0.007*Car(NS))*T1(NS)*T1(NS))/760*fgo(NS)/P(NS));

# CO2 Balance in liquid #
   Vl*$xstar(NS)*1250 = HW/dl*(B*Clif-
flo(NS)*x(NS))+R(NS)-(EXP((-47.91+112.8*Car(NS))+(0.7615-
1.668*Car(NS))*T1(NS)+
    (-
0.0029+0.007*Car(NS))*T1(NS)*T1(NS))/760*fgo(NS)/P(NS));
   x(NS) = 1250*xstar(NS);
   xhat(NS) = xstar(NS) - xs(NS);

# Mol balance #
   yno(NS)+yco(NS)+ywo(NS)=1;

# Energy Balance#
   (Vl*Cpl*dl/HW)*$T1star(NS)*35 = B*Cpl*(Tlif - T) +
       flo(NS)*Cpl*(T - T1(NS)) +
       fgo(NS-1)*Cpg1(NS)*(T1(NS-1) - T) +
fgo(NS)*Cpgo(NS)*(T - T1(NS)) +
       (fgo(NS-1)*ywo(NS-1) - fgo(NS)*ywo(NS))*Hvap +
R(NS) * Hr - Qla;

    T1(NS)-25 = T1star(NS)*35;
    T1hat(NS) = T1star(NS) - T1s(NS);

    Cpg1(NS) = Cpn*yno(NS-1) + Cpc*yco(NS-1) +
Cpw*ywo(NS-1);
    Cpgo(NS) = Cpn*yno(NS) + Cpc*yco(NS) + Cpw*ywo(NS);

    Car(NS)*Cmea = x(NS);
    Car(NS) = -3.024e-1*ph(NS) + 3.3419;

# Vapor pressure calculation #
   ywo(NS)*P(NS) = (A1*T1(NS)^3 + B1*T1(NS)^2 + C1*T1(NS)
+ D1)/ 760;
   ycoppm(NS) = 1000000 * yco(NS);

# Water leaving the absorber in the gas #
    watern = fgo(NS)*ywo(NS);


# GAS FEED EQUATIONS

#  N2 Balance in gas
    fg1*yn1 = fgof*ynof;

#  CO2 Balance in gas
   fg1*yc1 = fgof*ycof;

#  Mol Balance
   yc1 + yn1 = 1;
   ycof + ynof + ywof = 1;

# Outlet water vapor pressure calculation #
   ywof*Pf = EXP(A1f-B1f/(C1f+Tg1))/760;

   realflow = fg1*28.2;
   ycoperc = 100*ycof;

# Water entering the absorber in gas
  waterf = fgof*ywof;

# LEVEL MODEL
   zhat = z - h;
   (dl*Ad/HW)*$z = flo(1) - flout;

# MODEL FOR LEVEL CONTROLLER IN ABSORBER
   error = SP - z;
   $I_error = error;
   value = bias + gain*(error+I_error/rset);
   I_outhat = value - I_outs;

# DESORBER FEED VALVE
   gainvd*value = Istar*30+Tauvd*$Istar*30;
   flout = Istar*30;
   Ihat = Istar - Ist;
   (t_delayvd/3)*$out3star*1250+out3star*1250=x(1);
   out3star = out3/1250;
   out3hat = out3star - out3s;

# WATER MAKE-UP MODEL

 # Make-up water = Water lost in gas of top absorber +
 # water lost in gas leaving condenser - water in gas
feed

  fl = watern + waterc - waterf;

 # Overall balance
   flout + fl - flow = 0;

 # Concentration #
   flout*out3=flow*Clow;

# MODEL FOR DE MIXER BELOW CONDENSER

# Overall balance
   flow + L - Flom = 0;

# CO2 balance
  flow*Clow = Flom*Clom;

# Energy balance
  0 = flow*(T1m - T) + L*(Tc - T) + Flom*(T-Tlom);

# MODEL ABSORBER FEED VALVE

  gainav*Bsp = Bstar*30 + tauav*$Bstar*30;
  B = Bstar*30;
  Bhat = Bstar - Bs;
  (t_delayav/3)*$Cbstar*1250 + Cbstar*1250 = Cb;
  Clif = Cbstar*1250;
  Cbhat = Cbstar - Cbs;
  Real_Bsp = Bsp*20.13/1000;

# MODEL REBOILER

# Process Side Mass Balance #
  (dl*Adr/HW)*$zd = fld(1)-Vb-B;
  zrhat = zd - zs;

# Component Balance #
  Adr*zd*$xrstar*1250 = fld(1)*(Cl(1)-Cb)*HW/dl - Vb*(yc-
Cb*HW/dl);
  Cb = xrstar*1250;
  xrhat = xrstar - xrs;

# Vapor velocity #
  Vg = Vb*1.1515e+1;

# Mol Balance #
  yw = 1-yc;

# Vapor Pressure Calculation #
  yw*Pr = (( A1*Tr^3 + B1*Tr^2 + C1*Tr + D1 )/760)*xw;

# CO2 Partial Pressure#
  yc*Pr = E*EXP((-47.91+112.8*Carr) + (0.7615-
1.668*Carr)*Tr +
         (-0.0029+0.007*Carr)*Tr*Tr)/760;

# Carbonation ratio #
  Carr*Cmea = Cb;

# Energy Balance#
```

```
#Process Side#

  W=dl*Adr/HW;
  Cplr*Tr*W*$zd = fld(1)*Cplr*(T2(1)-T) + B*Cplr*(T-Tr)+
       Vb*Cpg*(T-Tr) - Vb*(yw*Hvap + yc*Hr) + Q - Qlr;

  Cpg = Cpc*yc + Cpw*yw;

# Steam side#
  Q=S*Hst;
  Sreal = S*18;
  Breal = B*20.13/1000;

# Pressure drop #
  Pr - Pd(1) = pltr*(h_dl + K_dh*0.77*Vg^2);

  Carr = -3.024e-1*phr + 3.3419;
  phmul = phr*10000;

# MODEL CONDENSER #

# Mass Balance in Condenser #
  fgd(HS) = L + V;

# Component Balance #
  fgd(HS)*ycd(HS) = V*ycc;

# Mol balance #
  ycc+ywc = 1;

# Vapor Pressure Calculation #
  ywc*Pc = ( A1*Tc^3 + B1*Tc^2 + C1*Tc + D1)/760;

# Energy Balance #

# Process Side#
  0 = fgd(HS)*Cpgi*(T2(HS) - T) - V*Cpgs*(Tc - T)
    -L*Cpl*(Tc - T) + L*Hvap - Qc;

  Cpgi = Cpc*ycd(HS) + Cpw*ywd(HS);
  Cpgs = Cpc*ycc + Cpw*ywc;

# Water Side#
  Qc = Cpl*Fw*(Two-Twi);

# Water leaving condenser as vapor #
  waterc = V*ywc;

# Model STEAM VALVE

  gains*Ssp = Sstar*3 + Taus*$Sstar*3;
  S = Sstar*3;
  Shat = Sstar - Ss;
  Real_Ssp = Ssp*18;

# Model OBJECTIVE

#  $J = Q1*((CO2ppm_SP - ycoppm(19))/100)^2 +
Q2*((phmul_SP - phmul)/200)^2
#       + R2*((Ssp/1000 - S_ini/18000))^2;

  $J =  Ssp;

  Lowliq = (0.05*Ssp*18 - 0.1)*1000/20.13-Bsp;
  Highliq = Bsp - (0.005926*Ssp*18 + 0.09074)*1000/20.13;
  dev_phmul = phmul_SP - phmul;
  dev_CO2ppm = CO2ppm_SP - ycoppm(5);


#    realflow = MIN(45,MAX(10000*(TIME-500),40));
#    realflow = 40;

    $V11 = MAX(0,(ycoppm(5)-100));


# MODEL DESORBER

# For I := 1

# Overall Balance #
  fld(2) + Vb = fld(1) + fgd(1);

# CO2 Balance #
  Vld(1)*$xdstar(1)*1250 = HW/dl*(fld(2)*Cl(2)-
fld(1)*Cl(1))+(Vb*yc)-
    (fgd(1)*ycd(1));
  Cl(1) = xdstar(1)*1250;
  xdhat(1) = xdstar(1) - xds(1);

# Vapor velocity #
  Vgd(1) = fgd(1)*1.1515e+1;

# Mol Balance #
  ycd(1)+ywd(1)=1;

# Vapor Pressure Calculation #
  ywd(1)*Pd(1) = (( A1*T2(1)^3 + B1*T2(1)^2 + C1*T2(1) +
D1 )/760)*xw;

# CO2 Partial pressure #
  ycd(1)*Pd(1) = E*EXP((-47.91+112.8*Card(1))+(0.7615-
1.668*Card(1))*T2(1)+
    (-0.0029+0.007*Card(1))*T2(1)*T2(1))/760;

# Carbonation ratio #
  Card(1)*Cmea = Cl(1);

# Energy Balance #
  0 = fld(2)*Cplr*(T2(2)-T) + fld(1)*Cplr*(T-T2(1)) +
       Vb*Cpgdi(1)*(Tr-T) + fgd(1)*Cpgdo(1)*(T-T2(1)) +
       (Vb*yw - fgd(1)*ywd(1))*Hvap + (Vb*yc -
fgd(1)*ycd(1))*Hr - Qld;

  Cpgdi(1) = Cpc*yc + Cpw*yw;
  Cpgdo(1) = Cpc*ycd(1) + Cpw*ywd(1);

# Pressure drop #
  Pd(1) - Pd(2) = plt(1)*(h_dl + K_dh*0.77*Vgd(1)^2);
  Vld(1) = 0.06012/(HS);


  For I := 2 TO HS-1 DO

# Overall Balance #
  fld(I+1) + fgd(I-1) = fld(I) + fgd(I);

# CO2 Balance #
  Vld(I)*$xdstar(I)*1250 = HW/dl*(fld(I+1)*Cl(I+1)-
fld(I)*Cl(I))+
  (fgd(I-1)*ycd(I-1))- (fgd(I)*ycd(I));
  Cl(I) = xdstar(I)*1250;
  xdhat(I) = xdstar(I) - xds(I);

# Vapor velocity #
  Vgd(I) = fgd(I)*1.1515e+1;

# Mol Balance #
  ycd(I)+ywd(I)=1;

# Vapor Pressure Calculation #
  ywd(I)*Pd(I) = (( A1*T2(I)^3 + B1*T2(I)^2 + C1*T2(I) +
D1 )/760)*xw;

# CO2 Partial pressure #
  ycd(I)*Pd(I) = E*EXP((-47.91+112.8*Card(I))+(0.7615-
1.668*Card(I))*T2(I)+
    (-0.0029+0.007*Card(I))*T2(I)*T2(I))/760;

# Carbonation ratio #
  Card(I)*Cmea = Cl(I);

# Energy Balance #
  0 = fld(I+1)*Cplr*(T2(I+1)-T) + fld(I)*Cplr*(T-T2(I)) +
       fgd(I-1)*Cpgdi(I)*(T2(I-1)-T) +
fgd(I)*Cpgdo(I)*(T-T2(I)) +
       (fgd(I-1)*ywd(I-1) - fgd(I)*ywd(I))*Hvap + (fgd(I-
1)*ycd(I-1)
        - fgd(I)*ycd(I))*Hr - Qld;

  Cpgdi(I) = Cpc*ycd(I-1) + Cpw*ywd(I-1);
  Cpgdo(I) = Cpc*ycd(I) + Cpw*ywd(I);

# Pressure drop #
  Pd(I) - Pd(I+1) = plt(I)*(h_dl + K_dh*0.77*Vgd(I)^2);
  Vld(I) = 0.06012/(HS);

  END

# FOR I := HS

  # Overall Balance #
  Flom + fgd(HS-1) = fld(HS) + fgd(HS);

# CO2 Balance #
  Vld(HS)*$xdstar(HS)*1250 = HW/dl*(Flom*Clom-
fld(HS)*Cl(HS))+
  (fgd(HS-1)*ycd(HS-1))- (fgd(HS)*ycd(HS));
  Cl(HS) = xdstar(HS)*1250;
  xdhat(HS) = xdstar(HS) - xds(HS);

# Vapor velocity #
  Vgd(HS) = fgd(HS)*1.1515e+1;

# Mol Balance #
  ycd(HS)+ywd(HS)=1;

# Vapor Pressure Calculation #
  ywd(HS)*Pd(HS) = (( A1*T2(HS)^3 + B1*T2(HS)^2 +
C1*T2(HS) + D1 )/760)*xw;

# CO2 Partial pressure #
  ycd(HS)*Pd(HS) = E*EXP((-47.91+112.8*Card(HS))+(0.7615-
1.668*Card(HS))*T2(HS)+
```

```
    (-0.0029+0.007*Card(HS))*T2(HS)*T2(HS))/760;

# Carbonation ratio #
  Card(HS)*Cmea = C1(HS);

# Energy Balance #
  0 = Flom*Cplr*(Tlom-T) + fld(HS)*Cplr*(T-T2(HS)) +
      fgd(HS-1)*Cpgdi(HS)*(T2(HS-1)-T) +
fgd(HS)*Cpgdo(HS)*(T-T2(HS)) +
      (fgd(HS-1)*ywd(HS-1) - fgd(HS)*ywd(HS))*Hvap +
      (fgd(HS-1)*ycd(HS-1) - fgd(HS)*ycd(HS))*Hr - Qld;

  Cpgdi(HS) = Cpc*ycd(HS-1) + Cpw*ywd(HS-1);
  Cpgdo(HS) = Cpc*ycd(HS) + Cpw*ywd(HS);

# Pressure drop #
  Pd(HS) - Pc = plt(HS)*(h_dl + K_dh*0.77*Vgd(HS)^2);
  Vld(HS) = 0.06012/(HS);


END #Model


PROCESS a

    UNIT
    AB AS CO2PLANT

    ASSIGN #Degress of freedom

    WITHIN AB DO


#*** Steady-State conditions ***


AB.SS := 2.333333333333333E-01 ;
AB.H := 5.500000794524512E-01 ;
AB.ZS := 3.864700609615142E-01 ;
AB.IST := 4.672885153285877E-01 ;
AB.I_OUTS := 1.401865541916288E+01 ;
AB.BS := 4.666666666666668E-01 ;

AB.XS(1)   :=        0.47944633         ;
AB.XS(2)   :=        0.42970987         ;
AB.XS(3)   :=        0.40450851         ;
AB.XS(4)   :=        0.39328951         ;
AB.XS(5)   :=        0.38592323         ;
AB.XRS     :=        0.39775777         ;
AB.XDS(1)  :=        0.38574402         ;
AB.XDS(2)  :=        0.38973394         ;
AB.XDS(3)  :=        0.39338103         ;
AB.XDS(4)  :=        0.39738971         ;
AB.XDS(5)  :=        0.40198706         ;
AB.XDS(6)  :=        0.40730844         ;
AB.XDS(7)  :=        0.41358059         ;
AB.XDS(8)  :=        0.42124105         ;
AB.XDS(9)  :=        0.43112473         ;
AB.XDS(10) :=        0.44491487         ;
AB.T1S(1)  :=        1.248718143        ;
AB.T1S(2)  :=        0.623628371        ;
AB.T1S(3)  :=        0.5467354 ;
AB.T1S(4)  :=        0.673048943        ;
AB.T1S(5)  :=        0.705953057        ;
AB.CBS     :=        0.39775777         ;
AB.OUT3S   :=        0.47944633         ;

#*** Uncertain parameters ***
     K2 :=           3.8367E-6; #4.5E-6;
     E :=            5.256E-1; #1;
     Cmea :=         1823; # mol/m3
     Q1a :=          2.69;
     Q1d :=          -3.55; #0;
     Q1r :=          -2.41; #0;

#*** Controler parameters ***
     Bsp  :=         14; #14;
     Ssp  :=         1;#0.7;

#*** Pilot Plant Conditions ***
     ycoperc         :=          2.7; #4.0;
     realflow        :=          42; #40;
     Tlif            :=          45;  # C
     Pf   :=         2.03;  # atm
     Tg1  :=         30;
     T1m  :=         90;
     Pc   :=         1;
     Twi  :=         24.5;
     Two  :=         36.4;
     Tc   :=         40;
     xw   :=         0.9513;
     P                :=         2.03;    # atm

#*** Objective Function parameters ***
     L_ini           :=          0.2832;
     S_ini           :=          18;

     CO2ppm_SP       :=          200;
     phmul_SP        :=          102363;


    END #within

PRESET
    RESTORE "CO2plant_values"


    INITIAL
#       STEADY_STATE
      WITHIN AB DO
        xhat = 0;
        T1hat = 0;
        zhat = 0;
        I_outhat = 0;
        Ihat = 0;
        out3hat = 0;
        Bhat = 0;
        Cbhat = 0;
        xrhat = 0;
        zrhat = 0;
        Shat = 0;
        xdhat = 0;

          V11 = 0;
          J = 0;

    END #Within

SOLUTIONPARAMETERS
#     OutputLevel := 2;
#     AbsoluteAccuracy := 0.001;


SCHEDULE



SEQUENCE

CONTINUE FOR 300

       RESET
          AB.Ssp := 1.2;
       END #RESET

CONTINUE FOR 360

       RESET
          AB.Ssp := 0.7;
       END #RESET


CONTINUE FOR 1200

#SAVE "kalman_ini"

END #Sequence

END #Process a
```

Appendix B

Parameter Sensitivity Experimental Data

Case 1.

Time	yco(5)	pHr	Bsp	Ssp	realflow	Ycoperc
0	394.1	10.076	13.86	1.035	42.030	4.000
30	394.1	10.076	13.86	1.035	42.031	3.972
60	394.1	10.076	13.82	1.036	42.011	4.000
90	394.0	10.076	13.81	1.075	42.021	4.023
120	393.9	10.076	13.81	1.083	42.087	4.032
150	394.2	10.080	13.74	1.119	42.107	4.026
180	395.0	10.086	13.68	1.127	42.042	4.017
210	396.6	10.091	13.64	1.121	42.011	3.994
240	398.7	10.096	13.50	1.117	41.979	3.970
270	401.3	10.099	13.44	1.100	41.953	3.948
300	403.5	10.103	13.27	1.099	41.913	3.951
330	405.1	10.108	13.20	1.090	41.876	3.949
360	406.8	10.108	13.12	1.085	41.891	3.892
390	408.3	10.102	13.05	1.076	41.906	3.869
420	409.6	10.102	12.92	1.074	41.931	3.967
450	411.3	10.109	12.90	1.049	41.990	4.065
480	414.0	10.108	12.90	1.047	42.079	4.017
510	415.8	10.101	12.95	1.026	42.130	3.964
540	417.9	10.098	12.99	1.025	42.080	4.005
570	419.8	10.097	12.98	1.033	42.041	4.062
600	419.8	10.097	13.07	1.035	42.058	4.045
630	418.6	10.097	13.13	1.037	42.047	4.003
660	417.8	10.097	13.17	1.037	41.977	3.978
690	417.4	10.099	13.14	1.037	41.943	3.972
720	415.6	10.102	13.18	1.045	41.932	3.985
750	414.0	10.108	13.11	1.044	41.927	3.985
780	412.3	10.107	13.10	1.036	41.910	3.939
810	412.0	10.102	13.08	1.033	41.932	3.880
840	412.6	10.098	12.98	1.032	41.992	3.844
870	415.0	10.096	12.94	1.035	42.041	3.874

Table B.1. Case 1, measurement set.

Case 2.

Time	yco(5)	xr	Bsp	Ssp	realflow	Ycoperc
0	394.2	0.403	13.68	1.127	42.042	4.017
30	395.0	0.400	13.64	1.121	42.011	3.994
60	396.6	0.398	13.50	1.117	41.979	3.970
90	398.7	0.396	13.44	1.100	41.953	3.948
120	401.3	0.395	13.27	1.099	41.913	3.951
150	403.5	0.394	13.20	1.090	41.876	3.949
180	405.1	0.391	13.12	1.085	41.891	3.892
210	406.8	0.391	13.05	1.076	41.906	3.869
240	408.3	0.394	12.92	1.074	41.931	3.967
270	409.6	0.394	12.90	1.049	41.990	4.065
300	411.3	0.391	12.90	1.047	42.079	4.017
330	414.0	0.391	12.95	1.026	42.130	3.964
360	415.8	0.394	12.99	1.025	42.080	4.005
390	417.9	0.395	12.98	1.033	42.041	4.062
420	419.8	0.396	13.07	1.035	42.058	4.045
450	419.8	0.396	13.13	1.037	42.047	4.003
480	418.6	0.396	13.17	1.037	41.977	3.978
510	417.8	0.396	13.14	1.037	41.943	3.972
540	417.4	0.395	13.18	1.045	41.932	3.985
570	415.6	0.394	13.11	1.044	41.927	3.985
600	414.0	0.391	13.10	1.036	41.910	3.939
630	412.3	0.392	13.08	1.033	41.932	3.880
660	412.0	0.394	12.98	1.032	41.992	3.844
690	412.6	0.395	12.94	1.035	42.041	3.874
720	415.0	0.396	12.92	1.046	42.095	3.955
750	417.6	0.396	13.05	1.037	42.107	4.011
780	420.9	0.396	13.13	1.029	42.056	3.958
810	424.7	0.396	13.17	1.025	42.036	3.820
840	428.3	0.396	13.16	1.024	42.053	3.830
870	431.2	0.396	13.68	1.127	42.042	4.017

Table B.2. Case 2, measurement set.

Appendix C

gOPT Sample Code

HORIZON

1560 : 1560 : 1560

INTERVALS

6

120 : 120 : 120

120 : 120 : 120

120 : 120 : 120

240 : 240 : 240

360 : 360 : 360

600 : 600 : 600

PIECEWISE-CONSTANT

AB.Ssp

INITIAL-PROFILE

0.7 : 0.7 : 0.7

0.7 : 0.7 : 0.899892900

0.7 : 0.7 : 1.099892900

0.94 : 0.7 : 1.31

0.78 : 0.7 : 1.61

0.83 : 0.7 : 1.61

PIECEWISE-CONSTANT

AB.Bsp

INITIAL-PROFILE

11.528130000 : 11.528130000 : 11.528130000

11.528130000 : 9.528130000 : 13.528130000

11.528130000 : 9 : 15.528130000

10 : 9 : 17.3

9 : 9 : 17.3

UNIV.